PROCEEDINGS OF IGY SYMPOSIUM

VOL. II

February 13-16, 1961, New Delhi

COUNCIL OF SCIENTIFIC & INDUSTRIAL RESEARCH

NEW DELHI

PROCEEDINGS OF
IGY SYMPOSIUM

PROCEEDINGS OF I G Y SYMPOSIUM

VOL. II

February 13-16, 1961, New Delhi

Under the auspices of

INDIAN NATIONAL COMMITTEE FOR IGY
PHYSICAL RESEARCH COMMITTEE OF CSIR
RADIO RESEARCH COMMITTEE OF CSIR

COUNCIL OF SCIENTIFIC & INDUSTRIAL RESEARCH
NEW DELHI

Editorial Staff

Editor
S. A. CHARI

Assistant Editor
C. P. AGARWAL

Production Officer
S. B. DESHAPRABHU

Technical Assistants
V. N. CHHIBBER
P. S. SHANKAR

PRINTED AT THE CATHOLIC PRESS, RANCHI, INDIA

CONTENTS

CONTENTS

CONTENTS

NUCLEAR RADIATION

The surface and interior of the earth*

M. S. KRISHNAN†

Department of Geophysics, Andhra University
Waltair

The surface of the earth exhibits different characteristics in different places, the several types of land areas being classed as shields, platforms, plains and mobile belts. The shields are the remnants of the very old parts of the crust composed generally of crystalline and metamorphic rocks, the typical areas being Canada, Brazil, South and East Africa, the Baltic region, the Indian Peninsula, etc. They contain rocks of various ages extending back to over 3000 million years as determined by the amounts of certain radioactive elements and the end-products of their decay, such as U-Pb, Th-Pb, K-A and Rb-Sr. During the last decade a great deal of data has been accumulated on the ages of minerals from various parts of the world. The study of these has shown that there are certain well-marked periods of mineral formation related to the mountain building movements[1]. The peaks of the mineral age frequencies obtained are: 50, 105, 350, 480, 620, 980, 1100, 1400, 1740, 1850, 2110, 2520 and 2610 (in million years). Those which occurred since life appeared on the earth are referred to as the late Pre-Cambrian, Caledonian, Hercynian, Nevadan and Alpine, their ages ranging from 650 to about 70 million years. These are more clearly recognized than the earlier ones. A periodicity of about 300 million years is also discernible though this has been obscured by averaging the age frequencies over the whole world.

Continents and Oceans

The continents and ocean basins have distinct characteristics in the nature of their material and in their structure. The former consist largely of light materials (sial), while the latter consist entirely of heavier basic rocks (sima). The continental crust is now known to have an average thickness of 32 or 33 km. down to the Mohorovicic discontinuity, while the oceanic crust is barely 6–10 km. thick. The continental crust consists of two (or three)

*Summary of opening talk
†Present address: National Geophysical Research Institute, Hyderabad

layers, the top being sial and the rest sima. When a third layer is distinguishable, it generally merges into the mantle rocks and the Moho often becomes indistinct. The different layers show distinct velocity ranges of P and S waves. On an average the P waves travel at 5·5 km./sec. in the sial and 6·5 km./sec. in the sima. When there is a lower simatic layer, the P wave velocity in it is about 7·5 km./sec. The mantle rock below the Moho shows a velocity of 8·2 or 8·3 km./sec. There is a thickening of the continental crust underneath the mountain chains, folded belts and island arcs. In mountain belts, the total thickness of the crust ordinarily varies from 40 to 60 km. and in extreme cases may even exceed 75 km.[2,3].

Island Arcs. The oceanic areas are of two types: one in which the margins consist of folded mountain ranges being thrust over the oceans as in the Pacific, and the other in which the margins are fractured coasts showing well-marked faults. The latter may be due to the fracturing of previously existing continents and later drifting of the fragments to the present positions. The Atlantic and Indian Oceans are of the latter type. The Pacific Ocean is encircled by a series of arc-like strings of islands (hence called island arcs). They have certain general characters. On the ocean side, they show a narrow, long and deep trench. On the concave side of the trench, often marked by emerging islands, is a zone of high negative gravity anomalies. Behind the negative anomaly zone are one or two zones of volcanic activity, the outer one being active. Further in (on the concave side) there is generally a shallow sea formed by the collapse of the continental margins in comparatively recent geological times. The whole of the arc appears to be thrust over the sea and the plane of thrust dips towards the continent. The outer arc shows a zone of shallow earthquakes, followed inward by one of the intermediate shocks (beneath the zone of volcanoes). Further behind, at a distance of 400–600 km. from the trench, comes the zone of deep earthquakes, the foci of which may extend down to a depth of 650–700 km. Benioff[4] has shown that the earthquake foci are arranged along two inward dipping zones, the upper one sloping in at about 30° from the horizontal and the lower one at about 60°. This general pattern is found everywhere around the Pacific, but island arcs are not present on the American side, though some of the characteristics of the arc are well developed in the Pacific coastal belt of South America. These arcs apparently indicate the areas which are being annexed to the continents from the ocean.

Mid-ocean Ridges. The oceans have been found to contain a median ridge situated more or less symmetrically between the opposite shores[5]. These mid-ocean ridges appear to conform to one of three general types. The ridges in the Atlantic and Indian Oceans are broad mountainous features which have a width of base of over 1000 km. and rise to within 2·5–3 km. of the sea level. Near their crest the topography is very rugged. The flanks

are cut by faults parallel to the length of the ridges. The top of the ridge is marked by a rift valley, 5–6 km. wide and a few kilometres deep, which is marked by shallow seismic activity and sometimes by volcanoes. The summit zone is one of high heat evolution, the amount of heat evolved being 8×10^{-6} cal./cm.^{2}/sec. which is about 6–8 times as high as the normal.

The second type of ridge is that of the southern Pacific. It is the ridge from Macquaire Island through Easter Island to the Galapagos, continuing into the western edge of North America. This ridge is a broad swell, about 3000–4000 km. wide and smooth in outline. It appears to be merely a gently arched part of the ocean bottom. Its central part, however, shows high heat evolution and occasional volcanic activity. This part is also characterized by a thin crust (barely 4–5 km. thick) but the flanks are thicker. The arching may be due to convection currents in the mantle rising under the ridge[6]. The interesting fact to note is that this south-east Pacific ridge has no rift valley along its top and is, therefore, not a tension feature as is the case with the mid-Atlantic and mid-Indian ridges. Alternatively, this ridge may possibly be due to a gentle compression of the oceanic crust in the southern Pacific.

The third type of ocean ridge is found in the central Pacific where a more or less continuous ridge runs in a north-westerly direction from the Easter Islands towards the Philippines, over a length of several thousand kilometres. This ridge is quite narrow compared to the other two types, and is generally surmounted by numerous sea-mounts as well as guyots, the latter being flat-topped, truncated cones. All these are volcanic cones which were active in the Cretaceous or Eocene times. Some of these which originally rose to the sea surface have since been truncated by wave action and then sunk to their present depth of about 3 km. below sea level. These ridges and their associated volcanic cones appear to mark a major zone of shear which came into being during the Cretaceous period. Volcanic eruptions along these shear zones built up the ridges which were later pierced by volcanoes whose cones now stand up as sea-mounts and guyots.

The north-eastern part of the Pacific between the Equator and Alaska seems to be a region which has undergone shear movements. There are more than half a dozen east-to-west fracture zones which now exhibit large fault scarps several hundred metres high. The blocks between these faults are at various levels, differing by as much as 2 km. in elevation. The fault zones often show sea-mounts or guyots, indicating that they were loci of volcanic activity. Magnetic measurements along some of these fractures have indicated that the blocks have moved along them for scores of kilometres, sometimes as much as 120–150 km. There are also minor fractures which run in a NE–SW and NW–SE directions so that the whole of the sea bottom has been sliced by a series of fractures along which the blocks have moved vertically as well as horizontally. At present, however, the margins of the

Pacific appear to indicate that the movement of the oceanic crust in the Pacific Ocean is generally in a counter-clockwise direction in relation to the continents around[7]. This observation is based partly upon the nature of the faults on the American side as well as observations on the first motions of earthquakes all around the Pacific.

The Arctic and Antarctic Areas

As a result of the work during the IGY and its continuation, we now possess a great deal more knowledge about these regions than before. In the Arctic area the Siberian coast is known to have a wide continental shelf, and this continues into the shelf of Alaska and Canada. The Arctic is roughly triangular in shape, opening out into the Atlantic Ocean. The mid-Atlantic ridge continues through Iceland and Jan Mayen and by the side of Franz Josef Land to the mouth of the Lena river, this feature being marked by high seismicity. The Verkhoyansk range bordering the valley of the Lena is now known to continue into New Siberian Islands and across the Arctic to the Canadian side as a submarine ridge. This important feature of the Arctic Ocean, known as the Lomonosov ridge, is of Mesozoic age. It rises to within 1000 m. of the surface and divides the Arctic Ocean into two parts with rather different characteristics[8].

The Antarctic is a huge continent with a permanent ice cap, rising to a maximum altitude of 3700 m. above sea level. It contains 85–90 per cent of the ice covering the earth and the total volume of ice is estimated at 30 million cu. km. The ice cap is in places as much as 3500 m. thick in East Antarctica. Data at present available indicate that snow is still accumulating on this continent, or at least that there is a balance between accumulation and depletion. Western Antarctica, which is the portion opposite South America, is largely under sea level and consists of island chains which are the continuation of the Scotia arc. They are mainly of Tertiary age and contain large quantities of volcanic rocks. Eastern Antarctica, on the other hand, is an ancient land mass in which there are rocks more than 1000 million years old as well as sediments of various later ages. It contains coal-bearing formations as well as marine formations which must originally have been laid down in warm seas as deduced from their fossil fauna. Seismic refraction studies show that East Antarctica possesses a normal continental crust, 35 km. thick. Palaeomagnetic measurements show that the Antarctica was well away from the Pole in former geological ages[9].

Interior of the Earth

Since our knowledge of the crust by actual observations extends only to a depth of 10,000 ft from the surface, that relating to the interior of the earth can only be indirect. For this purpose, seismic waves produced

either by natural earthquakes or by artificial explosions have been found to be very useful. Recent observations on volcanoes in the Hawaii Islands have indicated that lava is rising from magma chambers 40–60 km. deep[10]. Earthquake shocks originating in Japan and rising through the Klyuchevsky volcano area in Kamchatka show only primary waves. Gorshkov[11] has shown that the shear waves are cut off by bodies of fluid magma at a depth of about 60 km. and that the magma chamber under the volcano in question has an ellipsoidal shape with a length of 30–35 km. and a volume of about 20,000 cu. km.

Gutenberg[12] has postulated a low velocity layer in the upper mantle of the earth close to the Moho. This is inferred from the amplitudes of longitudinal waves which decrease gradually from a distance of 100 to 1000 km. from the epicentre and then increase rapidly. This may be due to the material at a depth of about 80 km. being plastic as a result of temperature increase.

High pressure techniques have now been used for studying the behaviour of minerals and rocks at pressures of the order of 200,000 atmospheres which correspond to a depth of 500 miles from the surface of the earth. As is now well known, artificial diamonds have been produced at a pressure of about 20,000 atmospheres and at a temperature of 2000°. Investigations have shown that at high pressures olivine changes into spinel; hexagonal boron nitride becomes cubic; soda feldspar changes to jadeite; quartz becomes coesite, and so on. In all cases the new mineral is about 15 per cent denser than the one from which it was formed. It is generally thought that there is a phase change at the Moho and that the basalt of the ocean bottom is converted into peridotite or eclogite in the mantle. The occurrence of earthquake shocks down to a depth of 700 km. will indicate that it is possible for the mantle to behave as a rigid material and to transmit short-term stresses as earthquake waves. But at greater depths, stresses are not accumulated and find expression in plastic flow. All seismologists agree that the earth has a layered structure, though there are differences of opinion regarding details. Several models of the earth's interior have been proposed, and all of them agree that there are major discontinuities in the earth at about 30–35 km. which is Mohorovicic, at 2900 km. which is the outer core boundary and at 4980 km. which is the boundary of the inner core. It is now known that the outer core, between 2900 and 4980 km., is fluid in character so that it does not transmit shear waves. But the inner core is inferred to be solid. There is a considerable difference of opinion regarding the nature and composition of the inner core. It is generally believed that it consists of a nickel-iron alloy. A modification of this is that it may contain also silicon to the extent of 20 per cent. Others have proposed that the core may consist of metallic hydrogen, whose characters would be entirely different from its normal behaviour at low pressures.

With an increase in the number of seismological stations all over the world, including the oceanic areas and the less developed countries, a great deal of information is being gathered about the structure of the crust and the interior in different places. With more experimental data, it would be possible in future to determine the real nature of the various zones of the interior of the earth.

References

1. Gastil, G., *Amer. J. Sci.*, **258** (1960), 1–35.
2. Woollard, G. P., *J. geophys. Res.*, **64** (1959), 1521–44.
3. Woollard, G. P., *Trans. Amer. geophys. Un.*, **41** (1960), 107–13; 351–55.
4. Benioff, H., *Bull. geol. Soc. Amer.*, **65** (1954), 385–400.
5. Menard, H. W., *Bull. geol. Soc. Amer.*, **69** (1958), 1179–86.
6. Menard, H. W., *Science*, **132** (1960), 1737–46.
7. Benioff, H., *Mechanics of Faulting*, Dominion Observatory, Ottawa Publ., **22**(2) (1957).
8. Hope, E. R., *J. geophys. Res.*, **64** (1960), 408–27.
9. Crary, A. P., *Trans. Amer. geophys. Un.*, **40** (1959), 331–39.
10. Eaton, J. P. & Murata, K. J., *Science*, **132** (1960), 925–32.
11. Gorshkov, G. S., *Bull. Acad. Sci. U.R.S.S., Ser. Geol.*, (1958), No. 11, 21–27.
12. Gutenberg, B., *Science*, **131** (1960), 953–63.

Upper tropospheric circulation over India

P. S. PANT

Meteorological Office
Poona

Meridional sections along 80°E depicting the month-to-month variation during 1958 of winds and temperatures have been prepared for the levels 9, 10·5, 12, 14 and 16 km. Charts showing streamlines and isotachs for the same levels and for the months January, April, July and October (representative of the four seasons) have been drawn. Corresponding sections and charts based on normal upper winds and temperatures have also been prepared.

On the basis of these charts the upper tropospheric circulation has been discussed with special reference to the onset and withdrawal of strong westerly and easterly winds of jet magnitude. The position of region of strongest winds, the horizontal and vertical shears associated with these winds and the characteristics of the tropopause have been examined. A few case studies during the IGY period have also been presented.

Some of the recent studies which have contributed to our knowledge of circulation in the high troposphere over India and of jet streams in particular are those of Venkiteshwaran[1], Choudhury[2], Krishna Rao[3], Krishna Rao and Ganesan[4], Koteswaram[5-7] and Koteswaram *et al.*[8,9]. Most of these have been based largely on the sounding balloon and the radiosonde data of upper air pressures, temperatures and humidities and the few pilot balloon observations available for the higher levels. There is, therefore, a need to review our knowledge of the circulation in the upper troposphere based on rawin data that have since become available. Special efforts have been made in India during the IGY period to obtain meteorological data at as high levels as possible. The network of aerological stations has also been expanded.

Data

The following data have been made use of in the study: (i) the upper wind data from all rawin and pilot balloon stations and the upper air temperature data from all the Indian radiosonde stations, based on ascents made at 1200 hours GMT during 1958; and (ii) the normal resultant upper winds over the 12 rawin stations, based on all ascents made at 1200 hours GMT up to the end of 1958 and the corresponding normals based on all available pilot balloon data up to about 1950 for all stations in India and Pakistan.

The data are presented in Figs. 1–9. Meridional sections along 80°E depicting the monthly mean resultant winds during 1958 at 12 and 14 km. are shown in Figs. 1 and 2 respectively. The number of observations on these

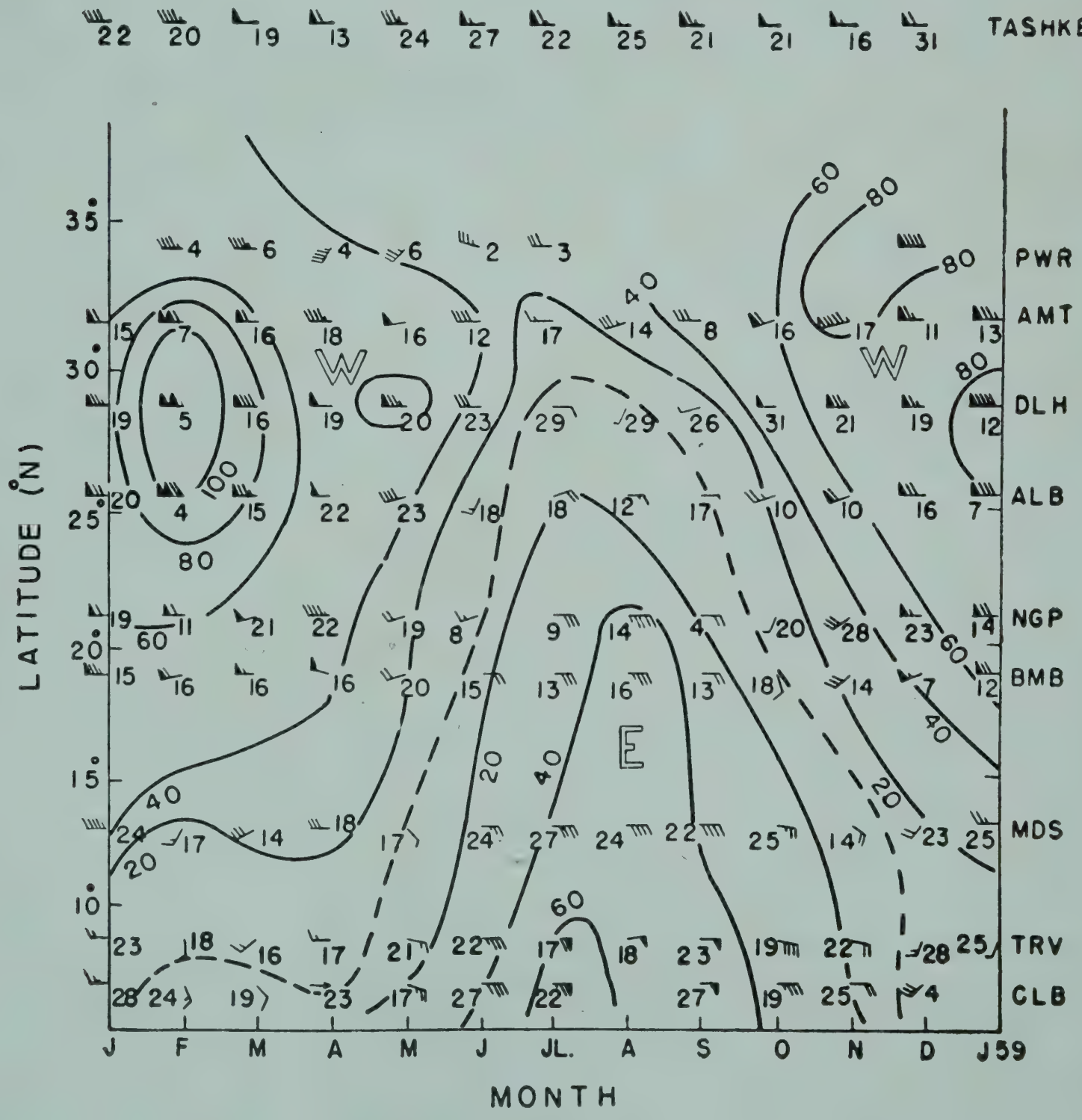

FIG. 1 — MONTHLY MEAN RESULTANT WINDS (KNOTS) AT 12 KM. NEAR 80°E DURING DIFFERENT MONTHS (1958)

sections and isotachs at intervals of 20 knots and the line of separation of easterlies and westerlies are also shown in the figures. The normal resultant wind cross-sections for levels 12, 14 and 16 km. are presented in Figs. 3–5. The temperature cross-sections along the same longitude for 300 mb. level, based on the monthly mean temperatures for 1958 and the normal temperatures, are shown in Figs. 6 and 7 respectively. Isotherms are drawn at intervals of 2° on these sections. Monthly mean height and temperature of tropopause observed during 1958 at Tashkent and New Delhi are shown in Table 1. The variation of wind speed with height at a few stations on January 20, 1958 at 1200 hours GMT is shown in Fig. 8. Similar diagram for July 21, 1957 at 1200 hours GMT is shown in Fig. 9.

TABLE 1 — MONTHLY MEAN TROPOPAUSE DATA FOR TASHKENT AND NEW DELHI DURING 1958

	First transition			Second transition		
	No.	Pr. (*mb.*)	T (OA)	No.	Pr. (*mb.*)	T (OA)
			TASHKENT			
Jan.	29	218	211·7	—	—	—
Feb.	28	222	210·5	—	—	—
Mar.	28	210	209·6	—	—	—
Apr.	28	207	212·2	4	148	211·5
May	29	233	217·0	2	105	211·0
June	28	217	219·4	7	103	211·9
July	18	329	242·7	25	94	206·5
Aug.	21	259	228·9	15	105	211·7
Sept.	19	255	227·0	20	125	210·3
Oct.	25	227	219·6	4	120	212·0
Nov.	26	224	214·0	1	96	210·0
Dec.	30	235	211·5	2	117	211·0
			NEW DELHI			
Jan.	13	206	216·0	4	101	207·5
Feb.	12	172	212·0	3	98	206·0
Mar.	18	138	209·6	6	95	206·0
Apr.	15	133	208·1	1	91	199·0
May	16	101	202·8	—	—	—
June	17	093	199·3	—	—	—
July	19	090	195·2	—	—	—
Aug.	21	100	195·4	—	—	—
Sept.	15	108	195·7	—	—	—
Oct.	19	106	200·3	—	—	—
Nov.	9	111	206·4	—	—	—
Dec.	7	161	212·3	—	—	—

Discussion

In the analysis, weightage has been given to rawin data, wherever they are available, as the number of rawin observations are greater than the pibal observations for levels at and above 9 km. The upper air data for Tashkent, Peshawar and Colombo are also made use of in the discussion.

The general features of the upper tropospheric wind and temperature distributions have been discussed. The spectacular seasonal changes that take place at these levels, the characteristics of the westerly and the easterly streams of jet magnitude and the changes in the tropopause structure associated with the changes in the upper tropospheric circulation have also been dealt with.

General Features of the Upper Troposphere. One of the very prominent features of the upper tropospheric circulation over India is the alternate

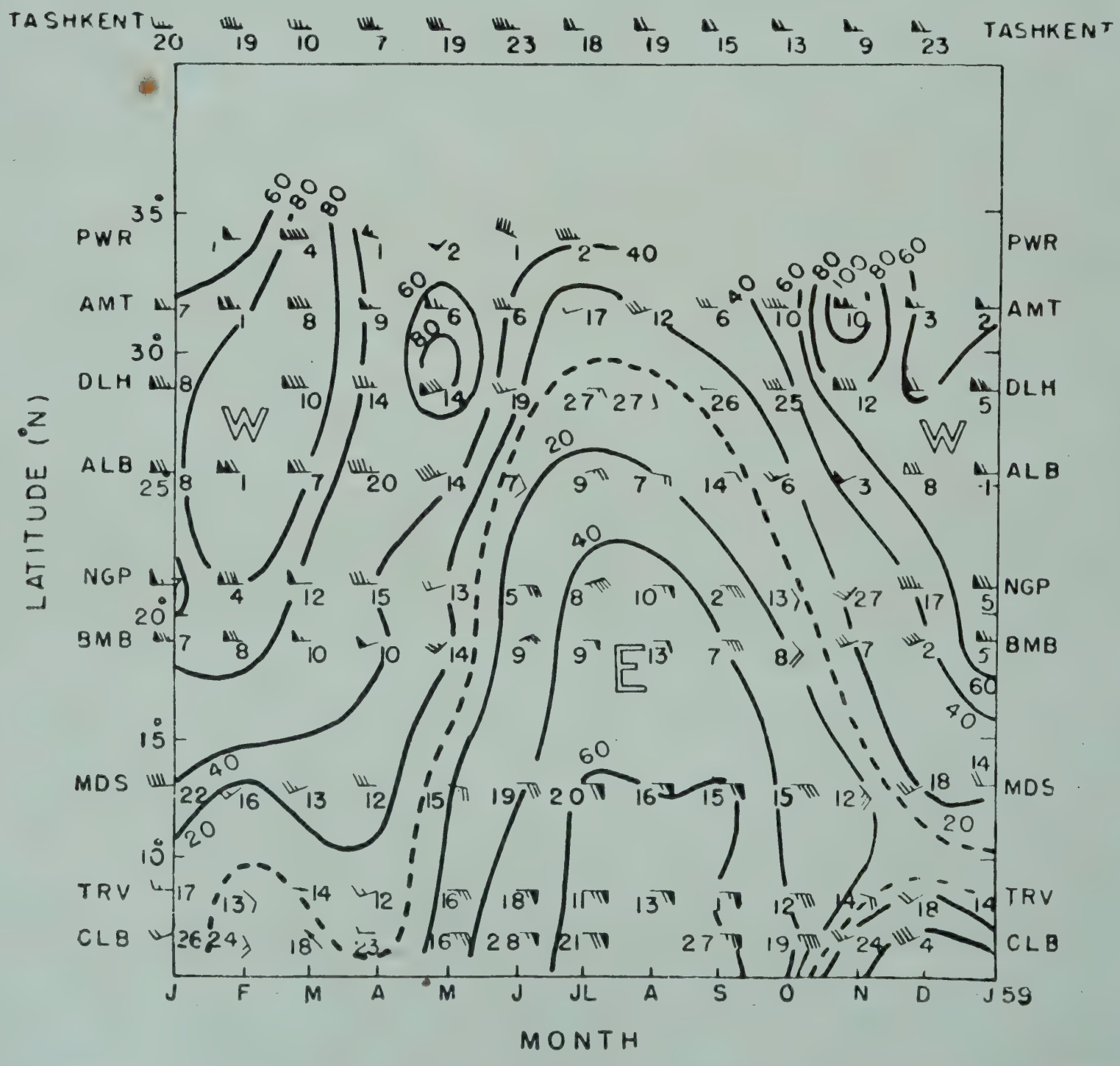

FIG. 2 — MONTHLY MEAN RESULTANT WINDS (KNOTS) AT 14 KM. NEAR 80°E (1958)

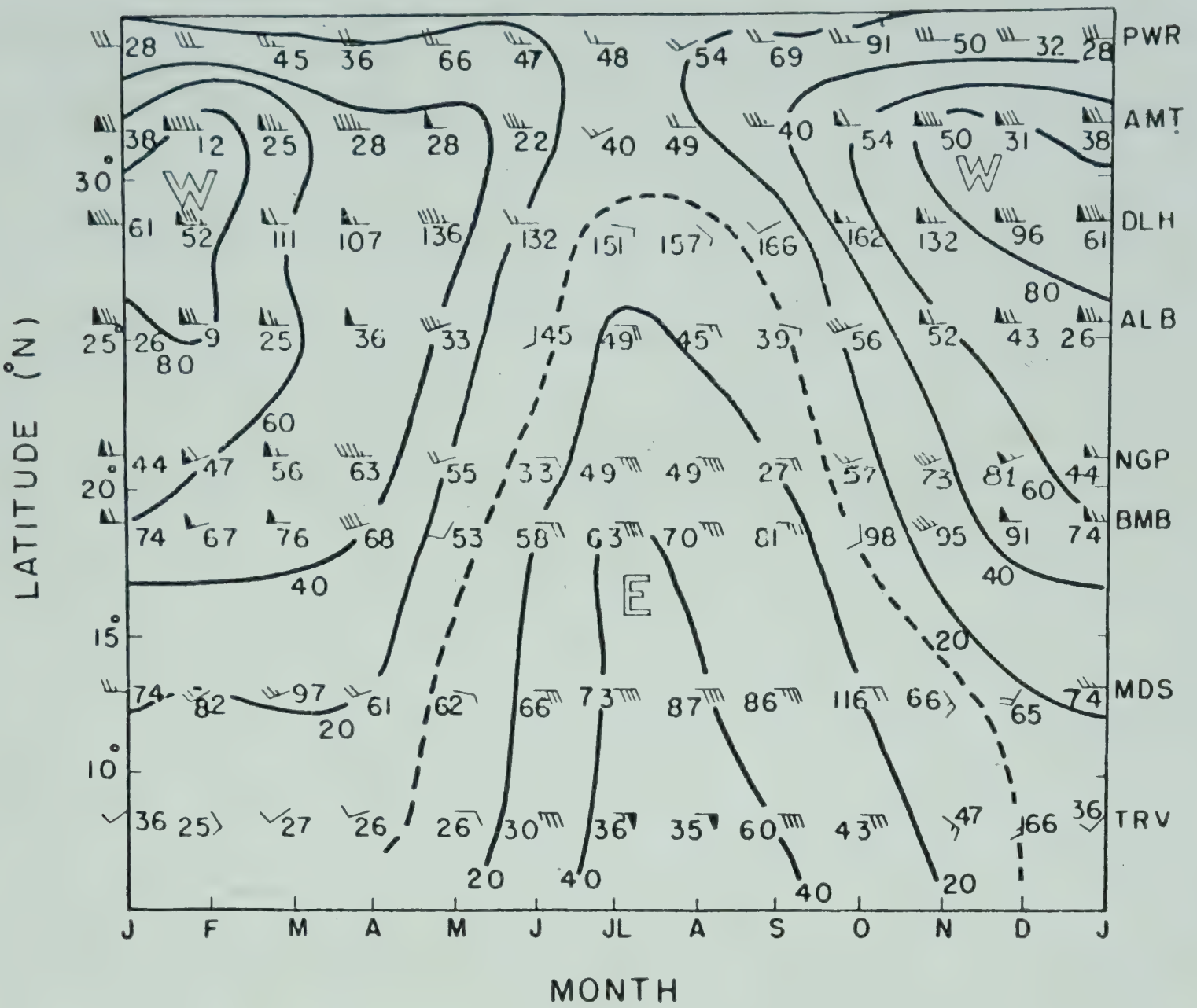

FIG. 3 — NORMAL RESULTANT WINDS (KNOTS) AT 12 KM. NEAR 80°E DURING DIFFERENT MONTHS

predominance of the westerlies and the easterlies; easterlies during the monsoon season and the westerlies during the dry season. In the winter months, the westerlies extend as far south as 5°N and in the monsoon months, the easterlies extend as far north as 30°N (Figs. 1–5). The westerlies strengthen and concentrate into winds of jet magnitude during the winter with their core around 27°N, and the easterlies, similarly, show a tendency to form into an easterly jet during the monsoon months. The westerlies are in general much stronger and are associated with larger shears.

There is a corresponding spectacular change in the thermal structure of the upper troposphere as the wind regimes change from the westerly to the easterly. The meridional temperature gradient is strongest during winter months, especially in the region north of 20°N, with temperatures decreasing from south to north (Figs. 6 and 7). It is in this region that the westerlies build up to jet magnitude. This temperature gradient weakens during March–May. During the monsoon months, a warm core at 300 mb. extending from 20°N to 30°N is noticed. This results in reversing the

gradient of temperature to the south of 20°N, and thus favours the strengthening of the easterlies in that region. One should, therefore, expect that the westerlies would reach their maximum speed during winter months and weaken considerably during the other months and the observed winds are in conformity with our expectation. In the vicinity of the sub-tropical jet, the temperature gradient weakens above 300 mb. and there are indications of a reversal of temperature gradient between 200 and 150 mb. This shows that in the mean, the jet core is around 200 mb. level. In the vicinity of the easterly jet, the temperature gradient favouring the strengthening of easterlies continues even up to 16 km. during the monsoon season. Hence the easterly jet builds up to 16 km.

Westerly Winds of Jet Magnitude. Examination of the winds at different levels of the upper troposphere reveals that the westerlies reach their maximum strength around 12 km. Fig. 1 shows that in 1958, winds of jet magnitude are over our region during January–March and October–December. During the period October–December they are confined to the region north of 25°N, with the core of strongest winds being north of 20°N. During

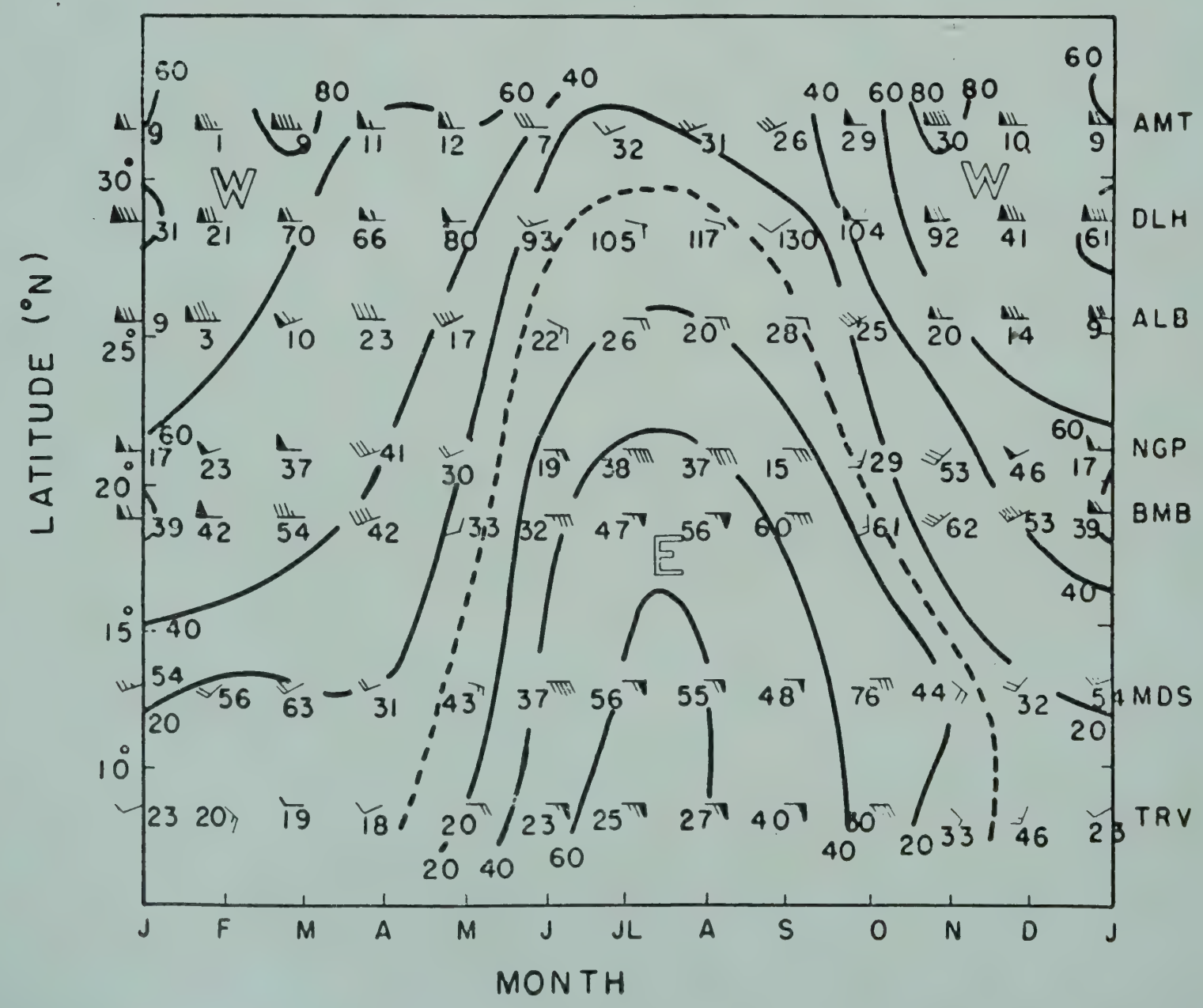

FIG. 4 — NORMAL RESULTANT WINDS (KNOTS) AT 14 KM. NEAR 80°E DURING DIFFERENT MONTHS

January–March 1958, the core of strongest westerlies is around 27°N with the speed at the core rising from 75 knots in January to 120 knots in February, and again decreasing to 80 knots in March. The mean westerly winds at 12 km. weaken from March to April falling below the jet magnitude even in the region north of 25°N. However, in May, westerly winds of jet magnitude (75 knots) reappear just over Delhi, and are not to be found during the entire monsoon season (June–September).

The seasonal changes in strength of the sub-tropical jet are in conformity with the changes in the meridional temperature gradient (Fig. 6). The horizontal shears associated with the jet stream are strongest in February and are 20 knots/1° lat. on the cyclonic side and about 12 knots/1° lat. on the anticyclonic side. In the other months the shears are much less. The corresponding vertical shear when the jet is strongest (in February) is 20 knots/km. below the core and about 25 knots/km. above.

The normal position of the sub-tropical jet is around 32°N in October with strength of just 60 knots and it gradually strengthens and shifts south

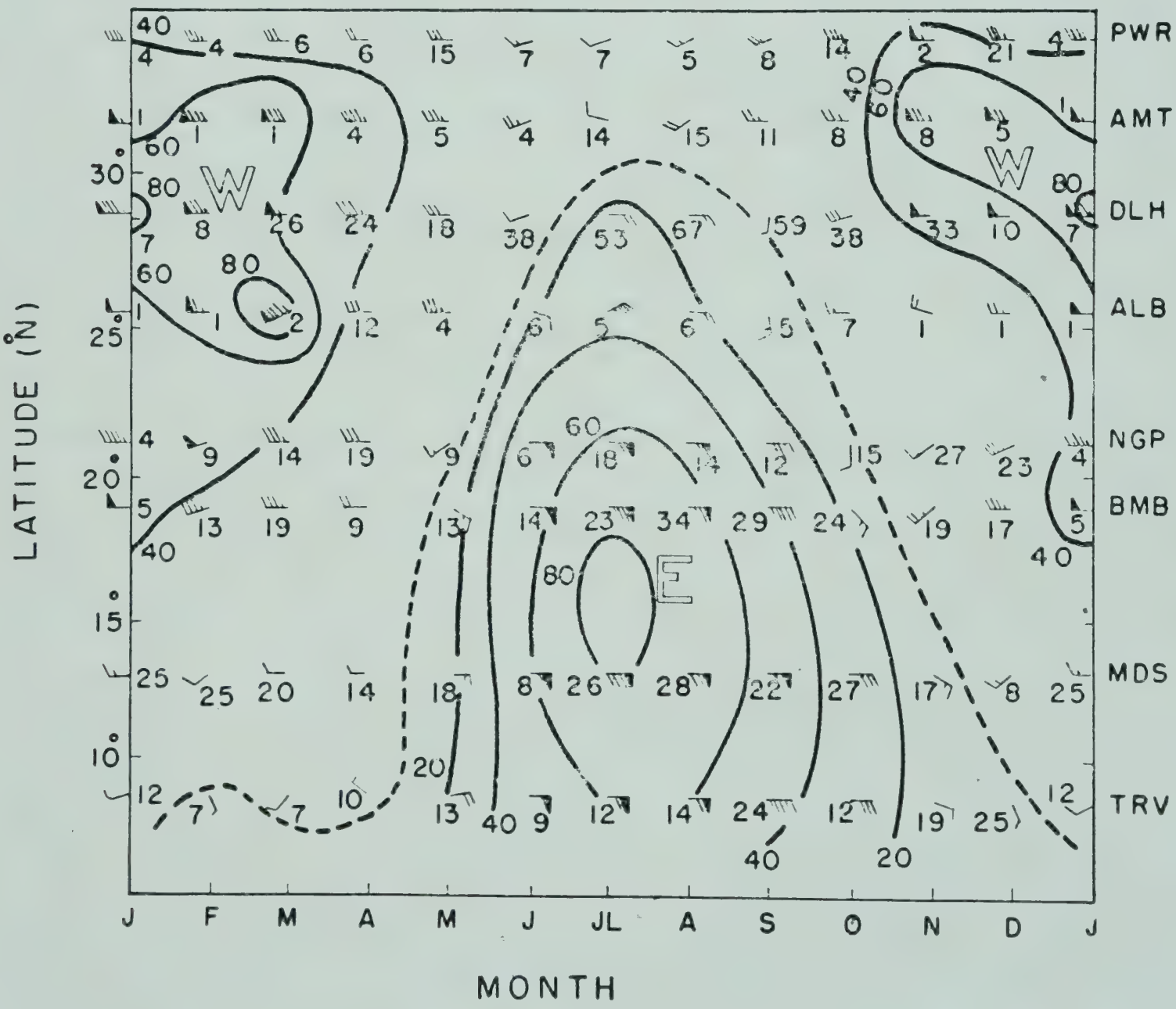

FIG. 5 — NORMAL RESULTANT WINDS (KNOTS) AT 16 KM. NEAR 80°E DURING DIFFERENT MONTHS

(Fig. 3). It has its southernmost position and is strongest in winter (90 knots). It weakens during the period March–May. The horizontal shears associated with it are 10 knots/1° lat. on the cyclonic side and about 5 knots/1° lat. on the anticyclonic side. The mean vertical shear is about 15 knots/km. below and above the jet.

The various characteristics of the westerly jet discussed on the basis of rawin data are largely in agreement with the findings of earlier studies[8,9]. However, the mean cross-sections presented here do not show the presence of the sub-tropical jet core with its characteristic shears in the months of April and May over our region. The absence of the jet core during April and May is in conformity with the rapid decrease of meridional temperature gradient observed during this period (Figs. 6 and 7). An examination of the reports of maximum winds over Delhi for four years reveals that there are reports of winds of over 60 knots from Delhi even in the months of April and May, but they are much less frequent than in the months of October–March.

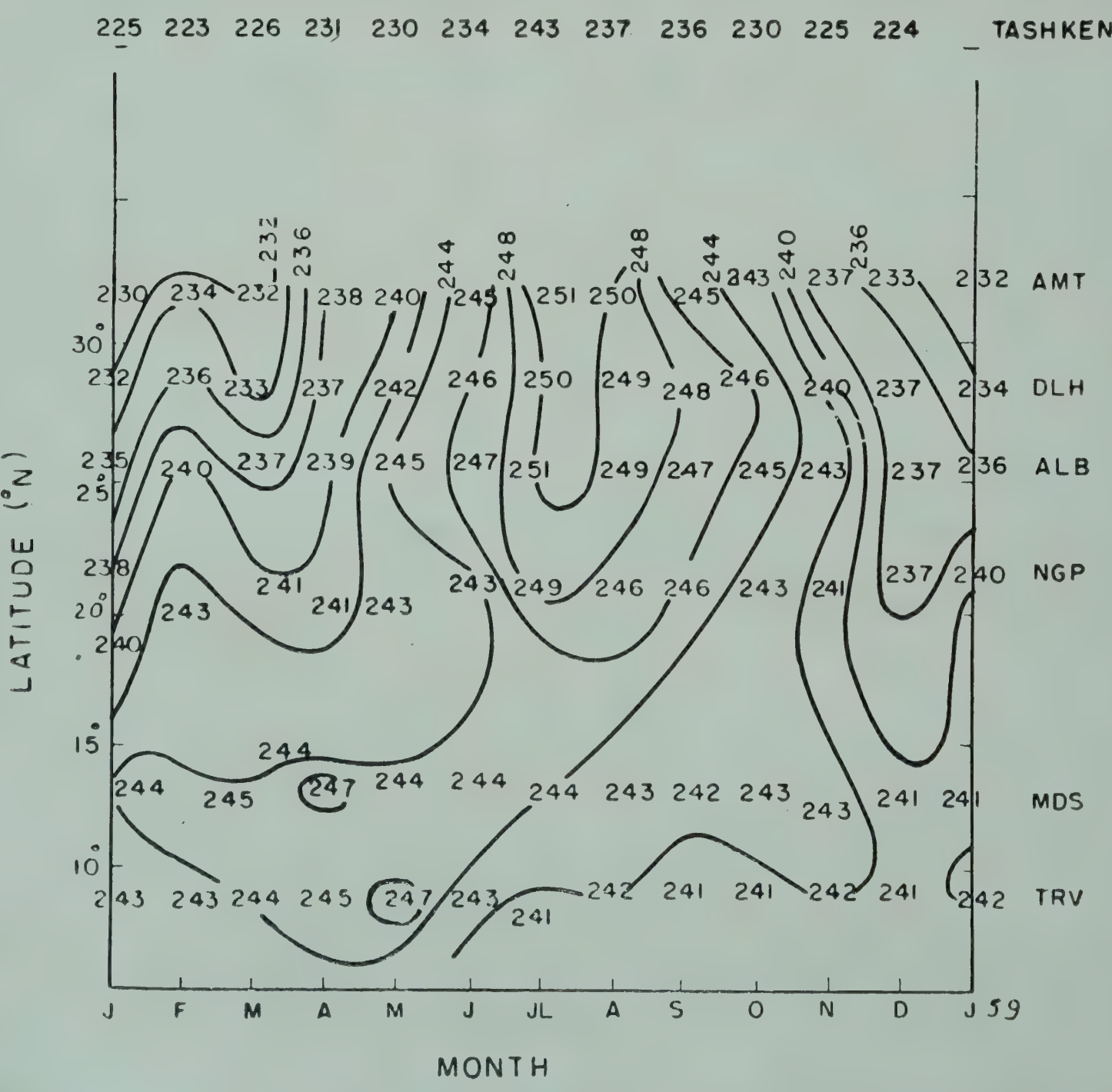

FIG. 6 — MONTHLY MEAN TEMPERATURE (°K.) AT 9 KM. NEAR 80°E (1958)

It has to be borne in mind that if the position of the jet is not steady during any period, it may not show up in the mean picture for that period.

The winds in the upper troposphere over Peshawar and Tashkent indicate that the sub-tropical jet disappears over our region and reappears later further north rather than gradually move northwards. Whereas it sets in over our region rather gradually, it appears first in October north of lat. 30°N and shifts southwards. It is also worth noting that westerlies over Tashkent are weakest during the period in which the jet is over our region, and comparatively strong during the other months.

Some interesting changes in the tropopause structure were noticed over Tashkent and Delhi during 1958 (Table 1). In the winter months, when the sub-tropical jet is far south, the middle latitude tropopause with its height around 200–230 mb. is observed over Tashkent with no upper tropical tropopause. In the same period, over Delhi, the lower tropopause characteristic of the middle latitudes along with the higher tropical tropopause is observed. During the period when the monsoon holds sway over our country, and the upper tropospheric easterlies spread farthest north, and when the jet

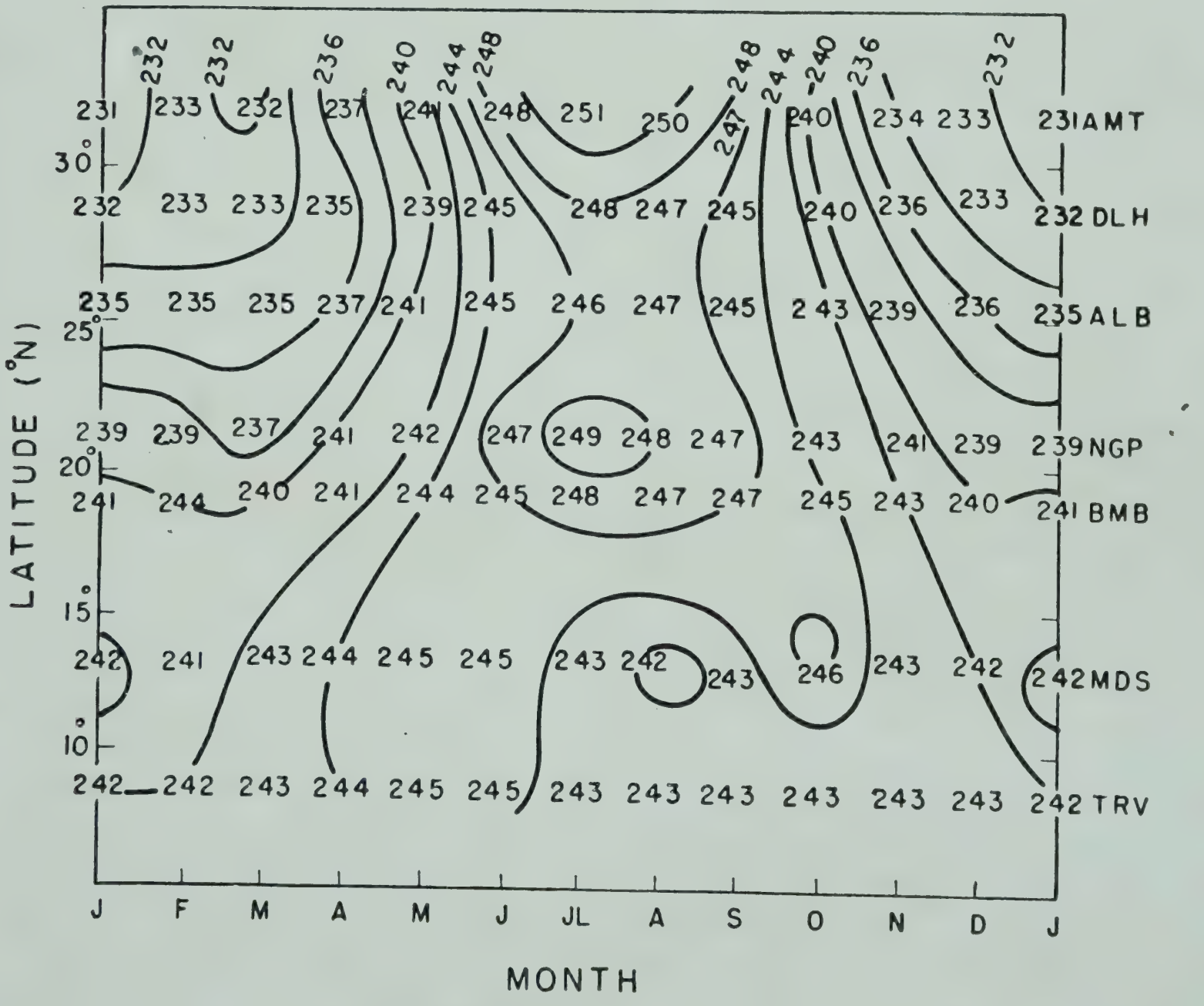

FIG. 7 — NORMAL TEMPERATURE (°K.) AT 9 KM. NEAR 80°E

is to the north of our region, the double tropopause is observed most frequently over Tashkent, whereas over Delhi, only the tropical tropopause is observed. These observations clearly show that with the shift in the position of the jet, the region where the double tropopause occurs also moves.

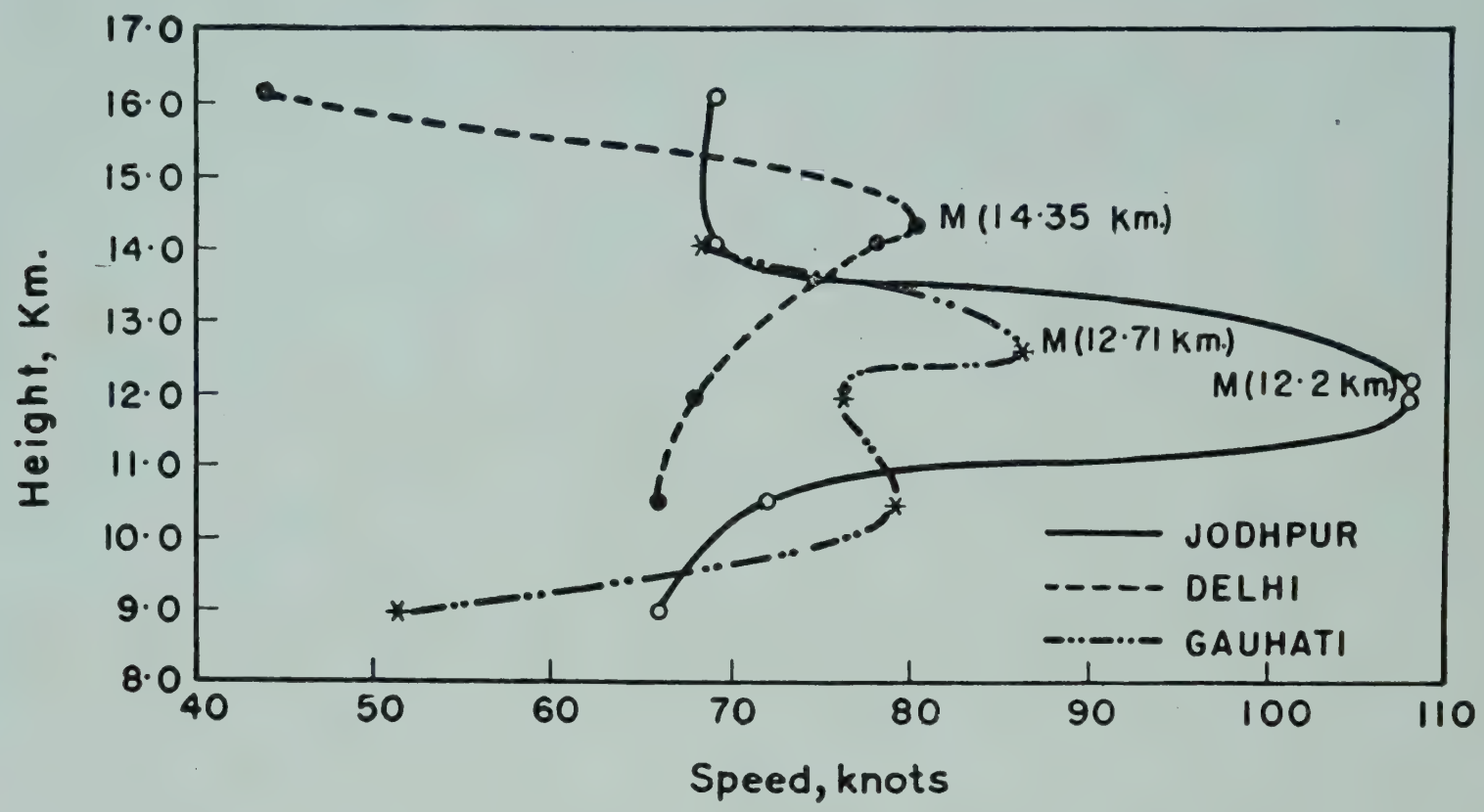

FIG. 8 — VARIATION OF WIND SPEED WITH HEIGHT AT A FEW STATIONS ON JANUARY 20, 1958 AT 1200 HOURS GMT

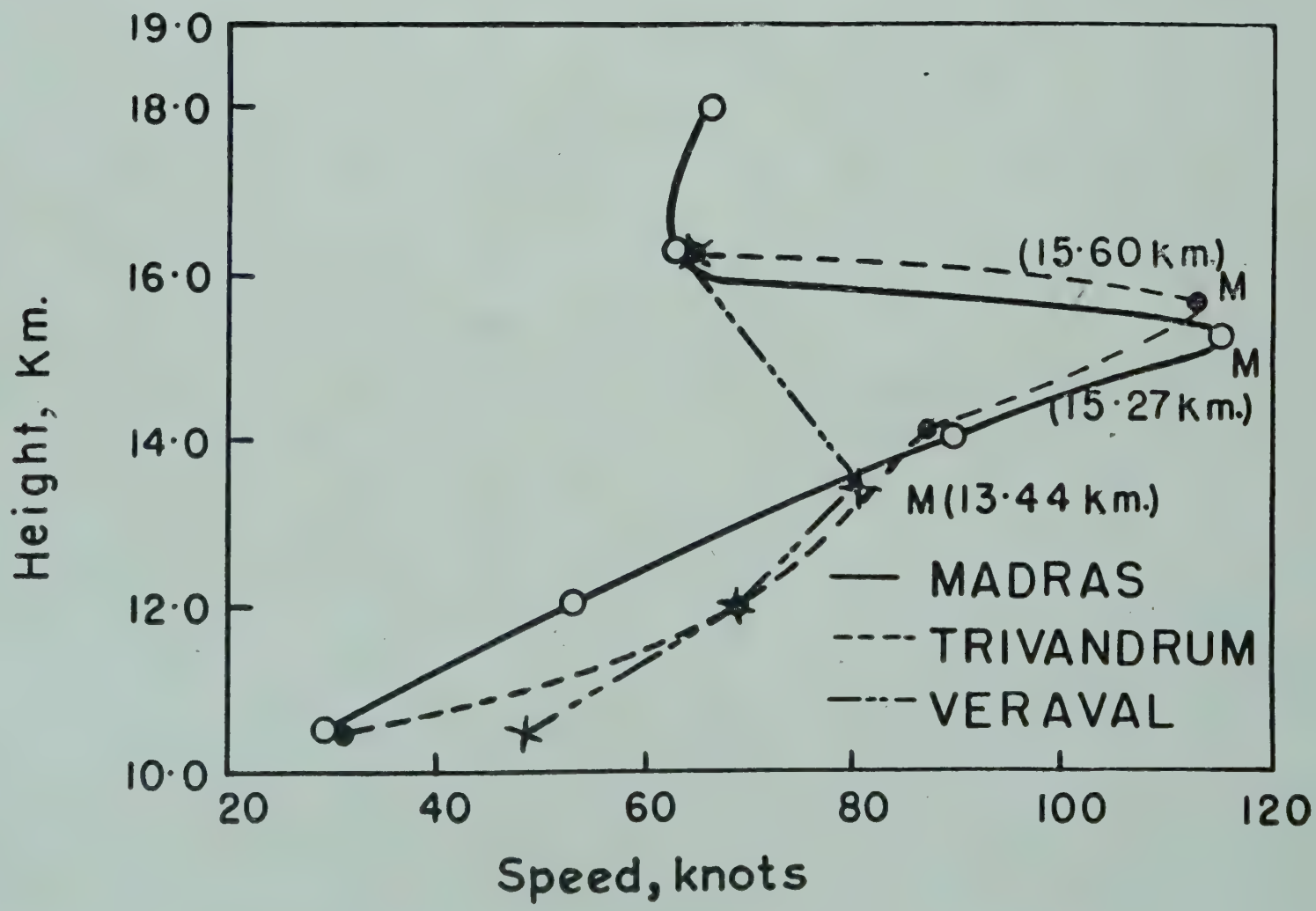

FIG. 9 — VARIATION OF WIND SPEED WITH HEIGHT AT A FEW STATIONS ON JULY 21, 1957 AT 1200 HOURS GMT

This is in accordance with the findings of Defant and Taba[10] on the basis of their world-wide study of tropopause structure. These observations show that in the monsoon season, the cold air adjacent to the tropical tropopause spreads out into the stratosphere of the middle latitudes carrying with it the tropical tropopause, whereas in winter, the stable air of the lower stratosphere of middle latitudes is drawn into the troposphere of lower latitudes. Such a meridional exchange of air has been suggested by Ramanathan and Kulkarni[11] to explain certain changes observed in the amount of ozone over Srinagar. The region of the tropopause break in the vicinity of the sub-tropical jet seems to be most favourable for such an exchange.

The appearance of the higher tropical tropopause over Tashkent or the increase in the frequency of its appearance during the monsoon season may have some relation to the spread of the upper tropospheric easterlies and, perhaps, to the behaviour of the monsoon as Sutcliffe and Bannon[12] have found over the Middle East. The latter aspect deserves further detailed study.

Westerly Jet Stream of January 20, 1958. Based on 1200 hours GMT wind observations it was possible to locate the jet core on this day. The winds at 12 km. clearly show that the core of the jet is to the south of Delhi and runs close to Jodhpur, Allahabad and Gauhati. The weaker winds over Calcutta show that the core is further north. The horizontal shears observed at the jet level are 20 knots/1° lat. on the cyclonic side and about 10 knots/1° lat. on the anticyclonic side. It is seen from Fig. 8 that the vertical shear is stronger near the jet core and is about 20 knots/km. both above and below the jet stream.

Double tropopause with the low transition around 230 mb. was observed over Jodhpur on this day. Even at Delhi, the lower tropopause was clearly seen at the same height as at Jodhpur, but the ascent did not reach the higher tropical tropopause. Further south, at Veraval, only the higher tropical tropopause was predominant. These observations coupled with those mentioned earlier lend support to the view that the westerly jet stream over our region in winter usually occurs in the region of the tropopause break, where the stable stratospheric air mass of the higher latitudes with its characteristic low tropopause comes over our region.

Easterly Winds of Jet Magnitude. Information about easterly jet stream over India is still very meagre, for it occurs at much higher levels than the westerly jet stream and wind observations for these levels are very scanty. The normal wind cross-sections along 80°E for 14 and 16 km. (Figs. 4 and 5) indicate that easterly winds of jet magnitude occur only in the months of July and August in the region south of 20°N with the core of maximum winds around 15°N. The speed at the core varies from 70 to 80 knots.

The easterly jet is not only weaker than the westerly but does not also possess the horizontal shears normally associated with jets. The horizontal shears associated with it are only about 5 knots/1° lat. Unlike the westerlies in winter, the easterly winds of jet magnitude seem to form a broad belt of strong winds and the core is not sharply defined. Thus they do not strictly satisfy the definition of jet stream[13]. The vertical shears associated with it are about 15 knots/km. both over and below jet core.

The mean wind cross-section for 1959 (Fig. 2) showing winds at 14·0 km. is based on much fewer observations than the corresponding normal wind cross-section (Fig. 4). On this cross-section the monthly mean resultant winds of Colombo are also shown. It is seen that the region of stronger easterlies is south of Madras at 14 km. in the period July–September. The observations for 16 km. are few, but the winds at this level show that the strong easterlies extend as far north as 20°N. This confirms the view expressed earlier that unlike the westerly winds of jet magnitude, the easterlies do not form a sharply defined core and are only a broad current of strong winds with large vertical shears. This is perhaps due to the fact that westerly jet during winter is formed in the region of confluence of the middle latitude air and the tropical air with the attendant sharply defined meridional temperature gradient, whereas the easterly winds in the upper troposphere are strengthened during the monsoon season by the thermally driven anticyclonic circulation over Tibet and North India[6,7] and the associated temperature gradient is not as strong as in the case of the westerly jet.

Easterly Jet Stream observed on July 21, 1957 (1200 hours GMT). Wind data were available for a number of stations in the south on this day, with ascents showing well-defined maxima. On an examination of winds at 14 km., it is seen that winds of jet magnitude are reported even over Port Blair, but that they reach their maximum strength over the peninsula, with the strongest winds occurring around 15°N. The horizontal shears are very small. The wind profiles for Trivandrum, Madras and Veraval (Fig. 9) indicate that the vertical shear below the maximum wind over Madras and Trivandrum is almost the same (20 knots/km.) and is higher above the maximum wind. At Veraval, which is farther away from the core, the shears are much less. The jet maximum occurs in association with the tropical tropopause, which is there both over Trivandrum and Madras.

Conclusion

(i) In the upper troposphere, the westerly winds, which are confined to the region north of 30°N during the monsoon, gradually strengthen and spread southwards and concentrate into a jet stream during the period October–March. From April onwards they weaken and shift northwards. During the monsoon season, the equatorial easterlies spread as far as 30°N.

(ii) During the winter, when the upper tropospheric westerlies and the sub-tropical jet stream are farthest south, the lower tropopause characteristic of the high latitudes along with the higher tropical tropopause is observed over North India. In the monsoon season when the upper tropospheric easterlies spread as far as 30°N, the tropical tropopause is observed quite frequently even over Tashkent. It is quite likely that the appearance of tropical tropopause over Tashkent and the behaviour of monsoon over India are closely related. This aspect deserves detailed study.

(iii) The sub-tropical jet stream, which is strongest during the winter and is around 27°N, occurs in the region of tropopause break and soundings in the vicinity of sub-tropical jet usually show the double tropopause. This lends support to the view that confluence of tropical air and the high latitude air is responsible for the formation of sub-tropical jet around 30°N.

(iv) The easterly winds of jet magnitude which are observed close to the tropical tropopause in the monsoon season in the region south of 20°N are weaker than their westerly counterparts during the dry period and are not associated with strong horizontal shears. Their core is not sharply defined.

Acknowledgement

The author is very thankful to Sarvashri B. Gopinatha Rao, D. S. V. Rao, N. R. Patole, K. M. Gokhale and R. N. Pendse who have helped him in different stages of the work.

References

1. Venkiteshwaran, S. P., *India met. Dep. Mem.*, **28** (Part 2) (1950), 55.
2. Choudhury, A. M., *Tellus*, **2** (1951), 56.
3. Krishna Rao, P. R., *Curr. Sci.*, **21** (1952), 63.
4. Krishna Rao, P. R. & Ganesan, V., *Indian J. Met. Geophys.*, **4** (1953), 193.
5. Koteswaram, P., *Indian J. Met. Geophys.*, **4** (1953), 13.
6. Koteswaram, P., Research Report, Dept. of Meteorology, Univ. of Chicago, 1956.
7. Koteswaram, P., *Tellus*, **10** (1958), 43.
8. Koteswaram, P. *et al.*, *Indian J. Met. Geophys.*, **4** (1953), 111.
9. Koteswaram, P. *et al.*, *Indian J. Met. Geophys.*, **5** (1954), 138.
10. Defant & Taba, *Tellus*, **9** (1957), 259.
11. Ramanathan, K. R. & Kulkarni, R. N., *Quart. J. roy. met. Soc.*, **86** (1960), No. 368, 144.
12. Sutcliffe, R. C. & Bannon, J. K., *Sci. Proc. Inst. Ass. Met. IUGG, Rome*, 1954, 322.
13. *World Meteorological Office, Technical Note No.* 19, 1958, 1.

A study of the onset of monsoon over India

P. S. PANT
A. D. VERNEKAR

Meteorological Office
Poona

The onset of the monsoon during the years 1957-59 has been examined. Meteorological data relating to 850 mb. level have been mainly considered, as this level is high enough to be free from local effects and low enough to be in the monsoon air, when it is just setting in and is not too deep. All the normally measured meteorological elements, namely temperature, humidity, wind speed and direction, and a few derived quantities, like lapse-rate, wet bulb potential temperature, have been examined.

The study broadly indicates that in the south the onset of monsoon does not result in a conspicuous change in the temperature and humidity of the air mass. The only characteristic change that comes over is the setting in of westerlies which are extremely steady and which can normally be separated from the winds existing earlier. Further north, especially at the interior stations, there is a conspicuous change in the thermal properties accompanied by rise in humidity.

Detailed discussion of onset of monsoon at some stations is presented.

Monsoon is one of the most important and dominating features of weather in India and its onset is of paramount importance to the farmer as well as the public in general. The onset of monsoon has so far been judged only by the rainfall it has caused. The normal dates of onset of the monsoon now in vogue in the India Meteorological Department[1] and the different studies on the onset of the monsoon[2,3] are all based on rainfall data only. Identifying the monsoon by the rainfall which it causes is not quite satisfactory, especially in regions where the amount of rain caused by pre-monsoon activity is comparable with the monsoon rainfall. There is, therefore, a need for a systematic study of the characteristics of the monsoon

air, so that criteria for declaring the onset of the monsoon over different parts of India can be evolved on the basis of these characteristics.

These criteria should be such that (i) they are less liable to local effects so that a meteorologist will be able to decide a little more objectively, and with greater ease, whether monsoon has set in over a place, and (ii) they should be based on data which are regularly available and should not, as far as possible, involve much of computation.

Data

The onset of monsoon over the two stations, Trivandrum and Bombay, on the west coast and the two inland stations, Nagpur and New Delhi, during IGY and IGC periods has been studied. Temperature, relative humidity, wind and wet bulb potential temperature (θ_{sw}) at 850 mb. level and the temperature difference (lapse) between 850 and 700 mb. levels based on 1200 hours GMT radiosonde and rawin observations have been examined. The 850 mb. level has been chosen as this is high enough to be free from local effects and at the same time is low enough to be in the monsoon air even when it is not very thick.

Diagrams showing the daily values of the first three elements along with the rainfall recorded at 0300 hours GMT during the months May, June and July of the years 1957, 1958 and 1959 are prepared, and the portions showing the data for about 15 days prior to and after the date of onset of the monsoon, fixed as explained below, are shown in Figs. 1–12. Wet bulb temperature and the difference in temperature between 850 and 700 mb. levels are shown in Tables 1–4. After a careful examination of the three years' data for each station, it has been possible to find out certain properties of the monsoon air which remain more or less invariant during the monsoon period and which are conspicuously different from the air mass properties during the pre-monsoon period. On the basis of such properties, criteria have been evolved for declaring the onset of monsoon at the four stations. Utilizing these criteria, dates of onset have been objectively fixed and are indicated in Figs. 1–12. Temporary changes caused in the upper air conditions over any place by the presence of a disturbance, either synoptic or local, should be distinguished from the regular changes that occur with the onset of monsoon. Detailed discussion of the changes that take place in the upper air over the four stations with the onset of the monsoon is presented below.

Discussion

Trivandrum. Being close to the source region of the monsoon air, Trivandrum does not show any spectacular changes in the air mass

TABLE 1 — SOME METEOROLOGICAL ELEMENTS DURING THE MONSOON PERIODS IN 1957, 1958 AND 1959: TRIVANDRUM

1957			1958			1959		
Date	Temp. difference between 850 & 700 mb.	θ_{sw} at 850 mb.	Date	Temp. difference between 850 & 700 mb.	θ_{sw} at 850 mb.	Date	Temp. difference between 850 & 700 mb.	θ_{sw} at 850 mb.
May			May			May		
4	8	24	9	8	25	2	9	23
5	9	22	10	8	23	3	12	21
6	8	23	11	7	24	4	8	24
7	8	22	12	9	24	5	8	23
8	10	23	13	7	25	6	7	21
9	9	26	14	10	21	7	8	25
10	9	23	15	6	21	8	10	22
11	11	24	16	9	23	9	8	23
12	—	—	17	9	21	10	10	21
13	—	—	18	9	23	11	7	23
14	11	23	19	12	23	12	8	24
15	—	24	20	8	23	13	12	23
16	—	—	21	9	25	14	12	24
17	—	—	22	8	24	15	9	23
18	—	—	23	9	23	16	10	24
19*	7	22	24*	8	24	17*	7	23
20	5	23	25	6	23	18	7	23
21	7	23	26	8	22	19	8	24
22	8	23	27	6	21	20	10	19
23	6	22	28	9	23	21	8	21
24	—	20	29	9	24	22	10	22
25	—	—	30	11	21	23	10	23
26	—	—	31	10	26	24	10	22
27	—	—	June			25	9	24
28	9	20	1	6	21	26	10	23
29	10	22	2	10	24	27	6	23
30	7	21	3	8	23	28	7	21
31	8	21	4	8	22	29	8	23
June			5	8	23	30	8	22
1	10	22	6	7	24	31	7	23
2	6	23	7	9	21	June		
3	9	22	8	6	23	1	7	22

*Date of onset of monsoon

characteristics with the onset of monsoon. This is illustrated by the fact that the normal temperature at 850 mb. level falls by only 1°C. from May to June, the dew point temperature by 1°C., and there is no change at all in the mean lapse (temperature difference) between 850 and 700 mb. levels[4]. The

TABLE 2 — SOME METEOROLOGICAL ELEMENTS DURING THE MONSOON PERIODS IN 1957, 1958 AND 1959: BOMBAY

1957			1958			1959		
Date	Temp. difference between 850 & 700 mb.	θ_{sw} at 850 mb.	Date	Temp. difference between 850 & 700 mb.	θ_{sw} at 850 mb.	Date	Temp. difference between 850 & 700 mb.	θ_{sw} at 850 mb.
June			June			June		
7	9	24	2	12	22	11	8	21
8	7	20	3	14	23	12	9	24
9	9	20	4	10	23	13	8	22
10	10	19	5	10	23	14	7	22
11	10	21	6	7	20	15	4	25
12	10	22	7	8	20	16	10	20
13	8	21	8	10	17	17	9	22
14	7	23	9	11	18	18	9	25
15	8	21	10	11	19	19	10	24
16	8	22	11	12	18	20	9	24
17	9	21	12	10	19	21	6	24
18	—	19	13	10	20	22	13	27
19	7	21	14	8	25	23	10	24
20	5	24	15	8	25	24	10	25
21	7	22	16	8	27	25	—	25
22*	9	25	17*	9	26	26*	9	25
23	10	24	18	9	27	27	9	24
24	7	24	19	10	25	28	8	25
25	8	23	20	9	25	29	8	25
26	6	27	21	8	26	30	12	26
27	7	24	22	9	25	July		
28	8	23	23	8	23	1	6	22
29	6	23	24	8	20	2	9	24
30	6	20	25	9	26	3	7	25
July			26	7	26	4	9	26
1	8	22	27	6	25	5	8	24
2	—	—	28	7	25	6	8	24
3	9	22	29	5	26	7	5	26
4	7	21	30	6	26	8	7	26
5	7	24	July			9	8	25
6	6	23	1	7	25	10	6	23
7	8	22	2	—	25	11	10	23

*Date of onset of monsoon

wet bulb potential temperature also does not show any significant change from pre-monsoon to monsoon months. Even the annual range of variations of these factors is small. The daily values of all the above mentioned parameters do not show any significant change in the period during which

TABLE 3 — SOME METEOROLOGICAL ELEMENTS DURING THE MONSOON PERIODS IN 1957, 1958 AND 1959: NAGPUR

1957			1958			1959		
Date	Temp. difference between 850 & 700 mb.	θ_{sw} at 850 mb.	Date	Temp. difference between 850 & 700 mb.	θ_{sw} at 850 mb.	Date	Temp. difference between 850 & 700 mb.	θ_{sw} at 850 mb.
June			June			June		
10	18	21	4	14	24	14	14	22
11	15	23	5	18	25	15	14	23
12	—	21	6	15	23	16	15	23
13	19	23	7	20	25	17	15	24
14	—	22	8	17	24	18	12	24
15	15	23	9	14	20	19	15	26
16	15	25	10	17	22	20	8	25
17	12	24	11	14	21	21	15	24
18	14	25	12	17	23	22	12	25
19	11	25	13	16	21	23	13	24
20	13	25	14	12	23	24	11	25
21	—	—	15	15	22	25	15	24
22	14	23	16	16	25	26	15	23
23	11	27	17	13	23	27	7	24
24	12	25	18	14	26	28	12	23
25*	10	25	19*	8	23	29*	11	25
26	10	26	20	11	26	30	7	24
27	7	24	21	12	25	July		
28	14	22	22	14	25	1	10	23
29	9	23	23	14	25	2	11	24
30	12	23	24	13	27	3	12	26
July			25	12	25	4	8	26
1	12	23	26	12	27	5	9	24
2	10	23	27	9	25	6	8	26
3	12	21	28	12	24	7	10	24
4	8	23	29	—	26	8	12	24
5	6	23	30	10	25	9	8	23
6	7	26	July			10	10	24
7	8	24	1	9	21	11	12	23
8	10	25	2	11	26	12	11	21
9	9	25	3	11	27	13	11	24
10	8	23	4	11	27	14	11	24

*Date of onset of monsoon

the monsoon is normally expected to set in over the region (Table 1). But one of the features for which monsoon is well known is the steadiness of winds with a preferential direction. Krishnan *et al.*[5] have shown that winds are extremely steady (steadiness factor $>$ 90 per cent) over the peninsula

TABLE 4 — SOME METEOROLOGICAL ELEMENTS DURING THE MONSOON PERIODS IN 1957, 1958 AND 1959: NEW DELHI

1957			1958			1959		
Date	Temp. difference between 850 & 700 mb.	θ_{sw} at 850 mb.	Date	Temp. difference between 850 & 700 mb.	θ_{sw} at 850 mb.	Date	Temp. difference between 850 & 700 mb.	θ_{sw} at 850 mb.
June			June			June		
24	15	23	14	20	23	17	17	23
25	15	25	15	15	21	18	15	20
26	16	26	16	12	22	19	14	25
27	15	24	17	16	25	20	17	24
28	10	22	18	12	24	21	12	24
29	—	23	19	15	22	22	16	24
30	—	—	20	14	25	23	17	27
July			21	14	24	24	16	27
1	12	25	22	12	23	25	15	23
2	11	21	23	13	25	26	11	23
3	16	25	24	17	27	27	11	21
4	12	26	25	14	28	28	12	27
5	16	23	26	12	23	29	12	25
6	12	24	27	10	24	30	12	26
7	13	26	28	10	25	July		
8	12	27	29*	10	—	1	11	25
9*	11	25	30	9	26	2*	8	25
10	12	27	July			3	12	28
11	13	26	1	11	25	4	11	27
12	14	28	2	10	27	5	11	28
13	10	25	3	11	27	6	9	28
14	13	27	4	16	26	7	8	26
15	16	25	5	11	25	8	7	27
16	15	24	6	11	25	9	13	26
17	10	26	7	8	26	10	12	28
18	15	25	8	8	27	11	13	28
19	14	25	9	11	24	12	8	24
20	16	25	10	9	26	13	12	23
21	16	25	11	6	26	14	7	23
22	14	27	12	11	27	15	11	26
23	—	25	13	11	25	16	14	24
24	16	24	14	8	25	17	12	27

*Date of onset of monsoon

south of lat. 20°N, during July at 1·5 km., whereas in the pre-monsoon months they are variable. This feature of the monsoon is very well shown by the charts for Trivandrum for all the three years (Figs. 1, 2 and 3). Winds which are weak and variable before the arrival of the monsoon

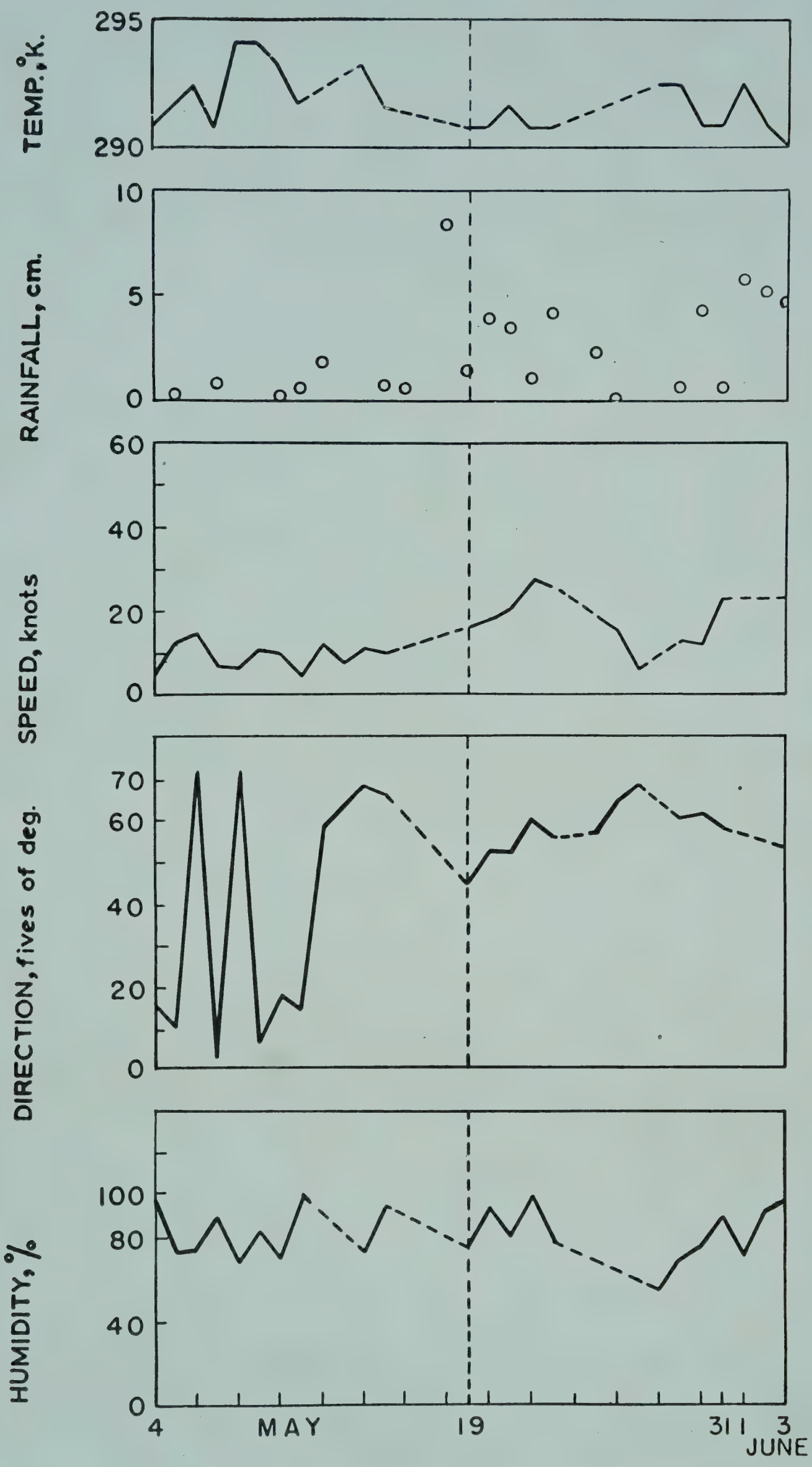

FIG. 1 — DAILY VALUES OF WIND SPEED AND DIRECTION, RELATIVE HUMIDITY, TEMPERATURE AND RAINFALL AT TRIVANDRUM DURING MAY–JUNE 1957

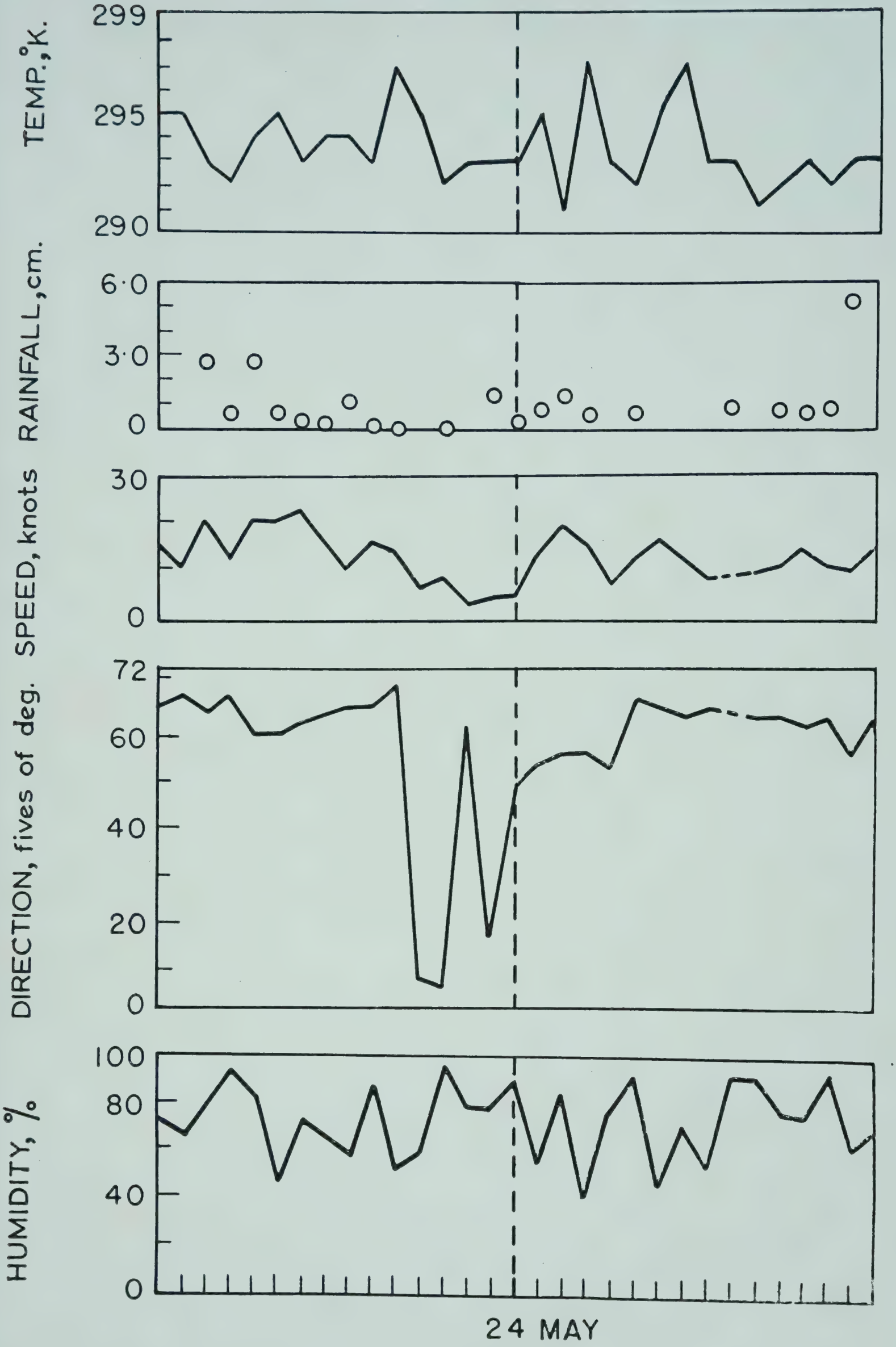

FIG. 2 — DAILY VALUES OF WIND SPEED AND DIRECTION, RELATIVE HUMIDITY, TEMPERATURE AND RAINFALL AT TRIVANDRUM DURING MAY 1958

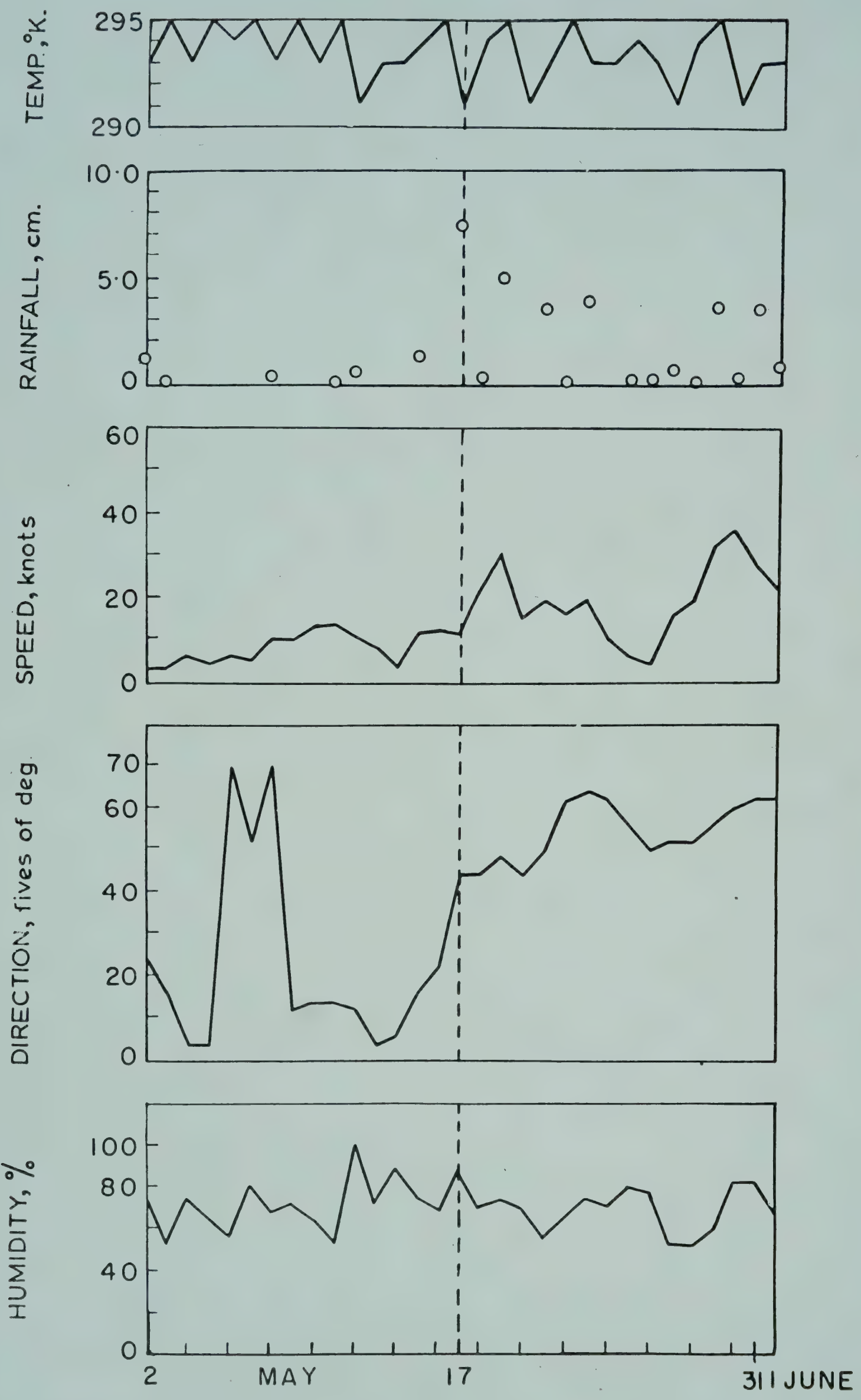

FIG. 3 — DAILY VALUES OF WIND SPEED AND DIRECTION, RELATIVE HUMIDITY, TEMPERATURE AND RAINFALL AT TRIVANDRUM DURING MAY–JUNE 1959

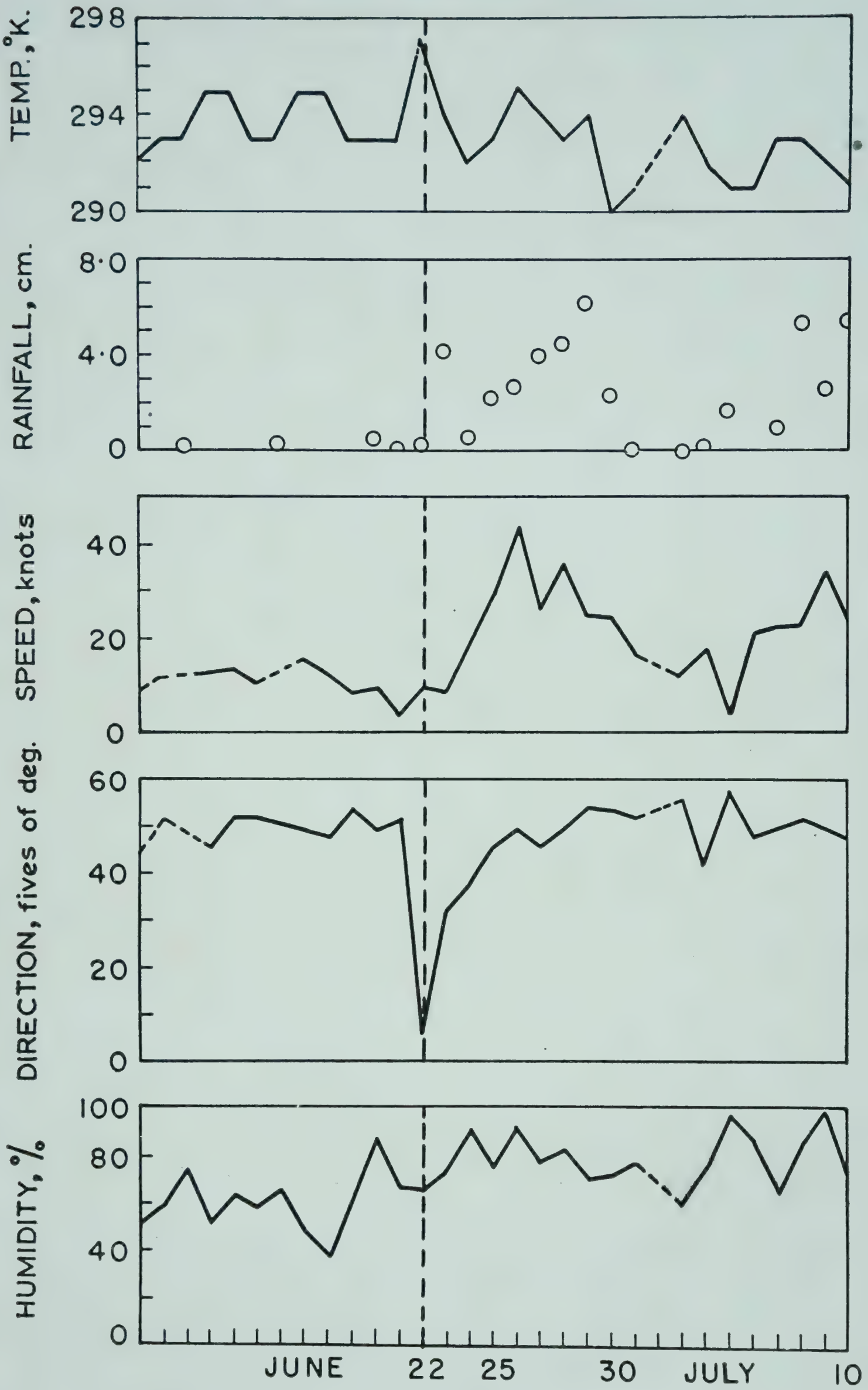

FIG. 4 — DAILY VALUES OF WIND SPEED AND DIRECTION, RELATIVE HUMIDITY, TEMPERATURE AND RAINFALL AT SANTACRUZ DURING JUNE–JULY 1957

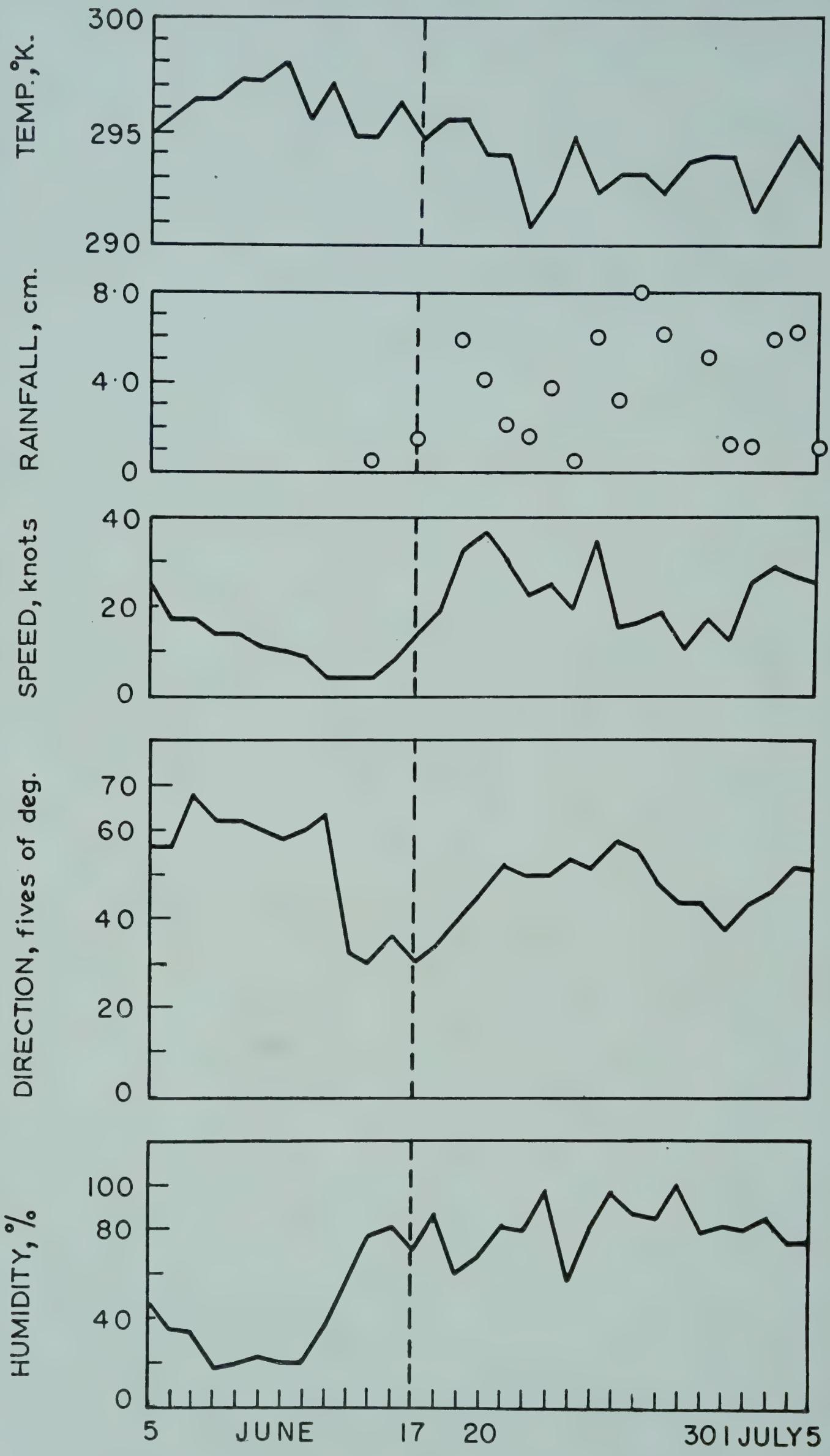

FIG. 5 — DAILY VALUES OF WIND SPEED AND DIRECTION, RELATIVE HUMIDITY, TEMPERATURE AND RAINFALL AT SANTACRUZ DURING JUNE–JULY 1958

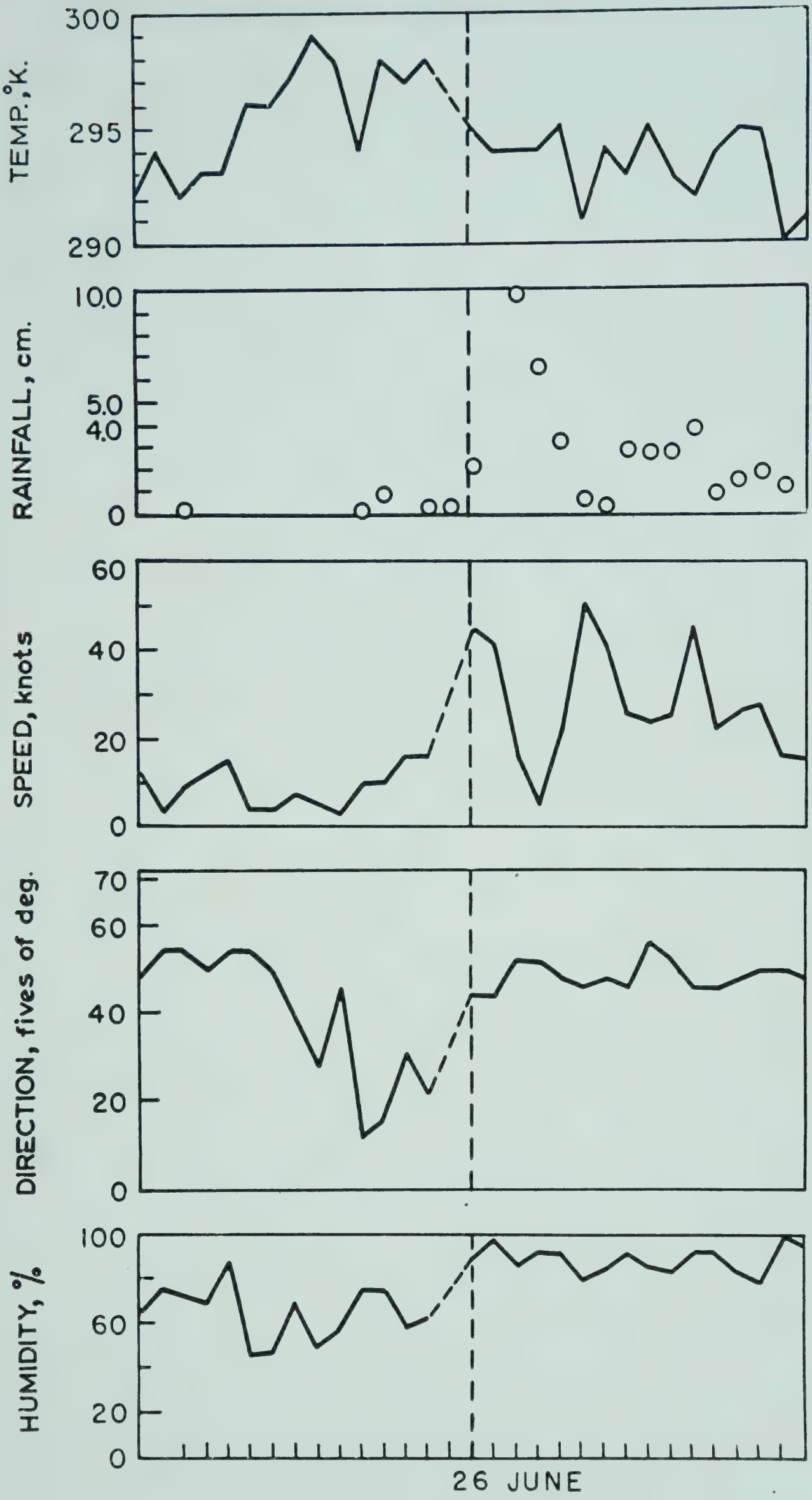

FIG. 6 — DAILY VALUES OF WIND SPEED AND DIRECTION, RELATIVE HUMIDITY, TEMPERATURE AND RAINFALL AT SANTACRUZ DURING JUNE 1959

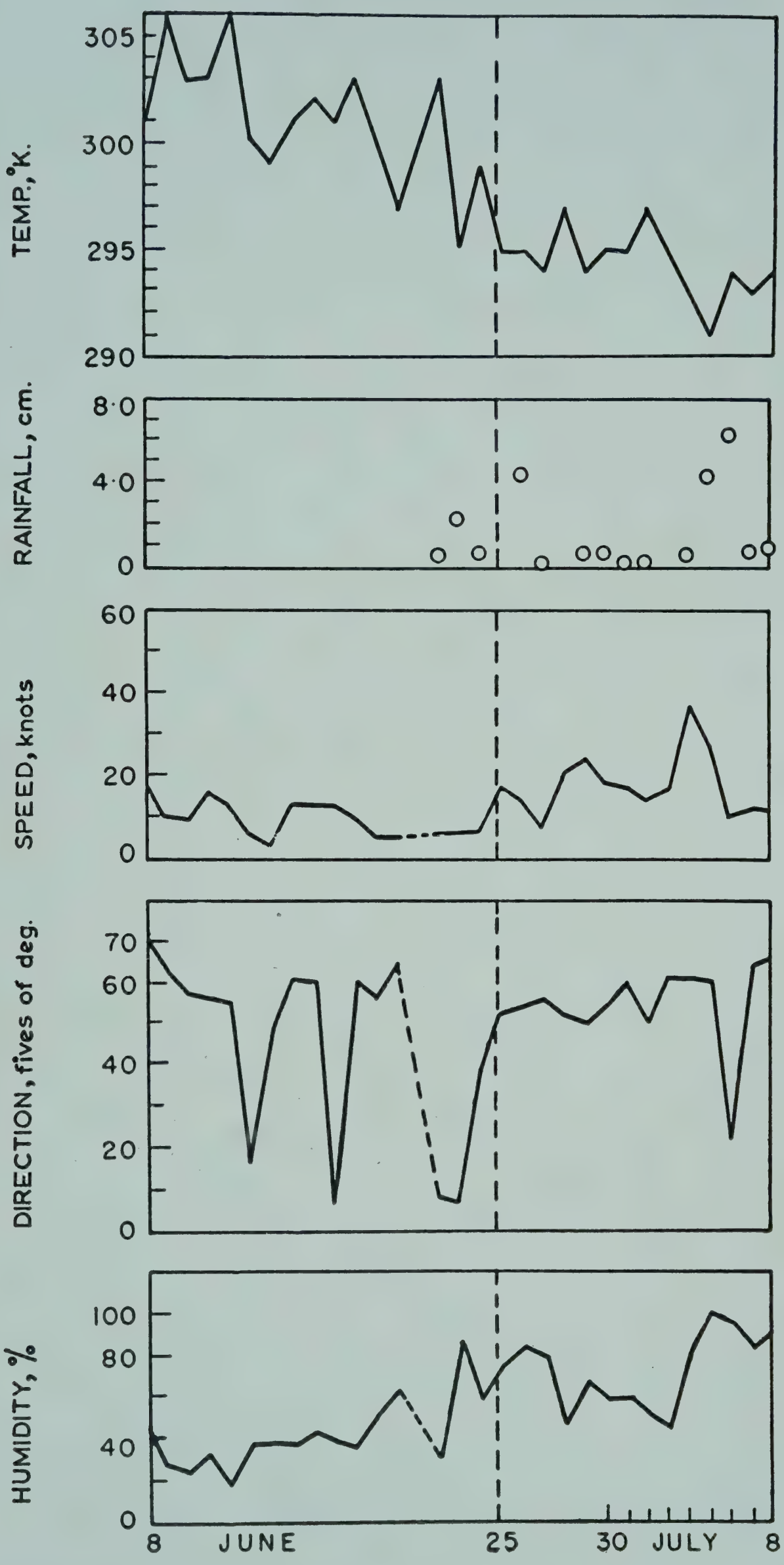

FIG. 7 — DAILY VALUES OF WIND SPEED AND DIRECTION, RELATIVE HUMIDITY, TEMPERATURE AND RAINFALL AT NAGPUR DURING JUNE–JULY 1957

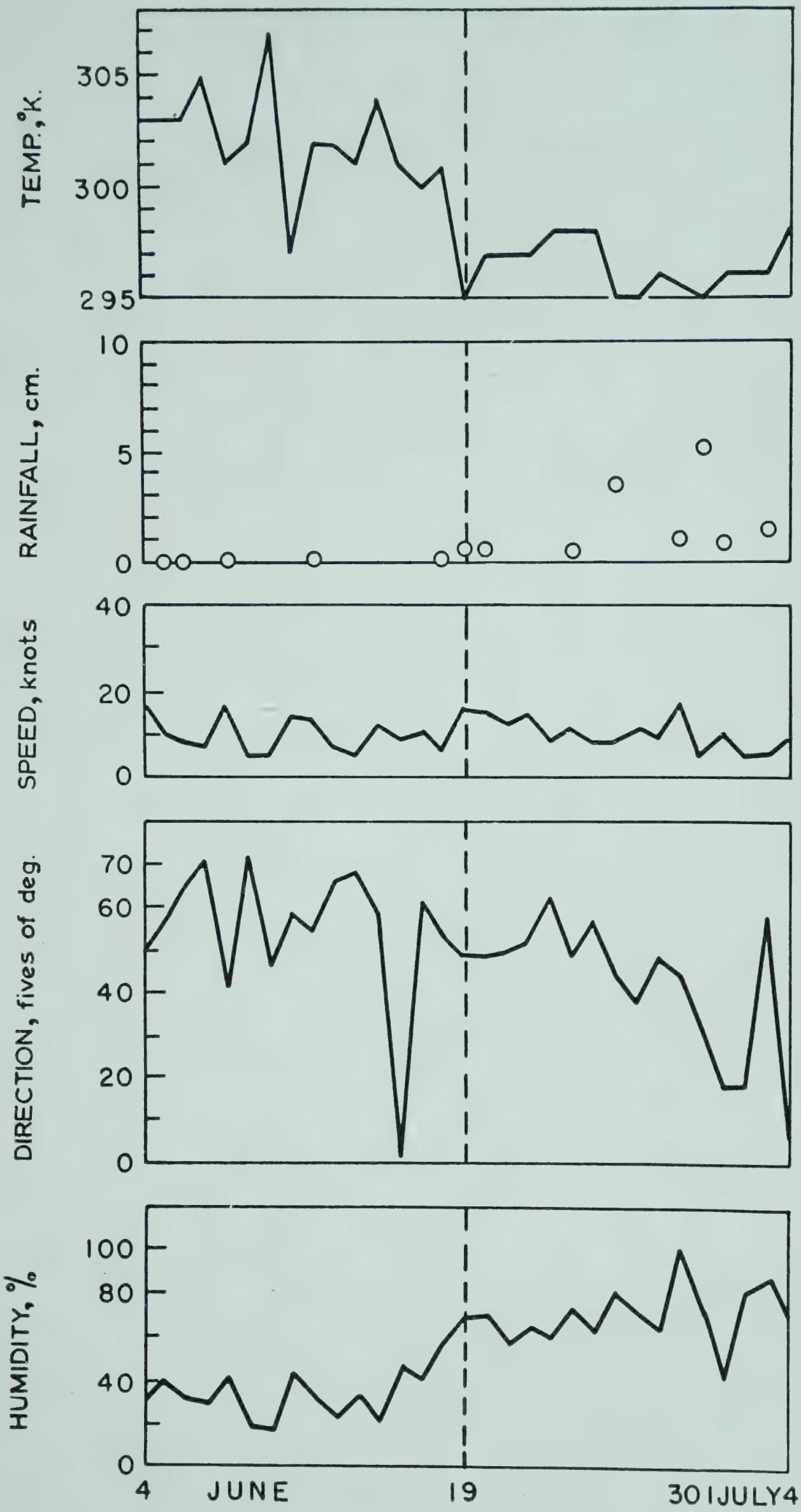

FIG. 8 — DAILY VALUES OF WIND SPEED AND DIRECTION, RELATIVE HUMIDITY, TEMPERATURE AND RAINFALL AT NAGPUR DURING JUNE–JULY 1958

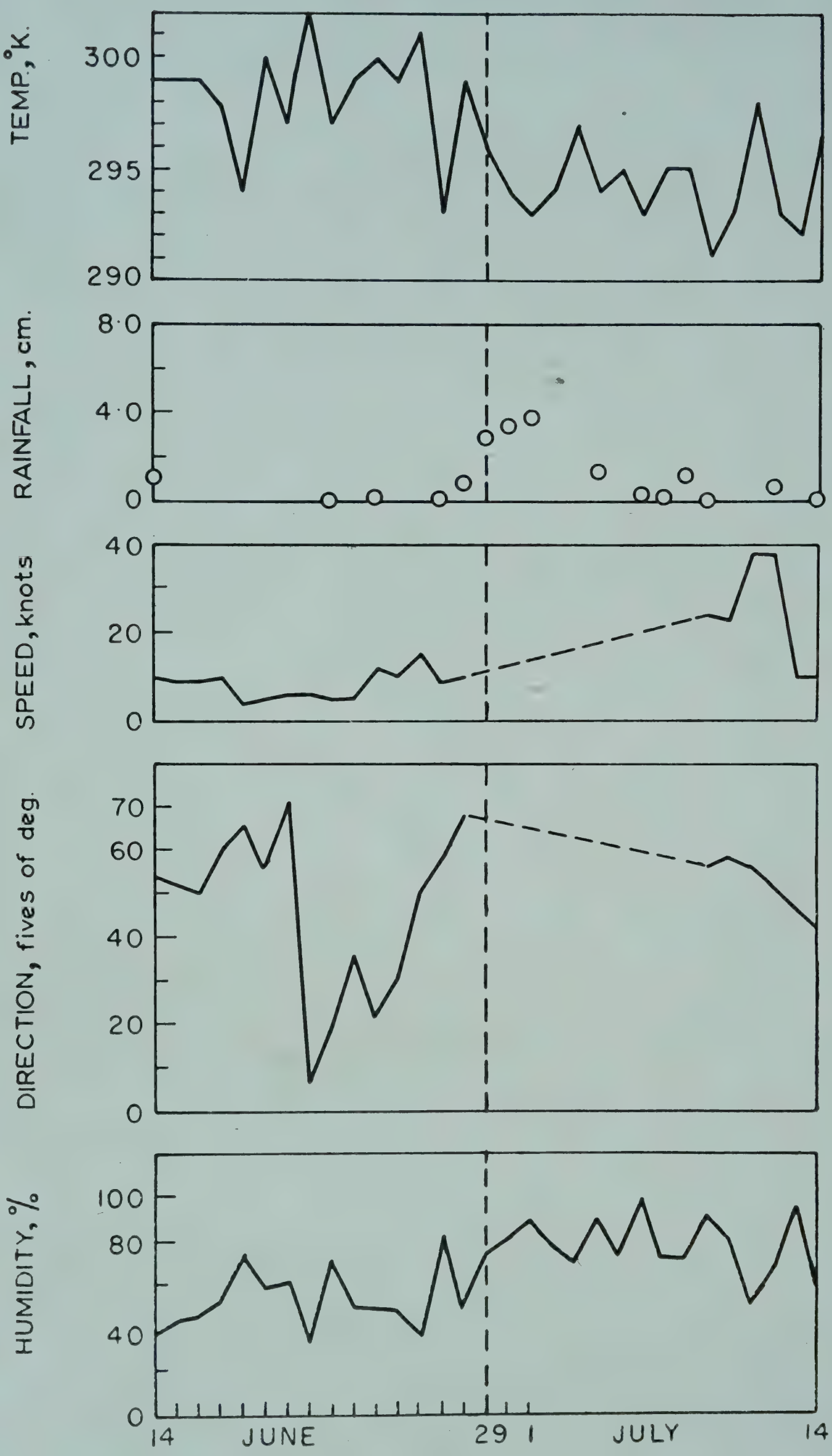

FIG. 9 — DAILY VALUES OF WIND SPEED AND DIRECTION, RELATIVE HUMIDITY, TEMPERATURE AND RAINFALL AT NAGPUR DURING JUNE–JULY 1959

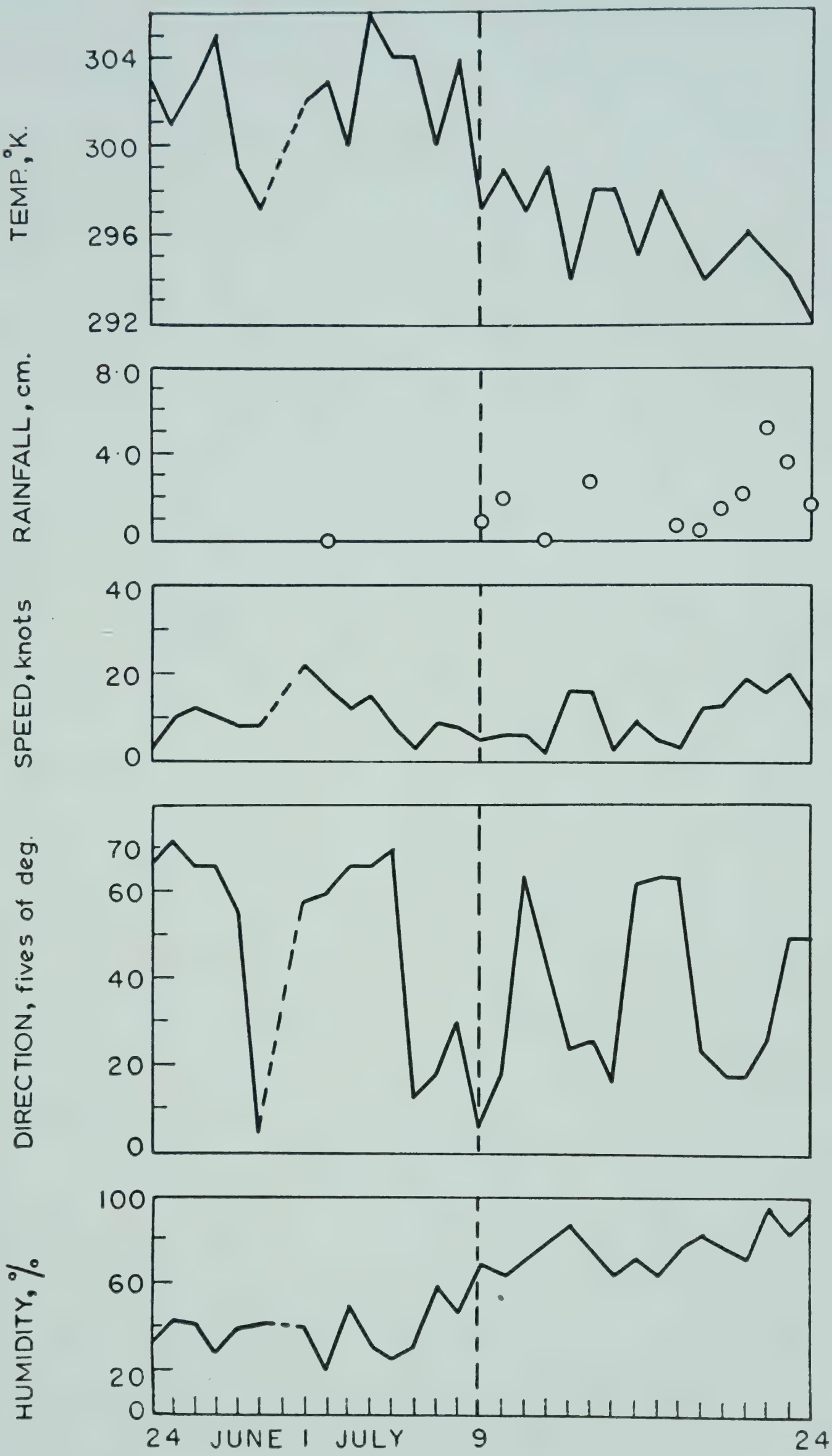

FIG. 10 — DAILY VALUES OF WIND SPEED AND DIRECTION, RELATIVE HUMIDITY, TEMPERATURE AND RAINFALL AT NEW DELHI DURING JUNE–JULY 1957

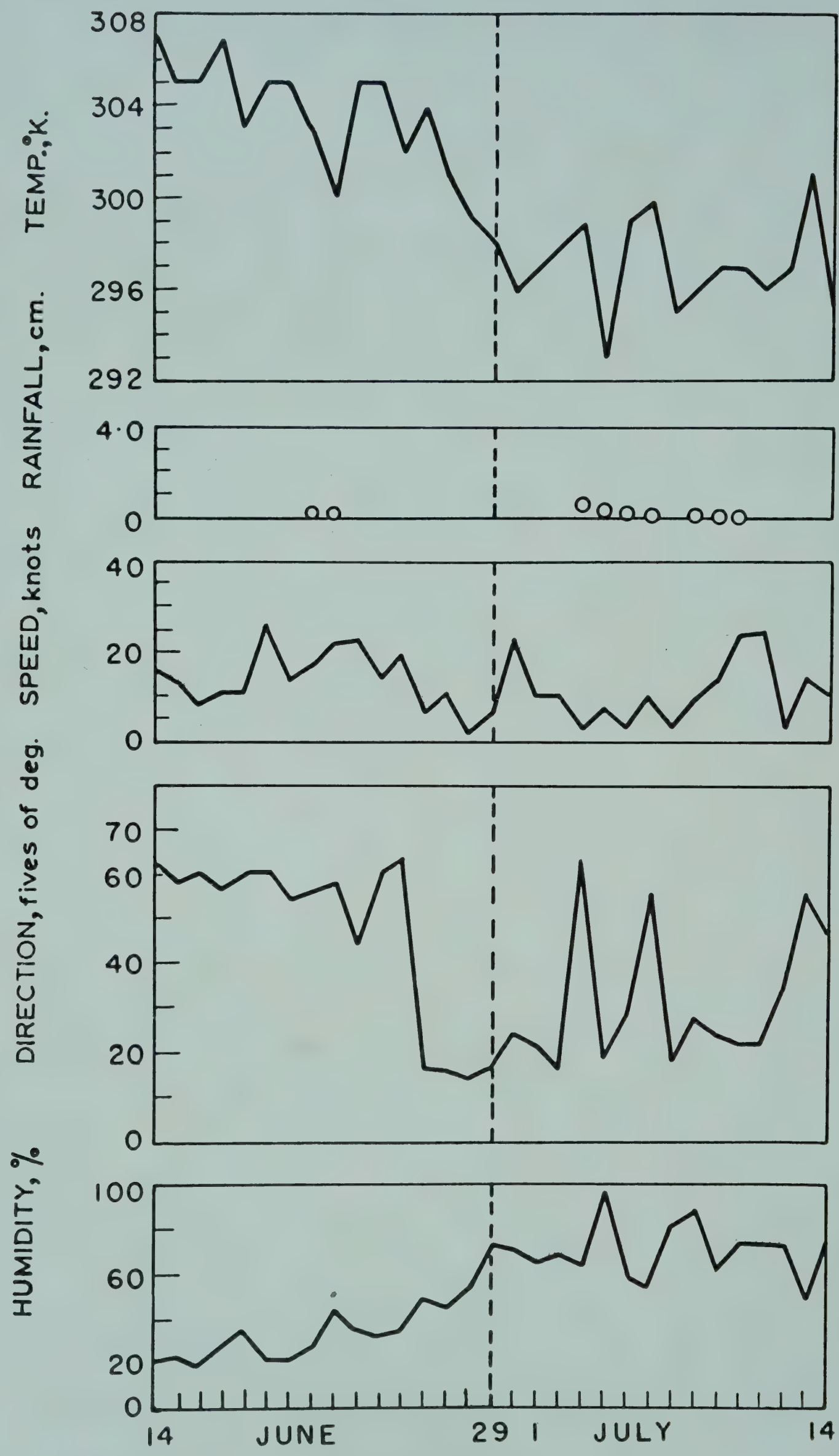

FIG. 11 — DAILY VALUES OF WIND SPEED AND DIRECTION, RELATIVE HUMIDITY, TEMPERATURE AND RAINFALL AT NEW DELHI DURING JUNE–JULY 1958

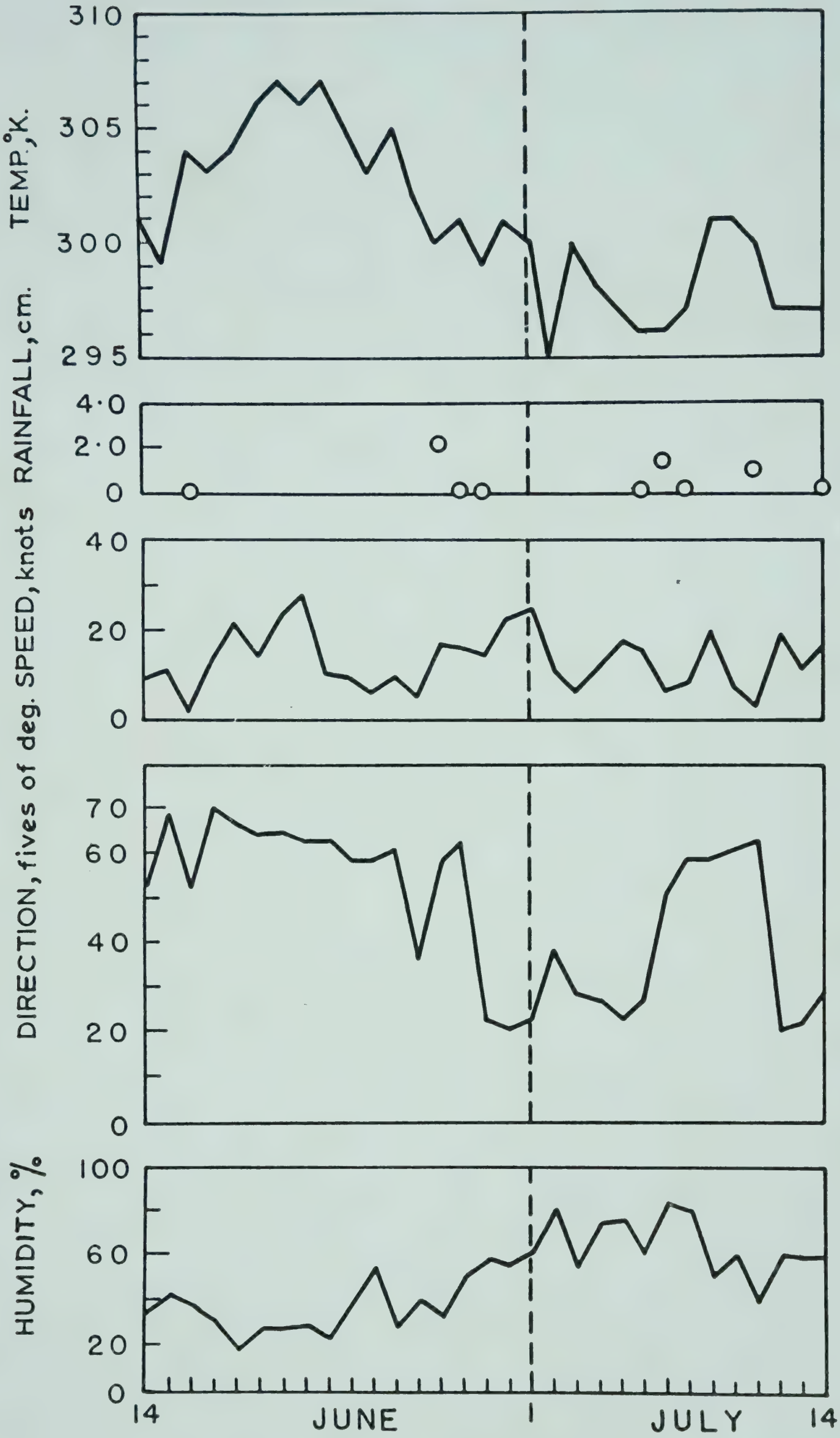

FIG. 12 — DAILY VALUES OF WIND SPEED AND DIRECTION, RELATIVE HUMIDITY, TEMPERATURE AND RAINFALL AT NEW DELHI DURING JUNE–JULY 1959

become steady with their directions at the time of change-over being between SW and NW gradually steadying toward west. The winds also strengthen considerably with the onset of monsoon. This change-over in the wind regime at Trivandrum is helpful in detecting the onset of monsoon.

The following criterion has been formulated for declaring the onset of monsoon over Trivandrum. Around the normal period for the onset of monsoon, the date on which winds at 850 mb. first become southwesterly (225° from north) or somewhere between southwesterly and northwesterly and remain so for the next 2 or 3 days can be taken to be the date of onset of monsoon. The above change in wind direction should be accompanied by considerable strengthening of winds and the relative humidity at 850 mb. level should be 60 per cent or above and remain so later on. On the basis of this criterion, the dates of onset of monsoon over Trivandrum for 1957, 1958 and 1959 have been fixed.

In 1957, there have been a number of days during May and June for which upper air data are not available. Though there are indications of the incursion of monsoon air earlier than May 19, the available data clearly show that monsoon was over Trivandrum from May 19 onwards.

In 1958, there was a temporary incursion of monsoon air as early as May 5. But it withdrew later and the regular onset took place on May 24. The relative humidity at 850 mb. was generally above 60 per cent after the onset and did not later fall below 50 per cent.

In 1959, the monsoon set in over Trivandrum on May 17 and during the 3 or 4 days' period prior to that date there was a continuous veering of winds from NNE to SW. This was accompanied by strengthening of winds. The relative humidity was all through above 50 per cent. In cases of gradual onset, when winds continuously veer over 2 or 3 days towards west, one can expect that the monsoon is likely to set in within the next 2–3 days. Although the above criterion may not enable a meteorologist to foresee the onset on all occasions, it will at least enable him to determine the date of onset objectively. This will also help introduce more uniformity in the matter of declaring the onset. It is also worth mentioning that the heavy falls of rain associated with the monsoon have generally occurred in Kerala after the dates of onset fixed by the above criterion.

Bombay. As this station is farther north from the source region of the monsoon air than Trivandrum, more prominent changes in the air mass properties are seen here. Temperature and wet bulb potential temperature at 850 mb. level and the lapse of temperature between 850 and 700 mb. levels do show a change with the onset of monsoon. But the change is gradual and is not very helpful for fixing the dates of onset unambiguously.

But, as at Trivandrum, there is a very prominent change in the wind direction as well as strength with the onset of the monsoon.

In addition to the change in winds at the 850 mb. level, a simultaneous and conspicuous change in relative humidity takes place. This is as should be expected, as the normal dew point temperature at 850 mb. level over Bombay increases by 8°C. from May to June. The charts for Bombay (Figs. 4, 5 and 6) reveal that relative humidity, which is 40 per cent or below in May prior to the onset of the monsoon, rises to values of 60 per cent or above at the time of onset of the monsoon and does very rarely fall below 50 per cent afterwards. When the monsoon is established, the relative humidity goes as high as 80 per cent. This change in relative humidity is helpful in separating the pre-monsoon and monsoon conditions.

The following criterion has been found to be helpful for fixing the date of onset of monsoon over Bombay. When the winds at 850 mb. level continuously veer over 2 or 3 days becoming southwesterly to westerly at the end of the period with a simultaneous rise in speed, and the relative humidity during this period being 60 per cent or above, then the first day of the above period can be taken to be the date of onset of monsoon. Applying this criterion the dates of onset of monsoon over Bombay during the years 1957, 1958 and 1959 have been fixed.

In 1957, there were temporary changes in the various factors around May 26 in association with the depression in the Arabian Sea off Karwar and South Konkan coast. But the regular onset of monsoon was on June 22. This was preceded by a continuous veering of winds from northeasterly to southwesterly and a simultaneous rise in speed. Relative humidity, which was about 40 per cent prior to the onset, has risen to 60 per cent or above and has remained above 60 per cent afterwards.

In 1958, the onset was on June 17 and was preceded by veering extending over 3 days from south-southeasterly to southwesterly direction with a simultaneous increase in wind speed.

In 1959, there was an incursion of weak monsoon current on May 26, which does not satisfy the criterion laid down above. But the regular onset was on June 26 or a day earlier (Data are not available for June 25, 1959).

The regular persistent monsoon rain over Konkan started after the dates fixed by the above criterion.

Nagpur. The changes that take place with the onset of the monsoon are more conspicuous at Nagpur, which is an inland station. The relative humidity at 850 mb. level, which is about 40 per cent in the pre-monsoon period, rises to 60 per cent or above, as at Bombay. This rise is accompanied by a conspicuous fall of temperature to a value much below the normal for June.

The lapse between 850 and 700 mb. and the θ_{sw} at 850 mb. also show a change, but these are not conspicuous enough to detect the onset of monsoon. Wind data for 850 mb. level have not been found to be useful for fixing the date of onset critically. Thus, it is seen that only the changes in humidity and temperature that take place at 850 mb. level over Nagpur are useful for fixing date of onset. The following criterion is found to be helpful in this connection.

The date on which the relative humidity at 850 mb. level rises to 60 per cent or above with the corresponding temperature being below the June normal, and both remaining so during the next two days, is taken to be the date of onset of the monsoon.

As per the above criterion, monsoon set in over Nagpur in 1957 on June 25. In 1958, the onset was on June 19. Prior to the onset, the relative humidity at 850 mb. level had gradually risen from 20 per cent on June 15 to 70 per cent on June 19. Between 18th and 19th there was a steep fall of temperature, from a value above the normal for June to a value below. In 1959, the monsoon was over Nagpur on June 29. Generally, persistent rainfall had occurred over Vidarbha only after the above-mentioned dates of onset in all the three years.

New Delhi. On a critical examination of the three years' data for New Delhi, it has been found that the criterion arrived at for Nagpur is applicable to New Delhi also.

In 1957, the monsoon set in over New Delhi on July 9. In the year 1958, it set in on June 29 and on July 1 in 1959. It may be mentioned that the persistent rainfall, characteristic of the monsoon, occurred over New Delhi and neighbourhood only three days after the dates mentioned above. This fact, if confirmed by analysis of data for longer number of years, will be of help for forecasting the monsoon rain at Delhi.

This study has shown that upper air data are quite useful in objectively fixing the date of onset of the monsoon over different stations. This would, no doubt, contribute to the introduction of uniformity in the matter of declaring the onset. It has also indicated the possibility that when the onset of monsoon is gradual, as it usually is at inland stations and even at coastal stations at times, it may be possible to foresee the onset of persistent monsoon rain at least a day or two before.

The conclusion arrived at in this study is based on the three years' data and hence can be treated as tentative. It is proposed to extend this study to include data for longer periods for the stations considered here and also to other stations.

Acknowledgement

The authors are very thankful to Shri B. Gopinatha Rao and other members of staff of the Upper Air Section, Poona, who have rendered considerable help to them in the preparation of this paper.

References

1. *Climatological Atlas for Airmen* (India Meteorological Department), 1943.
2. Bhullar, G. S., *Indian J. Met. Geophys.*, **3** (1952), 25.
3. Ramdas, L. A. *et al.*, *Indian J. Met. Geophys.*, **5** (1954), 305.
4. Rao, K. N., *Proceedings of the Symposium on Monsoons of the World*, 1958, New Delhi, 43.
5. Krishnan, A., Pant, P. S. & Ananthakrishnan, R., *Indian J. Met. Geophys.*, **12** (1961), 431.

M type thermistor as radiometer

B. PADMANABHAMURTY*
V. P. SUBRAHMANYAM

Department of Geophysics
Andhra University
Waltair

It is a well-recognized fact that almost the entire energy of the atmosphere as well as that of the upper layers of the soil is derived from incoming solar radiation. The measurement of this radiant energy with adequate accuracy has been made possible by the development of instruments based on principles of thermoelectricity which are in wide use all over the world. Thermistors have recently been found to be suitable as instruments of thermometry and anemometry[1-4].

In the present paper the use of thermistor (M 15 YHL, manufactured by Standard Telephones & Cables Ltd, England) as a radiometer has been studied. The thermistor element consists of a very small bead of the resistance material, about 0·02 in. diam. integrally deposited on two parallel platinum wires. The spacing of the wires, the chemical constitution of the bead material and the heat treatment of the bead element are the main factors that determine the cold resistance of the bead (which is 100,000 ohms at 20°C. in the present case). The bead is sealed to a flat copper disc by means of a thin layer of glass and connection to the bead is made by the platinum wire leads.

The thermistor was mounted on a circular mica sheet attached to the top of a Tufnol cylinder. The circular copper disc of the thermistor was given a uniform coat of turpentine soot and a hemispherical glass dome was provided over the tube as a protective cover. A small quantity of silica gel contained in a small receptacle screwed beneath served to absorb moisture present in the interior. The whole assembly was fixed to a rigid stand (Fig. 1).

---

*Present address: Meteorological Office, Poona 5

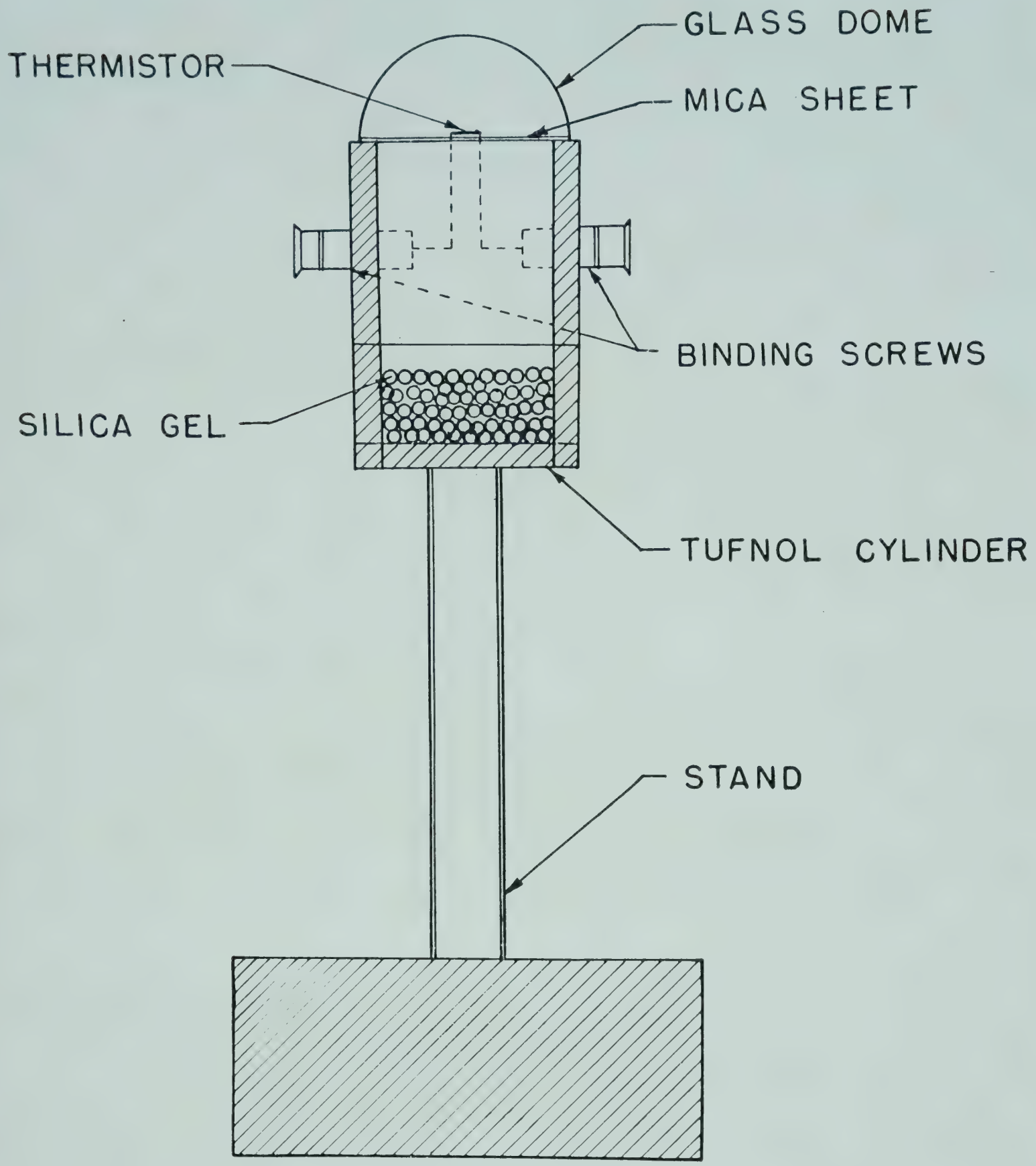

FIG. 1 — THERMISTOR RADIOMETER

The assembly was exposed to the incoming radiation from the sun and the sky beside a standard Eppley pyrheliometer. The resistances of the thermistor both when covered with an opaque box (R_0) and when fully exposed to radiation (R_1) were measured on a Wheatstone bridge. Simultaneously, the intensity of radiation was obtained by means of the Eppley pyrheliometer whose thermoelectric output was measured on a Beckman & Whitley portable millivolt indicator unit designed for climatic surveys. Plot of $(R_0-R_1)/R_0$ values against the Eppley observations yielded the standardization curve (Fig. 2) which was used for subsequent routine work.

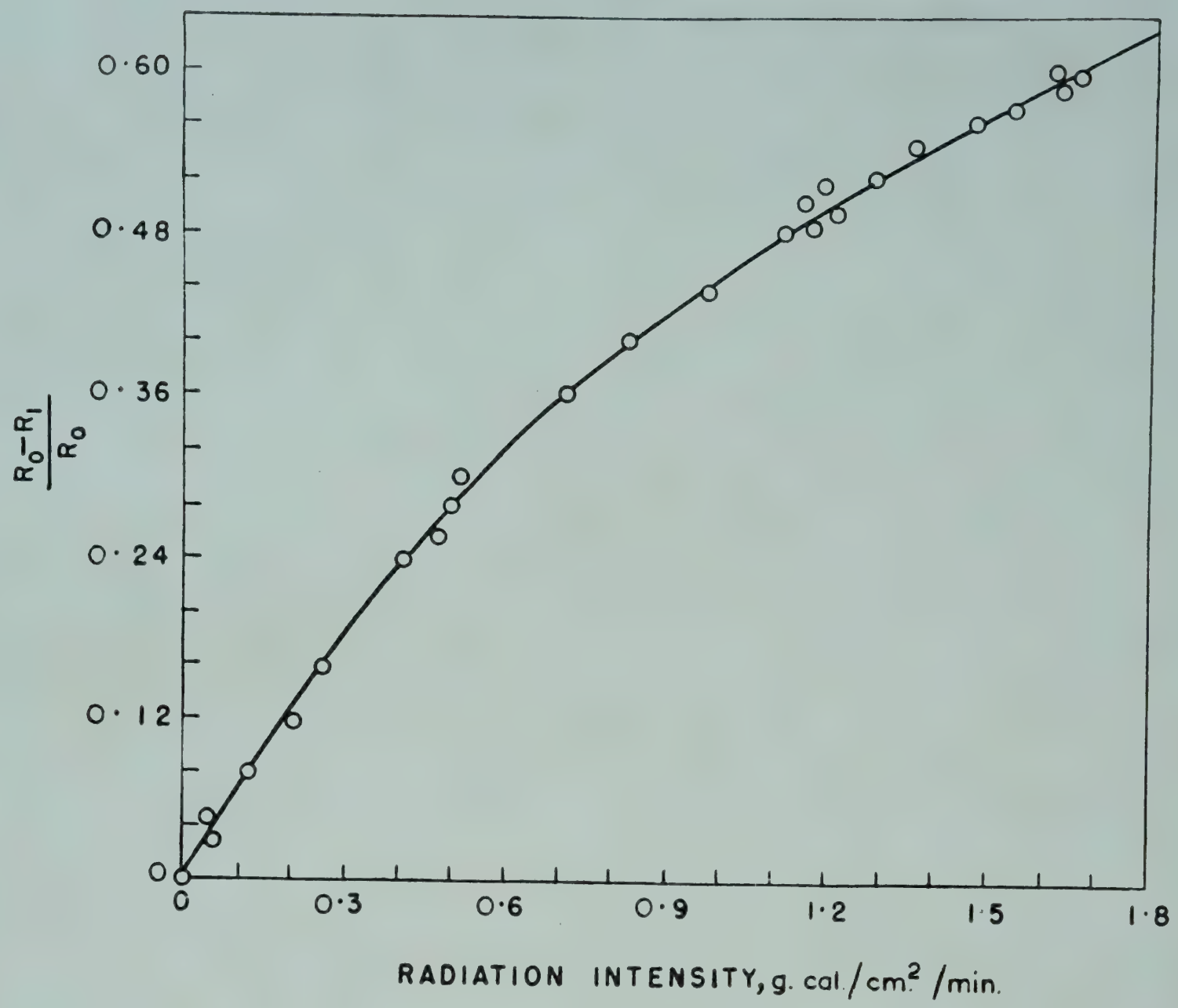

FIG. 2 — STANDARDIZATION CURVE FOR THERMISTOR RADIOMETER

Comparative observations were taken from early morning until noon-time on February 4, 1961 both with the thermistor radiometer and the standard Eppley pyrheliometer in order to study its performance. For a clear understanding of the response of the former to the direct solar and diffuse sky radiations, it was conventionally operated under shaded and unshaded conditions. Corresponding readings were simultaneously obtained with the pyrheliometer.

The data are graphically presented in Fig. 3. The remarkably close coincidence of the two sets of curves suggests that thermistors are admirably suited to radiometric work. Their simplicity of design, smallness in size and quickness of response on the one hand and reliability of performance as could be seen from Fig. 3 on the other, are all special features of this device which make it a very convenient instrument for general radiation surveys.

Work is in progress for the design of a thermistor of the same M type for measurement of long wave outgoing radiation from the ground. These two

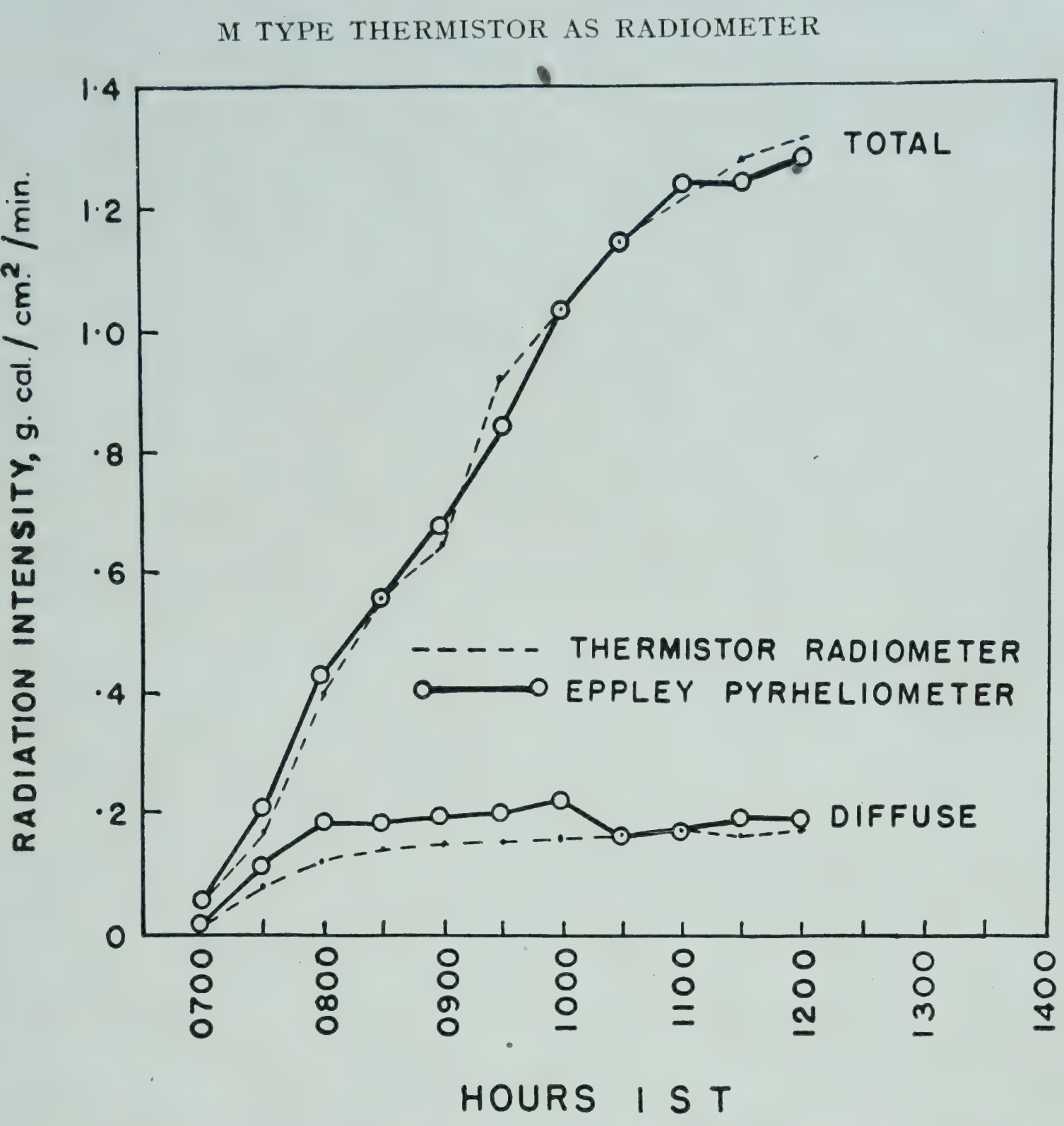

FIG. 3 — COMPARATIVE OBSERVATIONS WITH THERMISTOR RADIOMETER AND EPPLEY PYRHELIOMETER

instruments for separate measurement of the incoming and outgoing energies may constitute a very useful pair for quick investigations of radiation balance.

REFERENCES

1. HALES, WAYNE B., *Bull. Amer. met. Soc.*, **29** (1948), 495.
2. POORNACHANDRA RAO, C., *Indian J. Met. Geophys.*, **7** (1956), 321.
3. SUBRAHMANYAM, V. P., *Indian J. Met. Geophys.*, **8** (1957), 118.
4. SUBRAHMANYAM, V. P., *Indian J. Met. Geophys.*, **8** (1957), 458.

Some observations of nocturnal radiation at Poona and Delhi

ANNA MANI
OOMMEN CHACKO

Meteorological Office
Poona

Measurements of nocturnal and sky radiation have been made at Poona and Delhi during the IGY. The results confirm those obtained by earlier workers at Poona, with main reference to its seasonal variations and its dependence on the temperature and water vapour content of the lower layers of the atmosphere. The sky radiation at Delhi is greater than that at Poona as a consequence of the comparatively drier atmosphere over Poona. The values of sky radiation at Poona during 1945-58 are also much higher than those observed by Ramanathan and Desai in 1930-31 and the values calculated from Angstrom's formula.

Measurements of nocturnal atmospheric radiation using Angstrom compensation pyrgeometers were made as early as 1930 at Poona by Ramanathan and Desai[1]. They were extended by Raman[2,3] who studied its variations with time during the night and its dependence on the temperature and humidity in the lower layers of the atmosphere, and by Ramdas *et al.*[4,5] who measured the hourly variation in the nocturnal radiation coming from different altitudes of the night sky using a Moll microthermopile. The measurements were resumed by Chacko[6] in 1945 and continued in 1946 and 1949. Routine measurements of nocturnal radiation were introduced in July 1957 at Poona and Delhi, in connection with the implementation of a scheme of radiation measurements at a network of 14 stations in India. The results of measurements of nocturnal radiation during 1958 at Poona and Delhi are analysed and compared with the results obtained earlier.

Method of Measurement

The Angstrom compensation pyrgeometer consists of two black and two gilt strips. The former radiate energy to the atmosphere. The loss of

energy by the black strips is compensated by passing an electrical heating current i (measured by a precision milliammeter) through them. The equality of temperature of the black strips is indicated by thermocouples and a galvanometer fixed to their backs. If E is the outgoing radiation from the black strips at a temperature T°K. and S is the incoming long wave radiation (or the sky radiation), the difference $(E-S)$ is termed the infrared net or long wave effective outgoing radiation or nocturnal radiation (or now generally classified as outward terrestrial radiation), N. The nocturnal radiation is equal to Ci^2, where C is a constant depending upon the milliammeter. On the assumption that the emissivity of the black strips is unity, $E = \sigma T^4$, where σ is the Stefan-Boltzmann's constant and is equal to $8{\cdot}26 \times 10^{-11}$ cal./cm.^{2}/min./°K.^{4}. The sky radiation S is then given by $\sigma T^4 - Ci^2$. The technique of measurement of nocturnal radiation using this instrument has been described in detail earlier[1,2,6].

The nocturnal radiation was measured at 2030 hours IST every night whenever there was no rain with the pyrgeometer exposed horizontally on the roof of the radiation observatory buildings at Delhi and Poona where a practically free exposure to the entire sky was available.

The air temperature and relative humidity were measured with Assmann psychrometers. The constants of the pyrgeometers were determined at the Poona Central Radiation Unit with a standard instrument and checked later at the stations (Delhi and Poona) with a travelling standard.

Results

The radiation measurements were grouped into two categories — ' all nights ' and ' clear nights '. Nights with high cloud, or medium or low cloud near the horizon less than 1 octa, have been taken as clear nights. The observations on measurements of monthly and seasonal variation of sky radiation and nocturnal radiation are summarized below.

Delhi. The mean monthly values of sky radiation, long wave effective outgoing radiation, vapour pressure and air temperature for (i) all nights and (ii) clear nights at Delhi during 1958 are plotted in Figs. 1a and 1b respectively. No observations were available for December.

From Fig. 1a it can be seen that the sky radiation is a maximum in the months of June and July (mean value, 0·646 cal./cm.^{2}/min.) and continues to be near this till September (monsoon months). It is minimum in November (mean value, 0·450 cal./cm.^{2}/min.).

On clear nights the highest mean value (0·655 cal./cm.^{2}/min.) is reached in July and is lowest in November (Fig. 1b). The highest maximum recorded during the year is 0·701 cal./cm.^{2}/min. in June and the lowest minimum is

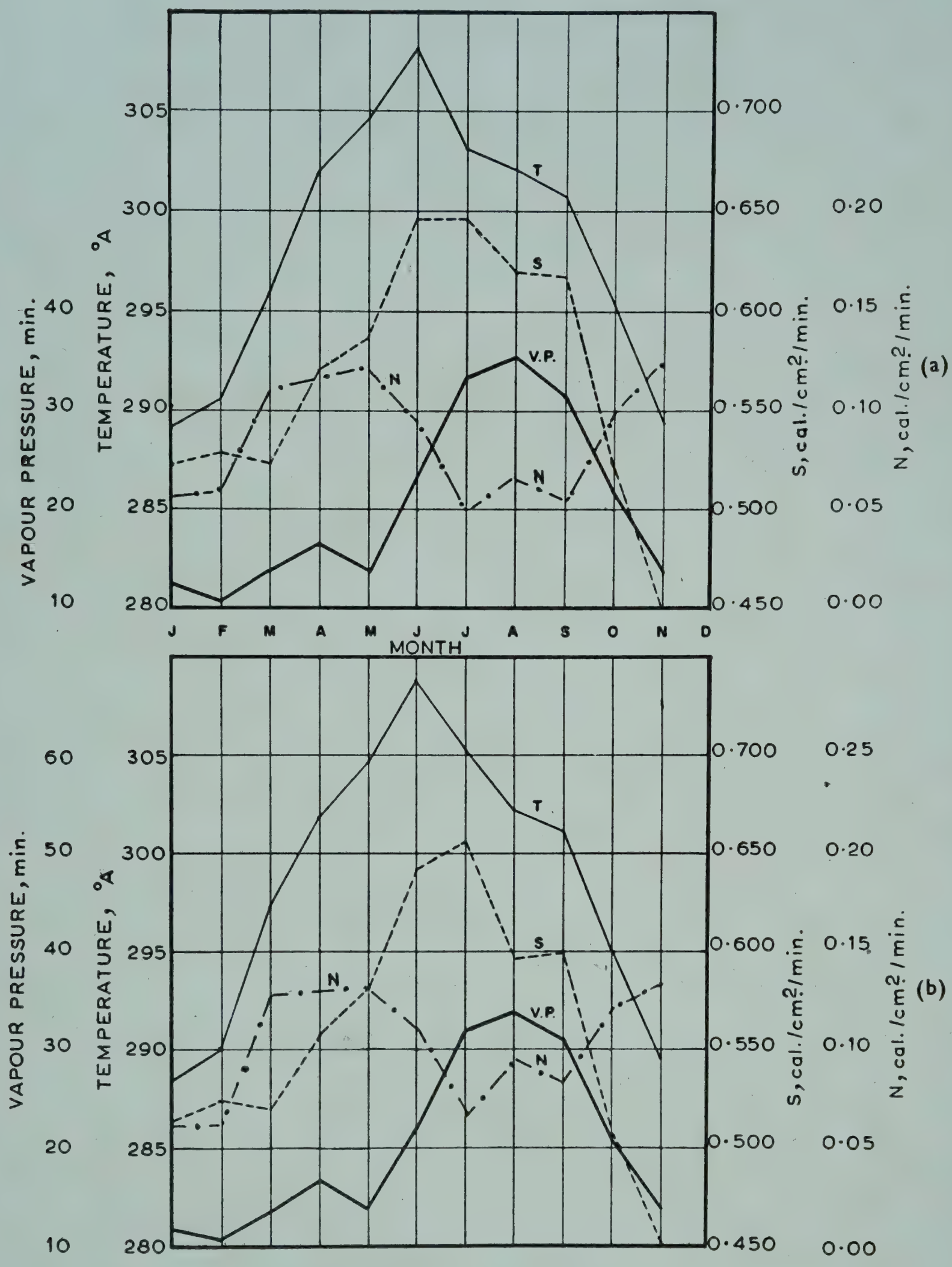

FIG. 1 — MARCH OF TEMPERATURE (*T*), VAPOUR PRESSURE (*V.P.*), SKY RADIATION (*S*) AND NOCTURNAL RADIATION (*N*) AT DELHI DURING 1958: (a) ALL NIGHTS, AND (b) CLEAR NIGHTS

0·385 cal./cm.²/min. in November. The mean value for the year is 0·567 cal./cm.²/min. in June and the lowest minimum is 0·385 cal./cm.²/min. in November. The mean value for the year is 0·567 cal./cm.²/min.; the mean

value for the monsoon is 0·657 cal./cm.^{2}/min. and for October–March it is 0·509 cal./cm.^{2}/min.

During June–September the sky radiation on all clear days reaches a value which is about 88 per cent of the black body radiation at the surface temperature. The mean of the ratio of the sky radiation to the black body radiation is 0·85, the range being 0·78–0·91. The nocturnal radiation curve is nearly the mirror image of the sky radiation curve, having a minimum in July–September and a maximum in winter. The temperature and vapour pressure curves show trends similar to the sky radiation curve, which is a function of the temperature and water vapour content of the lower levels of the atmosphere. In the hot summer months, the sky radiation shows an increase, while the water vapour content shows a fall.

Poona. Figs. 2a and 2b show the plot of the mean monthly values of sky radiation, long wave radiation, vapour pressure and air temperature for (i) all nights, and (ii) clear nights respectively during different months in 1958. No observations with clear skies were possible in July and August.

From Fig. 2a it can be seen that the sky radiation shows a steady increase from January (minimum mean value 0·488 cal./cm.^{2}/min.) to May, slight fall in June, rapid increase till July and August when the maximum value of 0·584 cal./cm.^{2}/min. is reached and a steady fall after that. It is maximum during the monsoon months July–September with a mean value of 0·576 cal./cm.^{2}/min. and minimum during the winter months December–February (mean, 0·498 cal./cm.^{2}/min.). The highest maximum recorded is 0·594 cal./cm.^{2}/min. in May and the lowest minimum 0·389 cal./cm.^{2}/min. in February.

The vapour pressure and sky radiation curves show the same general trend except for the fall in vapour pressure in February. The nocturnal radiation curve as at Delhi is a mirror image of the sky radiation curve.

The curves in Fig. 2b for clear nights show closer agreement between water vapour content and sky radiation.

During June–October, sky radiation on all clear days reaches a value which is about 81 per cent of the black body radiation at the surface temperature. The mean value for the ratio of the sky radiation to black body radiation is 0·78 and the range 0·76–0·85.

In Fig. 3 are reproduced the values of sky radiation obtained in 1958 with those obtained in 1930–31 by Ramanathan and Desai and the mean values obtained by Chacko in 1945, 1946 and 1949. The similarities are well marked, the maximum occurs in July–August and minimum in December–January. The mean values of sky radiation are roughly the same during

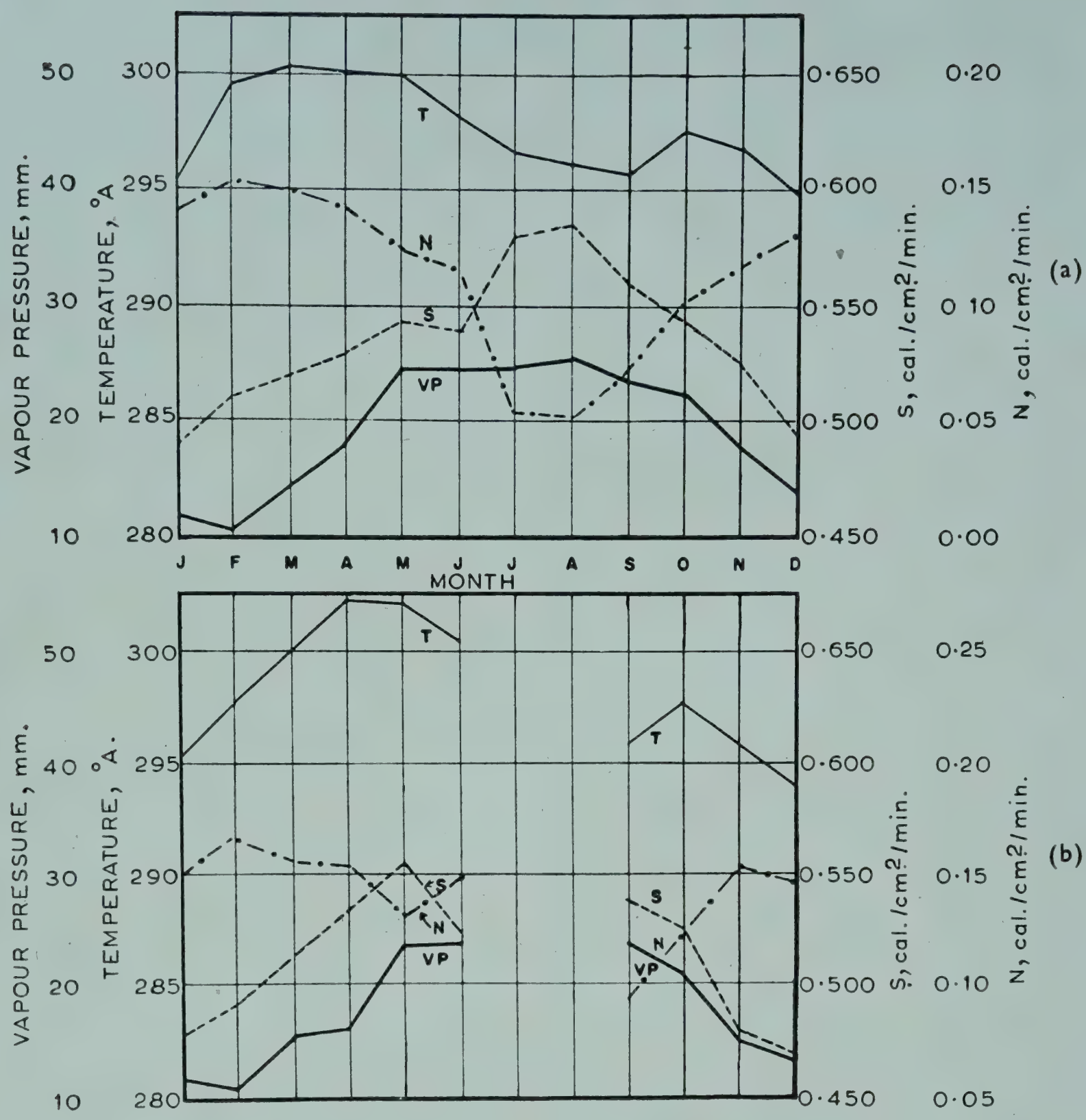

FIG. 2 — MARCH OF TEMPERATURE (*T*), VAPOUR PRESSURE (*V.P.*), SKY RADIATION (*S*) AND NOCTURNAL RADIATION (*N*) AT POONA DURING 1958: (a) ALL NIGHTS, AND (b) CLEAR NIGHTS

1945–49 and 1958, and are, however, markedly higher than those obtained during 1930–31 by Ramanathan and Desai.

DISCUSSION

The sky radiation for all nights has the highest value in the monsoon months. This can be explained as due to clouds which radiate like a black body. On cloudy nights the sky radiation depends mainly on the amount and type of the cloud. That the sky radiation for clear nights reaches maximum in July is due to the increased water vapour content in the atmosphere. The fall in the sky radiation in August at Delhi when water pressure registers

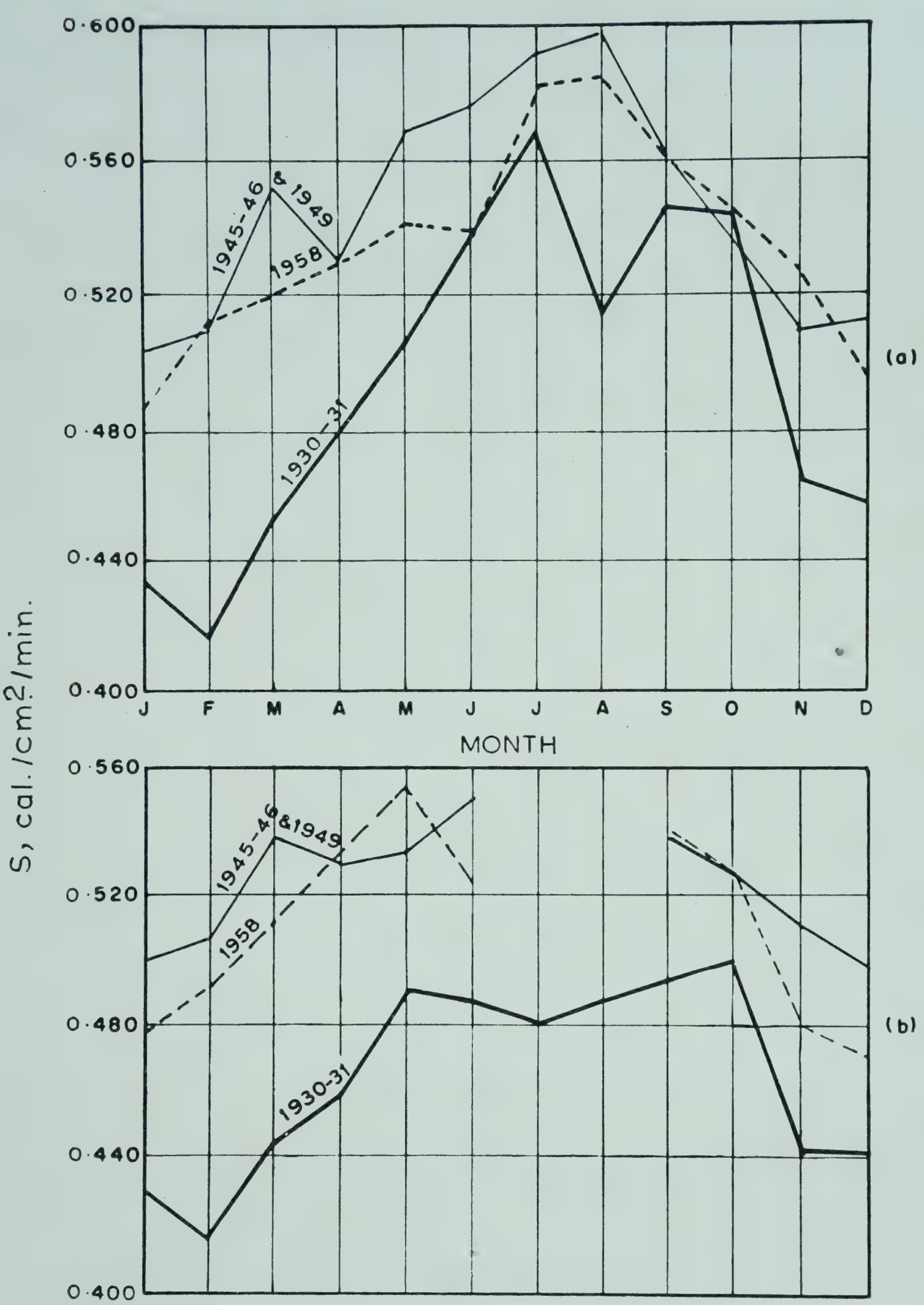

FIG. 3 — MARCH OF SKY RADIATION AT POONA DURING (i) 1930–31, (ii) 1945–46 AND 1949, AND (iii) 1958: (a) ALL NIGHTS, AND (b) CLEAR NIGHTS

a maximum should be ascribed to a fall in air temperature and to a very few observations in that month.

The close agreement between water vapour content and sky radiation (Fig. 2b) can be explained as due to the elimination of the effect of clouds on the sky radiation. The number of observations on clear nights during the monsoon months at both Poona and Delhi are, however, very few, being only 3 at Poona and 15 at Delhi. The results cannot therefore be considered to be conclusive. The mean value for the ratio of the sky radiation to the black body radiation at Poona is higher (0·78) than the value expected (0·75) on the basis that water vapour is the sole radiating constituent.

Comparison of Monthly Mean Values of Sky Radiation at Delhi and Poona. A comparative study of Figs. 1 and 2 shows that, taking the year as a whole, more radiation is received from the sky at Delhi than at Poona, the mean annual values being 0·567 cal./cm.^{2}/min. and 0·535 cal./cm.^{2}/min. for Delhi and Poona respectively for all nights and 0·558 and 0·510 cal./cm.^{2}/min. for clear nights. This is probably a consequence of the comparative dryness of the atmosphere over Poona. More sky radiation is received at Poona, however, during October and November than at Delhi, even on only clear nights, presumably as a result of the slightly higher vapour content at Poona and the slightly lower air temperatures at Delhi.

The nocturnal radiation taking the year as a whole is greater at Poona than at Delhi, the values being 0·113 cal./cm.^{2}/min. at Poona and 0·089 cal./cm.^{2}/min. at Delhi. On clear nights alone, the corresponding values are 0·143 and 0·100 cal./cm.^{2}/min. respectively. The Poona value is as much as three times that at Delhi in January and February and less than that at Delhi only during November and August.

The annual variation of the mean sky radiation at Delhi is roughly twice that at Poona and this is to be expected from the nature of the air supply over the two stations. Even during the monsoon, the air is drier at Poona than at Delhi, due to its location on the leeside of the Western Ghats; the annual variation in temperature is also lesser at Poona than at Delhi.

Dependence of Sky Radiation on Temperature and Vapour Pressure. Angstrom[8] has expressed the dependence of S on water vapour pressure p at the surface and air temperature T near the instrument as

$$S = E(0{\cdot}75 - 0{\cdot}32 \times 10^{-0{\cdot}069p})$$

According to this semi-empirical relationship, the value of the sky radiation from a clear sky will be between 75 and 43 per cent of that of a black body at the temperature of the atmosphere at the earth's surface. By a comparison of the monthly means of the observed radiation on clear nights with the values calculated according to Angstrom's formula, it will be seen that

TABLE 1 — MONTHLY MEAN VALUES OF OBSERVED AND COMPUTED VALUES OF SKY RADIATION FOR CLEAR NIGHTS AT DELHI AND POONA

(Values in cal./cm.²/min.)

Month	Delhi		Poona	
	Observed	Computed	Observed	Computed
Jan.	0·511	0·405	0·477	0·440
Feb.	0·524	0·408	0·491	0·451
Mar.	0·517	0·464	0·513	0·489
Apr.	0·557	0·503	0·535	0·507
May	0·581	0·513	0·555	0·521
June	0·642	0·565	0·524	0·509
July	0·655	0·549	—	—
Aug.	0·595	0·526	—	—
Sept.	0·599	0·519	0·540	0·478
Oct.	0·505	0·468	0·527	0·487
Nov.	0·450	0·417	0·480	0·462
Dec.	—	—	0·472	0·447

the observed values are always higher than the calculated values, and the difference is more for Delhi than for Poona (Table 1). This is in disagreement with the observations of Ramanathan and Desai[1] who found good agreement between the calculated and observed average monthly values in the drier part of the year and the calculated values to be higher than the observed values only during the wet months. They ascribed it either to the cloud haze often present in the atmosphere or to the imperfect applicability of the formula when the vapour pressures are high. A study of sky radiation data for longer periods and for more stations is considered necessary before any definite conclusions can be drawn on the extent of applicability of the formula.

References

1. Ramanathan, K. R. & Desai, B. N., *Beitr. Geophys.*, **35** (1932), 68.
2. Raman, P. K., *Proc. Indian Acad. Sci.*, **1A** (1935), 815.
3. Raman, P. K., *Proc. Indian Acad. Sci.*, **4A** (1936), 243.
4. Ramdas, L. A., Sreenivasaiah, B. N. & Raman, P. K., *Proc. Indian Acad. Sci.*, **5A** (1937), 45.
5. Ramdas, L. A., Sreenivasaiah, B. N. & Raman, P. K., *Proc. Indian Acad. Sci.*, **9A** (1939), 386.
6. Chacko, O., *Indian J. Met. Geophys.*, **2** (1951), 190.
7. Ramanathan, K. R. & Ramdas, L. A., *Proc. Indian Acad. Sci.*, **1A** (1935), 822.
8. Angstrom, A., *Beitr. Phys. frei. Atmos.*, **14** (1928), 8.

Measurements of diffuse solar (sky) radiation at Delhi and Poona

ANNA MANI
OOMMEN CHACKO

Meteorological Office
Poona

The results of measurements of diffuse radiation received on a horizontal surface at Delhi and Poona during 1959 have been summarized. The results bring out clearly the importance of the diffuse sky radiation in the total radiation budget, the seasonal and diurnal variations of diffuse radiation and the proportion of diffuse to total solar radiation at two representative stations in India. As expected, the diffuse radiation on all days is directly related to the amount of cloudiness and is maximum during the monsoon season. On clear days it is maximum in summer and minimum in winter.

Diffuse solar (sky) radiation is the short wave energy component of solar origin, scattered and diffused downwards by gas molecules, water vapour, dust particles and clouds in the atmosphere. With cloud-free skies, it depends mainly on the solar elevation, the latitude and altitude of the observing station, the degree of atmospheric turbidity and the amount of water vapour. With cloudy skies, the diffuse component varies markedly from day to day and hour to hour at the same place, the variability in the amount and type of cloud being the predominant cause.

A knowledge of all the radiation components is essential for a proper understanding of the radiation climatology of a region. In addition, measurements of diffuse radiation are of value in the estimation of the other radiation components and of daylight illumination, where such measurements are non-existent. They are also of importance to illumination engineers and architects, in interior illumination studies and building research particularly in the tropics, and in problems of utilization of solar energy.

MEASUREMENTS OF DIFFUSE SOLAR RADIATION AT DELHI AND POONA

While measurements of total incoming solar radiation over the earth's surface have been made at a large number of stations, observations of sky radiation have not been so extensive. Routine measurements of diffuse radiation have been made for many years at a number of stations in South Africa[1] and the Belgian Congo[2], and at the Blue Hill[3] and Kew[4] Observatories. Observations of sky radiation in India have not been made till the IGY. The results of the measurements of diffuse radiation at Poona and Delhi during the years 1958 and 1959 have been summarized in this paper.

Method of Measurement

The equipment used for the continuous registration of diffuse (sky) radiation is the same as that used[5] for recording the total incoming solar radiation on a horizontal surface, viz. a Moll Gorczynski solarimeter and Cambridge thread recorder with the addition of a shading ring to shade the thermopile element and the two hemispherical glass domes from direct sunshine. The shading ring is so mounted that its plane is in the plane of the apparent path of the sun's diurnal march across the sky and it shades the thermopile with its domes at all times and permits the solarimeter to measure only the scattered radiation received from the sky. The ring can be moved up or down on its two parallel supporting rods, without changing the position of its plane in space and allows for seasonal changes in the declination of the sun. The solarimeter is mounted at the centre of the shading ring so that its average distance from the ring remains constant throughout the year.

The exposure was the same as that for the total solarimeters — an unobstructed horizon over an azimuth range of 360°. The two instruments were installed about 1 m. apart, the diffuse solarimeter being mounted poleward of the total instrument, so that mutual interference was a minimum and not more than 1 per cent of the diffuse radiation as the total instrument is intercepted by the shading ring of the diffuse instrument.

The shading ring installed at Poona was built on the Schuepp[2] model and had a width of 5·1 cm. and a radius of 44·5 cm. The shading ring used at Delhi had a width of 5·1 cm. and a much smaller radius of 20·3 cm.

Shading Ring Correction. Corrections to compensate for the sky energy intercepted by the ring simultaneously with the eclipsing of the sun's disc were computed on the basis of the formula derived by Drummond[1].

$$\frac{X}{T} = \frac{2b}{\pi r} \cos^3 \delta \, (\sin \phi \sin \delta t_0 + \cos \phi \cos \delta \sin t_0)$$

where t_0 = hour angle of the sun at sunset
ϕ = latitude of the recorder

δ = sun's declination
b = width of the shading ring
r = radius of the shading ring
T = energy intensity on a horizontal plane receiver from the whole sky
X = energy intensity on a horizontal plane receiver for the part of the ring above the horizon.

The correction factor is $1/(1-X/T)$ for a sky of uniform brightness and b is small compared with r. Figs. 1 and 2 give the variations throughout the year of the computed shading ring correction factor for isotropic conditions for Poona and Delhi respectively. It can be seen that corrections vary from 4 to 8 per cent for Poona and from 7 to 18 per cent for Delhi, the correction factor being least in January and highest in April and September with a secondary minimum in July.

The correction factor to compensate for the diffuse energy intercepted by the shading ring is, as stated above, based on the assumption that the diffuse radiation from the sky is uniform and the receiver is an ideal one. Corrections for the non-uniform nature of the sky radiation which includes the marked variations in the intensity of the circumsolar radiation have, however, to be made. Drummond[1] found that theoretically derived corrections for his standard ring (width, 5·1 cm. and diam., 30·5 cm.), expressed as a percentage of the measured diffuse radiation, required the addition of 7 per cent for completely cloudless skies and 3 per cent for completely cloudy skies. Schuepp[2] found an addition of 3–5 per cent necessary for clear skies and no addition for cloudy and overcast skies. The exact corrections to be applied for Indian conditions are under investigation.

Standardization of the Equipment. The solarimeters and recorders were standardized, initially at the Central Radiation Unit at Poona before installation and later at the stations during annual inspection, (i) by direct standardization against a working standard Angstrom pyrheliometer and (ii) by comparison over a suitable period with a standardized solarimeter under natural conditions of exposure, as in the case of the total radiation instruments.

Results and Discussion

Total and Diffuse Radiation. Figs. 3 and 4 show the monthly means of the total (T) and diffuse (D) daily radiation for the year 1959 at Delhi and Poona respectively. The values of the ratio D/T and the hours of bright sunshine (SS) and cloudiness (C) are also plotted. While data for all the twelve months are available for both IGY and IGC for Delhi, only the data from October 1958 to December 1959 are available for Poona. Only the

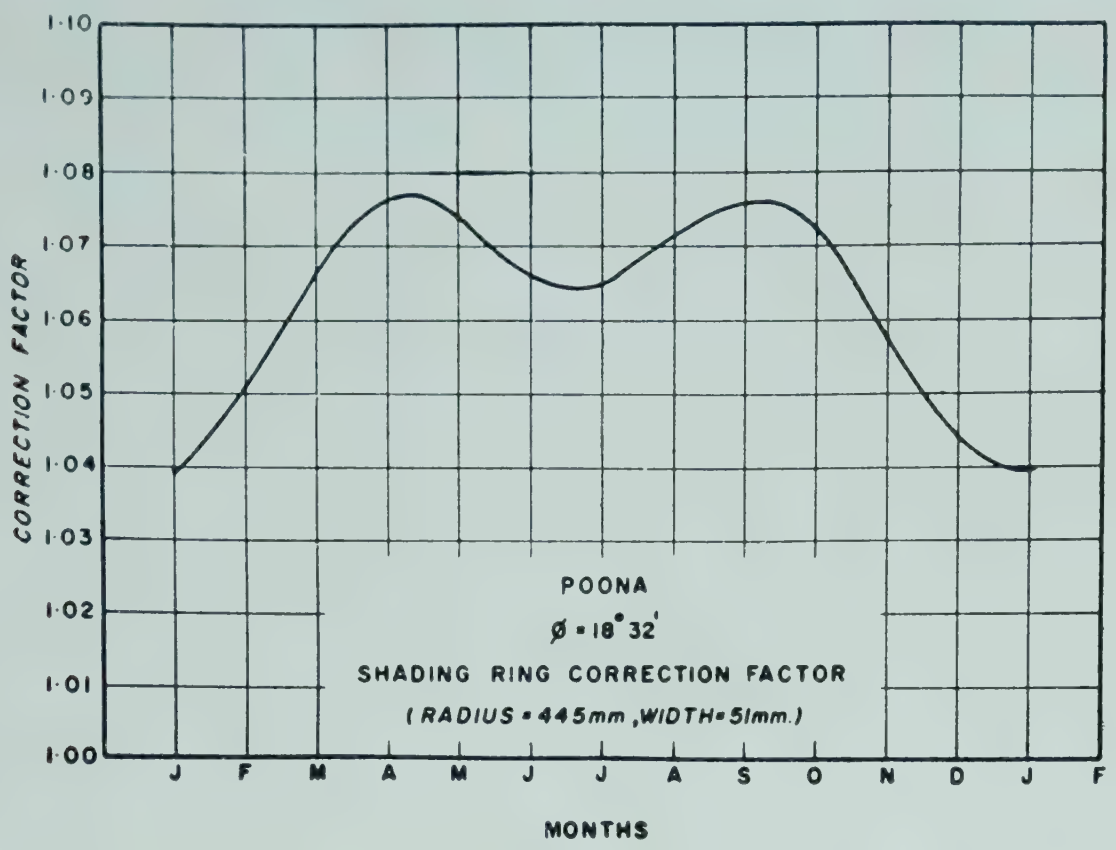

FIG. 1 — SHADING RING CORRECTION FACTOR FOR DIFFERENT MONTHS AT POONA

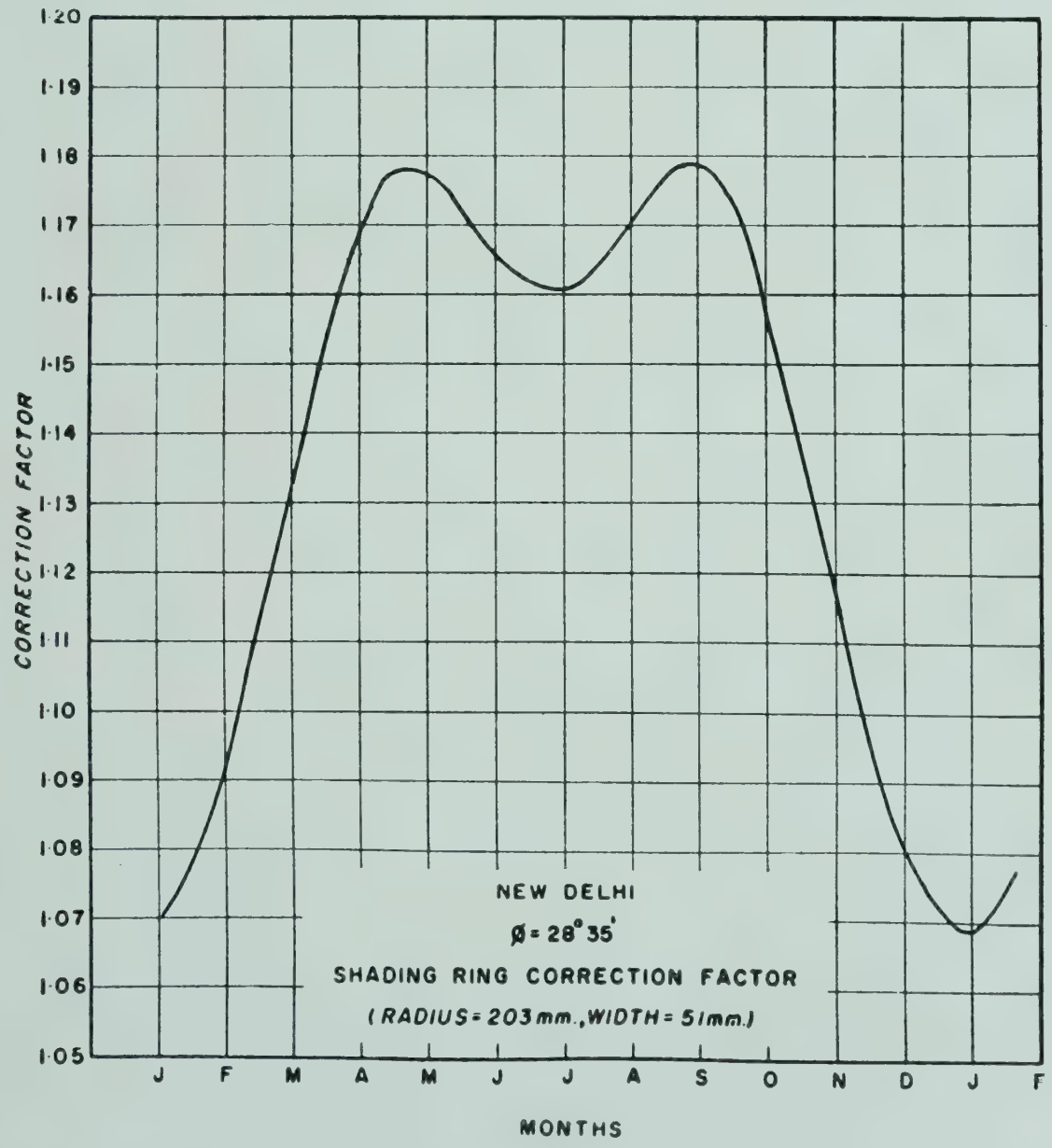

FIG. 2 — SHADING RING CORRECTION FACTOR FOR DIFFERENT MONTHS AT DELHI

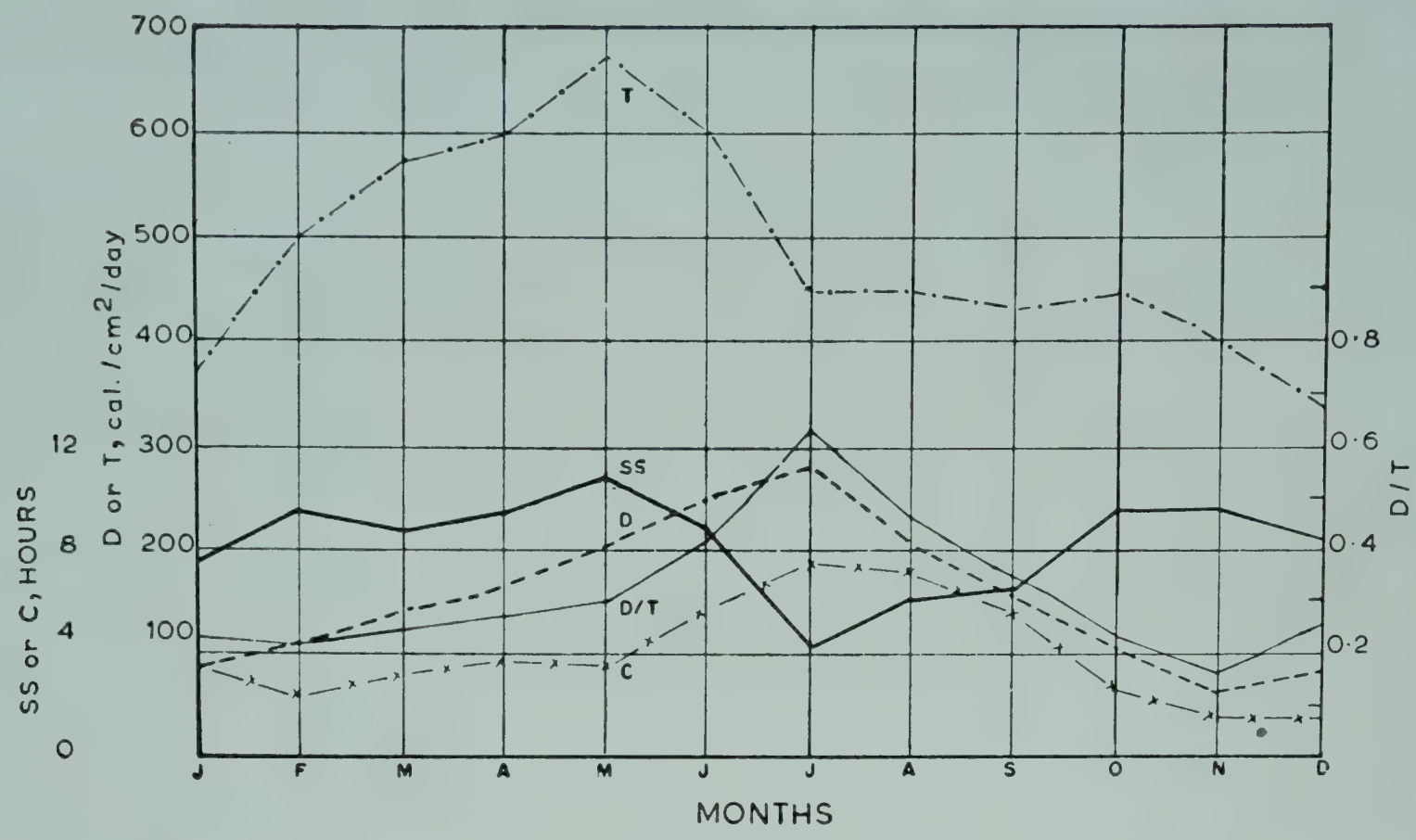

FIG. 3 — MARCH OF TOTAL SOLAR RADIATION (T), DIFFUSE SKY RADIATION (D), HOURS OF BRIGHT SUNSHINE (SS), MEAN HOURS OF CLOUDINESS (C) AND RATIO D/T AT DELHI ON ALL DAYS DURING 1959

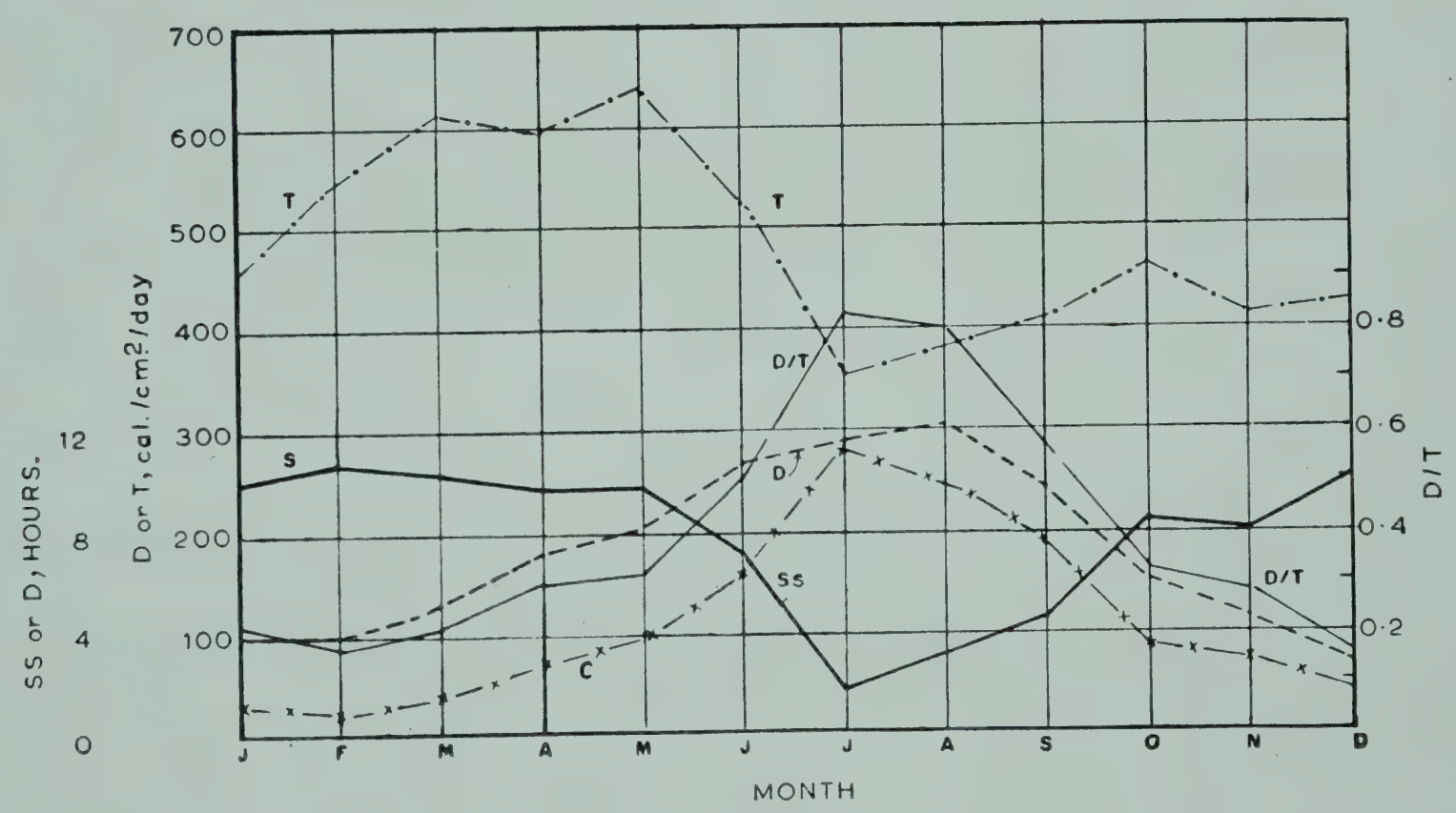

FIG. 4 — MARCH OF TOTAL SOLAR RADIATION (T), DIFFUSE SKY RADIATION (D), HOURS OF BRIGHT SUNSHINE (SS), MEAN HOURS OF CLOUDINESS (C) AND RATIO D/T AT POONA ON ALL DAYS DURING 1959

data for 1959 which are available for both Delhi and Poona have been discussed.

Diffuse radiation at Delhi constituted 33 per cent of the total solar and sky radiation received during 1958 and 1959. The ratio D/T for Poona during

1959 was 37 per cent. The daily totals of diffuse radiation averaged 152 cal./cm.^{2} for Delhi and 179 cal./cm.^{2} for Poona for the year 1959. Over the year as a whole, 58 k.cal./cm.^{2} were received indirectly at Delhi and 66 k.cal./cm.^{2} at Poona. These values compare well with corresponding values at Kew (49), Brussels (47), Berlin (43), Tananarive (70) and South Africa (45–50)[1].

The mean daily diffuse radiation attains its maximum value at Poona in August (303 cal./cm.^{2}) and at Delhi in July (282 cal./cm.^{2}), the highest diffuse radiation recorded on any day being 356 cal./cm.^{2} for Delhi in July and 378 cal./cm.^{2} for Poona in November. The mean total radiation, on the other hand, reaches the maximum in May at both Poona (637 cal./cm.^{2}) and Delhi (668 cal./cm.^{2}). The mean duration of bright sunshine is, however, least during July at both Poona (1·8 hr) and Delhi (4·2 hr). There were no clear days in July at both Poona and Delhi and the high values of D in July are the direct result of monsoon clouding.

The mean daily diffuse radiation reaches its minimum value in November at Delhi (61 cal./cm.^{2}) and in December at Poona (70 cal./cm.^{2}), the lowest diffuse radiation recorded on any day being 49 cal./cm.^{2} in December at Poona and 45 cal./cm.^{2} in November at Delhi. These are also the months when the duration of bright sunshine is a maximum (9·5 hr at Delhi and 10·2 hr at Poona) and cloudiness is minimum.

On the whole, diffuse radiation is maximum during the summer and monsoon months, May–September, as a result of the increased turbidity in summer and clouding during the monsoon months and minimum during the clear winter months, November–February. The values of the total solar radiation are, on the other hand, highest during the summer months, March–June, and least during the monsoon and winter months. The mean daily diffuse radiation is less than 100 cal./cm.^{2} during winter and about 250-300 cal./cm.^{2} during the monsoon.

The mean values of D for the three main seasons of the year, October–January, February–May and June–September, are tabulated with the percentage of annual diffuse radiation received in each of the seasons at both Poona and Delhi (Table 1). It can be seen from the table that Poona received more diffuse radiation throughout the year than Delhi except during February and March, the two clearest months at Poona, when it is slightly less. This is obviously due to (i) greater clouding at Poona during the monsoon months, June–September, when the proportions of diffuse to total radiation are 68 and 46 per cent respectively for Poona and Delhi, and (ii) higher values of T at Poona during the remaining winter and summer months, October–April, when D/T is the same (*c.* 25 per cent) for both stations. The rates of increase and decrease in the diffuse radiation values during the year are naturally higher at Poona than at Delhi.

TABLE 1 — MEAN DAILY DIFFUSE RADIATION (*D*) AND PERCENTAGE OF ANNUAL DIFFUSE RADIATION (*DP*) FOR THREE MAIN SEASONS AT DELHI AND POONA

(*Values in cal./cm.*^{2})

Station	Oct.–Jan.		Feb.–May		June–Sept.	
	D	*DP*	*D*	*DP*	*D*	*DP*
Delhi	82	18	153	34	222	48
Poona	109	21	151	28	275	51

TABLE 2 — MAXIMUM AND MINIMUM VALUES OF *T* AND *D* AND MONTHS IN WHICH THESE VALUES ARE ATTAINED DURING 1959 AT DELHI AND POONA

(*Values in cal./cm.*^{2}*/day*)

	$T_{max.}$		$T_{min.}$		$D_{max.}$		$D_{min.}$	
	Value	Month	Value	Month	Value	Month	Value	Month
DELHI								
All days	668	May	336	Dec.	282	July	61	Nov.
Clear days	695	May	363	Dec.	210	June	56	Nov.
Cloudy days	643	May	317	Dec.	282	July	67	Nov.
POONA								
All days	637	May	354	July	303	Aug.	70	Dec.
Clear days	671	Apr.	432	Dec.	210	June	57	Dec.
Cloudy days	630	May	354	July	303	Aug.	81	Dec.

It is interesting to note that 50 per cent of the diffuse radiation received during the year is received during the monsoon months and about one-third during summer. The percentage of annual radiation received at both stations during the different seasons is roughly the same, the percentage being slightly higher during winter and monsoon at Poona and in summer at Delhi.

There were 95 clear and 152 cloudy days at Delhi and 96 clear and 234 cloudy days at Poona during 1959. The maxima and minima for *T* and *D*, for all categories of days — all days, clear days and cloudy days — occur generally in the same months at both stations. The maximum and minimum values for *T* and *D* at Delhi and Poona during 1959 and the months in which these values are attained are given in Table 2.

The clearest atmospheric conditions, therefore, occur during the winter months (November–January at Delhi and October–January at Poona) when diffuse radiation is a minimum and the most turbid in the hot summer

months May and June when diffuse radiation is a maximum. The diffuse radiation received at Poona and Delhi throughout the year on clear days is roughly the same.

The upper limiting daily value of cloudless sky radiation T is about 747 cal./cm.^{2} in May, of which the D component accounts for 13 per cent at Delhi. The corresponding values for Poona are 722 cal./cm.^{2} in May and 16 per cent respectively. The lowest value of T is 145 cal./cm.^{2} in September at Poona in which a flux of about 94 per cent is contributed from the sky. The corresponding value for Delhi is 87 in January. No record of D was, however, available for the day.

Considering the daily totals of T for all days, the highest and lowest daily means occur during the same months as for cloudless sky conditions, the values being naturally higher for the latter. Table 3 gives the highest and lowest daily sums of T and D during 1959 at Delhi and Poona.

There is a remarkable constancy in the daily total radiation fluxes during November and December at Delhi and during February at Poona, the difference between the highest value and the average of all days being only 40–50 cal./cm.^{2} or 8 per cent of the total. Although the lowest value of mean T is recorded in December at Delhi and July at Poona, the greatest variability is exhibited in January at Delhi and in September at Poona.

Similarly the month of most constant daily diffuse flux is July at Delhi and August at Poona, the ratio between the highest and lowest values being only 1·7 and 1·9 respectively. The greatest variability in D is shown during August at Delhi and November at Poona.

Ratio of Diffuse to Total Radiation. The annual march of the ratio of diffuse to total radiation (D/T) month by month is illustrated in Figs. 3 and 4 for all days of the year and in Figs. 5 and 6 for clear days.

It will be seen that the maximum value of D/T occurs in July at both Poona (83 per cent) and Delhi (63 per cent) and the minimum (16 per cent) in December at Poona and in November at Delhi. For the whole year, the trend is similar to that of D, being highest during the monsoon months and least during the winter months. The average value during June–September is 68 per cent at Poona and 46 per cent at Delhi and only about 25 per cent during the remaining eight months. It is generally higher at Poona than at Delhi throughout the year, except during December–March.

On clear days the trend is markedly different, with a maximum of 32 per cent in June for both Poona and Delhi and a minimum of 12 per cent in August for both Delhi and October for Poona (Figs. 5 and 6). The mean value for the whole year is only 19 per cent at both stations. The annual variation at Delhi and Poona is similar with a maximum in the turbid

TABLE 3 — HIGHEST AND LOWEST DAILY SUMS OF *T* AND *D* AT DELHI AND POONA DURING 1959

(*Values in cal./cm.*^{2})

DELHI

		Jan.	Feb.	Mar.	Apr.	May	June	July	Aug.	Sept.	Oct.	Nov.	Dec.	Year
T	Highest	464	558	634	681	747	693	570	623	597	500	432	377	747
	Lowest	87	389	418	190	608	300	238	198	249	246	303	265	87
Ratio	Highest / Lowest	5·3	1·4	1·5	3·6	1·2	2·3	2·4	3·1	2·4	2·0	1·4	1·4	8·6
D	Highest	138	245	201	294	342	339	356	293	262	184	143	139	356
	Lowest	54	69	87	95	100	122	211	73	95	69	45	49	45
Ratio	Highest / Lowest	2·5	3·6	3·5	3·1	3·4	2·8	1·7	4·0	2·8	2·7	3·2	2·8	7·9

POONA

T	Highest	551	600	669	699	722	679	539	590	609	575	502	447	722
	Lowest	303	504	469	277	344	191	160	196	145	217	190	350	145
Ratio	Highest / Lowest	1·8	1·2	1·4	2·5	2·1	3·6	3·3	3·0	4·2	2·6	2·6	1·3	5·0
D	Highest	199	137	187	324	334	371	373	367	350	320	378	125	178
	Lowest	51	68	90	114	114	163	155	194	131	60	54	49	49
Ratio	Highest / Lowest	3·9	2·0	2·0	2·8	2·9	2·3	2·4	1·9	2·7	5·3	7·0	2·5	7·7

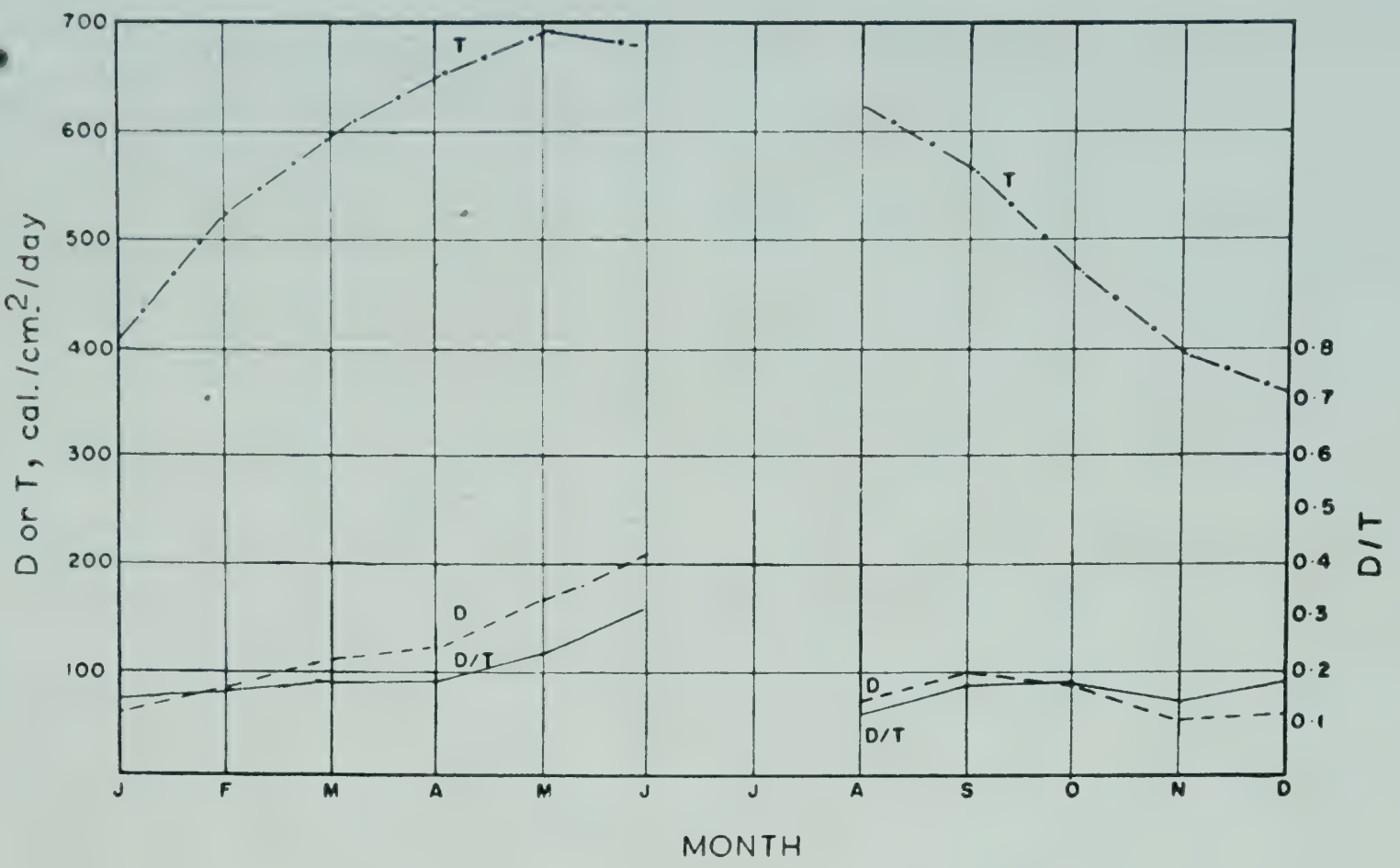

FIG. 5 — MARCH OF TOTAL SOLAR RADIATION (T), DIFFUSE SKY RADIATION (D) AND RATIO D/T AT DELHI ON CLEAR DAYS DURING 1959

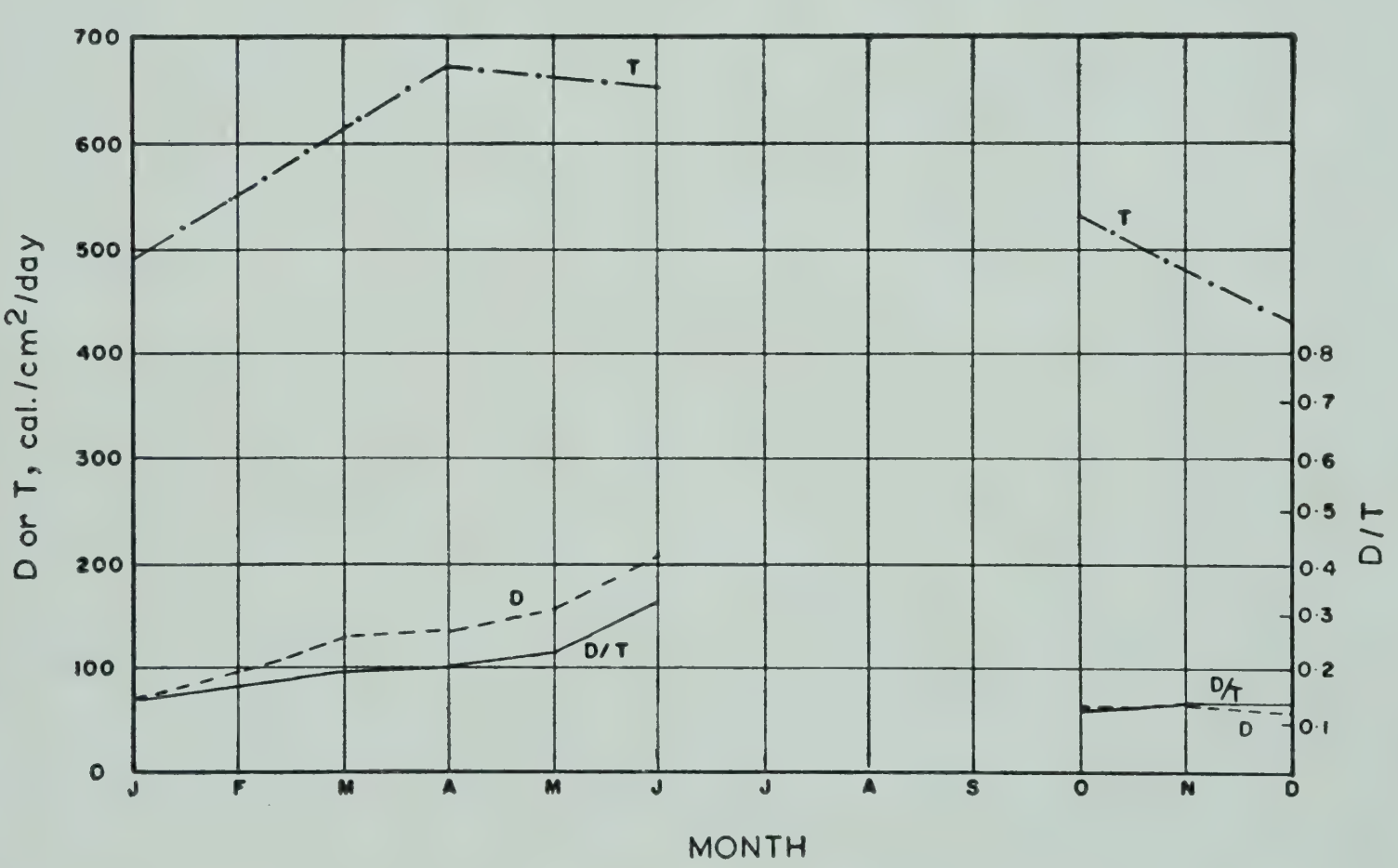

FIG. 6 — MARCH OF TOTAL SOLAR RADIATION (T), DIFFUSE SKY RADIATION (D) AND RATIO D/T AT POONA ON CLEAR DAYS DURING 1959

summer months and a minimum in the clear winter months. The ratio D/T is slightly higher at Delhi than at Poona during the winter months, indicating the atmosphere over Delhi to be less transparent, since on clear days

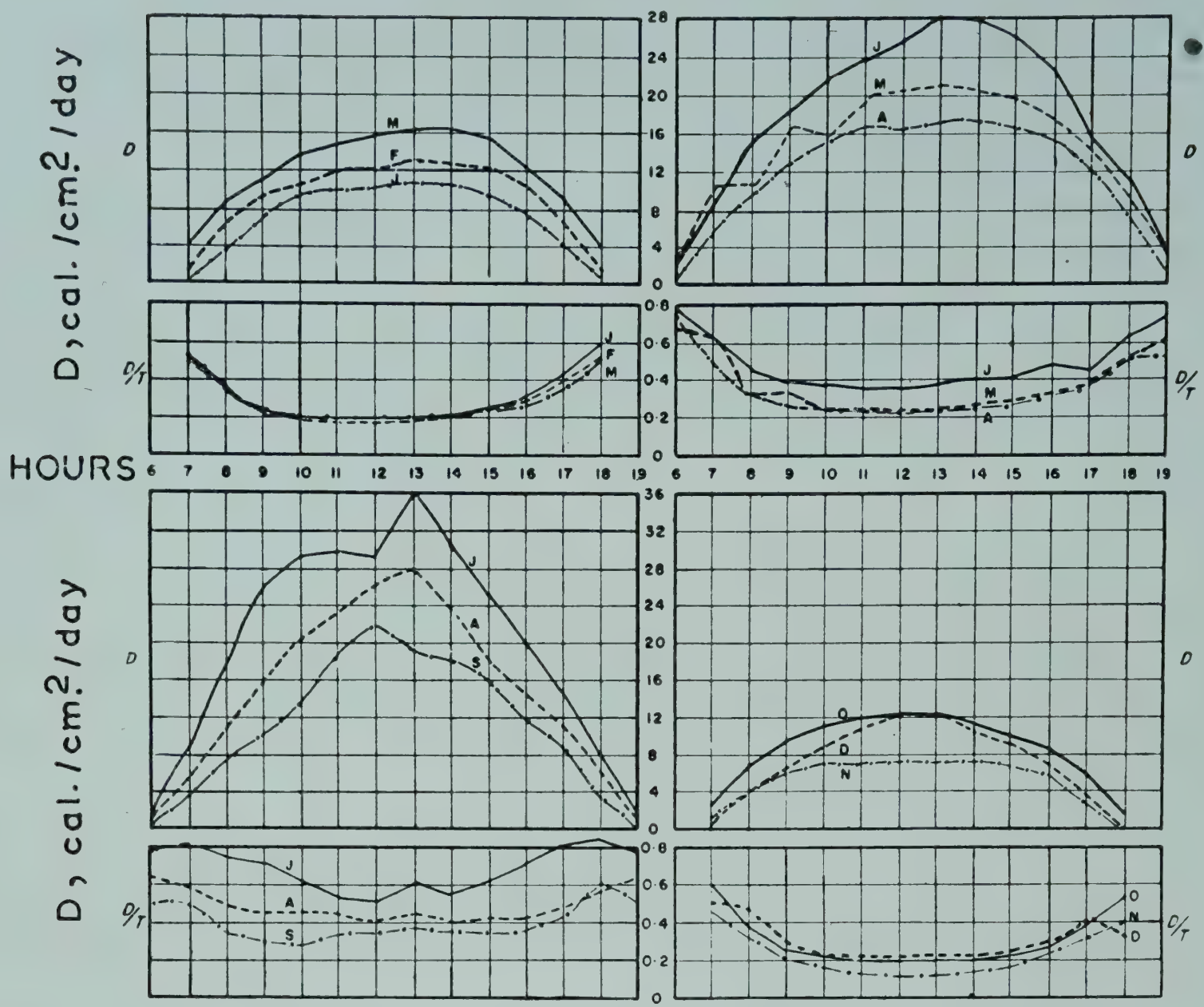

FIG. 7 — HOURLY VARIATION OF DIFFUSE SKY RADIATION (D) AND D/T AT DELHI DURING 1959

D/T is a function mainly of the turbidity and water vapour content of the atmosphere. The increased pollution and the result of increased convective effects, which disperse dust and water vapour in the atmosphere during summer account for the higher values in summer at both stations.

A study of the values for the ratio D/T for various stations in the world shows that it is lowest (0·05) at Mt Evans and highest (0·58) at Leopoldville.

Frequency Distribution of Daily Totals. The percentage frequency distribution of daily sums of diffuse radiation for all days at Delhi and Poona in each month has been recorded. This shows that more than 60 per cent of the values of D exceeded 300 cal./cm.^{2} during the monsoon months July and August at Poona, less than 5 per cent being below 200 cal./cm.^{2}. During December–March at Poona, nearly 80 per cent lies in the group 51–150 cal./cm.^{2}. At Delhi nearly 100 per cent lies in the range 51–150 cal./cm.^{2} during the winter months and 201–350 cal./cm.^{2} during the monsoons.

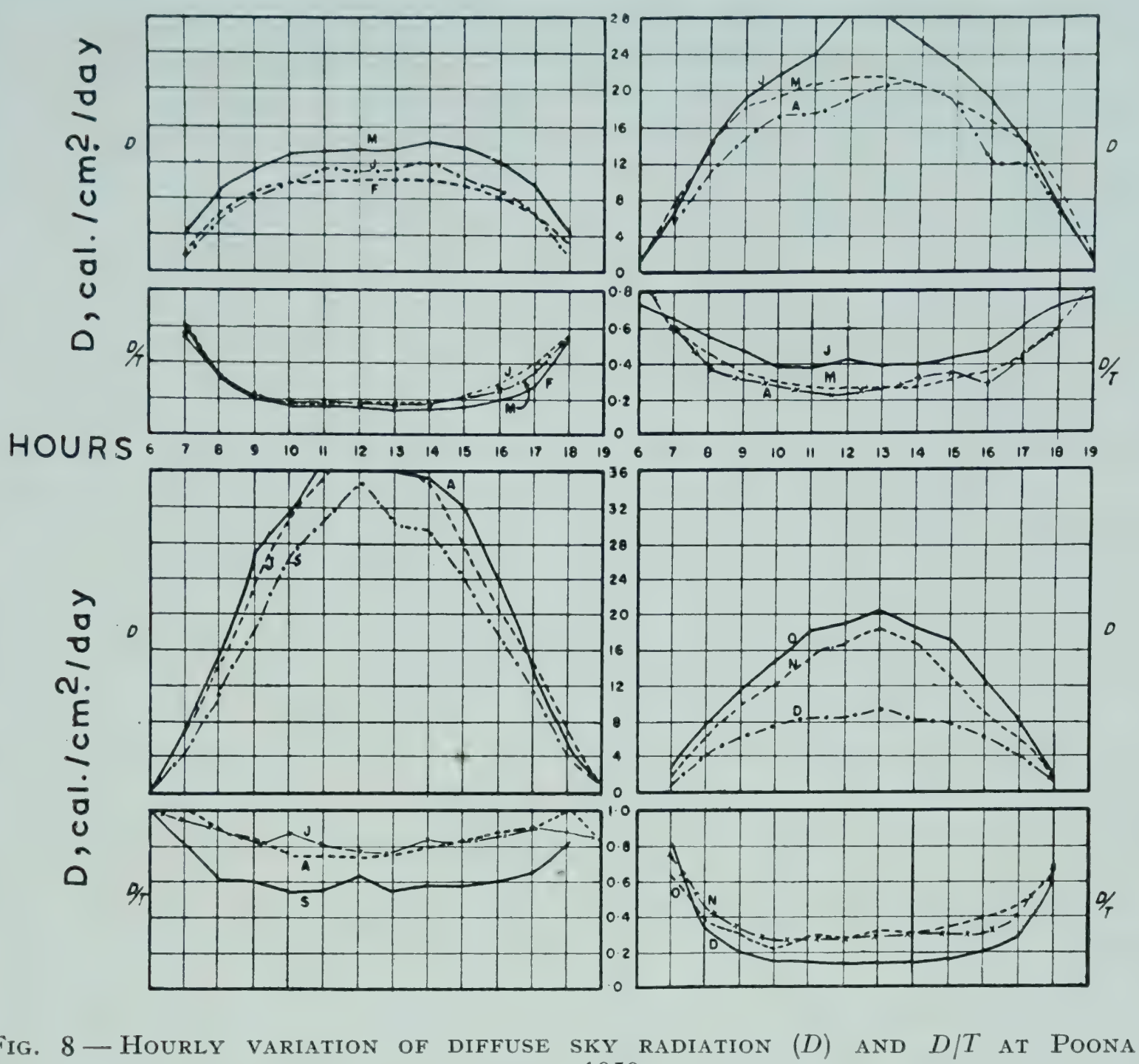

FIG. 8 — HOURLY VARIATION OF DIFFUSE SKY RADIATION (D) AND D/T AT POONA DURING 1959

Taking the year as a whole, maximum diffuse radiation is received in the interval 51–100 cal./cm.^{2} at both stations, followed by that in the intervals 101–150 cal./cm.^{2}.

Mean Hourly Variation of D during Different Months of the Year. For many practical purposes it is desirable to have a knowledge of the diurnal variation of T and D through all seasons of the year. The hourly variation of diffuse sky radiation and D/T at Delhi and Poona is illustrated in Figs. 7 and 8 respectively. Figs. 9a and 9b show isopleth diagrams in which lines of equal intensity of radiation have been drawn for Delhi and Poona.

Delhi. It will be noticed that the intensity of diffuse radiation increases from sunrise and shows a maximum between 1200 and 1400 hours (LAT), thereafter it decreases till after sunset. During the months May–September, the variations are irregular, showing fluctuations in intensity throughout the day with the maximum around 1300 hours (LAT). The intensity

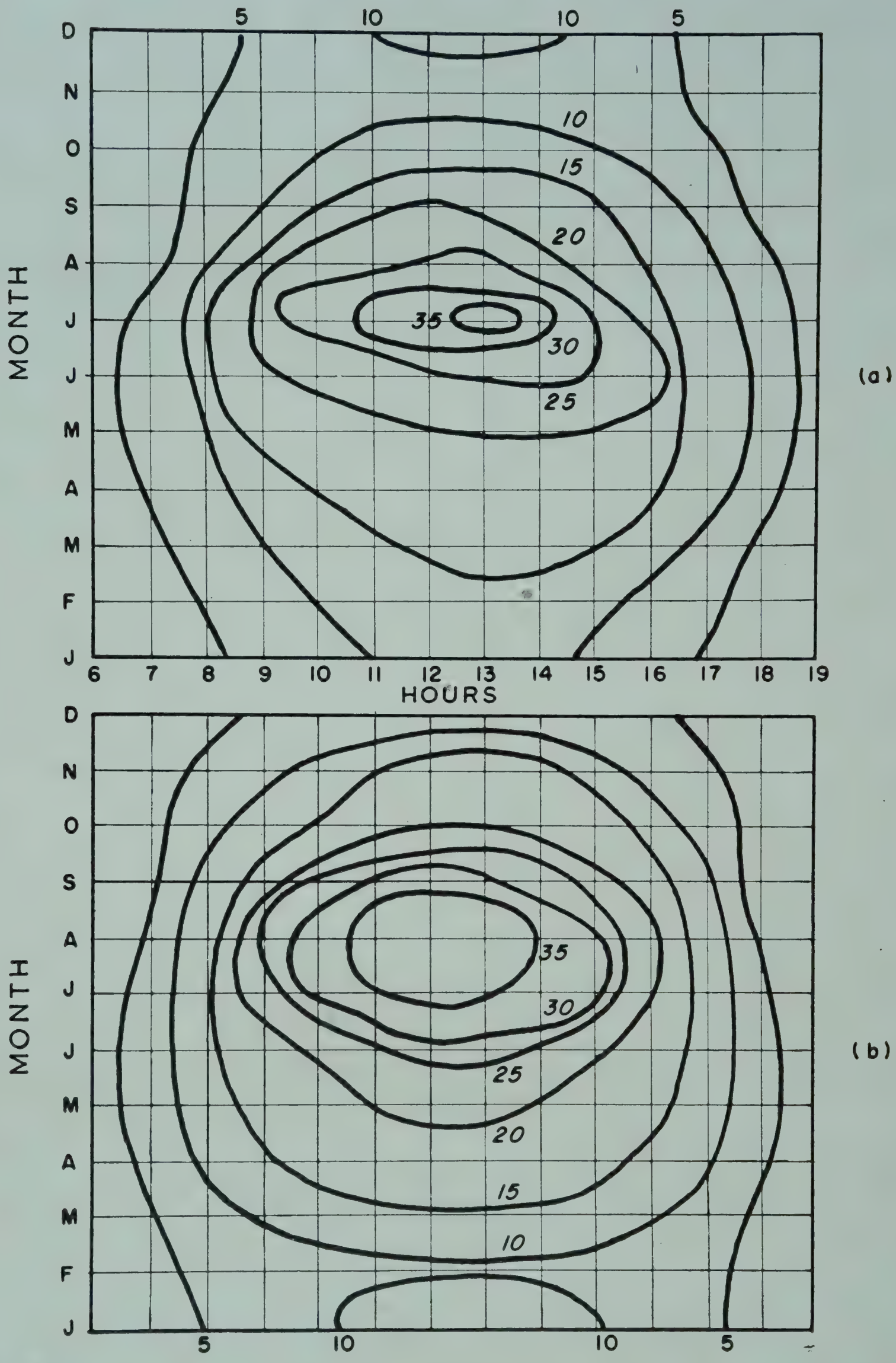

FIG. 9 — ISOPLETH OF DIFFUSE SKY RADIATION, D (CAL./CM.^{2}/HR) SHOWING HOURLY VARIATION IN DIFFERENT MONTHS: (a) DELHI, AND (b) POONA

during each hour increases from January to March by nearly 2 cal./cm.^{2} per month, till June by about 4 cal./cm.^{2} per month and falls after July at about the same rate with a sudden drop of about 8 cal./cm.^{2} from September to October.

The maximum values of hourly diffuse radiation received vary from 10·6 cal./cm.^{2}/hr in January to 36·2 cal./cm.^{2}/hr in July, the average value around 1300 hours (LAT) being about 18 cal./cm.^{2}/hr.

Poona. The intensity is generally symmetrical around noon during the months May–September and around 1300 hours (LAT) during the months October–April. The variations are large as at Delhi during the summer and monsoon months, while during the winter months December–February the curve is flatter and more regular. The intensity of diffuse radiation in each hour increases month to month by about 2 cal./cm.^{2} from January to March, 4 cal./cm.^{2} from April to June, 8 cal./cm.^{2} from July to September and then falls again by about 3 cal./cm.^{2} from October to December.

The maximum value reached by the hourly diffuse radiation is 40 cal./cm.^{2} in July–August, 30 in June, 20 in April–May and October–November, 10 in January–March and 9 in December, the average value being about 20 cal./cm.^{2}.

The hourly means around noon are highest in May for T (83 cal./cm.^{2}) and in July for D (36 cal./cm.^{2}) at Delhi. The corresponding values for Poona are 84 cal./cm.^{2} in March and 39 cal./cm.^{2} in August respectively. The lowest hourly value for T and D at Delhi were 53 and 7 cal./cm.^{2}. The corresponding values at Poona were 48 and 8 cal./cm.^{2}. Over the whole year T and D reached 82·3 and 21·6 cal./cm.^{2} when the sun was highest in the sky.

Hourly Values of D/T. The hourly variations of the ratio D/T for all the months for 1959 at Delhi and Poona are illustrated in Figs. 7 and 8. It will be seen that the progression in values of the ratio from 0700 to 1800 hours is a very smooth one during the winter and summer months October–May. They are very irregular from June to September during the monsoon at both Delhi and Poona. The variations are symmetrical around noon, minimum at noon during October–March. The minimum occurs between 1000 and 1400 hours (LAT) during the remaining months. The maxima are about sunrise and sunset, since with low solar elevations much of the energy received then is indirectly from the sky.

Direct Solar Radiation. Direct solar radiation I_H received in a horizontal surface is given by $T-D$ and the mean values of I_H month by month for both Delhi and Poona have been calculated. It is found that the annual variation of I_H is similar to that of T. The more important parameters are

I_V the direct solar radiation received on a vertical surface in the direction towards the sun and I_N that at normal incidence. These will be discussed in a separate paper.

References

1. Drummond, A. J., *Arch. Met. Wien*, **7** (1956), 413.
2. Schuepp, W., *Bull. Serv. met. Congo Belge*, No. 8 (1952), 11.
3. Hand, I. F. & Wollaston, F. A., *Tech. Pap. No.* 18, *U.S. Weath. Bur., Washington*, 1952.
4. Blackwell, M. J., M.R.P. No. 895, *Air Ministry Met. Res. Com.*, London, 1954.
5. Mani, A., Chacko, O. & Venkiteshwaran, S. P., *Indian J. Met. Geophys.*, **13** (1962), 337.

* * *

Seasonal Variation of Potential Gradient in Free Atmosphere over Poona. Anna Mani, B. B. Huddar, N. R. Kachare, M. S. Swaminathan & G. P. Srivastava, Meteorological Office, Poona, and S. P. Venkiteshwaran, National Aeronautical Laboratory, Bangalore [*Indian J. Met. Geophys.*, **11** (1960), 285].

The techniques developed at Poona for the measurement of electrical potential gradient in the free atmosphere have been described and the results of observations made over Poona during 1957–58 on the day-to-day and diurnal variations of potential gradient in the troposphere as well as the seasonal variations have been discussed. The variation of potential gradient with height follows the theoretical values only during the monsoon months, showing an increase above 300 mb. in winter and steady values above 500 mb. during summer. (*Abstract*)

Measurements of Atmospheric Turbidity with Angstrom Pyrheliometers at Poona and Delhi. Anna Mani & Oommen Chacko, Meteorological Office, Poona.

Measurements of the direct solar radiation, both for selected spectral regions and for the whole spectrum, have been made at Poona and Delhi using the Angstrom pyrheliometer and standard Schott glass filters OGI, RG2 and RG8. From these values, Angstroms turbidity coefficient (β) has been computed for both stations for the years 1958 and 1959. The diurnal and seasonal variations in the atmospheric turbidity at both stations are discussed and compared with similar measurements in the tropical and middle latitudes. (*Abstract*)

Observations of Electric Potential Gradient near the Ground at Poona. K. R. Sivaraman & A. K. Banerjee, Meteorological Office, Poona [*Indian J. Met. Geophys.*, **13** (1962), 192].

A detailed study of the diurnal and seasonal variations in the electrical potential gradient near the ground has been made from the records of a Cambridge photographic electrograph installed at the Meteorological Office, Poona. Variations of potential gradient with various meteorological factors have been discussed and an explanation for the observed variations has been offered. (*Abstract*)

Measurements of the Total Radiation from Sun and Sky in India. Anna Mani & Oommen Chacko, Meteorological Office, Poona, and S. P. Venkiteshwaran, National Aeronautical Laboratory, Bangalore [*Indian J. Met. Geophys.*, **13** (1962)].

The radiation data obtained with the Moll-Gorczynski solarimeter, Bellani pyranometer and the Campbell-Stokes sunshine recorder at Poona, Delhi, Calcutta and Madras have been summarized. The seasonal and diurnal variation of radiation from the sun and sky in the representative regions of India have been brought out clearly for the first time. (*Abstract*)

SFE and S_q vectors at Indian geomagnetic stations

P. R. PISHAROTY
P. V. JOSEPH

Colaba Observatory
Bombay

The ΔH values corresponding to the maxima of geomagnetic crochets associated with optical solar flares of importance 3^+ and 3 were measured for fifteen crochets well recorded on the H-magnetograms of Alibag, Annamalainagar and Trivandrum, during 1957–59 (Figs. 1–3). They show a diurnal variation somewhat similar to the S_q (the daily inequality of the solar daily variation of the quiet days) in H, also shown in the same figures. However, a comparison of the two curves shows that there is a difference in phase between the two, the maxima of the SFE daily variation being about one hour earlier than that of the S_q daily variation. The lead of one hour in phase was confirmed by plotting the ΔH (SFE) values on the x-axis and the S_q

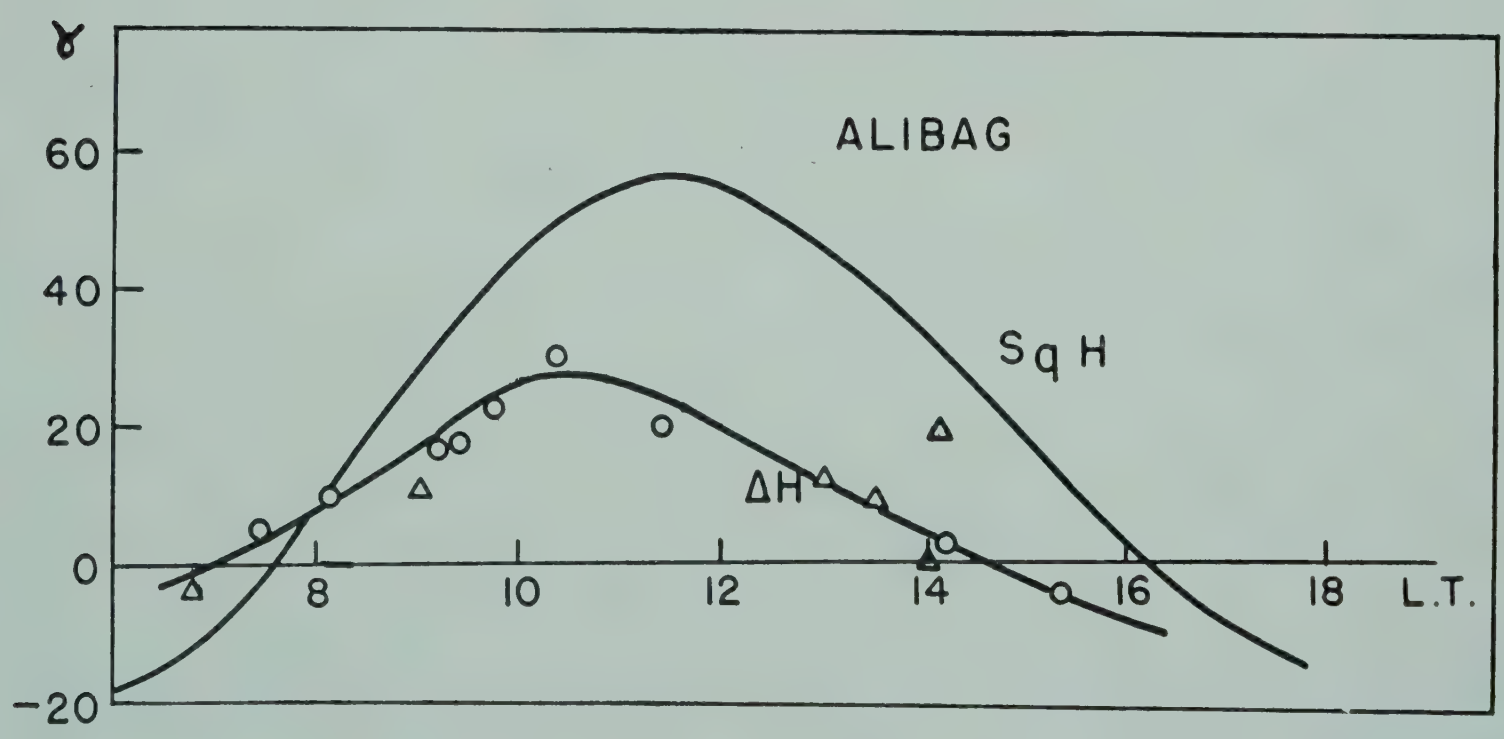

FIG. 1 — DIURNAL VARIATION OF S_q AND ΔH: ALIBAG [UPPER CURVE REPRESENTS THE DAILY INEQUALITY OF $S_q(H)$ FOR SUMMER 1958; CIRCLES REPRESENT THE ΔH VALUES CORRESPONDING TO MAXIMUM OF SFE FOR CROCHETS DURING SUMMER AND TRIANGLES FOR OTHER SEASONS]

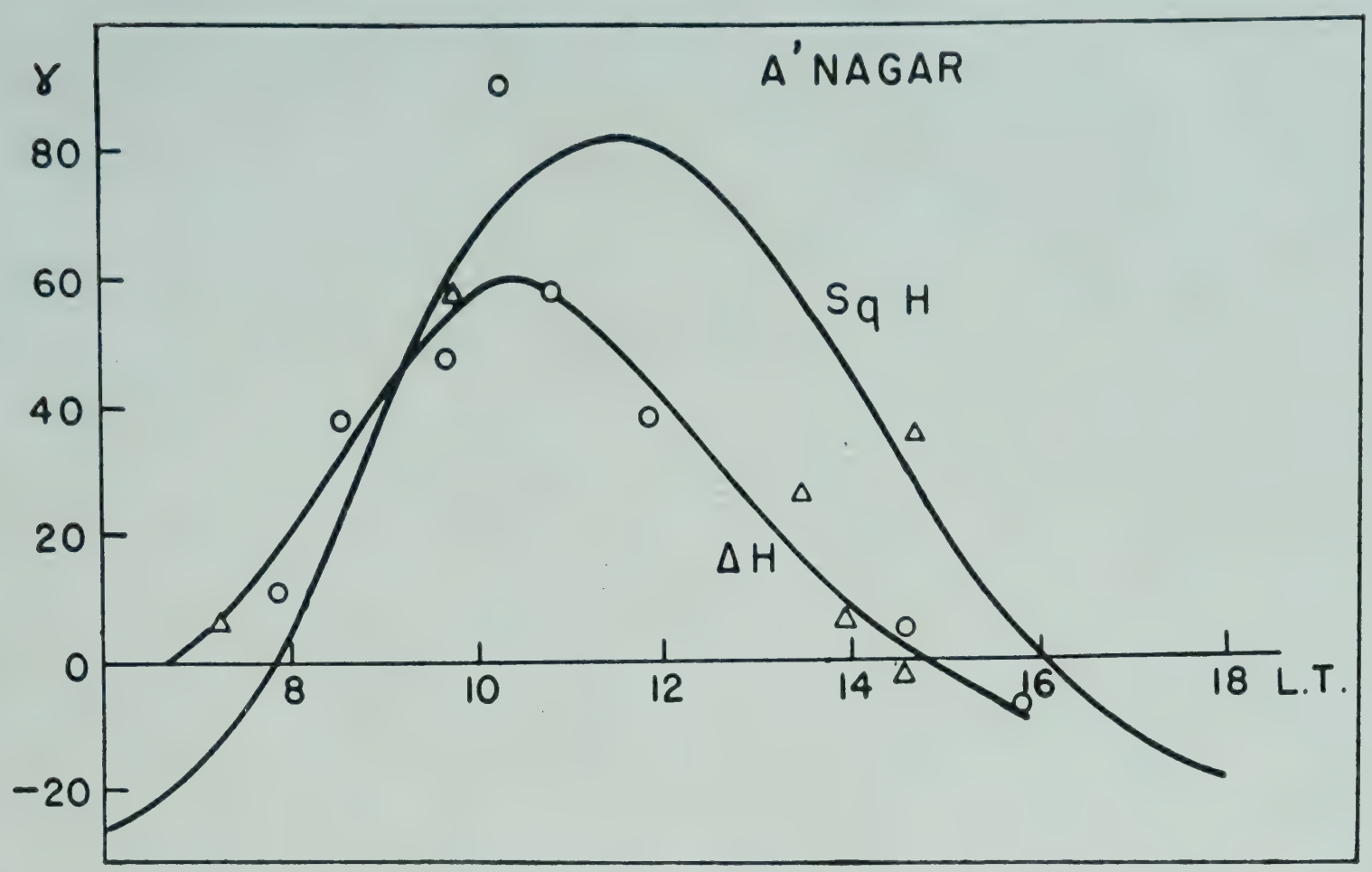

FIG. 2 — DIURNAL VARIATION OF S_q AND ΔH: ANNAMALAINAGAR [UPPER CURVE REPRESENTS THE DAILY INEQUALITY OF $S_q(H)$ FOR SUMMER 1958; CIRCLES REPRESENT THE ΔH VALUES CORRESPONDING TO MAXIMUM OF SFE FOR CROCHETS DURING SUMMER AND TRIANGLES FOR OTHER SEASONS]

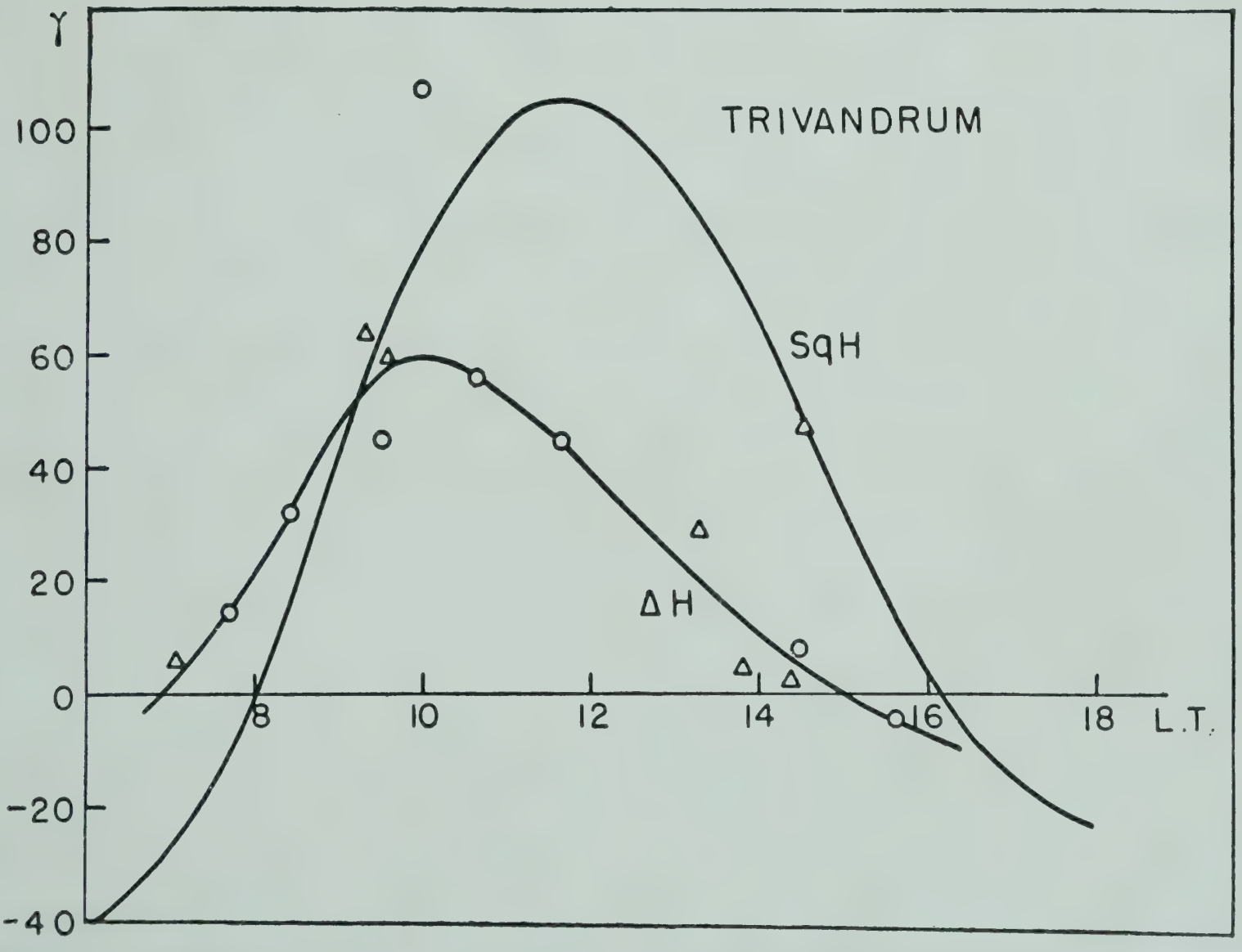

FIG. 3 — DIURNAL VARIATION OF S_q AND ΔH: TRIVANDRUM [UPPER CURVE REPRESENTS THE DAILY INEQUALITY OF $S_q(H)$ FOR SUMMER 1958; CIRCLES REPRESENT THE ΔH VALUES CORRESPONDING TO MAXIMUM OF SFE FOR CROCHETS DURING SUMMER AND TRIANGLES FOR OTHER SEASONS]

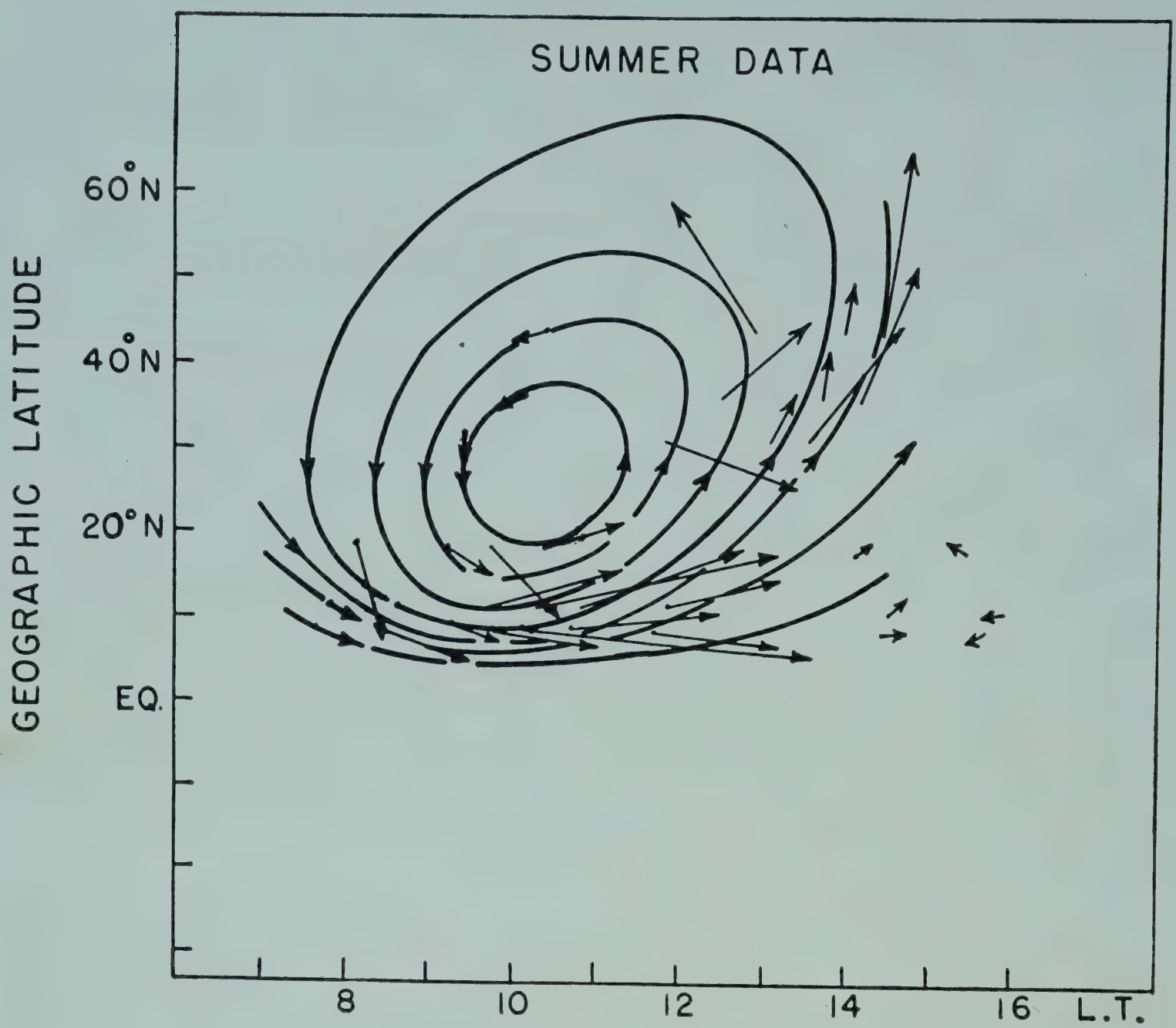

FIG. 4 — SFE CURRENT SYSTEM (TENTATIVE) [ARROWS INDICATE THE HORIZONTAL CURRENT VECTORS RESPONSIBLE FOR THE CROCHETS OF SUMMER SEASON; OVAL LINES REPRESENT CURRENT SYSTEM ASSUMED TO BE RESPONSIBLE FOR THE SFEs]

values with different phase differences on the y-axis. The points were found to lie on a straight line for a phase difference of about an hour, but on ellipses for other phase differences.

The amplitudes of the curves suggest that the ionization currents associated with the solar flare effects is about 60–70 per cent of the normal S_q currents, if both flow at the same height. However, the existence of the phase difference suggests that they flow at different levels, where apparently the winds and the ionization combine to produce the observed effects.

The horizontal magnetic vectors of the SFE crochets and of the corresponding instantaneous vectors of the solar daily variations were computed. The angular separation at Alibag for large crochets (between 0800 and 1200 hours local time) was of the order of 20°, while the corresponding separation at Trivandrum and Annamalainagar was of the order of 5°.

SFE AND S_q VECTORS AT INDIAN GEOMAGNETIC STATIONS

With the data available from published records of three Japanese stations and those of the Indian stations, a tentative SFE current system (showing only the directions of current flow) has been drawn (Fig. 4). It will be seen that the local time at which the D values of the SFE crochets would exhibit a sharp change in sign (east or west) is different for different latitudes. These times appear to be 0948 hours for latitude 10°N, 1006 hours for latitude 20°N, 1036 hours for latitude 40°N and 1054 hours for 50°N.

A detailed paper will be published in the *Indian Journal of Meteorology and Geophysics.*

Geomagnetic storms in July 1959

A. J. SHIRGAOKAR
B. J. SRIVASTAVA

Colaba Observatory
Bombay

Features of the three major geomagnetic SSC-type storms recorded on July 11, 15 and 17, 1959 at the magnetic observatories at Alibag, Annamalainagar and Trivandrum have been discussed. A list of geomagnetic storms with SSC(H) $> 75\gamma$ [mean range of S_q(H) at Alibag] during 1921–58 is also presented and the dependence of SSC(H) amplitudes on S_q(H) discussed. Some of the noteworthy features of the July 1959 storms are given below.

Storm of July 11, 1959. Associated with the solar flare (3^+) on July 10 at 0206 hours GMT, the storm occurred 38 hr after the flare at night-time, the initial phase lasted about 6 hr and no marked main phase developed thereafter. The entire disturbance lasted about 10 hr. Only small fluctuations of the geomagnetic field were noticed in the records of the three stations. It was a moderate storm on the whole, without the main phase. Highest K index during the storm at Alibag was 6 over one 3 hr interval (K = 9, for a range of 300γ disturbance at Alibag).

Storm of July 15, 1959. Associated with the solar flare (3^+) of July 14 at 0332 hours GMT, the storm occurred 28·5 hr later in day-time at about the maximum time for H. Initial phase lasted about half an hour. Another SSC-like movement was recorded at 1327 hours GMT (Alibag: $\Delta H = 46\gamma$, $\Delta Z = -11\gamma$, ΔD = record lost; Annamalainagar: $\Delta H = 59\gamma$, $\Delta Z = 30\gamma$, $\Delta D = -2'{\cdot}0$; Trivandrum: $\Delta H = 57\gamma$, $\Delta Z = 45\gamma$, $\Delta D = 0'{\cdot}5$). Another flare effect was seen in the magnetogram at 1400 hours GMT on July 14 (2^+) which might be associated with this. It was a very severe storm with the three phases, initial, main and recovery, all well defined. In the main phase occurred the second SSC, and thereafter its morphology differed from the storms of July 11 and 17, 1959 in which a second SSC was not noticed, nor was the main phase well developed. Perhaps the second SSC helped in the formation of the main storm bay, which is sufficiently deep in the H-record. The time interval between the SSC and the minimum in

TABLE 1 — GEOMAGNETIC STORMS OF JULY 1959

Station	Date	Storm-time (GMT)			Sudden commencement amplitudes (SSC-type)			Ranges			S_q(H) for the hour preceding SSC γ
		Beginning *hours*	Ending *date*	Ending *hours*	D	H	Z	D	H	Z	
Alibag	11	1625	12	0200	−1·5	+88	−19	7	136	49	3
	15*	0802	16	0900	−1·1	+80	−18	17	751‡	137	44
	17	1638	18	1900	−2·7	+148	−18	11	305	73	45†
Annamalainagar	11	1625	12	0200	−3·9	+113	+63	7	173	73	−1
	15*	0802	16	0900	−4·5	+132	—	15	814	212	61
	17	1638	18	1900	−5·8	+174	+96	14	362	165	49†
Trivandrum	11	1625	12	0200	+0·4	+104	+99	5	173	118	11
	15*	0802	16	0900	+0·5	+189‡	106‡	12	865‡	342‡	70
	17	1638	18	1900	+0·6	+148	+157	7	332	277	41†

*Another SSC-like movement recorded at 1327 hours on July 15, whence the activity became intense
†Values unusable since the period preceding the SSC happened to be disturbed
‡Approximate values

TABLE 2 — LARGE SSCs ($\Delta H > 75\gamma$) AT ALIBAG (1921-58)

Date	Time of occurrence of SSC GMT	Amplitude of SSC in H γ	$S_q(H)$ for the hour preceding SSC γ
1921 May 13	1311	130	95*
May 14	2215	230	−68*
1927 Aug. 21	0739	180	59
1928 July 7	2328	280	12
1938 Jan. 16	2232	167	−10
Apr. 16	0545	130	75
1939 Apr. 23	0547	84	78
May 5	2045	97	10
1942 Mar. 1	0727	82	67*
1946 Mar. 28	0635	82	16
July 26	1845	148	−11
1947 July 17	1748	108	8
1958 Feb. 11	0126	80†	−2
July 8	0748	96	58

*Values unusable since the period preceding the SSC happened to be disturbed
†Approximate value

H during the storm was about 11 hr. Pulsations of the period of 20 sec. or so were seen in the initial and main phase of the storm at all the Indian stations in H, Z and D. The storm yielded two K indices of 8 at Alibag. It has been described as a 'noise storm' by Ellis[1], since it is associated with strong bursts of radio noise at kilocycle frequencies during the main phase, about 3 hr after its onset.

This storm resembles in certain respects the intense geomagnetic storm of February 11, 1958 (beginning 0126 hours GMT) which was associated with the solar flare of importance 2 (Hawaii) on February 9 at 2108 hours GMT. The time interval between the beginning of the flare and the SSC is 28·3 hr. The minimum in H of the storm is reached 10 hr after the SSC. There were three K indices of 8 at Alibag during the storm of February 11, 1958.

Storm of July 17, 1959. Associated with a solar flare (2) at 1604 hours GMT on July 16, the storm occurred after 24 hr at night-time; the initial phase lasted about 2 hr. The main phase was not well developed. Sharp, short-period, large-amplitude oscillations (period 3–4 min.) were superposed on long-period (1 hr or more) oscillations throughout. Several sharp rises and falls in the main phase showing pulsatory changes in the geomagnetic

field were recorded. Pulsations were noticed in the initial and main phase but not in the recovery phase. According to Ellis[1] this is not a 'noise storm'. It yielded one K index of 8 at Alibag.

The special features of the storms are that the amplitudes of the three SSCs on these days in H at Alibag (88γ, 79γ and 148γ respectively) are well above the magnitude of the SSCs usually recorded at Alibag (about 30γ in H). The SSC on July 11 and 17 occurred during the night-time (Table 1).

The largest of the SSCs(H) during 1921–58 (Table 2) occurred on July 7, 1928 in two stages at 2328 hours GMT (night-time), its magnitude being 280γ. Perhaps it should not be treated as a single SSC but as a complex one. The magnitude of the SSCs recorded (1921–58) does not bear any definite relation to the S_q(H) at the time of its occurrence at Alibag. This is in contrast with the general observation of day-time enhancement of SSCs at stations affected by the electroject, and therefore suggests that Alibag is outside the effects of the equatorial electroject. This is in conformity with the observation Maeda and Yamamoto[2] that the effect of the electrojet does not extend beyond 20° dip-latitude. The annual mean value of the dip at Alibag (for 1958) is 24°38′·5.

References

1. Ellis, G. R. A., *J. geophys. Res.*, **65** (1960), 1705.
2. Maeda, H. & Yamamoto, M., *J. geophys. Res.*, **65** (1960), 2538.

Severe geomagnetic storms recorded at the Indian stations

B. J. SRIVASTAVA

Colaba Observatory
Bombay

Ten severe geomagnetic storms (range > 300γ in H at Alibag) were recorded during the IGY. The elements of these storms are given in Table 1.

The greatest storm was recorded on February 11, 1958, the range in H being 688γ. This storm was remarkable in that it showed unusual fluctuations during its initial phase at Alibag, somewhat similar to those of geomagnetic storms recorded in higher latitudes and similar to the storm recorded at Alibag on July 8, 1928.

There were three SC-type storms commencing on September 29, 1957 and December 4 and 13, 1958. These were remarkable in that the onset of their main phases was considerably delayed (8–14 hr) after the corresponding SSCs. Usually the main phase starts ½–3 hr after the SSC. In the case of the storm of September 29, 1957, the main phase started about 14 hr after the SSC, while in the case of the storms of December 4 and 13, 1958, the main phase began 8 and 12 hr respectively after the SSC.

It was found that the SSC*s (reverse storm sudden commencements), whenever they occurred, were recorded prominently at Trivandrum, less so at Annamalainagar, while they were just perceptible at Alibag. Five of these occurred between 0800 and 1200 hours local time on June 2 and 28, September 25 and October 22 and 28, 1958. The reverse preliminary kicks could be clearly seen in the traces of all the three elements D, H and Z. Kakioka has also listed four of these as SSC*, while that of October 28 has been recorded as a normal SSC at that station.

A detailed paper will be published in the *Indian Journal of Meteorology and Geophysics.*

TABLE 1 — SEVERE GEOMAGNETIC STORMS DURING THE IGY

Station	Date		Storm-time (GMT)			Sudden commencement (SSC-type) amplitudes			Ranges		
			Beginning	Ending		D	H	Z	D	H	Z
			hours	*date*	*hours*	/	γ	γ	/	γ	γ
Alibag	1957	Sept. 2	0314	4	0800	—	+22	−9	—	333	137
		4	1300	6	2000	−0·7	+37	−9	10	418	69
		13	0046	14	1800	−0·5	+17	−7	13	582	121
		21	1006	22	1300	−2·4	+74	−31	8	355	59
		29	0016	Oct. 1	1200	−0·2	+14	−2	8	483	89
	1958	Feb. 11	0126	12	2300	−2·2	+80*	−29	12	668	126
		July 8	0748	10	0000	−2·2	+95	−31	14	610	113
		Sept. 3	0842	5	2100	—	+36	−11	11	501	78
		Oct. 24	0730	25	1400	−0·9	+33	−16	5	309	41
		Dec. 4	0035	5	1200	−0·6	+21	−7	8	315	85
Annamalainagar	1958	Feb. 11	0126	12	2300	−3·0	—	—	18	—	—
		July 8	0748	10	0000	−7·0	—	+72	15	682	127
		Sept. 3	0842	5	2100	†−2·0	+65	+24	11	512	—
		Oct. 24	0730	25	1400	−2·5	+97	+20	8	383	84
		Dec. 4	0035	5	1200	−1·0	+37	+20	6	341	91
Trivandrum	1958	July 8	0748	10	0000	+0·5	+146	—	9	741	>344
		Sept. 3	0842	5	2100	+0·5	+71	+68	6	541	188
		Oct. 24	0730	25	1400	+0·5	+111	+85	4	394	175
		Dec. 4	0035	5	1200	+0·1	+28	+33	7	355	203

Approximate †SSC type

Geomagnetic variations at Alibag, Annamalainagar and Trivandrum

A. YACOB
P. R. PISHAROTY

Colaba Observatory
Bombay

Magnetic observatories at Trivandrum and Annamalainagar are situated close to and on either side of the magnetic equator. The geographic and the geomagnetic coordinates of these two observatories as well as those of the Alibag Magnetic Observatory are given in Table 1; their dip angles are also given.

Mean Geomagnetic S_q Field. Complete data are available for all the three observatories for the period October 1957–December 1958 only of the IGY. The S_q variations of the three elements H, Z and D derived from the International Quiet Days falling within the above period are presented in the form of the mean of the element plus the first four harmonic components:

$$M + \sum_{n=1}^{n=4} C_n \sin (n\theta + \phi_n)$$

ϕ_n being reckoned from zero hour LMT.

Alibag

$$\begin{aligned} H = 38{,}686 &+ 30 \sin (\theta + 269^\circ) \\ &+ 14 \sin (2\theta + 105^\circ) \\ &+ 6 \sin (3\theta - 56^\circ) \\ &+ 2 \sin (4\theta - 222^\circ) \end{aligned}$$

Annamalainagar

$$\begin{aligned} H = 40{,}619 &+ 46 \sin (\theta + 271^\circ) \\ &+ 23 \sin (2\theta + 110^\circ) \\ &+ 10 \sin (3\theta - 36^\circ) \\ &+ 4 \sin (4\theta - 185^\circ) \end{aligned}$$

TABLE 1 — GEOGRAPHIC AND GEOMAGNETIC COORDINATES AND DIP ANGLES AT TRIVANDRUM, ANNAMALAINAGAR AND ALIBAG OBSERVATORIES

Station	Geographic		Geomagnetic		Dip
	Lat.	Long.	Lat.	Long.	
Trivandrum	8°29′N	76°50′E	0°53′S	145°50′E	−0°36′
Annamalainagar	11°22′N	79°42′E	1°26′N	149°42′E	5°25′
Alibag	18°38′N	72°52′E	9°30′N	143°36′E	24°38′

Trivandrum

$$H = 40{,}084 + 60 \sin(\theta + 270^\circ) + 31 \sin(2\theta + 105^\circ) + 13 \sin(3\theta - 33^\circ) + 4 \sin(4\theta - 176^\circ)$$

The mean ranges of $S_q(H)$ at the three stations are respectively 70γ, 113γ and 149γ, the highest value being for Trivandrum.

The values of $S_q(Z)$ in γ are:

Alibag

$$Z = 17{,}737 + 7 \sin(\theta + 52^\circ) + 5 \sin(2\theta - 75^\circ) + 5 \sin(3\theta + 134^\circ) + 3 \sin(4\theta - 16^\circ)$$

Annamalainagar

$$Z = 3{,}852 + 17 \sin(\theta + 61^\circ) + 8 \sin(2\theta - 115^\circ) + 2 \sin(3\theta + 105^\circ) + 1 \sin(4\theta + 35^\circ)$$

Trivandrum

$$Z = -420 + 16 \sin(\theta - 42^\circ) + 12 \sin(2\theta + 139^\circ) + 5 \sin(3\theta - 2^\circ) + 2 \sin(4\theta - 156^\circ)$$

The mean ranges of $S_q(Z)$ at the three stations are respectively 31γ, 43γ and 50γ, the highest value being for Trivandrum.

The values of $S_q(D)$ in minutes of arc are:

Alibag

$$D = -48'{\cdot}2 + 0'{\cdot}8 \sin(\theta + 25^\circ) + 0'{\cdot}8 \sin(2\theta - 131^\circ) + 0'{\cdot}7 \sin(3\theta + 66^\circ) + 0'{\cdot}2 \sin(4\theta - 87^\circ)$$

Annamalainagar

$$\begin{aligned} D = & -164'{\cdot}6 + 0'{\cdot}5 \sin(\theta + 73^\circ) \\ & + 0'{\cdot}6 \sin(2\theta - 100^\circ) \\ & + 0'{\cdot}4 \sin(3\theta + 82^\circ) \\ & + 0'{\cdot}1 \sin(4\theta - 63^\circ) \end{aligned}$$

Trivandrum

$$\begin{aligned} D = & -174'{\cdot}6 + 0'{\cdot}1 \sin(\theta + 31^\circ) \\ & + 0'{\cdot}3 \sin(2\theta - 103^\circ) \\ & + 0'{\cdot}3 \sin(3\theta + 63^\circ) \\ & + 0'{\cdot}1 \sin(4\theta - 100^\circ) \end{aligned}$$

The ranges of $S_q(D)$ at the three stations are respectively 3′·9 (45γ), 2′·4 (29γ) and 1′·2 (14γ), the least value being for Trivandrum.

Mean Geomagnetic SD Field. The solar daily disturbance values for the elements H, Z and D were determined for the period under study by subtracting the mean hourly values for the International Quiet Days from the corresponding mean hourly values for the International Disturbed Days. The mean depression of H during disturbed days and the daily disturbance variation SD(H) in gammas (θ being reckoned from zero hour LMT) are:

Alibag

$$\begin{aligned} H = & -59 - 10{\cdot}7 \sin(\theta + 139^\circ) \\ & - 4{\cdot}0 \sin(2\theta + 120^\circ) \\ & - 0{\cdot}8 \sin(3\theta - 51^\circ) \\ & - 0{\cdot}4 \sin(4\theta - 287^\circ) \end{aligned}$$

Annamalainagar

$$\begin{aligned} H = & -61 - 9{\cdot}7 \sin(\theta + 150^\circ) \\ & - 6{\cdot}0 \sin(2\theta + 124^\circ) \\ & - 2{\cdot}1 \sin(3\theta - 30^\circ) \\ & - 1{\cdot}0 \sin(4\theta - 200^\circ) \end{aligned}$$

Trivandrum

$$\begin{aligned} H = & -61 - 8{\cdot}2 \sin(\theta + 160^\circ) \\ & - 8{\cdot}1 \sin(2\theta + 127^\circ) \\ & - 2{\cdot}9 \sin(3\theta - 28^\circ) \\ & - 1{\cdot}0 \sin(4\theta - 194^\circ) \end{aligned}$$

The ranges in the SD(H) values are 27γ, 29γ and 31γ respectively.

Storm-time Changes in H due to Disturbance Field. Storm-time changes in H for individual storms of the SC-type, in respect of each observatory, was derived by subtracting the appropriate S_q values (of the particular month in which the storm occurred) from the corresponding hourly values during the period of the storm. The difference in H thus obtained for each hour will be the total of SD, D_{st} and D_i averaged for the hour.

A comparison of these values for the three stations was effected by superposing them. The three superposed curves keep close together during the night hours, but tend to separate out during the daylight hours. When the trend is a fall, the Trivandrum values are lower during the day and when the trend is a rise the Trivandrum values are higher during the day; Annamalainagar values take intermediate positions (The equatorial enhancements are much less than the enhancements in the S_q field for the corresponding hours). The day-time equatorial enhancements become more prominent during the later phases of a storm, particularly during the recovery phase.

Rapid Fluctuations in H. Sharp fluctuations of short duration, mostly less than about 10 min., were considered as rapid fluctuations. These, therefore, included all sudden commencements and all sudden impulses, positive and negative. In all, 827 simultaneous fluctuations distributed during the different hours of the day and night were studied. For each fluctuation (i) the ratio of the magnitude at Trivandrum to that at Alibag, (ii) the ratio of the magnitude at Annamalainagar to that at Alibag, and (iii) the ratio of the magnitude at Trivandrum to that at Annamalainagar were computed.

It was found that the ratios (i) and (ii) shoot up with sunrise and reach peak values ranging between 3 and 4 about the time of the local noon. The mean value of the ratio during daylight hours is about 2·5, while during the night hours it is about 1. The day-time ratio (iii) is about 1·2 showing that the enhancement of SSCs and SIs increases towards the magnetic equator.

A detailed paper on the intercomparisons is being published in the *Indian Journal of Meteorology and Geophysics.*

An estimate of geomagnetic manifestation of solar activity

A. YACOB

Colaba Observatory
Bombay

It is well known that the magnitudes of the geomagnetic variations on the quiet as well as the disturbed days show a correspondence with the level of solar activity as exhibited by the spottedness of the sun's disc. In the present note the effect of the wave radiation from the sun during the IGY, a period of high solar activity at the Alibag Magnetic Observatory, is compared with that during July 1953–December 1954, a period of low solar activity, by simply comparing the mean ranges in H for the five I_Q days of each month. To compare the effects of the corpuscular radiation during the above two periods, the K indices and the equivalent amplitude, a_k, are used. The frequency of occurrence of the K indices, 0–9, were counted and the percentage frequencies of each index computed for the two periods. Then the equivalent range amplitudes of disturbances, a_k, were summed up and the two values for the two periods were compared.

The mean quiet-day ranges in H for the IGY period and the quiet period July 1953–December 1954 are shown monthwise in Table 1. It will be seen that for most of the months, the ranges during the IGY are more than double the ranges for the epoch of sunspot minimum. The mean ratio is 2·24, showing an increase of 124 per cent during the IGY over that during the other period.

The percentage frequencies of K indices for the two periods are given in Table 2. A quantitative increase of the disturbance for the IGY period was obtained by summing the equivalent disturbance range amplitudes a_k for the two periods. The mean ratio of the sums of the values of a_k for the two periods is 1·43, showing an increase of 43 per cent in equivalent disturbance effect during IGY over that during the other period.

It is thus seen that while wave radiation from the sun enhances its geomagnetic manifestation by 124 per cent during the IGY as compared with the

TABLE 1 — MEAN RANGES IN H OBTAINED FROM THE FIVE I_Q DAYS FOR IGY AND FOR THE MINIMUM PERIOD, JULY 1953-DECEMBER 1954

Month	S_q(H) range in		
	IGY	Min. period selected	Ratio
July	67	28	2·39
Aug.	63	33	1·91
Sept.	78	38	2·05
Oct.	76	35	2·17
Nov.	79	37	2·14
Dec.	53	22	2·41
Jan.	63	26	2·42
Feb.	69	22	3·14
Mar.	80	36	2·22
Apr.	85	40	2·13
May	86	37	2·32
June	84	29	2·90
July	75	42	1·79
Aug.	73	34	2·15
Sept.	73	34	2·15
Oct.	78	34	2·29
Nov.	63	45	1·40
Dec.	55	23	2·39
Mean ratio			2·24

TABLE 2 — PERCENTAGE FREQUENCIES OF THE K INDICES FOR IGY AND FOR THE MINIMUM PERIOD, JULY 1953-DECEMBER 1954

K indices	Percentage frequency	
	IGY	Min. period selected
0	0·43	1·09
1	15·92	25·98
2	41·53	44·39
3	24·17	18·31
4	11·84	7·95
5	4·26	2·01
6	1·37	0·27
7	0·27	0·0
8	0·21	0·0
9	0·0	0·0
Sum of a_ks	74,358	52,060
Mean ratio	1·43	

minimum activity period, the corpuscular radiation enhances its geomagnetic manifestation by only 43 per cent. Perhaps an increase in wave radiation is not necessarily associated with an increase in corpuscular radiation on all occasions.

The mean critical frequency for noon for the E layer of the ionosphere, the seat of the S_q currents, during the IGY period for Ahmedabad was 4·3 Mc/s., while the corresponding value during the period July 1953–December 1954 was 3·1 Mc/s. Assuming these values to be representative for Alibag and assuming the electron densities to be proportional to square of the critical frequencies, the conductivity of the E layer at noon during the IGY was nearly double the value $[=(4{\cdot}3/3{\cdot}1)^2]$ corresponding to the sunspot minimum epoch selected. The increase in conductivity, compared with the increase in the S_q range at Alibag, is a little less. This is understandable as the S_q currents would increase not only with increased conductivity but also with the increased winds consequent on the greater heating effects associated with an enhancement in the wave radiation.

* * *

Solar Radiation Theory of Earth's Magnetism. J. S. Chatterjee, Jadavpur University, Calcutta.

A new theory of earth's magnetism is presented. It is shown that due to non-linear properties of the mantle of the earth, the solar corpuscular radiation will cause a small uni-directional current to flow in the mantle and liquid core of the earth. This uni-directional current grows through successive disturbances and the final value of the current is such as to explain the observed magnetic field of the earth. The crust also will be permanently magnetized to saturation. The secular variation and reversed rock magnetism can be easily explained by this theory. (*Abstract*)

Seasonal Variation of Lunar and Solar Geomagnetic Tides in the Geomagnetic Equatorial Region. K. S. Raja Rao, Meteorological Office, Poona [*J. atmos. terr. Phys.*, **20** (1961), 289].

Following the method outlined by Chapman and Miller, the lunar L(H) and solar S(H) geomagnetic tides at Kodaikanal (geomag. lat. +0·6°) have been determined for the three seasons — December solstice, June solstice and equinox — making use of the hourly values of horizontal intensity for

the years 1950–55. Comparison of the seasonal variation of the amplitude of L(H) at Kodaikanal with similar results for Huancayo (geomag. lat. −0·6°) and Ibadan (geomag. lat. +10°) shows that the amplitude of L(H) at Kodaikanal is larger in December solstice than in June solstice, similar to the variation at Huancayo and Ibadan. It is, therefore, concluded that the ionospheric currents causing geomagnetic tides are not symmetrical with respect to the geomagnetic equator; but the southern hemispheric currents extend into the northern hemisphere up to 10°N geomagnetic latitude in December solstice. It is likely that the region of separation of the northern and southern hemispheric currents is not static, but oscillates northwards and southwards across the geomagnetic equator. There is no significant seasonal variation in the amplitude of S(H) in the magnetic equatorial region. (*Abstract*)

Study of night airglow at Mt Abu: OI 5577 Å

B. S. DANDEKAR

Physical Research Laboratory
Ahmedabad

The airglow photometer used for measuring the diurnal and seasonal variations of the OI green line in airglow at Mt Abu is described and the results are discussed.

The variations in intensity have been found to have no correlation with either sunspot or magnetic activity. An increase in the intensity of OI 5577 Å has been observed on the night following a number of solar flares.

For the study of tropical airglow, an observation station was started by the Physical Research Laboratory, Ahmedabad, at Mt Abu (lat. 24°·6N: long. 72°·7E; height, 1200 m.) in December 1955. The emission of 5577 Å has been observed over a period of about four years. The present paper gives an account of the instrumentation used and discusses the diurnal and seasonal variations of the intensity of airglow. An attempt is also made to find if there is any effect of solar and magnetic activity on the variations of OI 5577.

Description of Airglow Photometer

A block diagram of the airglow equipment using a photoelectric photometer is shown in Fig. 1. The high tension for the photomultiplier was obtained from a stabilized H.T. supply. The output current of the phototube was amplified by a three-stage d.c. amplifier. The filaments of the amplifier valves were heated from a 6 V. accumulator to ensure the stability of the amplifier. The power for the amplifier was derived from a low-tension, electronically stabilized power supply. The amplified output was finally fed to a 0–1 ma. d.c. Evershed pen recorder.

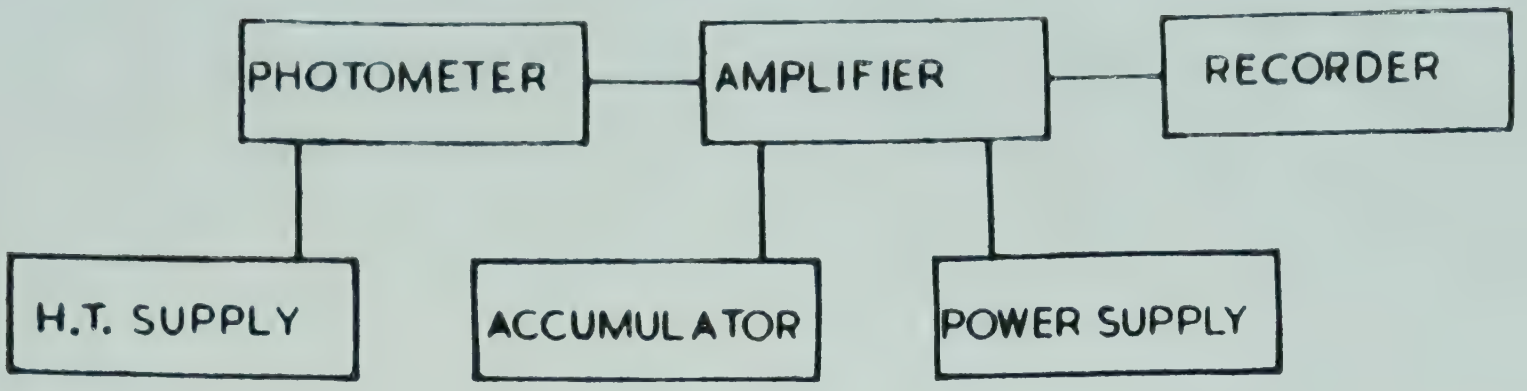

FIG. 1 — BLOCK DIAGRAM OF EQUIPMENT USED FOR AIRGLOW OBSERVATIONS AT MT ABU

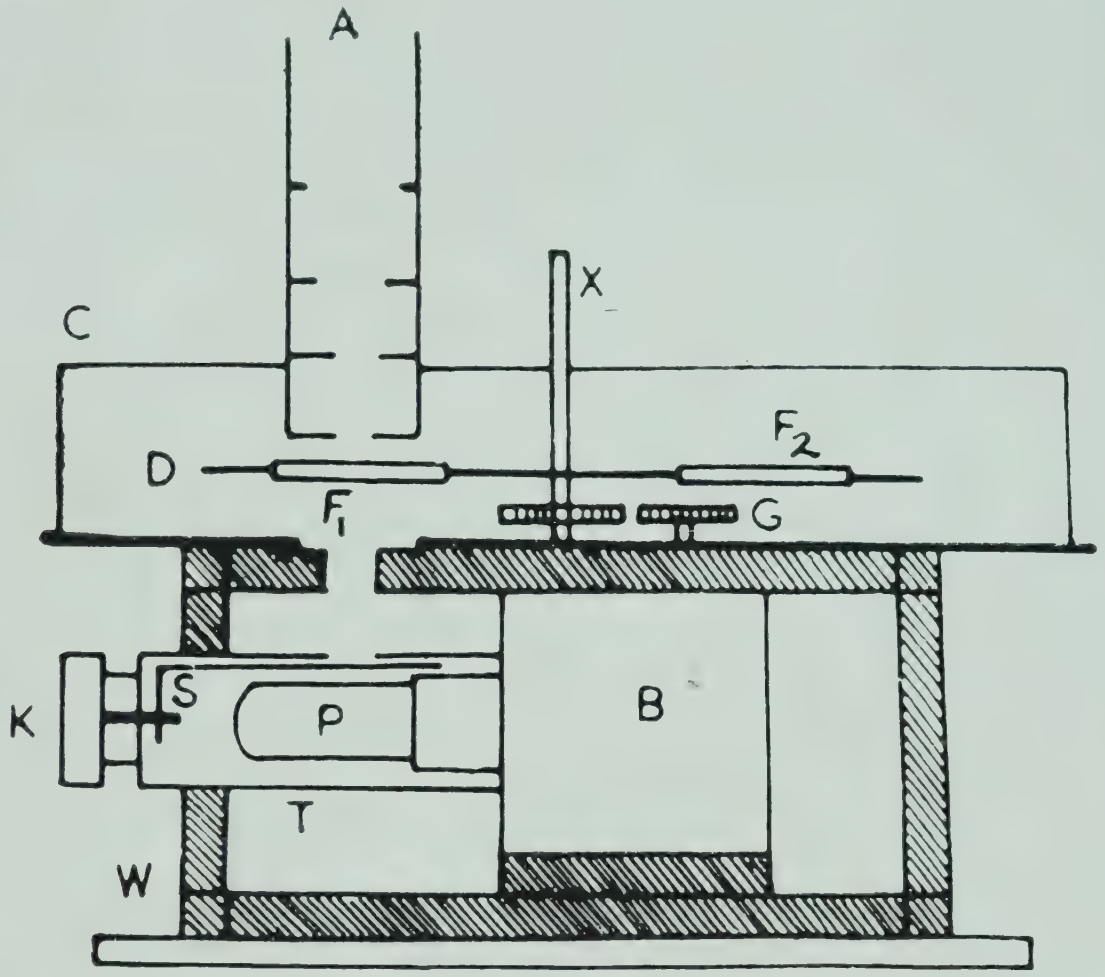

FIG. 2 — POLAR AIRGLOW PHOTOMETER [W, WOODEN BOX; B, BLEEDER; T, TUBE; K, KNOB; S, SHUTTER; P, PHOTOTUBE (RCA 931-A); C, COVER; D, DISC; X, AXLE; G, GEARS; F_1 & F_2, FITTERS; A, APERTURE]

The arrangement of the airglow photometer is shown schematically in Fig. 2. P is an RCA 931-A photomultiplier. Two interference filters F_1 and F_2, one of which has its peak transmission at 5580 Å and the other at 5300 Å, are employed. The former allows the selection of the OI green line and the latter serves to estimate the background radiation. The filters are mounted on a rotatable metal disc D. The disc D is fitted on the axle X of a wheel which can be rotated by a motor through a system of gears G. Light falls on the phototube through each of the filters for about $2\frac{1}{2}$ min., one after the other. During a rotation, the disc C cuts off the light for a part of the time and thereby the dark current level is also recorded. The projecting cylindrical tube contains apertures A which define the angle subtended by the photometer. The photometer covers a circular field of 11°·2 diameter.

The interference filters used are of Barr & Stroud make. The equivalent band-widths of 5300 and 5580 Å filters were 90 and 135 Å respectively. An ON 16 Corning glass filter was used in conjunction with the 5580 Å interference filter to cut off some of the unwanted yellow region of the spectrum. The characteristics of these filters are shown in Fig. 3. The continuous line shows the dependence of the filter transmission upon wavelength. The dotted lines are the relative curves of filter transmission multiplied by the photomultiplier response.

The photometer was directed towards the pole to avoid the effect of varying stellar background. The observations were made only on clear nights when there was no moon. A typical airglow record is shown in Fig. 4. The record with the higher amplitudes relates to the OI green line. The other record with lower amplitudes refers to the background radiation near 5300 Å.

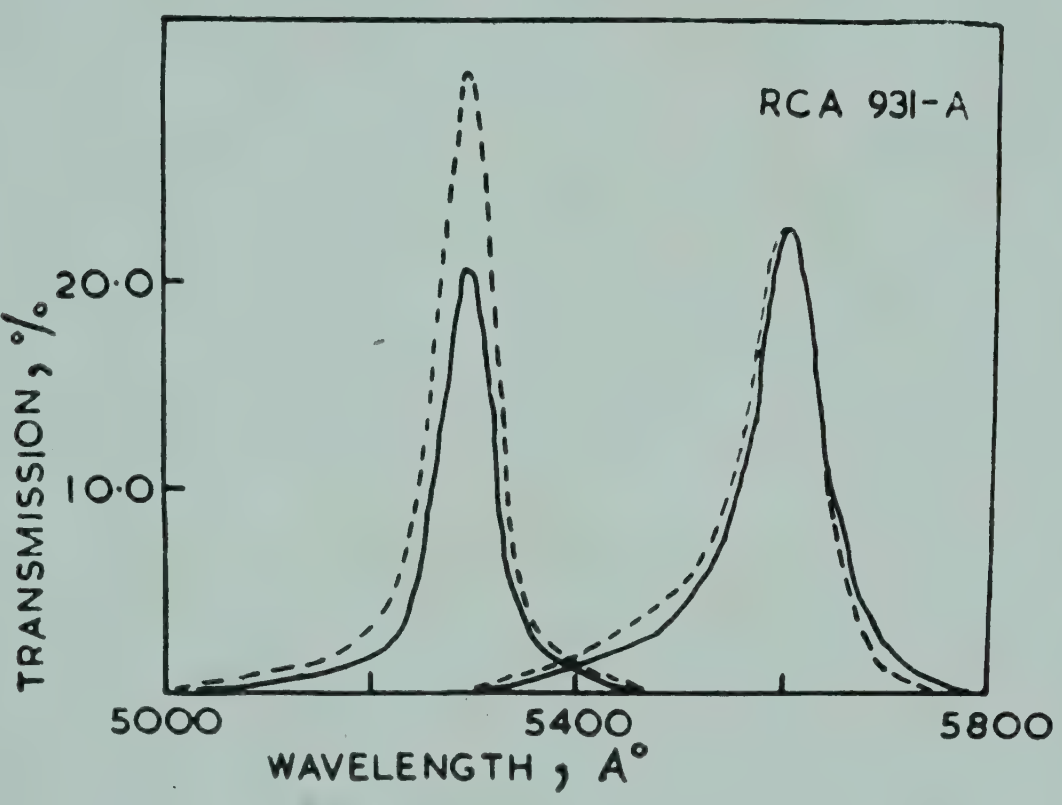

FIG. 3 — TRANSMISSION CHARACTERISTICS OF OPTICAL FILTERS

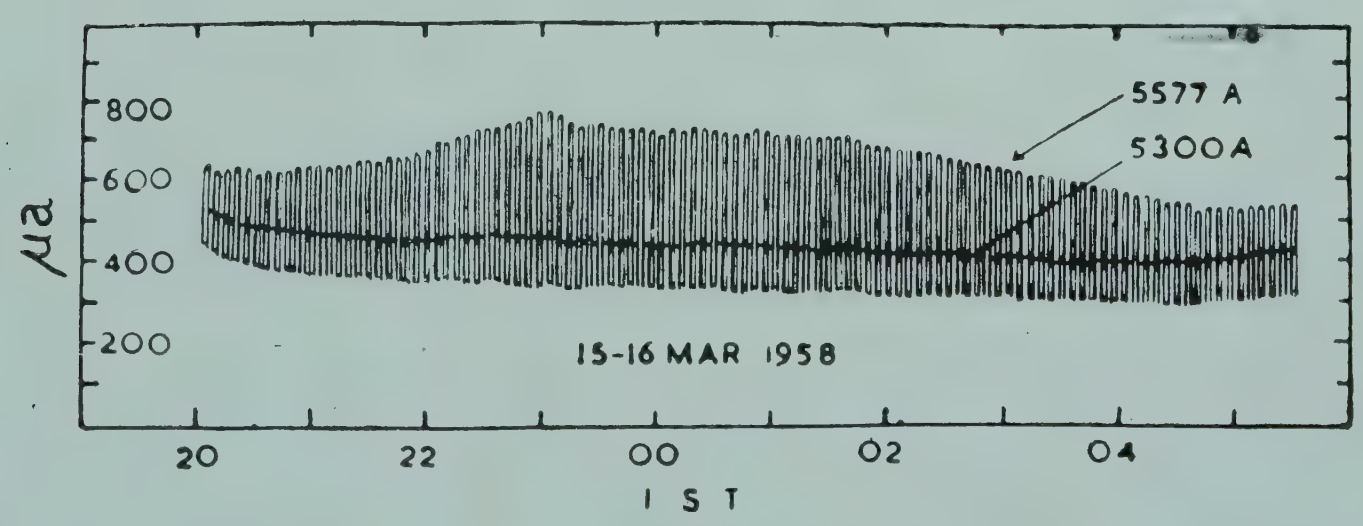

FIG. 4 — SAMPLE RECORD OF AIRGLOW INTENSITIES (5577 Å AND 5300 Å)

The stability of the airglow photometer was checked by measuring every day the deflection caused by the light from a radioactive source.

The photometer was calibrated against Roach's travelling standard photometer when Dr F. E. Roach[1] visited India in May 1958. The calibration yielded the following empirical relation

$$I_{5577} = 2{\cdot}37\ (d_{5577} - 65) \qquad (1)$$

where I_{5577} is the intensity of the airglow in Rayleighs corrected for the background radiation, and d_{5577} is the deflection in μa. caused by the light transmitted by the 5577 filter.

Later, the photometer was independently calibrated against a tungsten W-4 type ribbon filament lamp obtained from Messrs Philips. An artificial sky was produced in a dark room by illuminating a screen coated with magnesium oxide with the light from the ribbon filament lamp maintained at a constant temperature. The photometer was exposed to the artificial sky. The conversion factor was obtained by taking into consideration the filament temperature, its effective area used for illuminating the screen, the angle between the beam of light and the perpendicular to the screen, the filter transmission, its band-width and the photomultiplier response.

It was found that 1 μa. corresponded to 1·71 Rayleighs for 5300 Å and to 2·26 Rayleighs for 5577 Å.

As these agree reasonably well with the former calibration (with Roach's photometer), the empirical relation [Equation (1)] was used for the reduction of the data.

The observations towards the pole were reduced to zenith by dividing by a factor 2·0 which was determined from full-sky scanning observations.

Table 1 gives the number of observations from October to June during 1955–60.

Variation of Intensity during the Night

The data from October 1957 to December 1959 were grouped according to seasons: (i) autumn (October–November), (ii) winter (December–February), and (iii) spring (March–May). In the monsoon months June–September, data are lacking owing to cloud and rain.

The nocturnal variation in each of the above three seasons is shown in Fig. 5. The minimum and maximum intensities are shown by crosses and circles respectively. The curves in each group represent the boundaries above which 25, 50 and 75 per cent of the observations lie. All the groups show an increase in intensity during the first part of the night. The intensity reaches a maximum generally before midnight and is followed by a fall towards the early morning.

TABLE 1 — NUMBER OF OBSERVATIONS IN EACH MONTH DURING THE PERIOD OF OPERATION

Month	No. of observations					Total (Nights)
	1955–56	1956–57	1957–58	1958–59	1959–60	
Oct.	—	—	3	8	6	17
Nov.	3	—	4	14	11	32
Dec.	8	—	17	13	11	49
Jan.	7	7	18	14	17	63
Feb.	10	11	17	14	2	54
Mar.	8	9	16	17	—	50
Apr.	2	11	16	15	—	44
May	2	11	17	10	—	40
June	—	—	9	—	—	9
Total	40	49	117	105	47	358

The maximum in autumn occurs at about 2200 hours (local time), in winter at 2100 hours and in spring at about zero hour. The hour of maximum intensity thus changes from season to season. The median intensities were 350 Rayleighs in autumn, 280 Rayleighs in winter and 390 Rayleighs in spring. The nocturnal variation was maximum in spring.

In the same figure, the nocturnal variations at Mt Abu are compared with the nocturnal variations at Tamanrasset which is situated at the same geographic latitude in the Sahara (long. 5°30′E). At Tamanrasset, the maxima occur at a later hour. There is no strict correspondence between the day-to-day variations at the two places. The reasons for this are not clear. It may be that, as suggested by Roach *et al.*[2], the increases and decreases of airglow occur in cells with a diameter of the order of 2500 km. There may also be differences in the daily variation of atmospheric transparency at Mt Abu and Tamanrasset. It may be mentioned that at Poona the maximum intensity of 5577 Å occurs before midnight[3].

From the observations at Haute Provence and Cactus Peak, Roach, Williams and Pettit[4] concluded that the OI green line exhibits a maximum one hour after local midnight. Thus most of the stations record a maximum of intensity for the OI green line, around local midnight, though the exact time of occurrence of the maximum varies.

Seasonal Variations

For studying the seasonal variations, use was made of the data for all nights on which observations at 2300, zero and 0100 hours (local time) were

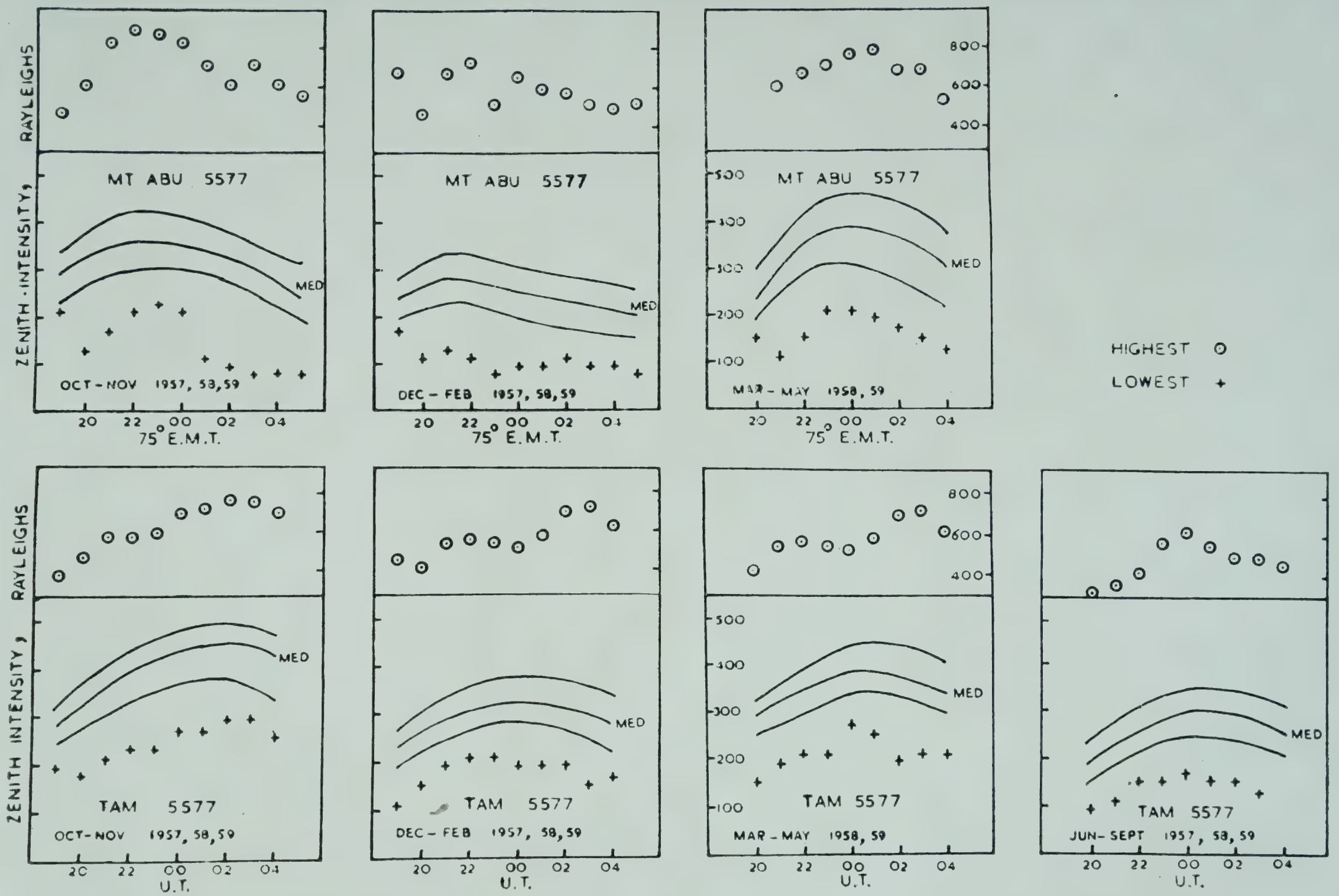

FIG. 5 — NOCTURNAL VARIATION OF INTENSITY AT MT ABU AND TAMANRASSET IN DIFFERENT SEASONS

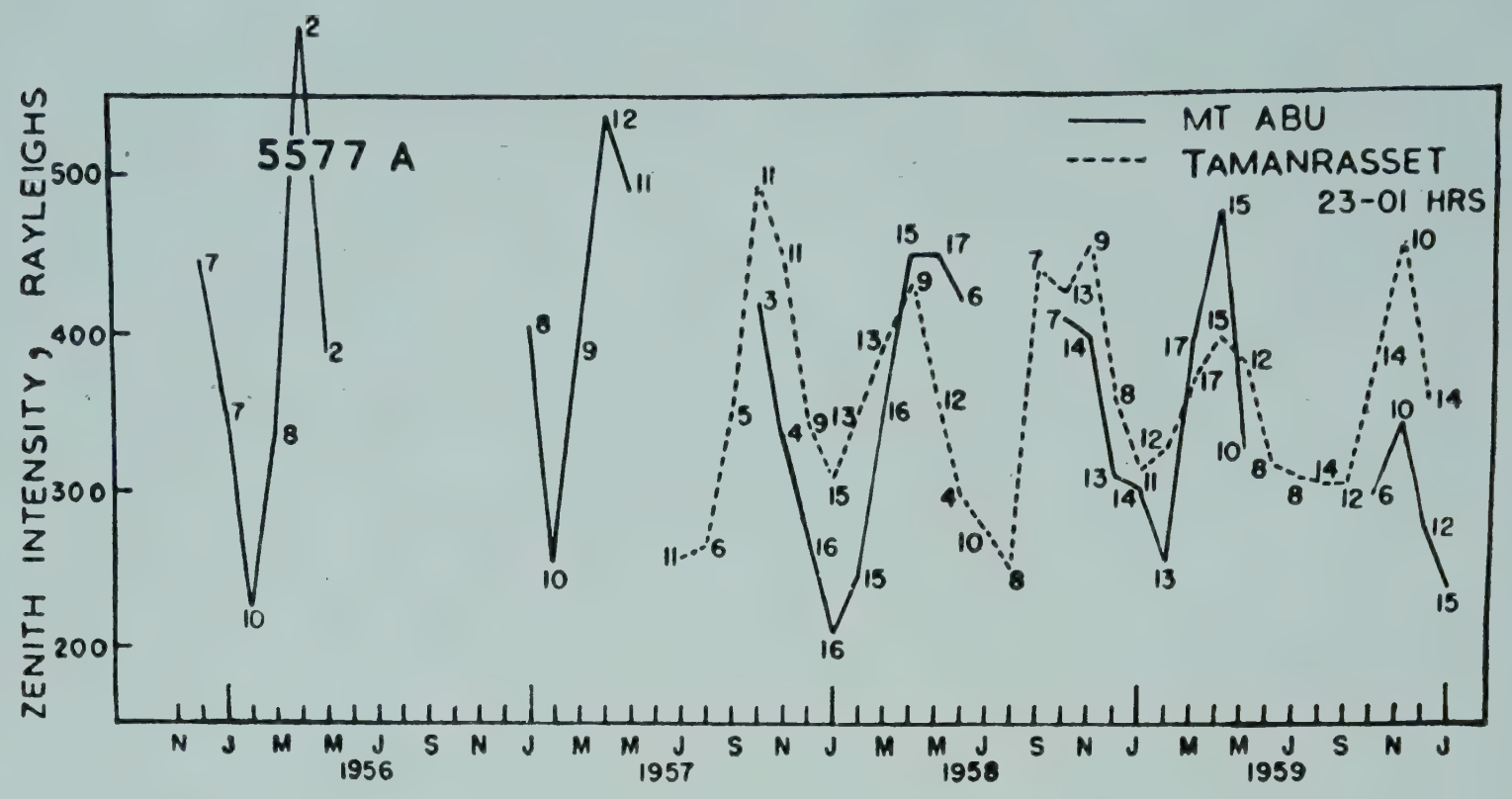

FIG. 6 — SEASONAL VARIATION OF AIRGLOW (5577 Å) AT MT ABU AND TAMANRASSET

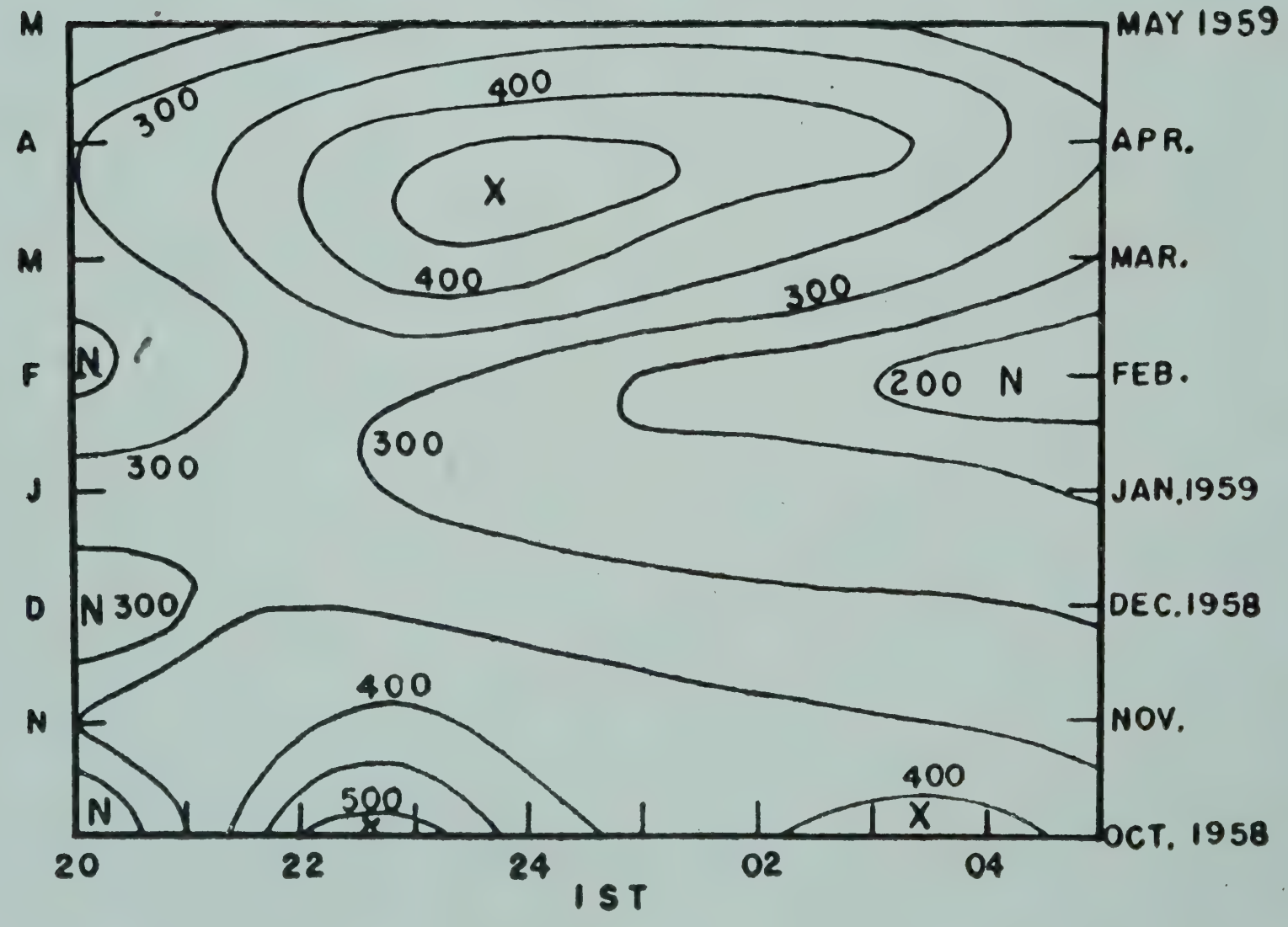

FIG. 7 — ISOPLETHS OF ZENITH AIRGLOW (5577 Å) INTENSITIES AT MT ABU DURING 1958–59

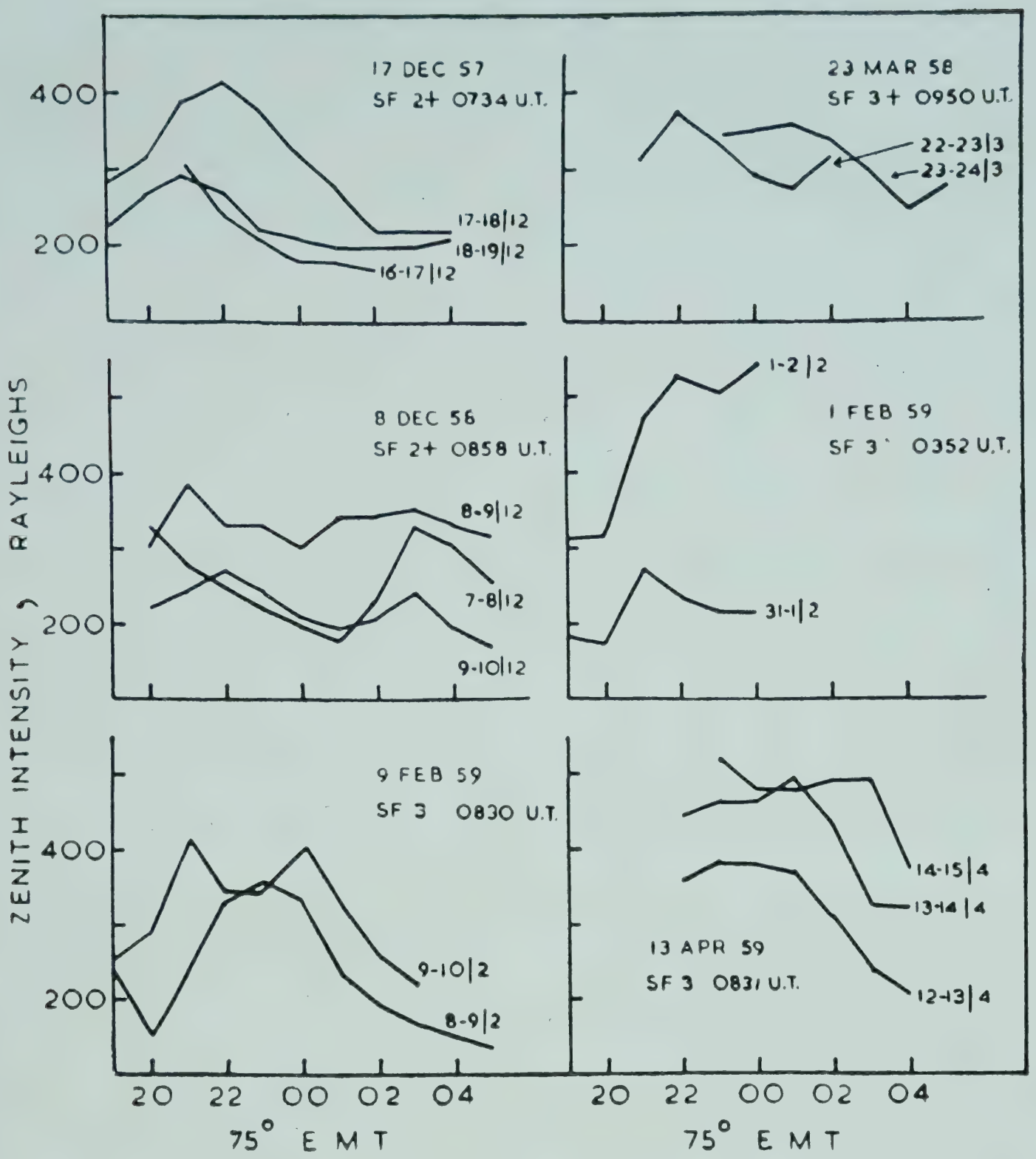

FIG. 8 — EFFECT OF SOLAR FLARES ON INTENSITY OF NIGHT AIRGLOW (5577 Å) AS OBSERVED AT MT ABU

made. The monthly mean intensities thus obtained (Fig. 6) clearly show a minimum in January–February and a maximum in April. In the same figure are shown the seasonal variations (data treated in the same way) at Tamanrasset during the IGY and IGC period. The seasonal variations at the two stations are similar in character.

The isopleth map in Fig. 7 summarizes the behaviour of the variations during the night in different seasons, of the zenith sky intensity, from October 1958 to May 1959. The diagram shows maxima in April and October and a minimum in February.

Tamanrasset observations show another minimum in June–September (Fig. 6).

The 5577 Å line thus shows in the sub-tropical regions two maxima during the year in the two equinoctial seasons and minima in winter and summer.

Effect of Magnetic Activity, Sunspot Frequency and Solar Flares on the Intensity of 5577 Å

An attempt was made to find if there is any effect of solar and magnetic activity on the intensity of OI 5577 Å line in the airglow. For this, only observations on nights for which data at 2300, zero and 0100 hours were available were used.

The seasonal variations were first removed in the following way:

The mean of the observations at 2300, zero and 0100 hours (local time) was obtained for each night. The monthly mean and annual average values were calculated from them. The ratio of the monthly mean to the annual mean was taken to be a characteristic of the month. The observed three-hourly intensities on each day were normalized by dividing the observed value by the ratio appropriate to that month. It is believed that this process would effectively remove the seasonal variations. These computed values were used for further analysis.

The data were divided in three groups depending on the magnetic activity of the day: (i) $\Sigma K < 10$, (ii) $10 < \Sigma K < 18$, and (iii) $\Sigma K \geqslant 18$. The data for magnetic activity at the nearest magnetic observatory, Alibag, were taken from Volumes 6–11 of the *Indian Journal of Meteorology and Geophysics* (1955–60). The mean intensities were obtained for each group. The results do not show any significant effect of magnetic activity on the variations of airglow.

In a similar way, the daily Zürich sunspot number (obtained from CRPL publication) were compared with the intensity of the airglow. It was observed that there was no relation between the airglow and sunspot number on a day-to-day basis.

It may be mentioned that Roach[5] from his studies at Cactus Peak and other low latitude stations did not find any significant correlation of airglow with either sunspots or magnetic activity.

An interesting result of the effect of some solar flares of class 2^+ and 3 on airglow has been observed and is illustrated in Fig. 8. Only flares which occurred from 0800 to 1600 hours (local time) were considered. Each set shows the intensities on three successive nights, one preceding the solar flare and the other two following the solar flare. The time of occurrence and the size of the flare (taken from CRPL data) are also mentioned. On the night following the solar flare an increase in the intensity of OI 5577 Å was generally observed.

Acknowledgement

The author is thankful to Prof. K. R. Ramanathan, Director, Physical Research Laboratory, for guidance and encouragement in the work.

References

1. Roach, F. E., *Rep. nat. Bur. Stand.*, (1958), 5591.
2. Roach, F. E., Tandberg-Hanssen & Megill, *J. atmos. terr. Phys.*, **13** (1958), 113.
3. Chiplonkar, M. W. & Kulkarni, P. V., *Indian J. Met. Geophys.*, **9** (1958), 133.
4. Roach, F. E., Williams, D. R. & Pettit, H. B., *J. geophys. Res.*, **58** (1953), 73.
5. Roach, F. E., *Ann. Geophys.*, **11** (1955), 214.

Atmospheric ozone over Mt Abu-Ahmedabad and its comparison with that over other stations in India and elsewhere

G. M. SHAH

Physical Research Laboratory
Ahmedabad

The results of ozone measurements made during 1952-59 at Mt Abu with Dobson spectrometer are summarized. The day-to-day and seasonal variations of ozone at Mt Abu are compared with those at other Indian stations and also at a few stations in Japan and Europe.

The amount of ozone at Mt Abu has been found to be the lowest in 1952 compared to other years. Large differences in ozone amounts have been observed between Mt Abu and Marcus Island and between Srinagar and Tateno. These differences have been discussed with reference to the air movements in the lower stratosphere and upper troposphere over India and over North-East Asia and North-West Pacific.

Vertical distributions of ozone calculated from 38 sets of umkehr measurements made during IGY-IGC at Mt Abu have also been presented. Significant changes of ozone have been found to take place particularly between 12 and 24 km. when the total ozone changes.

Comparison of ozone amounts measured by using the wavelength pair CC′ (3114/3324) and the pair AD (3055/3176) shows that measurements with AD are less subject to irregular variations.

Ozone is formed in the earth's upper atmosphere by the photochemical action of sun's ultraviolet radiation. Although present in small amounts, it plays an important part in the heat economy of the atmosphere and is also a very valuable tracer for studying dynamical processes in the atmosphere.

The quantity of ozone in the atmosphere is determined by measuring with a spectrophotometer the relative intensities of two narrow bands of solar

ultraviolet radiation, one well within the Hartley absorption band and the other just outside it.

The instrument most widely used for measurements of atmospheric ozone is the Dobson photoelectric spectrophotometer[1].

Ozone observations at Mt Abu have been regularly made since 1952 and they are available for studying long-term variations. Up to June 1957, ozone observations at Mt Abu were made with Dobson spectrophotometer No. 39. Dobson spectrophotometer No. 54 having metallized wedges was received at the Physical Research Laboratory, Ahmedabad, in May 1956. It was assembled and tested at Ahmedabad in September 1956.

The wavelength settings were checked using the emission lines 3021 Å and 3129 Å from a Philips mercury discharge lamp and 3404 Å from a cadmium lamp. The wedges were calibrated by using perforated thin blackened metal sheets of known transmission ratios.

New tables for the wavelength settings and for converting the dial readings R to log I/I' were prepared from the calibration of wedges at Ahmedabad in October 1956. Both total ozone and umkehr observations were made at Ahmedabad to test the consistency of the observations.

The instrument was transferred to Mt Abu (24°N) in June 1957 and the instrumental adjustments were again tested and the wedge was re-calibrated. Some small changes necessary in the λ settings were made. No appreciable change was found in the wedge calibration and the table for converting R to N prepared at Ahmedabad could be used at Mt Abu.

Regular ozone observations with the wavelength pairs $\lambda\lambda CC'$ and $\lambda\lambda AD$ were started at Mt Abu from July 1, 1957 with Dobson spectrophotometer No. 54. Umkehr measurements with wavelength pairs $\lambda\lambda A$, $\lambda\lambda C$ and $\lambda\lambda D$ were made on days of clear weather and especially when the total ozone amount was found to change rapidly. Umkehr curves were obtained on about 100 days and some of them were selected for calculating the vertical distribution of ozone.

Zenith sky measurements with Dobson spectrophotometer No. 54 were also made during 1957–58 on days when the zenith sky was covered with uniform clouds, but direct sun observations also were possible within a few hours of the zenith sky measurements. The aim of these measurements was to connect empirically the amount of total ozone obtained from zenith cloudy sky observations with those obtained with the direct sun.

Comparison of Values of Total Ozone in the Atmosphere measured with Dobson Spectrophotometer by using Wavelength Pairs $\lambda\lambda CC'$ and $\lambda\lambda AD$. The total ozone amount x, expressed in cm. at STP, is the thickness of a column of ozone of unit cross-section when the volume of

ozone present in the atmosphere is reduced to standard temperature and pressure.

Total ozone amounts were calculated at Mt Abu from direct sun observations with λλCC′ (λλ 3114/3324 and 3324/4536) according to the modified formula given by Ramanathan and Karandikar[2].

$$x = \frac{(L_0-L)-(\beta-\beta')m}{\mu(\alpha-\alpha')} - \frac{K'}{(\alpha-\alpha')}(\delta'-\delta'')$$

$$= \frac{(N-N_0)-100\,(\beta-\beta')m}{100\;\mu(\alpha-\alpha')} - \frac{K'}{(\alpha-\alpha')}(\delta'-\delta'')$$

where $100\ (L_0-L) \equiv (N-N_0)$.

In this method, observations both with short wavelengths and long wavelengths have to be taken; the latter were used to calculate $(\delta'-\delta'')$ which represents the effect of large particle scattering. Taking $\alpha-\alpha'$ to be 0·865, the correction term becomes 0·241 $(\delta'-\delta'')$.

Ozone amounts were also calculated from direct sun observations with λλAD using a difference method according to the formula given in the IGY Observers' Handbook for the ozone spectrophotometer[1].

Putting in the numerical values given in the Handbook, for observations with λλAD,

$$x = \frac{(N-N_0)_A-(N-N_0)_D}{1{\cdot}388\ \mu} - 0{\cdot}008$$

Values of total ozone amount determined by the AD method and by the CC′ method have been compared at Kodaikanal (10°N), Mt Abu (24°N)–Ahmedabad (23°) and Srinagar (34°N). The monthly mean differences between x_{AD} and $x_{CC'}$ are given in Table 1.

It can be seen from the table that on an average x_{AD} was greater than $x_{CC'}$ by about 0·007 cm. at Kodaikanal, 0·004 cm. at Mt Abu and 0·009 cm. at Srinagar. A few large fluctuations were found on some individual days at Srinagar. The advantage of using the AD difference method over the CC′ method is that the correction due to haze or large particle scattering is practically eliminated.

Day-to-day Variations of Ozone over Mt Abu during 1952-59. Fig. 1 gives the daily values of total ozone amount at Mt Abu from 1952 to 1959.

During 1952–55, the maximum amount of ozone occurred in May–June and in 1956–58 in March–April. The quantity of ozone generally starts falling in June, remains constant during the monsoon months and then undergoes a further decrease, reaching a minimum in November–December. In

TABLE 1 — MONTHLY MEAN DIFFERENCES BETWEEN x_{AD} AND $x_{CC'}$ AT KODAIKANAL, MT ABU AND SRINAGAR

(Number in brackets denotes the number of observations for the month)

Year	Month	Kodaikanal	Mt Abu	Srinagar
1957	June	—	0·006 (25)	—
	July	—	0·006 (16)	—
	Aug.	—	0·005 (14)	0·006 (28)
	Sept.	—	0·004 (26)	0·012 (15)
	Oct.	—	0·004 (28)	0·010 (21)
	Nov.	—	0·004 (28)	0·010 (24)
	Dec.	—	0·005 (29)	0·010 (17)
1958	Jan.	—	0·005 (29)	0·010 (20)
	Feb.	—	0·004 (28)	0·010 (10)
	Mar.	—	0·004 (31)	0·010 (21)
	Apr.	—	0·005 (29)	0·010 (29)
	May	0·015 (17)	0·005 (31)	0·009 (30)
	June	0·014 (13)	0·003 (26)	0·004 (30)
	July	0·013 (13)	0·003 (4)	0·004 (22)
	Aug.	0·014 (4)	0·003 (16)	0·006 (31)
	Sept.	0·014 (20)	0·004 (9)	0·005 (28)
	Oct.	0·010 (11)	0·004 (25)	0·004 (29)
	Nov.	0·011 (23)	0·003 (28)	0·008 (28)
	Dec.	0·011 (23)	0·003 (29)	0·006 (9)
1959	Jan.	0·011 (22)	0·003 (28)	0·014 (10)
	Feb.	0·011 (20)	0·003 (26)	0·011 (20)
	Mar.	0·005 (30)	0·003 (27)	0·010 (27)
	Apr.	0·005 (17)	0·004 (29)	0·014 (29)
	May	0·005 (16)	0·004 (29)	0·008 (16)
	June	0·004 (10)	0·004 (23)	0·009 (30)
	July	0·003 (8)	—	0·008 (28)
	Aug.	0·007 (12)	—	0·008 (30)
	Sept.	0·007 (13)	0·004 (5)	0·006 (25)
	Oct.	0·009 (9)	0·005 (18)	0·004 (28)
	Nov.	0·006 (13)	0·003 (24)	0·009 (29)
	Dec.	0·002 (16)	0·004 (29)	0·006 (31)
1960	Jan.	0·004 (21)	0·005 (20)	0·005 (24)
	Feb.	0·006 (14)	0·003* (24)	0·006 (17)
	Mar.	0·005 (22)	0·004* (24)	0·007 (21)
	Apr.	0·004 (20)	0·005* (27)	0·013 (26)
	May	0·005 (10)	0·005* (28)	0·014 (27)
	June	0·005 (14)	0·005* (20)	0·011 (27)
	July	0·005 (7)	0·005* (7)	0·010 (29)
	Aug.	0·005 (12)	0·005* (3)	0·012 (23)
	Sept.	0·007 (8)	0·005* (22)	0·011 (28)
	Oct.	0·006 (6)	0·005* (26)	0·012 (29)
	Nov.	0·004 (7)	0·004* (28)	0·011 (27)
	Dec.	0·005 (22)	0·005* (24)	0·006 (18)
	Av.	0·007	0·004	0·009

*Observations were made at Ahmedabad and not at Mt Abu

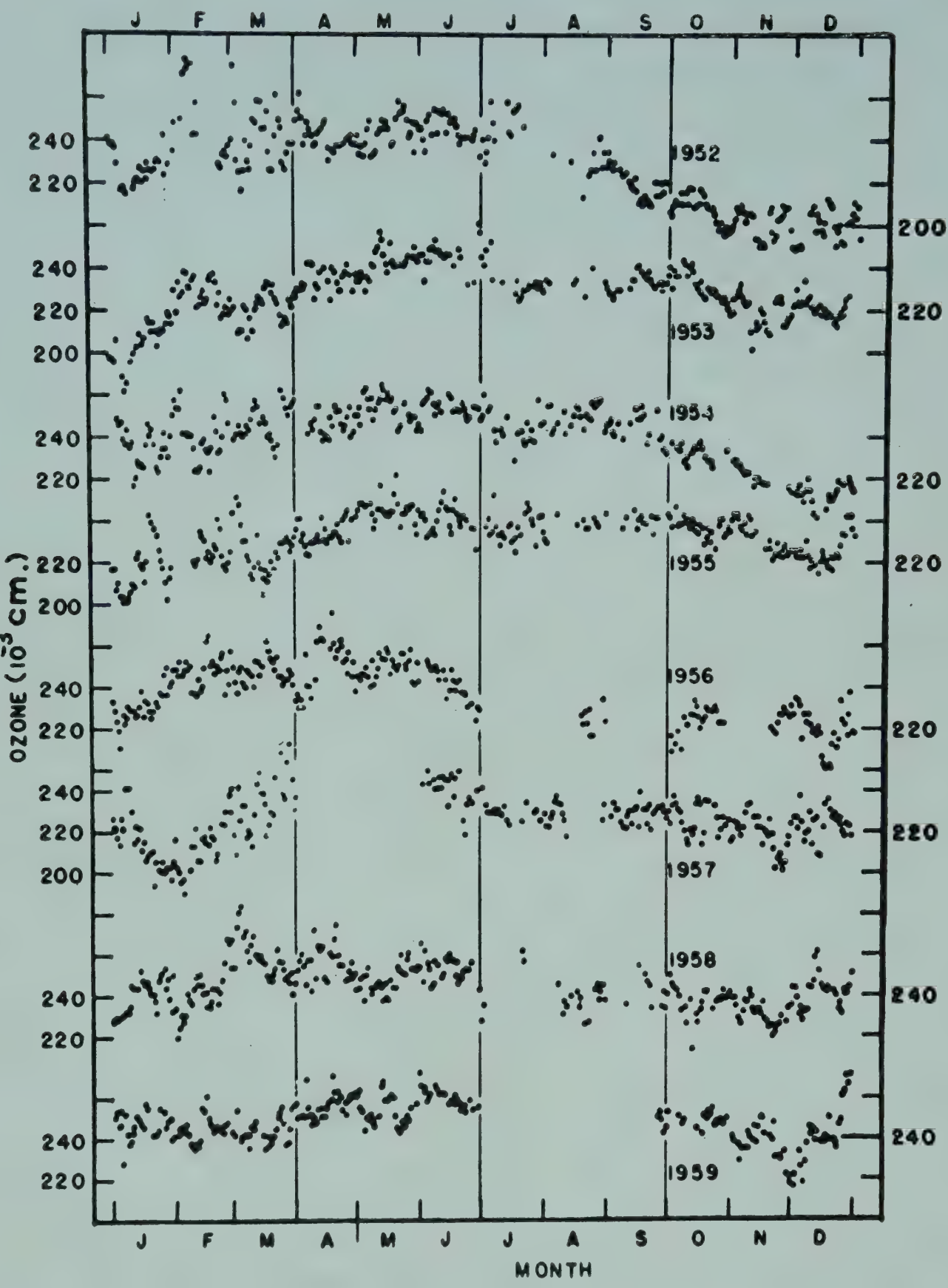

FIG. 1 — DAILY VALUES OF OZONE OVER MT ABU (1952–59)

January the ozone amount begins to rise. In the autumn of 1952, the ozone amounts were lower than those in the autumn of other years, the mean value with Vigroux' coefficients being 0·190 cm.

Comparison of day-to-day Variations of Ozone Amounts over Mt Abu with those of other Indian Stations during 1957-59. The day-to-day values of ozone amounts over Srinagar (34°N), Delhi (28·5°N), Mt Abu (24°N) and Kodaikanal (10°N) during 1957, 1958 and 1959 are given by Figs. 2, 3 and 4 respectively.

The noteworthy point is that over North India the day-to-day fluctuations in ozone amounts are largest in January–March when active western

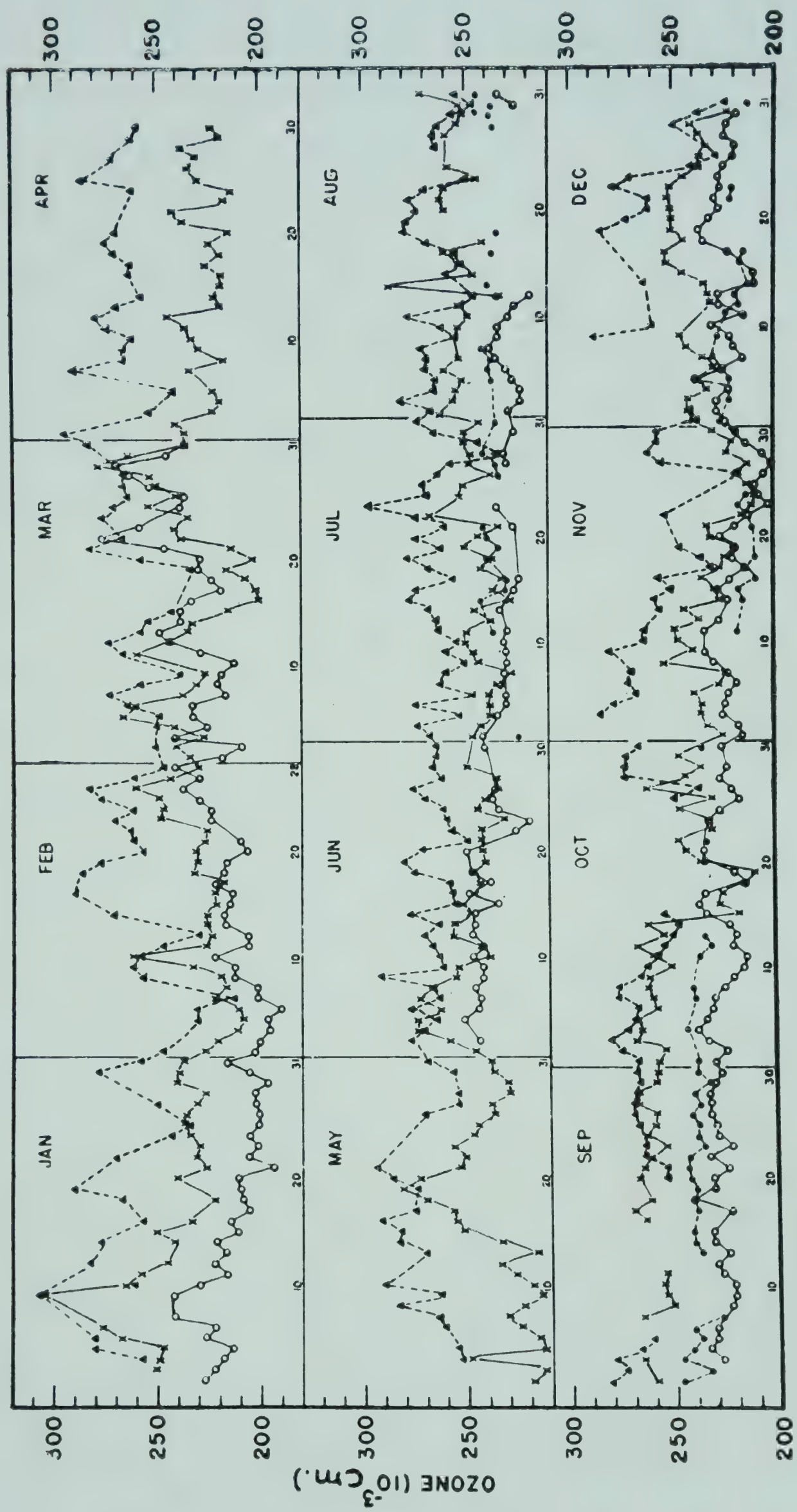

FIG. 2 — DAILY VALUES OF OZONE AT SRINAGAR, DELHI, MT ABU AND KODAIKANAL (1957)

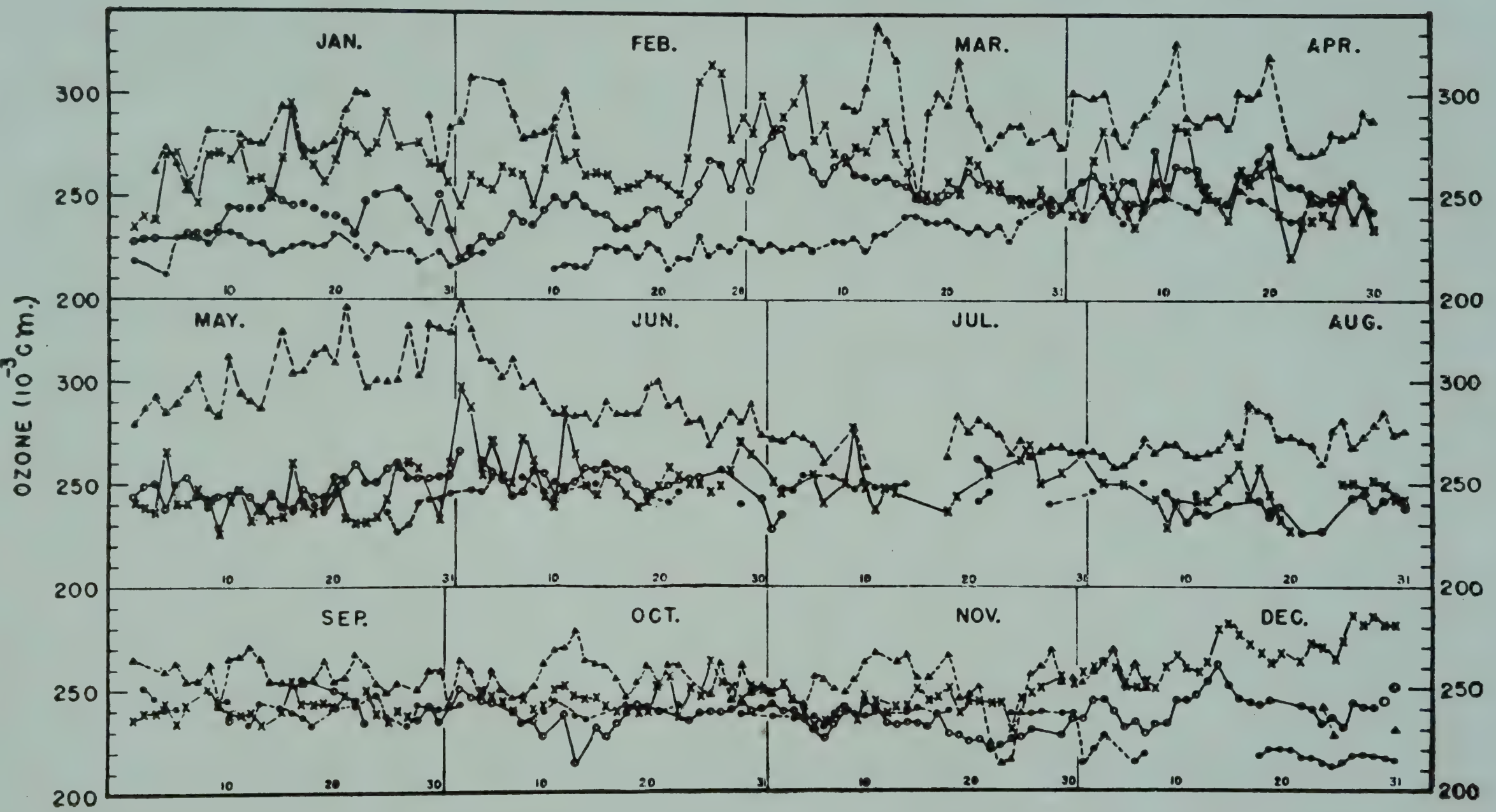

FIG. 3 — DAILY VALUES OF OZONE AT SRINAGAR, DELHI, MT ABU AND KODAIKANAL (1958)

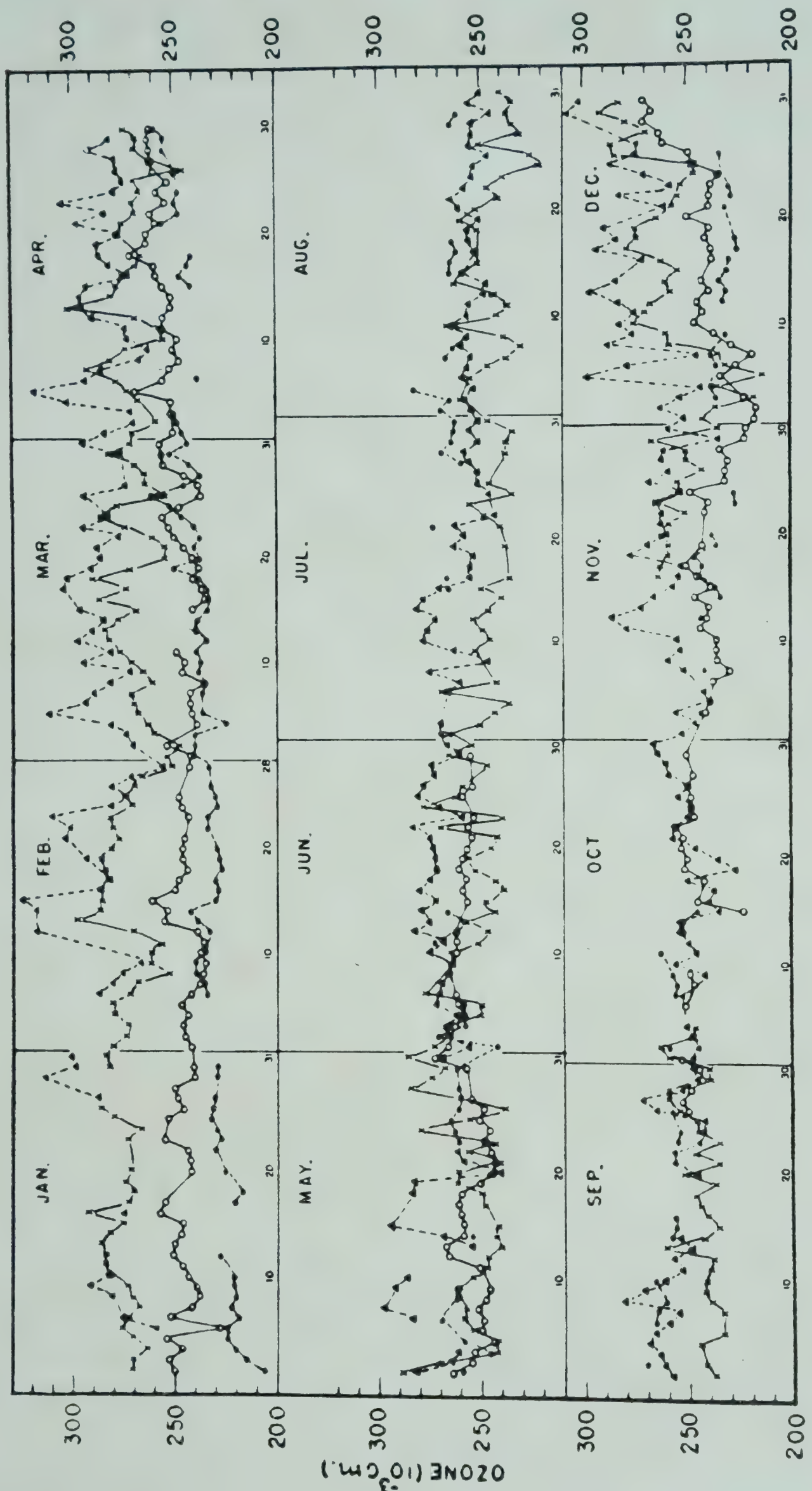

FIG. 4 — DAILY VALUES OF OZONE AT SRINAGAR, DELHI, MT ABU AND KODAIKANAL (1959)

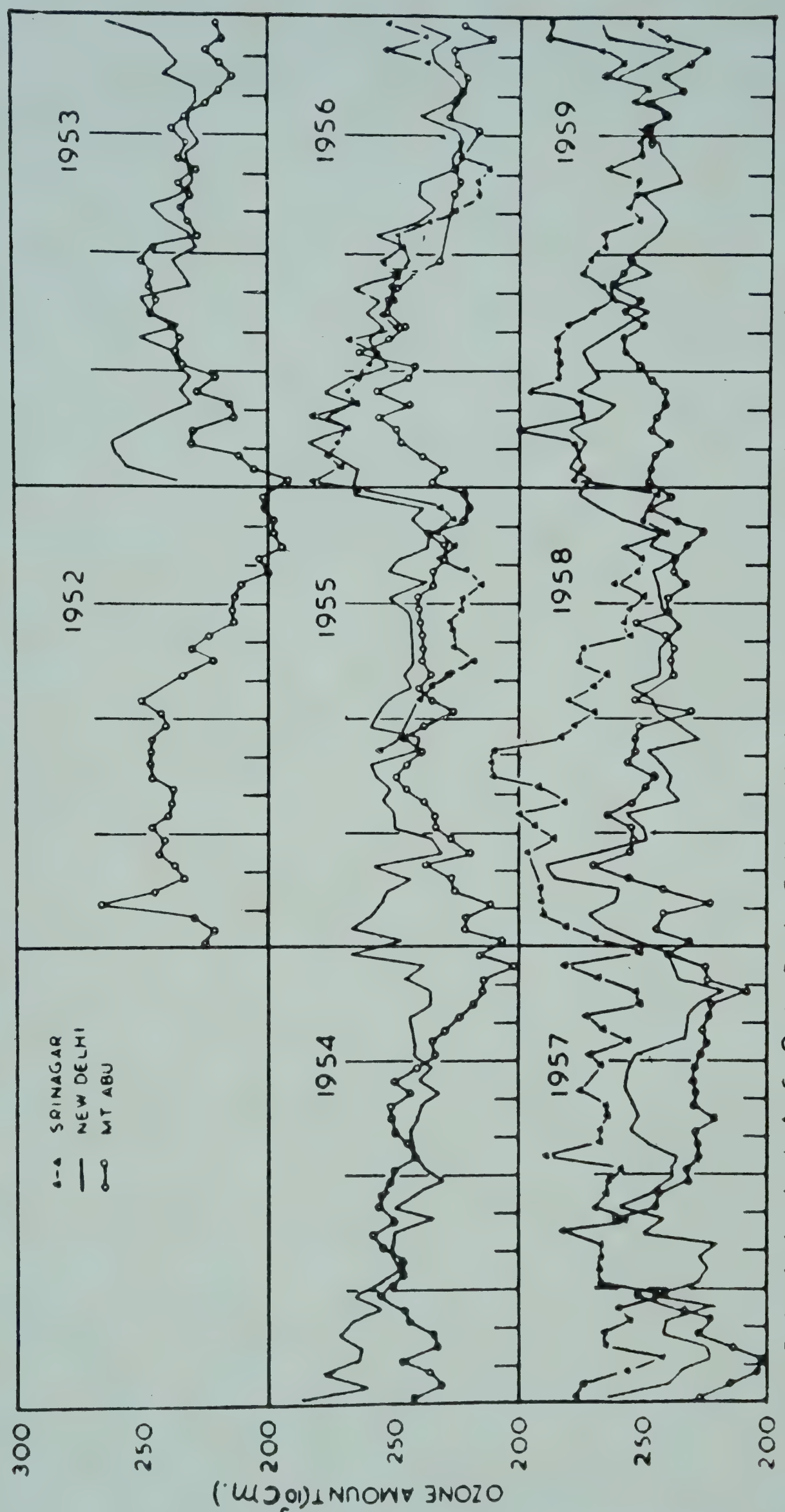

FIG. 5 — TEN-DAY MEAN OZONE AMOUNTS AT SRINAGAR, DELHI AND MT ABU (1952–59)

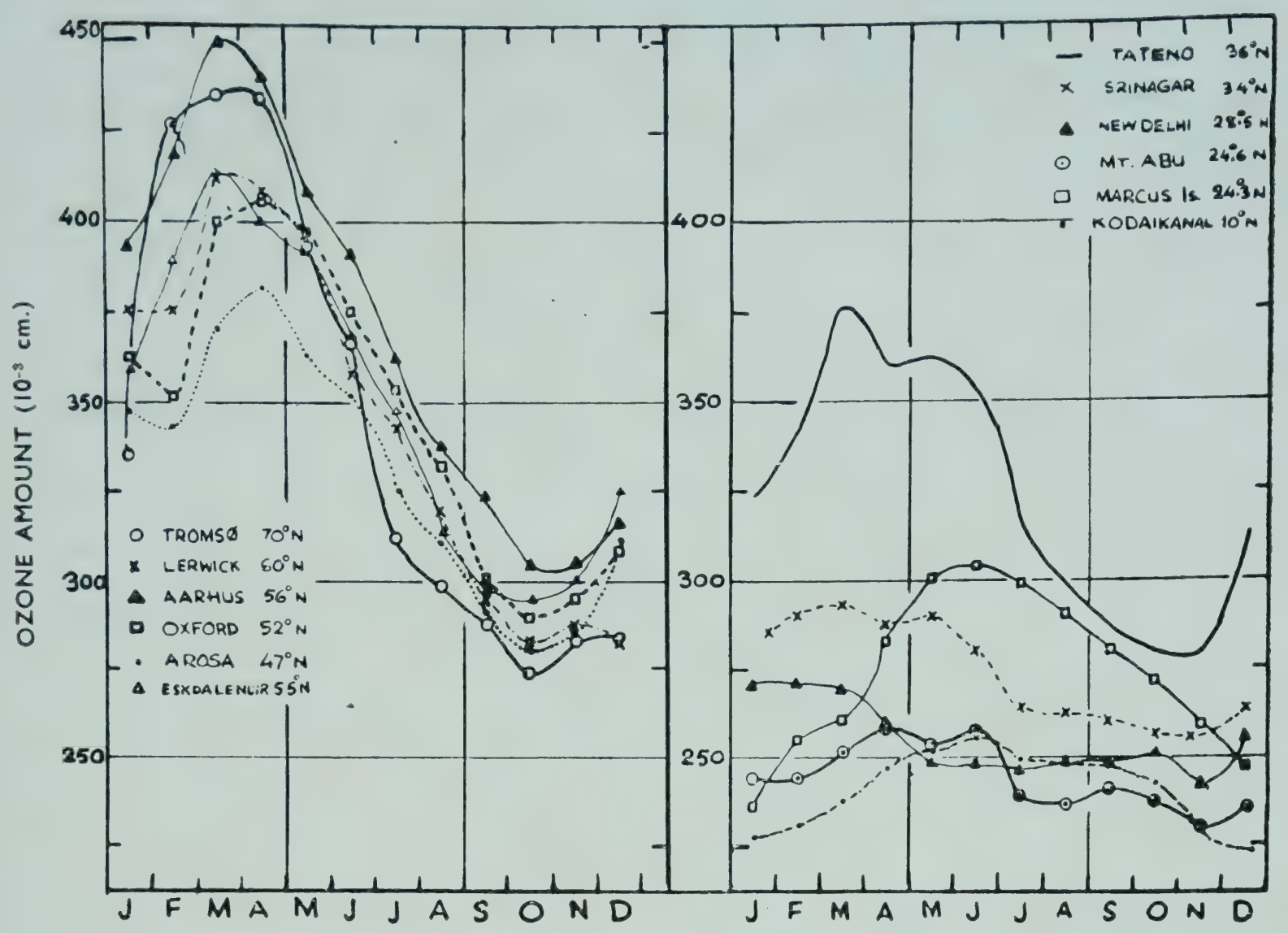

FIG. 6 — MEAN MONTHLY OZONE AMOUNTS AT A FEW SELECTED STATIONS IN EUROPE AND ASIA (1957–59)

disturbances pass across the country. The gradient of ozone amount between South India and North India is greatest in January–February. In 1957–58, there were large gradients of ozone between Delhi and Srinagar even in April–May.

Seasonal Variations of Ozone over Mt Abu and other Indian Stations. The ten-day means of ozone amounts at Mt Abu, Srinagar and Delhi from 1952 to 1959 are shown in Fig. 5.

At Srinagar and Delhi, the maximum ozone values occur in January–February, whereas at Mt Abu it is shifted to April–May.

The minimum at Mt Abu occurs in autumn. It occurs earlier in the year both at Delhi and Srinagar. By the end of November, the ozone values at Delhi start increasing, while at Mt Abu a slow rise takes place in the beginning of December, followed by a more rapid rise in the middle of January. In Srinagar, the rise of ozone takes place even earlier than at Delhi. Both at Srinagar and Delhi the decrease in ozone starts in April and the minimum is reached in October–November.

The maximum values at Srinagar, Delhi and Mt Abu increase with latitude.

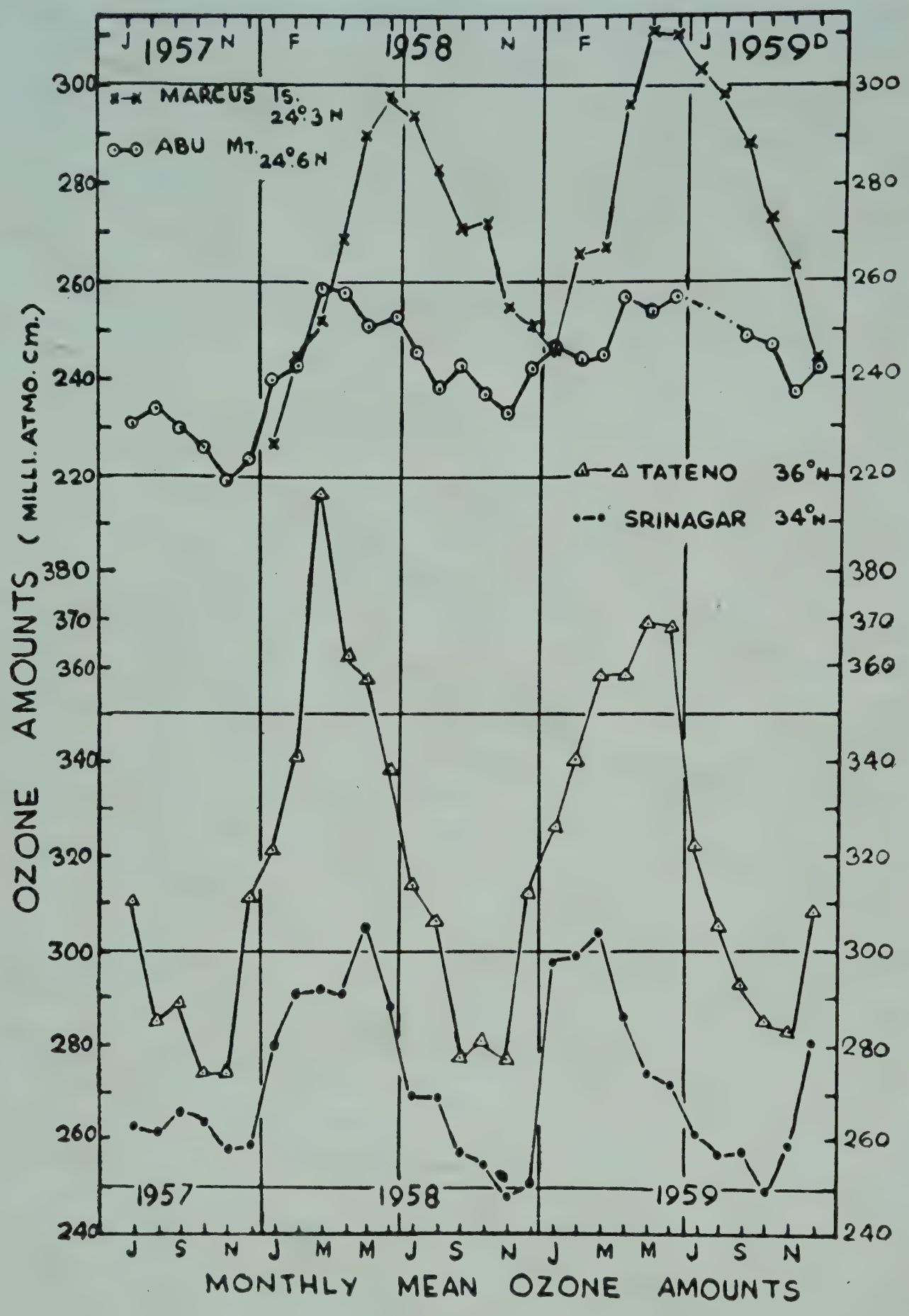

FIG. 7 — MONTHLY MEAN OZONE AMOUNTS AT (i) MARCUS ISLAND AND MT ABU, AND (ii) SRINAGAR AND TATENO

Fig. 6 gives the mean monthly ozone amounts at a few selected stations in the northern hemisphere in Europe and Asia. The monthly mean values of ozone for Tromsø (70°N), Lerwick (60°N), Aarhus (56°·2N), Eskdalemuir (55°·3N), Oxford (52°N) and Arosa (47°N) in Europe, and Tateno (36°N), Srinagar (34°N), Delhi (28°·5N), Mt Abu (24°·6N), Marcus Island (24°·3N) and Kodaikanal (10°N) in Asia, are based on the average of ozone data collected during the IGY–IGC period.

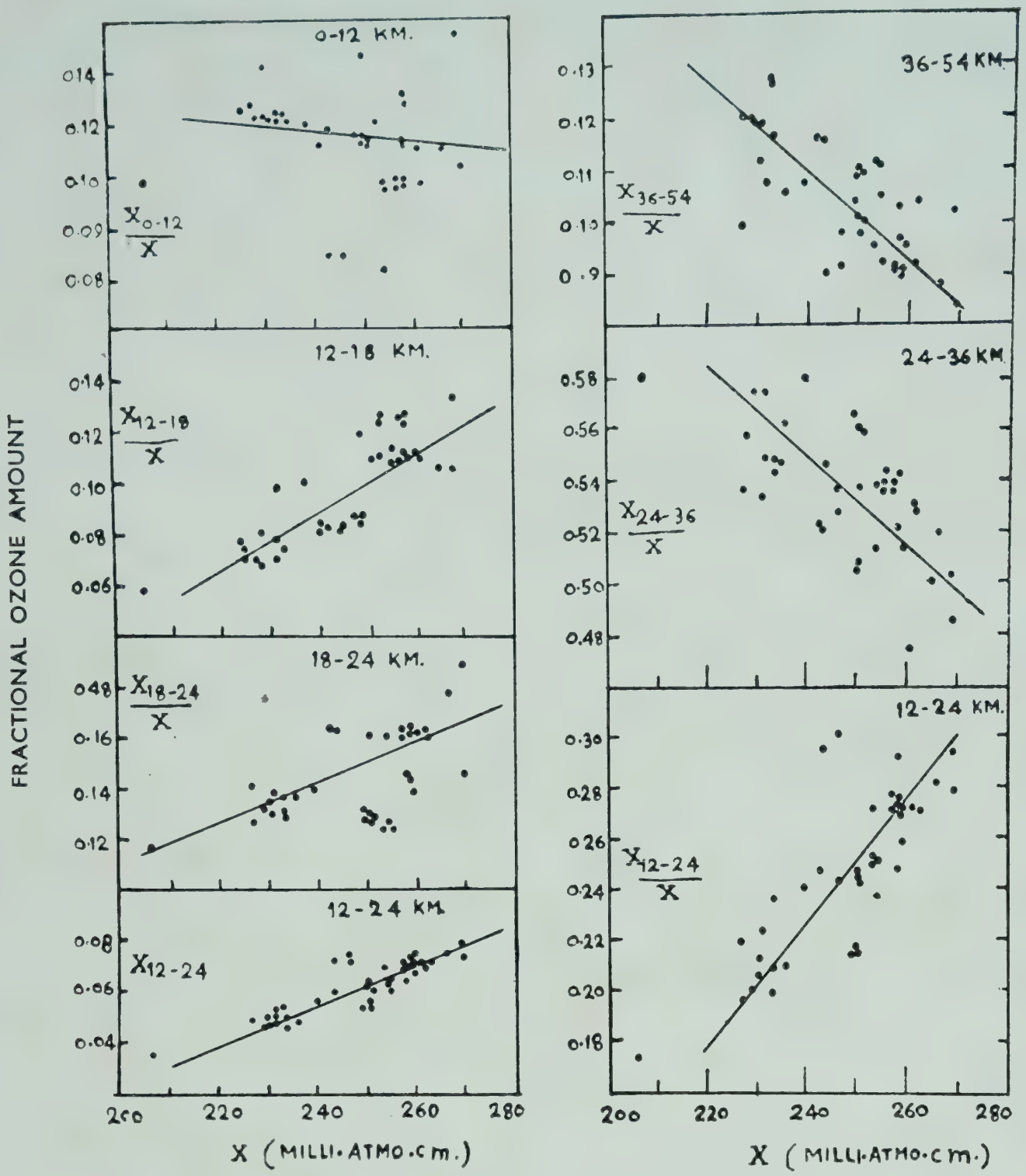

FIG. 8 — SCATTER DIAGRAM OF FRACTIONAL OZONE AMOUNTS IN VARIOUS 12 KM. LAYERS ABOVE SEA LEVEL OVER MT ABU AGAINST TOTAL OZONE AMOUNTS

The interesting feature of the diagram is that all the Indian stations including Srinagar fall in a group apart from Japanese stations with low ozone values. Tateno and Marcus Island in Japan fall in a group corresponding to higher latitudes where seasonal variations of ozone amounts are markedly larger, even though the latitudes of these two stations are nearly equal to those of Srinagar and Mt Abu respectively.

Fig. 7 gives the monthly mean ozone amounts of (i) Mt Abu and Marcus Island, and (ii) Tateno and Srinagar for the IGY–IGC period. The ozone values at Marcus Island become comparable to those at Mt Abu in November–December.

Similarly, Tateno in Japan shows much higher values than Srinagar in India in winter months, even though both are nearly at the same latitudes (36°N

TABLE 2 — VERTICAL OZONE DISTRIBUTION OVER MT ABU FROM UMKEHR OBSERVATIONS

(*Each layer is* 6 *km. thick. Layer* 1 *is* 0–6 *km., layer* 2 *is* 6–12 *km., etc.*)

Date	Total ozone *m. atm.-cm.*	Amount of ozone in layers *m. atm.-cm. km.*$^{-1}$								
		1	2	3	4	5	6	7	8	9
18-6-57	239	1·3	2·7	4·0	5·6	15·3	8·6	2·7	0·8	0·8
23-11-57	207	1·3	2·0	2·9	4·9	13·3	6·0	2·7	0·8	0·7
26-11-57	207	0·7	2·0	2·0	4·0	12·6	8·0	2·8	0·8	0·7
27-11-57	202	1·3	2·0	2·7	3·8	11·7	8·0	2·7	0·9	0·7
6-1-58	233	2·0	2·0	2·7	5·1	14·6	7·5	2·9	1·1	0·9
8-1-58	229	1·3	2·7	2·9	4·6	13·3	8·6	2·9	1·1	0·5
26-1-58	249	1·3	2·7	3·6	5·3	15·3	9·0	2·7	0·8	0·5
30-1-58	254	0·7	1·3	4·6	5·3	16·0	10·5	2·4	0·8	0·7
3-2-58	229	2·0	2·0	2·7	5·1	14·6	7·3	2·7	0·9	0·9
7-2-58	230	2·0	2·0	2·7	5·1	14·6	7·4	2·7	0·9	0·9
10-2-58	254	0·5	2·7	5·3	5·3	14·6	9·3	2·7	1·3	0·4
11-2-58	244	0·7	2·0	4·0	7·7	14·6	7·3	2·4	1·2	0·9
13-2-58	250	1·3	2·7	3·6	6·7	15·4	7·8	2·7	1·1	0·4
22-2-58	243	2·0	2·0	3·3	6·7	14·6	7·3	2·9	1·3	0·4
23-2-58	250	1·3	2·7	3·6	5·3	15·4	8·8	2·7	1·1	0·8
25-2-58	269	1·3	2·4	4·6	8·5	15·4	7·8	2·9	0·9	0·7
23-4-58	257	0·9	2·7	4·8	7·1	14·6	8·5	2·4	1·2	0·8
25-4-58	250	1·3	2·7	3·6	5·3	15·4	8·8	2·8	1·1	0·7
18-5-58	243	0·7	1·3	3·3	8·7	14·6	8·4	2·0	0·9	0·7
19-5-58	246	0·7	1·3	3·3	9·1	14·6	8·3	2·0	0·9	0·8
21-5-58	257	0·7	2·7	4·7	6·9	14·6	9·3	1·6	1·2	1·1
22-5-58	266	1·3	2·7	4·6	7·8	14·6	9·3	1·6	1·2	1·1
24-5-58	258	0·7	2·7	4·8	7·0	14·6	9·3	1·7	1·2	0·9
27-5-58	258	0·7	2·7	4·8	6·9	14·6	9·8	1·6	1·2	1·1
30-10-58	242	1·8	2·0	3·3	6·7	14·6	7·3	3·1	1·3	0·3
19-11-58	227	2·0	2·0	2·7	4·8	14·6	7·3	2·7	0·9	0·9
22-11-58	223	2·0	2·4	3·3	4·4	13·3	7·3	2·9	0·9	0·7
24-11-58	229	2·0	2·7	4·0	4·4	13·3	7·3	2·9	0·9	0·7
24-12-58	233	2·0	2·0	3·1	5·1	14·6	7·4	2·9	0·9	0·7
7-4-59	250	2·0	3·3	4·9	5·3	14·1	7·8	2·7	1·1	0·4
8-4-59	250	2·0	3·3	4·6	5·6	14·1	7·8	2·7	1·1	0·4
13-4-59	254	0·5	2·7	5·3	5·3	14·6	9·1	2·7	1·3	0·7
15-4-59	254	0·5	2·7	5·0	5·6	14·6	9·0	2·8	1·3	0·7
17-4-59	259	1·3	3·3	5·4	5·7	14·0	9·2	1·6	1·3	0·9
22-4-59	262	0·7	2·7	4·8	7·5	14·6	9·3	2·4	1·2	0·9
1-5-59	269	2·7	3·3	6·0	6·5	13·3	9·3	1·6	1·2	0·9
7-5-59	253	1·3	4·0	7·0	9·6	10·6	5·3	2·7	0·7	0·5
14-5-59	261	1·2	2·7	4·8	7·5	14·6	9·3	1·6	1·2	1·0

and 34°N). In August–September the difference between the ozone values of Tateno and Srinagar is small.

Discussion

The larger ozone amounts at Tateno and Marcus Island compared to those at Srinagar and Mt Abu may be explained as due to the frequent occurrence of subsidence of air in the lower stratosphere and upper troposphere over Japan from the region of the Siberian anticyclone and the associated cold waves from the north-west[3].

The Indian summer monsoon and the Himalayas are responsible for throwing up considerable quantities of water vapour into the upper troposphere and lower stratosphere, and this would exert a depressing influence on the ozone amounts in the monsoon region south of the Himalayas.

For a better understanding of the seasonal variation of ozone it is necessary to know the changes in its vertical distribution. It is found that when the total ozone amount changes, significant changes of ozone take place, particularly in 12–24 km. Fig. 8 shows a scatter diagram of the fractional ozone amounts in various 12 km. thick layers over Mt Abu against the total ozone amounts. These were calculated from umkehr observations on different days during the period 1957–59 by the method B, suggested by Ramanathan and Dave[4]. Table 2 gives ozone distributions on different days.

Acknowledgement

Thanks of the author are due to the Director-General of Observatories of the India Meteorological Department for making available the data collected by the observers of the Department. Thanks are also due to the Director of the Aerological Observatory at Tateno who sent regularly the bulletins of the Tateno Observatory containing ozone and upper air data of Japanese stations. The author is greatly indebted to Prof. K. R. Ramanathan for his interest and guidance at all stages of the work.

References

1. Dobson, G. M. B., *Ann. IGY*, **5** (1957–58), 46–81.
2. Ramanathan, K. R. & Karandikar, R. V., *Quart. J. roy. met. Soc.*, **75** (1949), 257.
3. Kulkarni, R. N., Angreji, P. D. & Ramanathan, K. R., *Met. & Geophys., Japan*, **10**(2) (1959), 85.
4. Ramanathan, K. R. & Dave, J. V., *Ann. IGY*, **5** (1957), 23.

Airglow observations on OI 5577 Å at Srinagar (1958-60)

P. D. ANGREJI

Physical Research Laboratory
Ahmedabad

Airglow data on OI 5577 Å obtained during 1958-60 at Srinagar (ϕ 34°N) have been compared with those obtained at Mt Abu, Tamanrasset and Kakioka. The monthly means of nocturnal and seasonal variations have also been analysed. An attempt is made to see any possible covariation of the airglow intensity with the magnetic activity (u_1) and the sunspot number (R_z).

As part of the IGY programme, regular observations of OI 5577 Å in the night airglow were started at Srinagar, Kashmir (ϕ 34°05′N : 74°50′E; 1586 m.), in March 1958 and continued till November 1960. During this period, observations were possible on about 340 clear moonless nights. On about 300 of these nights, continuous observations could be taken for 3 hr or more. The main results of the analysis of these observations are presented in this paper.

Description and Calibration of Photometer

The night sky photometer, which was made at the Physical Research Laboratory, Ahmedabad, and used at Srinagar, covers a circular field of 10°·2 diam. Its sensing element consists of a photomultiplier (RCA 931-A) combined with two interference filters. The filters are mounted on a rotatable metal disc and can be manipulated by a suitable clock mechanism to occupy positions in front of the photomultiplier one after the other after every 3 min. At every change of the filter, there is an interval of 15 sec. during which all light is cut off from the photomultiplier and the dark current level recorded. The output signal is fed to a high-gain, differential type d.c. amplifier, and the amplified current is recorded by an Evershed-Vignoles

recorder, the chart speed used being 1 in./hr. The filters have peak transmissions near 5600 and 5300 Å, the former transmits the 5577 Å line and latter is used to monitor the background continuum radiation.

The spectral characteristics of the optical filters and the net transmission of the photometer assembly are shown in Fig. 1. The continuous lines give the filter transmissions and the broken lines show (in arbitrary units) the effective spectral response of the optical assembly taking into account the relative response of the photomultiplier. The half band-widths of the 5300 and 5600 Å filters were 115 and 85 Å, and the equivalent band-widths (or integrated effective transmission in terms of the transmission at 5577 and 5300 Å) taking into account the photomultiplier response were 208 and 129 Å respectively.

The photometer was pointed towards the celestial pole to avoid the varying stellar background. The constancy of the sensitiveness of the photometer was checked by taking records on the same chart, both before and after every night's observation, of the light of a radioactive luminescent source.

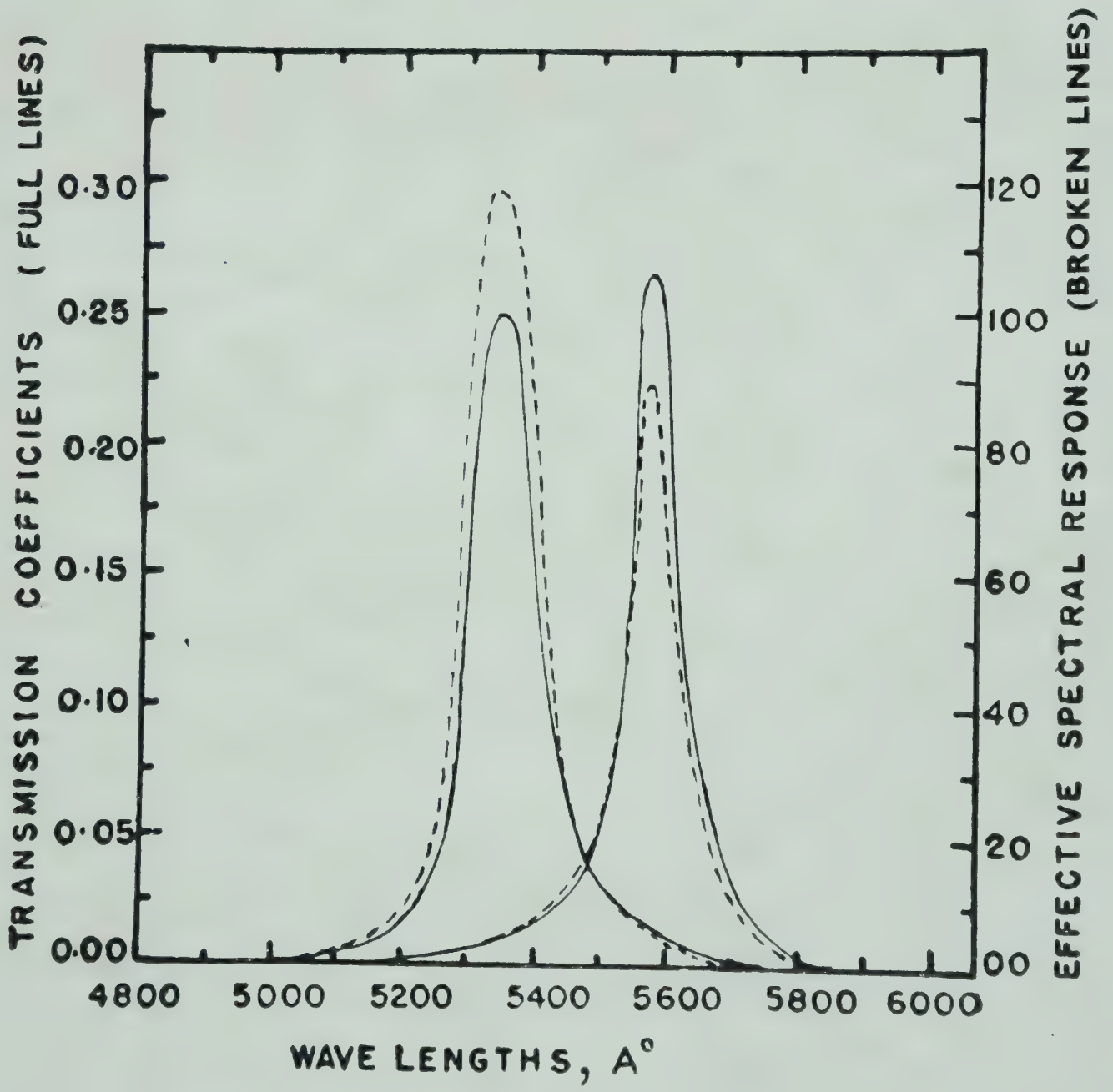

FIG. 1 — SPECTRAL CHARACTERISTICS OF OPTICAL FILTERS AND NET TRANSMISSION OF PHOTOMETER ASSEMBLY

The photometer was independently calibrated against the brightness of a magnesium oxide diffusing screen illuminated by a standard Philips type W-4 tungsten filament lamp of known spectral characteristics. It was found that a recorder current of 1 μa. corresponds to 1·721 Rayleighs for 5577 Å, and to 1·316 Rayleighs for 5300 Å, the normalized equivalent bandwidths being 100 Å. The radioactive luminescent source at Srinagar was compared in January 1958 with the photometer at Mt Abu. The latter was intercompared in May 1958 with the portable standard photometer of Dr Roach[1].

The values of I_z/I_0 relating to Cactus Peak[2], which is at nearly the same latitude and elevation as Srinagar, have been used for converting the poleward intensities to zenith sky intensities. The values are:

$$I_{\text{zenith}} = I_{\text{pole}}/1{\cdot}637 \text{ for } 5577 \text{ Å}$$

and

$$I_{\text{zenith}} = I_{\text{pole}}/1{\cdot}134 \text{ for } 5300 \text{ Å}$$

Following the two-colour method of Roach[1], the reported intensities for 5577 Å were corrected for the contaminating radiation due to background continuum. As the two-colour method in the case of 5577 Å very nearly eliminates the contamination due to OH band[3], no special correction for it was made.

Results

Nocturnal Variations. The systematic trends in the nocturnal variations come out clearly in spite of some sporadic variations of small magnitude and low frequency, their contributions being averaged out in summation. The annual and the seasonal mean variations are shown in Fig. 2.

A study of the figure leads to the following inferences:

(i) The intensity of 5577 Å is maximum at about midnight; in the summer months, the maximum is broad and occurs later than midnight, whereas in the winter period the maximum is relatively well defined and occurs shortly after midnight. In autumn and winter, the pre-dawn values are lower than post-dusk values, while in spring and summer, the pre-dawn values are higher.

(ii) In the equinoctial periods, the intensities are higher; the autumn values are the highest.

(iii) In the equinoctial months, the rates of increase of intensity in the pre-midnight hours are higher, the highest being in September and the next highest in April.

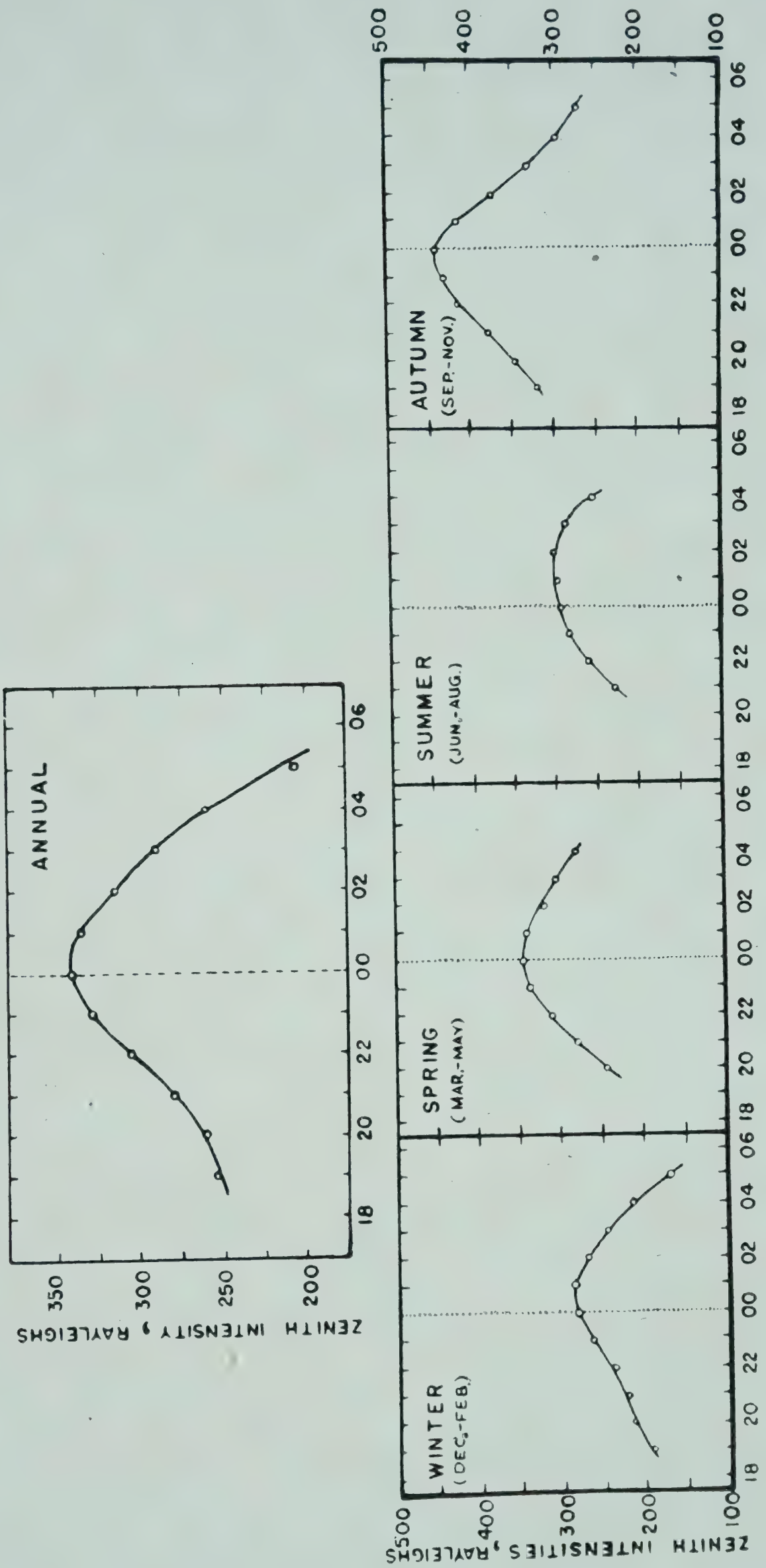

FIG. 2 — MEAN AND SEASONAL NOCTURNAL VARIATIONS

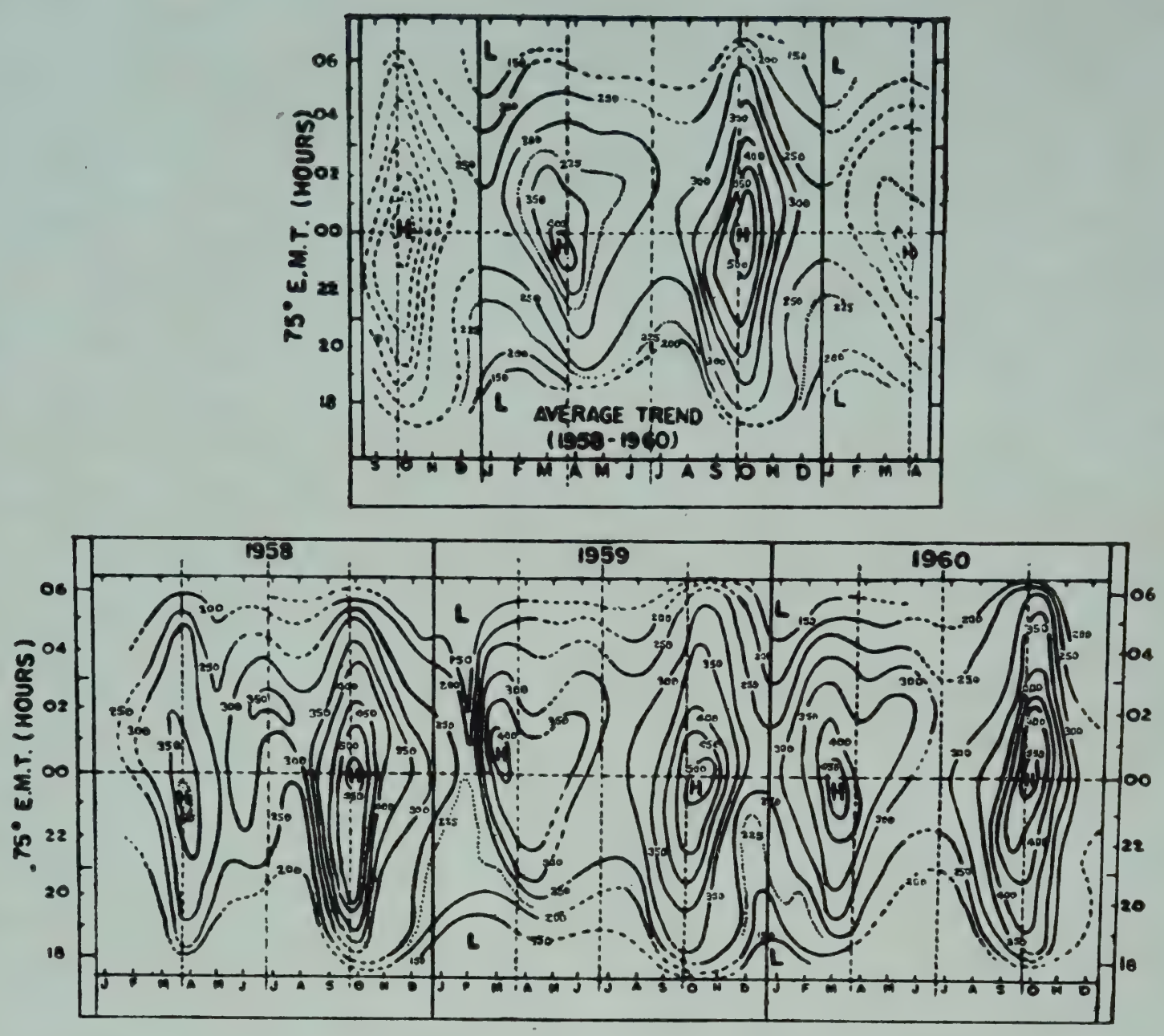

FIG. 3 — ISO-PHOTO MAPS (INTERVAL — 50 R) OF AIRGLOW 5577 Å INTENSITIES AT SRINAGAR (1958–60)

(iv) In general, the earlier the time of maximum (measuring from the twilight end) the faster is the change in intensity.

Seasonal Variations. The contour map (Fig. 3) displays all the nocturnal and seasonal features. The upper part of the figure gives a pictorial resume of the variations. In the lower portion is given the actual behaviour in the individual months of the whole period 1958–60. The missing data are indicated by broken lines. There is a regular annual variation with maxima in the equinoxes and minima in the solstices.

Year-to-Year Variations. In Fig. 4 the mean values of the intensity of 5577 Å (I) for each month of the period June 1957–December 1960, the monthly means of the Zürich relative sunspot number (R_z) and of the magnetic activity (u_1)[4] are shown along with the available concurrent data of other stations in middle and low latitudes (The data of Tamanrasset are based on one-colour method[1]). The u_1 values plotted in the figure were obtained from the H-data of Alibag, Kodaikanal, Trivandrum and Huancayo for

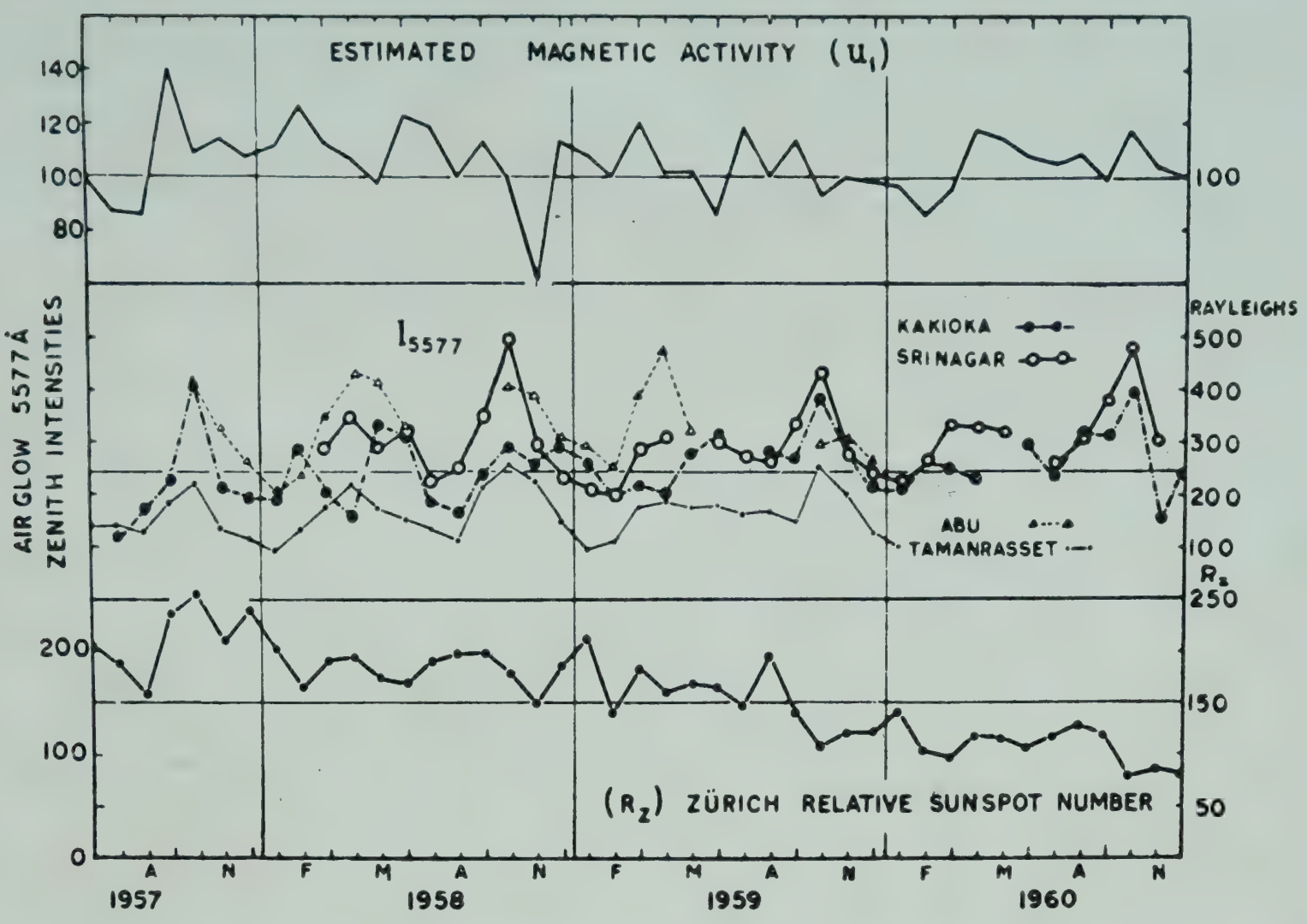

FIG. 4 — AIRGLOW 5577 Å INTENSITY (MONTHLY MEANS OF MIDDLE AND LOW LATITUDE STATIONS) AND RELATIVE SUNSPOT NUMBER AND GEOMAGNETIC ACTIVITY DURING IGY AND IGC

the period 1957–59, and for 1960, they were obtained by extrapolation from R_z and C_i, the relationship between the two being derived from an analysis of u_1, R_z and C_i for the period 1884–1949.

The Kakioka values, though smaller than the values at Srinagar, show very similar variations. Tamanrasset also behaves similar to Srinagar. Though a comparison on a round-the-year basis is not possible with the Mt Abu data, due to discontinuities during the monsoon months, it is clearly seen that the Mt Abu values are markedly larger than those at Tamanrasset and Kakoika, and sometimes larger than the Srinagar values also.

The airglow intensity does not show any large decrease from 1957 to 1960, although the sunspot number decreased to about one-third; there is, however, a suggestion of some relationship with u_1, consistent with the findings of McCaulley *et al.*[5].

ACKNOWLEDGEMENT

The author expresses his grateful thanks to Prof. K. R. Ramanathan for his interest and encouragement at all stages of work; and to Dr R. V. Bhonsle for his help in the construction and calibration of the photometer at Srinagar.

Thanks are due to Dr B. S. Dandekar for his help in intercomparing the luminescent sources.

References

1. Roach, F. E., *The Intercalibration of Airglow Photometers*, N.B.S. Rep. No. 5591, 1958.
2. Roach, F. E. & Meinel, A. B., *Astrophys. J.*, **122** (1955), 530.
3. Roach, F. E., *Aurora and Airglow*, IGY Instruction Manual No. IV (Pergamon Press, London), 1956.
4. Chapman, S. & Bartels, J., *Geomagnetism* (Oxford University Press, Oxford), 1940, 366.
5. McCaulley, J. W., Roach, F. E. & Matsushita, S., *J. geophys. Res.*, **65** (1960), 1499.

Night airglow at Mt Abu: OI 6300 Å

B. S. DANDEKAR

Physical Research Laboratory
Ahmedabad

The nocturnal variations at Mt Abu of the red airglow in different seasons are discussed and compared with those occurring at Haute Provence. The intensity of the OI red lines increases with increase in the critical frequency of the F layer. The rate of increase is enhanced when the critical frequency exceeds 14 Mc/s.

The equipment used for the study was similar to that used by the author (*p.* 88) for the OI green line. An EMI 6095 photomultiplier was fitted in a cylindrical tube. The voltages to the dynodes of the phototube were fed through a bank of resistances. An interference filter with peak transmission at 6300 Å was used. A plano-convex lens with an aperture of 2 in. and a focal length of 4 in. was mounted in such a way that the photocathode lay in its focal plane. The lens focused the incoming light on the photocathode. The aperture in front of the photocathode covered a circular field of 7° diam. A small radioactive source was fitted in a shutter which could be brought directly over the photocathode for calibrating the instrument. The photometer (Fig. 1) was placed on an alt-azimuth mounting with scales for measuring the altitude and azimuth.

The equivalent band-width of the filter multiplied by the relative photomultiplier response was 140 Å. In Fig. 2, the continuous curve shows the filter transmission and the dotted line represents the filter transmission multiplied by the photomultiplier response.

The photometer was directed towards the celestial north pole and observations were made only on clear moonless nights. Fig. 3 shows a typical record. The record with the higher amplitude relates to the Na-D lines and the one with the lower amplitude to the OI red lines. The smaller amplitude of the OI lines is due to the lower response of the photomultiplier at that wavelength.

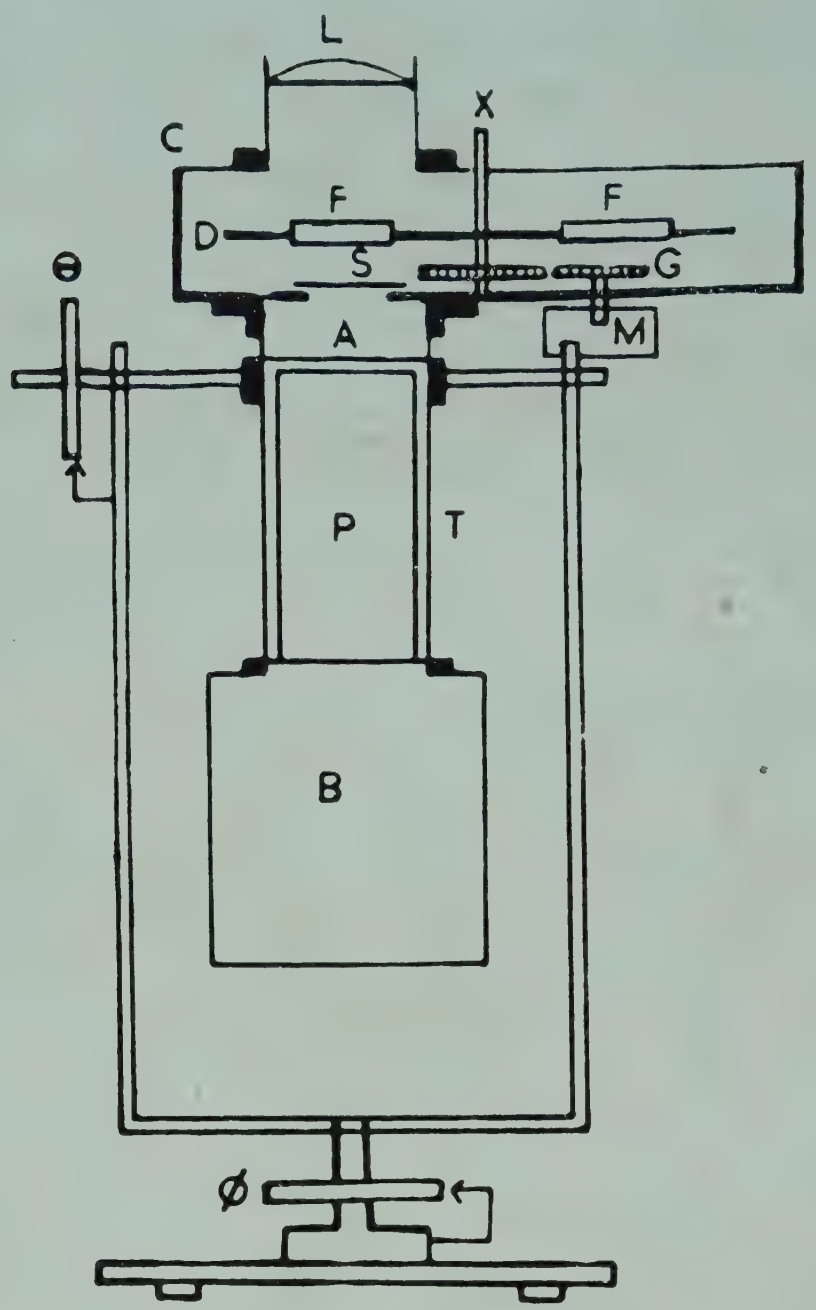

FIG. 1 — ALT-AZIMUTH PHOTOMETER [L, LENS; C, COVER; X, AXLE; F, FILTER; D, DISC; S, SHUTTER; A, APERTURE; G, GEARS; M, MOTOR; T, TUBE; B, BLEEDER BOX; θ, ALTITUDE SCALE; ϕ, AZIMUTH SCALE; P, PHOTOTUBE (EMI 6095)]

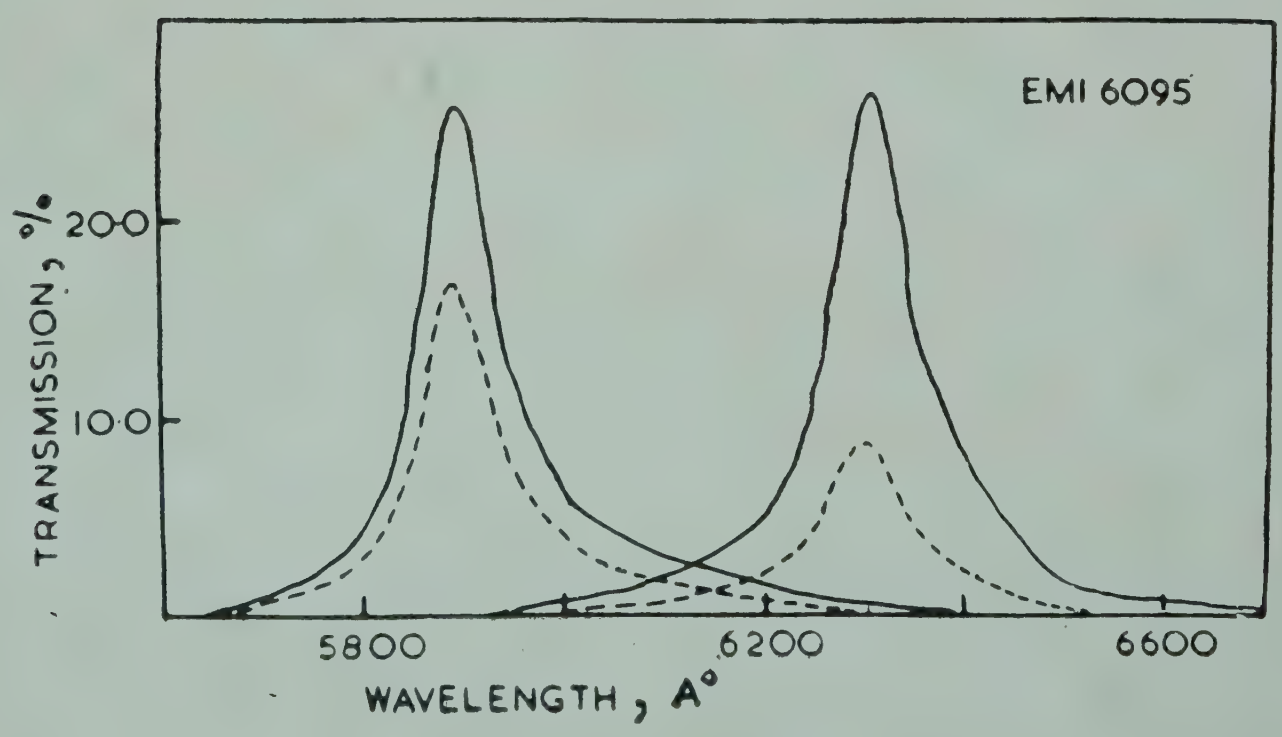

FIG. 2 — DEPENDENCE OF FILTER TRANSMISSION ON WAVELENGTH

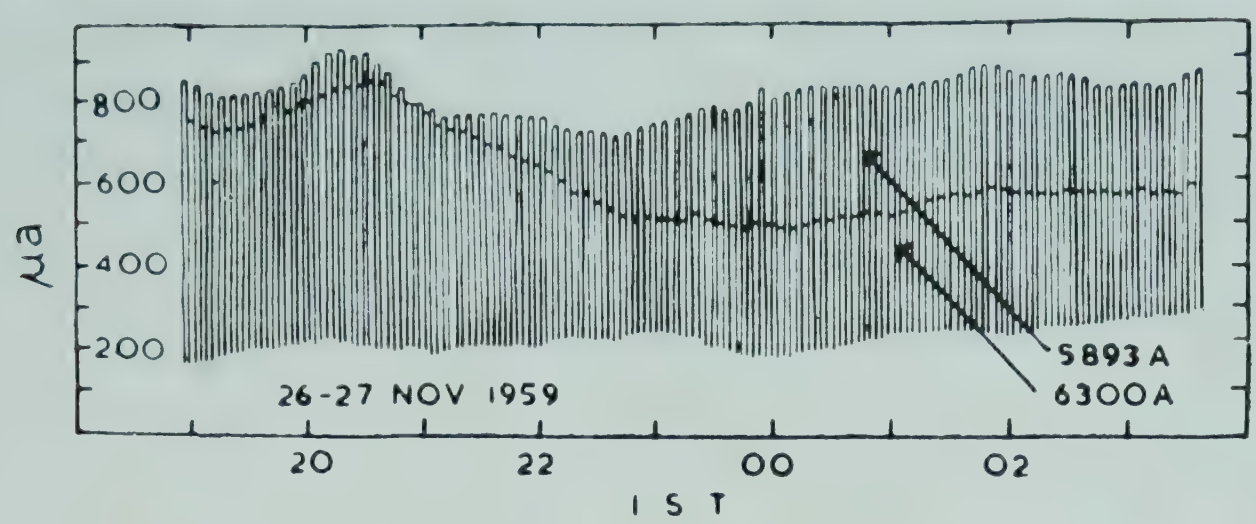

FIG. 3 — SAMPLE RECORD EXHIBITING NOCTURNAL VARIATION OF OI RED (6300 Å) AND Na-D (5893 Å) LINES

TABLE 1 — NUMBER OF OBSERVATIONS MADE FROM OCTOBER TO MAY (1957/58-1959/60)

MONTH	NO. OF OBSERVATIONS			TOTAL
	1957–58	1958–59	1959–60	
Oct.	5	—	8	13
Nov.	4	14	11	29
Dec.	—	3	12	15
Jan.	12	10	16	38
Feb.	5	14	2	21
Mar.	15	17	—	32
Apr.	—	15	—	15
May	6	10	—	16
			Total	179

The photometer was calibrated for the OI red lines in the same way as for the 5577 Å line against a Philips tungsten W-4 type ribbon filament lamp. It was found that 1 μa. corresponds to 1·39 Rayleighs for the 6300 Å filter. The correction for the background was estimated from similar records with a 5300 Å filter. The data were reduced by the use of the following relation:

$$I_{6300} = 1{\cdot}39 d_{6300} - 115$$

where I_{6300} is the intensity of the airglow (in Rayleighs) corrected for the background radiation and d_{6300} is the deflection (in μa.) caused by the light transmitted by the filter. The observations towards the pole were reduced to zenith by dividing by a factor 1·7. This was determined from zenith and pole observations taken one after the other on a number of days.

Table 1 gives the number of observations in each month during the period of operation.

The background radiation was estimated with the help of the 5300 Å filter. The filter transmits the weak OH band (6–0), whereas the 6300 Å filter transmits the strong (9–3) band of OH. No correction was made for the effect of this contamination.

Variation of Intensity of the Red OI Lines during Night

The data from October 1957 to December 1959 were grouped according to season: (i) autumn (October–November), (ii) winter (December–February), and (iii) spring (March–May). Data could not be obtained during the monsoon months, June–September, due to cloud and rain.

Fig. 4 shows the nocturnal variation in each of these seasons. The maximum and minimum intensities are also shown. The curves in each group represent the boundaries above which 25, 50 and 75 per cent observations lie. All the groups show a rapid decrease in intensity up to about local midnight followed later by a steady uniform intensity. This post-crepuscular effect is quite prominent in autumn and less so in spring. The intensities after midnight in spring are higher than those in winter.

It is interesting to note that Roach[1] and Barbier[2] have observed a similar post-crepuscular effect for the OI red lines, with the intensity decreasing rapidly in the first four hours of the night and later remaining more or less steady for a few hours. In their latitudes, however, they find another rise of intensity in the pre-dawn hours which is well correlated with magnetic activity. Barbier[2] has stated that the post-crepuscular effect was strong in November and absent in summer.

Huruhata and coworkers[3] estimate the average height of the 6300 Å emission layer to be about 270 km. Barbier[4] deduced a height of about 300 km. for the same emission. Rocket observations[5] suggest that the emission layer is situated at a height beyond 160 km., which is the maximum height reached by the rocket. The Van Rhijn technique yielded heights which varied widely but were greater than 180 km. The results in general indicate that the OI red emission takes place somewhere in the F region of the ionosphere.

The oxygen red lines are easily excited due to their low excitation potential and also due to the abundance of atomic oxygen at all heights in the ionosphere. Bates and Massey[6] and independently Nicolet[7] suggested the following dissociative recombination process for the OI red radiation:

$$O_2^+ + e \rightarrow O(1_D) + O \qquad (1)$$

The formation of O_2^+ ions would be either by charge transfer process

$$O^+ + O_2 \rightarrow O_2^+ + O(3_P) \qquad (2)$$

or by ion-atom interchange.

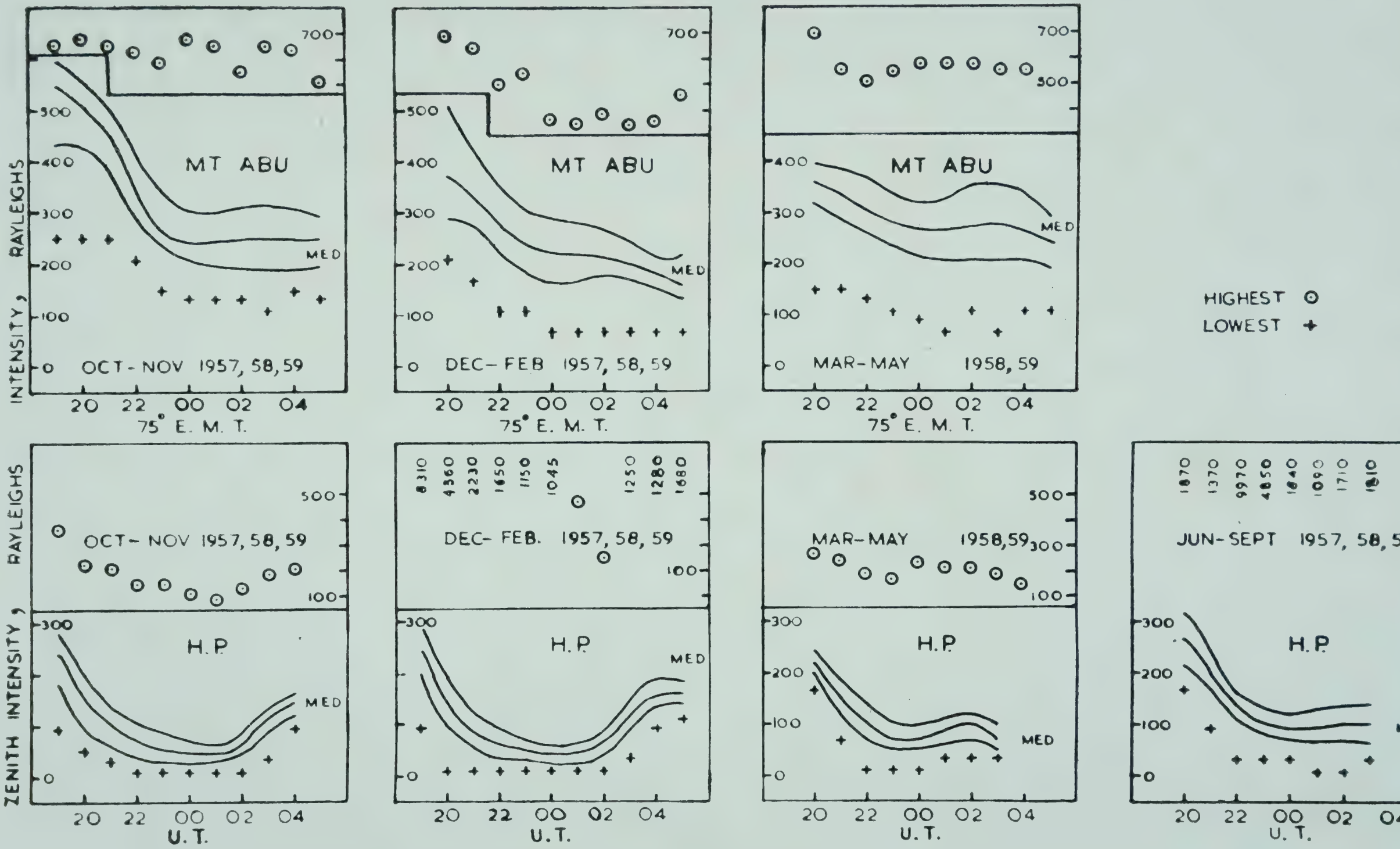

FIG. 4 — NOCTURNAL VARIATION OF OI RED LINES IN DIFFERENT SEASONS AT MT ABU AND AT HAUTE PROVENCE

Process (1) is supposed to be the most effective for the disappearance of electrons in the F layer. As it can also give rise to OI red lines, one should expect a correlation between the intensity of the OI red lines and the physical parameters of the F layer. The correlation of these has been studied by Amand[8] and Barbier[9].

An attempt was made to investigate the relation between the variation of the intensity of the red lines of the airglow and the variations of the critical frequency of the F layer. For this purpose the airglow data at Mt Abu (geog. lat. 24°·6N: long. 72°·7E) were compared with f_0F_2 data obtained from the ionograms of the Physical Research Laboratory at Ahmedabad (geog. lat. 23°·0N: long. 72°·6E). The data of the year 1959 were used. The hourly airglow intensities were divided into a number of groups according to the values of the critical frequency at that time. All the observations available from late evening to pre-dawn were used. The results are shown in Fig. 5, in which full circles show the median values for each group, which included an interval of 1 Mc. in the values of f_0F_2. The vertical lines show the range of variations; 50 per cent of the observations lay within that range, with 25 per cent above and 25 per cent below the median value. The curve joining the circles exhibits a slow rise of intensity up to 10 Mc/s. and a more rapid rise later. Beyond 14 Mc/s. the gradient of the curve increases rapidly exhibiting a larger influence of f_0F_2 above 14 Mc/s. on the airglow.

Barbier[9] derived an empirical relation

$$I = 583 \times 10^6 f_0^2 e^{-(h'-275)/80}$$

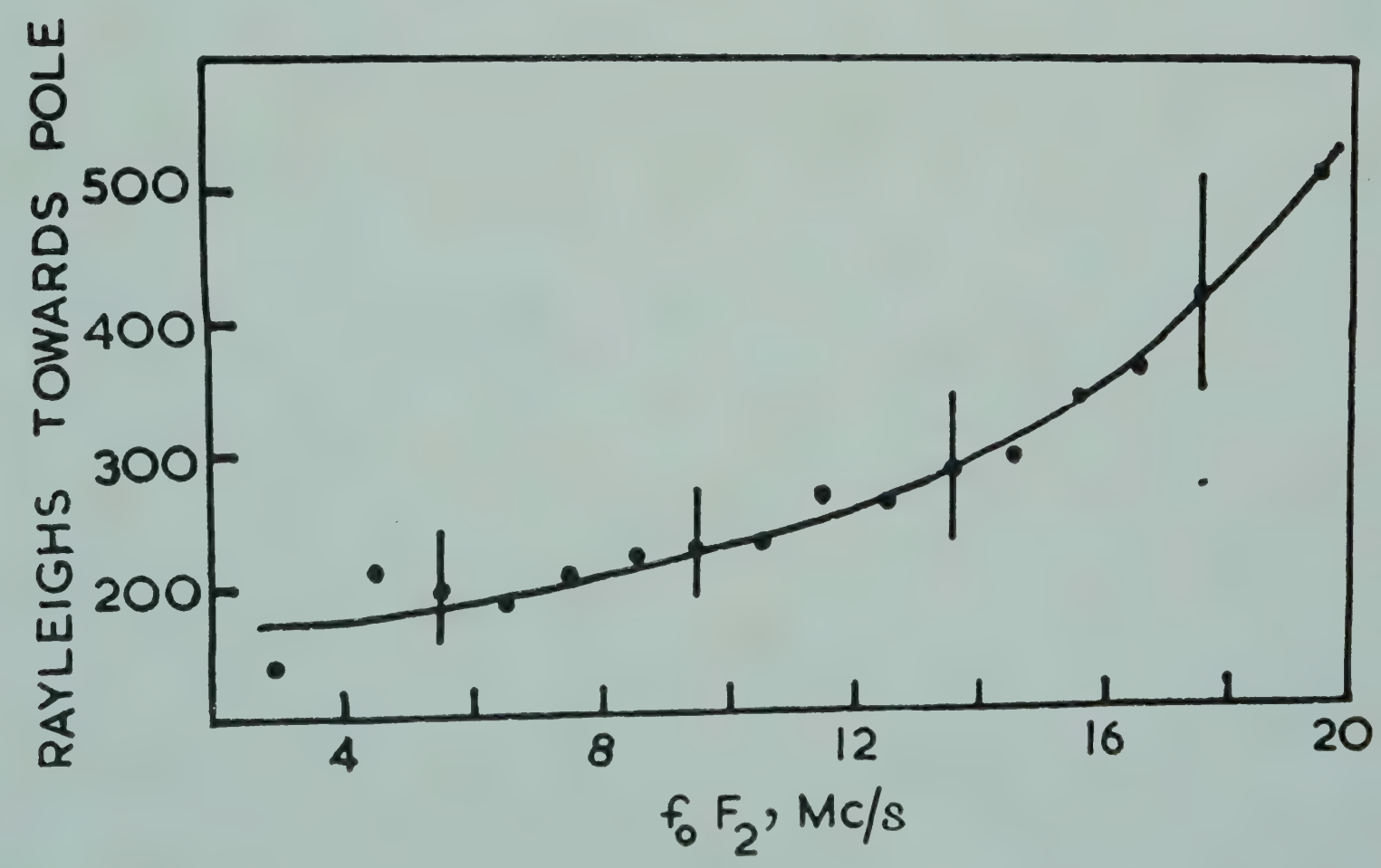

FIG. 5 — DEPENDENCE OF THE INTENSITY OF OI RED LINES ON THE CRITICAL FREQUENCY f_0F_2 OF THE F LAYER

relating the nocturnal intensity of the OI red lines with f_0F and its equivalent height h', but the relation was found to hold only in the first part of the night. As mentioned previously, late night enhancement of 6300 Å in middle latitudes has been found to be correlated with magnetic activity and possibly also with aurorae. From the observations over the whole night Huruhata *et al.*[3] observed that the OI red radiation was approximately proportional to the maximum electron density $(f_0F_2)^2$ of the F layer.

Acknowledgement

The author is thankful to Prof. K. R. Ramanathan, Director, Physical Research Laboratory, Ahmedabad, for his kind guidance in the work.

References

1. Roach, F. E., *Proc. nat. Acad. Sci.*, **40** (1954), 950.
2. Barbier, D., *The Airglow and the Aurorae* (Pergamon Press), 1956, 38.
3. Huruhata, M., Nakamura, T. & Tanabe, H., *Rep. Ionosph. Space Res. Japan*, **13** (1959), 283.
4. Barbier, D., *C.R. Acad. Sci.*, **244** (1957), 1809.
5. Heppner, J. P., Stolarik, J. D. & Meredith, L. H., *Trans. Amer. geophys. Un.*, **38** (1957), 394.
6. Bates, D. R. & Massey, H. S. W., *Proc. roy. Soc.*, **192** (1947), 1.
7. Nicolet, M., *Phys. Rev.*, **93** (1954), 633.
8. Amand, P., *Ann. Geophys.*, **11** (1955), 450.
9. Barbier, D., *Ann. Geophys.*, **17** (1961), 3.

* * *

Simultaneous Study of the λλ 5577, 5893 and 6300 Emissions of Night Airglow at Poona. M. W. Chiplonkar & V. V. Agashe, Physics Department, Poona University, Poona [*Ann. Geophys.*, **17** (1961), 231].

In continuation of our previous investigations carried out at Poona during the IGY and the IGC on λ5577 emission in the night airglow, some more results of simultaneous measurements of the three prominent night sky emissions have been presented. These measurements were carried out on 17 clear moonless nights during the period January–April 1960. It was observed that in general the λ5893 emission was the strongest while the λ5577 emission was the weakest. Further, λ5893 emission showed little variation from night to night as compared with those of the other two radiations. One of the most peculiar features revealed during the present study is the azimuthal variation of the λ6300 emission, which changes as the night progresses, at first more rapidly till about midnight and then gradually during the early morning hours. Attention is drawn to a similar observation made by the French workers at Tamanrasset. (*Abstract*)

Change of strength of the source of daily variation of cosmic rays with solar cycle

H. RAZDAN

Physical Research Laboratory
Ahmedabad

The daily variation of cosmic rays as observed with narrow angle and wide angle telescopes has been discussed. The results obtained with narrow angle telescopes reveal that the amplitude decreases with increasing solar activity. Theoretical implications of this conclusion are discussed.

In the interpretation of the processes responsible for the solar anisotropy of cosmic radiation, the change of strength of the source of solar daily variation of cosmic ray intensity during the period of a solar cycle of activity is of considerable significance. It is widely recognized that the density of plasma and the conductivity of interplanetary space should in general be higher during years when the sun is active than during a period of minimum solar activity. If the anisotropy of the primary radiation is related to the acceleration or the deceleration of cosmic ray particles passing through beams of solar plasma with frozen magnetic fields as suggested by several workers[1-3], the source should be weak during a period of high solar activity. On the other hand, if the strength of the source related to anisotropy is stronger during years of maximum solar activity than at sunspot minimum, then the acceleration in beams is not the dominating process causing anisotropy.

The most significant changes in the form of daily variation from year to year are seen when observations are made at low latitudes[4]. The twelve-month mean daily variation of meson intensity at Huancayo during June–November 1954 has been reported to have a negligible amplitude, barely

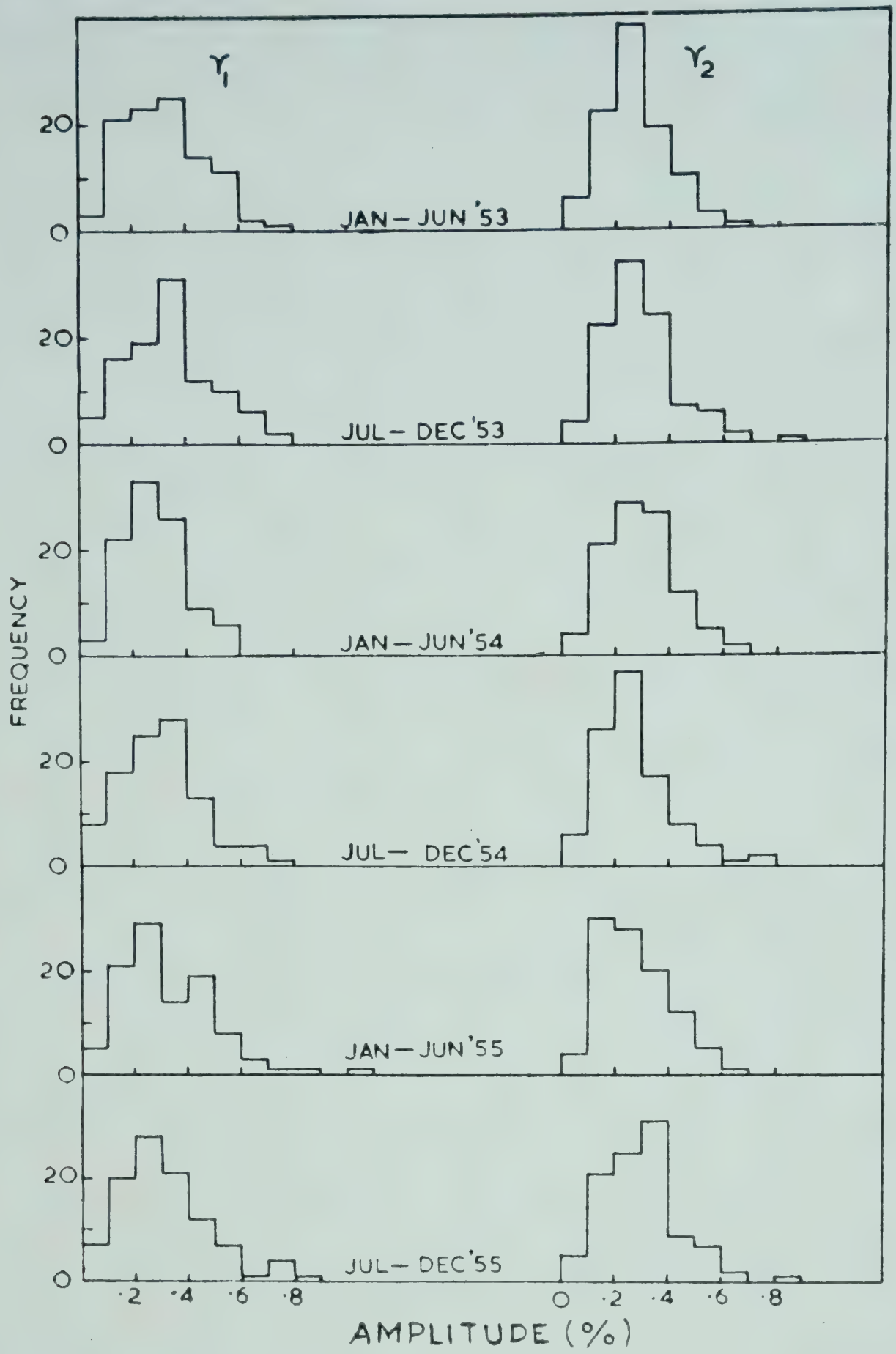

FIG. 1 — r_1 AND r_2 HISTOGRAMS AT HUANCAYO FOR SUCCESSIVE SIX-MONTHLY PERIODS FROM 1953 TO 1955

above noise level[5,6]. It has been suggested by Glokova[6] that during this period the solar daily variation was absent.

The daily variation of meson intensity at Huancayo and at Ahmedabad on individual days during the period 1953–55 has been analysed. The histograms of r_1 and r_2, the amplitudes of the diurnal and the semidiurnal component respectively, and of ϕ_1 and ϕ_2, the time of maximum of the two components when the amplitudes of the variation are significant at the 2σ level

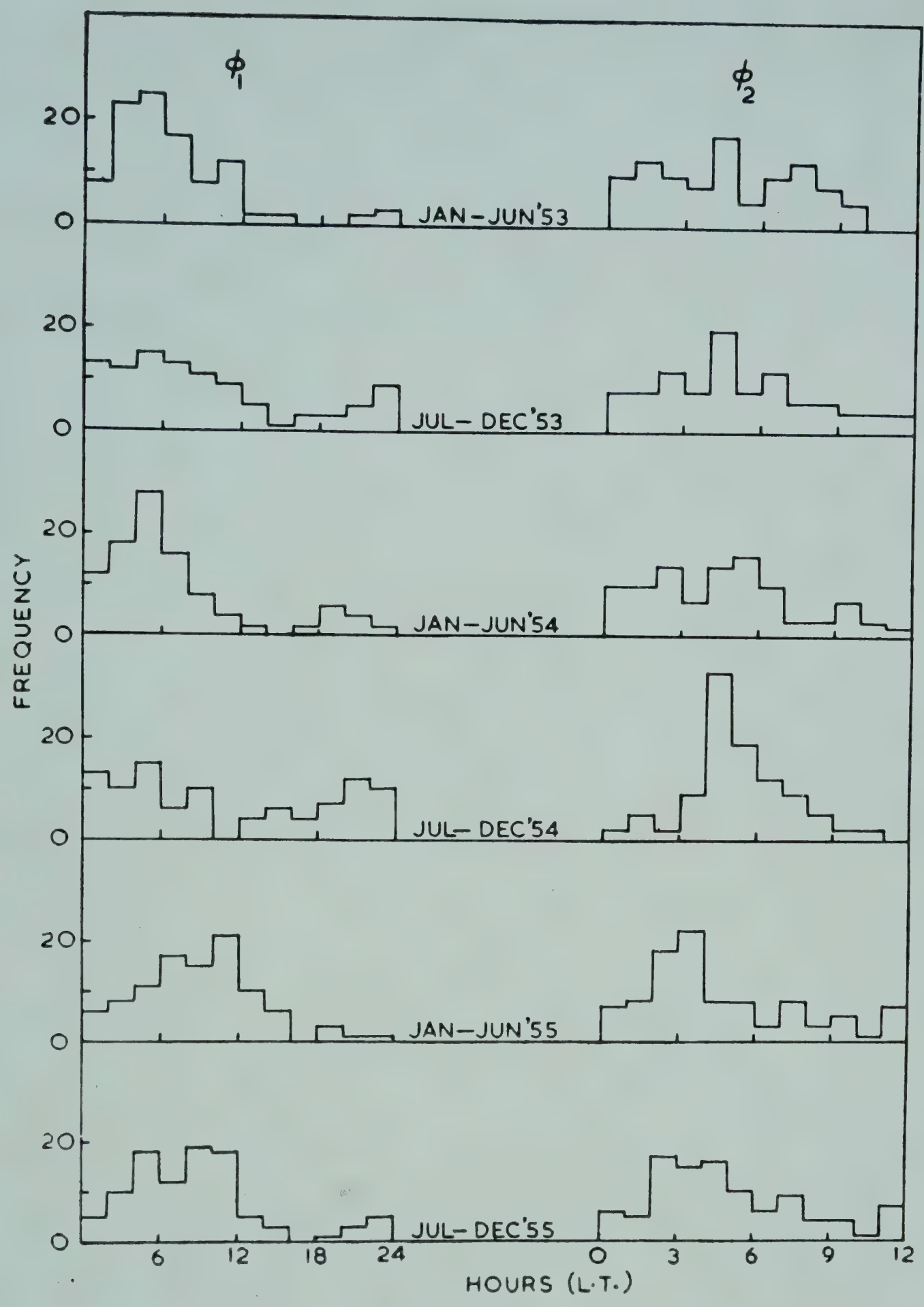

FIG. 2 — ϕ_1 AND ϕ_2 HISTOGRAMS AT HUANCAYO FOR SUCCESSIVE SIX-MONTHLY PERIODS FROM 1953 TO 1955

(σ being the Poisson standard error) are shown in Figs. 1, 2 and 3. Separate histograms give the distribution of r_1, r_2 and ϕ_1, ϕ_2 during the successive six-monthly periods for which the data were available at the two stations. The comparison of r_1 or r_2 histograms is made by comparing their means which are presented in Table 1. The application of the '*t*' test shows that there is no significant difference between r_1 and r_2 histograms during this

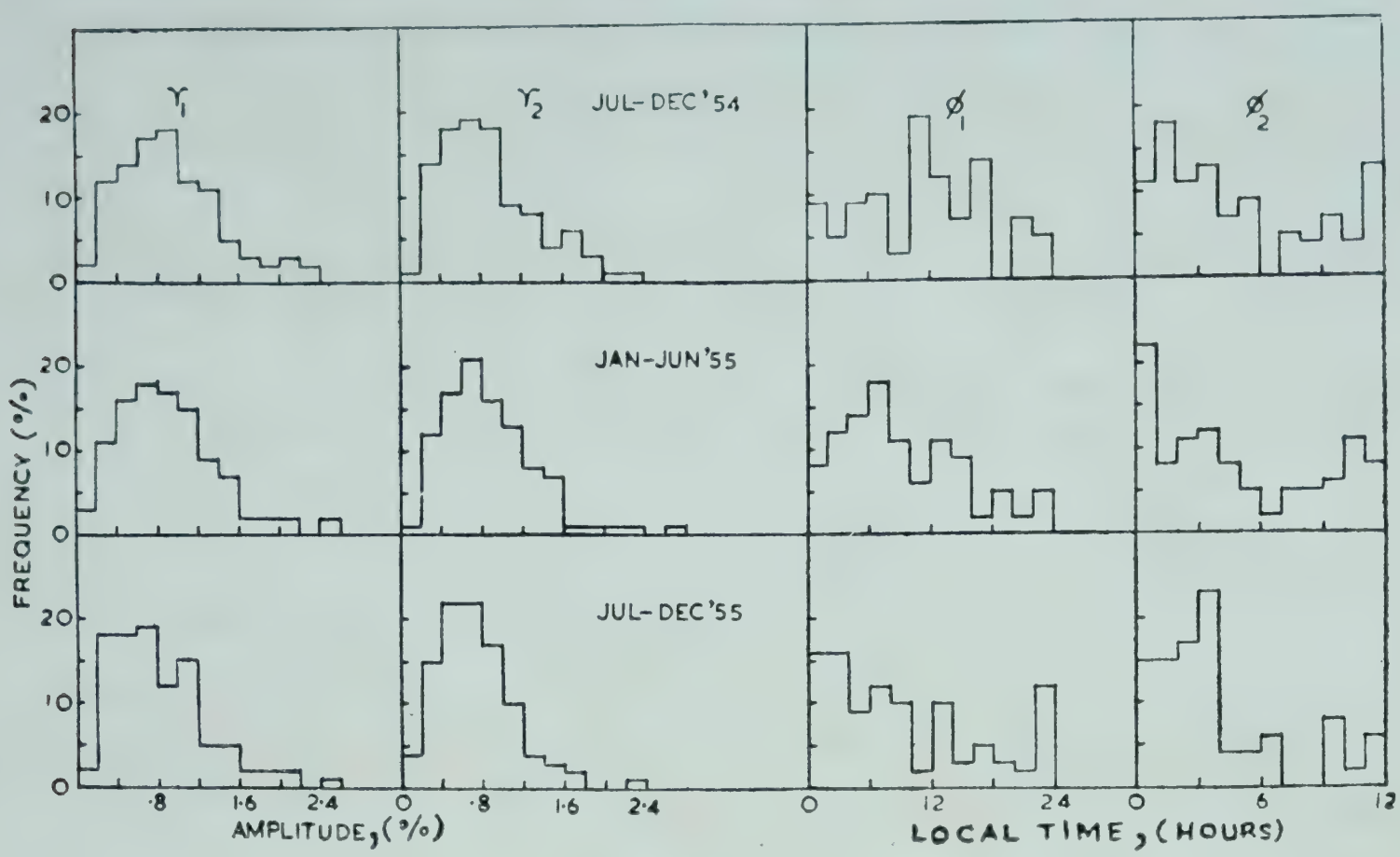

FIG. 3 — r_1, r_2 AND ϕ_1, ϕ_2 HISTOGRAMS AT AHMEDABAD FOR THREE SUCCESSIVE SIX-MONTHLY PERIODS FROM JULY 1954 TO DECEMBER 1955

period. Moreover, the χ^2 test demonstrates that the time of diurnal maximum is significantly more variable during the period July–December 1954 than during other periods. It can, therefore, be concluded that the negligible amplitude of the mean daily variation during the period June–November 1954 is due to the great variability of the time of maximum rather than to any inherent decrease of the strength of anisotropy during that period.

Studies were made at Ahmedabad with narrow angle telescopes for the period 1954–58 in addition to wide angle telescopes. The data of each individual day were corrected for the daily variation of atmospheric pressure and temperature effects as discussed by Sarabhai *et al.*[4]. The means of r_1 and r_2 histograms for various periods are presented in Table 2 for the two types of telescopes. It is seen that the means of r_1 and r_2 histograms at Huancayo are in general smaller than the corresponding values at Ahmedabad (Table 1). Similarly, the means of r_1 and r_2 histograms of various years observed with the wide angle telescope are smaller than the values obtained from the narrow angle telescope (Table 2). Such a difference is explained as due to the difference in the counting rates of various detectors, it being maximum in ionization chamber at Huancayo and minimum in the narrow angle telescope at Ahmedabad*.

It can also be seen from Table 2 that the diurnal amplitudes on individual days have decreased significantly from a period of minimum solar activity

*The effect of the counting rate of an instrument on the observed amplitude of daily variation will be discussed elsewhere

TABLE 1 — MEANS OF r_1 AND r_2 HISTOGRAMS AT HUANCAYO AND AHMEDABAD FOR VARIOUS SIX-MONTHLY PERIODS FROM 1953 TO 1955

Period	Huancayo mean (%)		Ahmedabad mean (%)	
	r_1	r_2	r_1	r_2
Jan.–June 1953	0·27	0·22	—	—
July–Dec. 1953	0·29	0·24	—	—
Jan.–June 1954	0·23	0·25	—	—
July–Dec. 1954	0·25	0·22	0·86	0·82
Jan.–June 1955	0·27	0·22	0·81	0·82
July–Dec. 1956	0·26	0·25	0·75	0·67

Error for the mean is $\pm 0{\cdot}02$ per cent at Huancayo and $\pm 0{\cdot}05$ per cent at Ahmedabad

TABLE 2 — MEANS OF r_1 AND r_2 HISTOGRAMS OBSERVED WITH WIDE ANGLE AND NARROW ANGLE TELESCOPES AT AHMEDABAD DURING VARIOUS PERIODS FROM 1954 TO 1958

Period	Wide angle telescope ($22° \times 37°$) mean (%)		Narrow angle telescope ($5° \times 19°$) mean (%)	
	r_1	r_2	r_1	r_2
Sept. 1954–July 1955	$0{\cdot}70 \pm 0{\cdot}5$	$0{\cdot}64 \pm 0{\cdot}04$	$1{\cdot}61 \pm 0{\cdot}08$	$0{\cdot}93 \pm 0{\cdot}04$
1956	$0{\cdot}64 \pm 0{\cdot}03$	$0{\cdot}53 \pm 0{\cdot}02$	—	—
1957	$0{\cdot}64 \pm 0{\cdot}05$	$0{\cdot}59 \pm 0{\cdot}04$	$1{\cdot}09 \pm 0{\cdot}08$	$0{\cdot}96 \pm 0{\cdot}06$
1958	$0{\cdot}59 \pm 0{\cdot}02$	$0{\cdot}52 \pm 0{\cdot}02$	$1{\cdot}02 \pm 0{\cdot}07$	$0{\cdot}87 \pm 0{\cdot}07$

TABLE 3 — MEANS OF r_1 AND r_2 HISTOGRAMS OBSERVED WITH A WIDE ANGLE TELESCOPE AT KODAIKANAL AND TRIVANDRUM DURING VARIOUS PERIODS FROM 1955 TO 1958

Period	Kodaikanal mean (%)		Trivandrum mean (%)	
	r_1	r_2	r_1	r_2
1955	$0{\cdot}70 \pm 0{\cdot}20$	$0{\cdot}52 \pm 0{\cdot}02$	$0{\cdot}69 \pm 0{\cdot}04$	$0{\cdot}62 \pm 0{\cdot}03$
1956	$0{\cdot}55 \pm 0{\cdot}02$	$0{\cdot}51 \pm 0{\cdot}02$	$0{\cdot}64 \pm 0{\cdot}03$	$0{\cdot}56 \pm 0{\cdot}03$
1957	$0{\cdot}51 \pm 0{\cdot}02$	$0{\cdot}52 \pm 0{\cdot}02$	$0{\cdot}62 \pm 0{\cdot}02$	$0{\cdot}53 \pm 0{\cdot}02$
1958	$0{\cdot}50 \pm 0{\cdot}03$	$0{\cdot}46 \pm 0{\cdot}03$	$0{\cdot}61 \pm 0{\cdot}02$	$0{\cdot}55 \pm 0{\cdot}02$

to a period of maximum solar activity. Similar changes have been observed with wide angle meson telescopes at Kodaikanal and Trivandrum as seen from Table 3. The data in these cases have been corrected for only atmospheric pressure changes. Since the diurnal variation of ground temperature at these places is rather small ($\sim \pm 3°$), it is unlikely that the results will change after temperature correction. It is, therefore, concluded that the strength of the source of daily variation decreases with increasing solar

activity which is consistent with an origin of anisotropy of primary radiation due to acceleration of the cosmic ray particles in beams of solar plasma with frozen magnetic fields.

References

1. Nagashima, K., *J. Geomag. Geoelect.*, **7** (1955), 51.
2. Nerurkar, N. W., *Proc. Indian Acad. Sci.*, **45A** (1957), 341.
3. Dorman, L. I., *Time Variation in Cosmic Rays* (State Publishing House, Moscow), English translation, 1957.
4. Sarabhai, V., Desai, U. D. & Venkatesan, D., *Phys. Rev.*, **99** (1955), 1490.
5. Possener, M. & van Heerdan, I. J., *Phil. Mag.*, **1** (1956), 253.
6. Glokova, E. S., *Proceedings of the Moscow Conference on Cosmic Rays*, Vol. 4, 1960, 243.

Correlated changes of geomagnetism and east-west asymmetry of cosmic rays

U. R. RAO

Physical Research Laboratory
Ahmedabad

A study of the correlated changes of east-west asymmetry and of geomagnetism has been conducted for the first time at Ahmedabad during 1957-58. The study indicates that days with high east-west asymmetry are associated with geomagnetically quiet days and a cosmic ray daily variation consistent with a source situated at an angle of $112 \pm 10^{\circ}$ to the left of the earth-sun line and having an energy spectrum of the type $a\epsilon^{-0.8 \pm 0.3}$. The increases in asymmetry and the associated daily variation for east and west can be explained by the acceleration of cosmic ray particles crossing beams of width 3×10^{12} cm. with a frozen magnetic field of 10^{-6} gauss and a radial velocity of about 10^{8} cm./sec. The implications of such a theory have been examined.

Days with low asymmetry have been found to occur 3-4 days after the onset of cosmic ray storms associated with geomagnetic storms, usually of the SC-type.

Directional counter telescopes at low latitudes, particularly those pointing east and west, are a powerful tool for understanding the time variations of cosmic rays and the electromagnetic variations in interplanetary space. Since at low latitudes east and west pointing telescopes scan the same part of the celestial sphere, an anisotropy of primary radiation shows up as a daily variation with a characteristic shift of 6 hr between east and west telescopes inclined at 45° to the zenith. On the other hand, a local source of daily variation situated within the influence of the geomagnetic field shows up as a daily variation with the same pattern for east and west

directions. Moreover, since the east-west asymmetry of cosmic radiation is largest at equatorial latitudes, changes of the energy spectrum of primary cosmic radiation can be followed through the time variations of east-west asymmetry.

The results of investigation relating to changes of east-west asymmetry during 1957–58 at Ahmedabad (geomagnetic coordinates, 13°·9N : 143°·9E and altitude, sea level) are presented and interpreted in this paper. The details of the experimental set-up, the corrections for meteorological factors and the calculations are presented elsewhere[1]. The daily variation of meson intensity has been corrected for the daily variation of atmospheric temperature and pressure and in the calculation of the daily mean east-west asymmetry, correction for harmonic pressure has been applied.

Correlated Changes of East-West Asymmetry and Daily Variation

East-west asymmetry which is defined as $[2(W-E)/(W+E)]\times 100$, where W and E are daily mean intensities for west and east, has a mean value of $14{\cdot}97\pm 0{\cdot}55$ per cent at Ahmedabad. Days on which the east-west asymmetry has a value above 16·1 per cent or below 13·9 per cent are called days of high and low asymmetry respectively. During the period of observation there are 491 days with normal, 28 days with high and 26 days with low east-west asymmetry.

Fig. 1 shows the daily variation of meson intensity for east and west and of neutron intensity at stations situated in middle and equatorial latitude belts on days of high asymmetry. The particulars of the stations representing middle latitude belt covering the range 55°–75° geomagnetic latitude and equatorial latitude belt covering the range 15°N–15°S are given in Table 1. The parameters of the daily variation of meson and neutron intensities on days of high asymmetry are shown in Table 2.

The average daily variation of meson intensity for both east and west has a large amplitude with a characteristic difference of 6 hr in the time of their diurnal as well as their semidiurnal maximum. Thus the daily variation on days of high asymmetry is consistent with its being produced by an anisotropy of primary radiation. The similarity of form and amplitude of the daily variation observed in neutron intensities at equatorial and middle latitudes and the earlier time of diurnal maximum of the daily variation at equatorial stations confirm the above conclusion. The semidiurnal component, however, has a significant amplitude only for neutron intensity at equatorial latitudes. Thus the primary anisotropy observed at equatorial stations, with neutron monitors or meson telescopes, has an inherent semidiurnal component associated with it. This proves that the doubt cast by

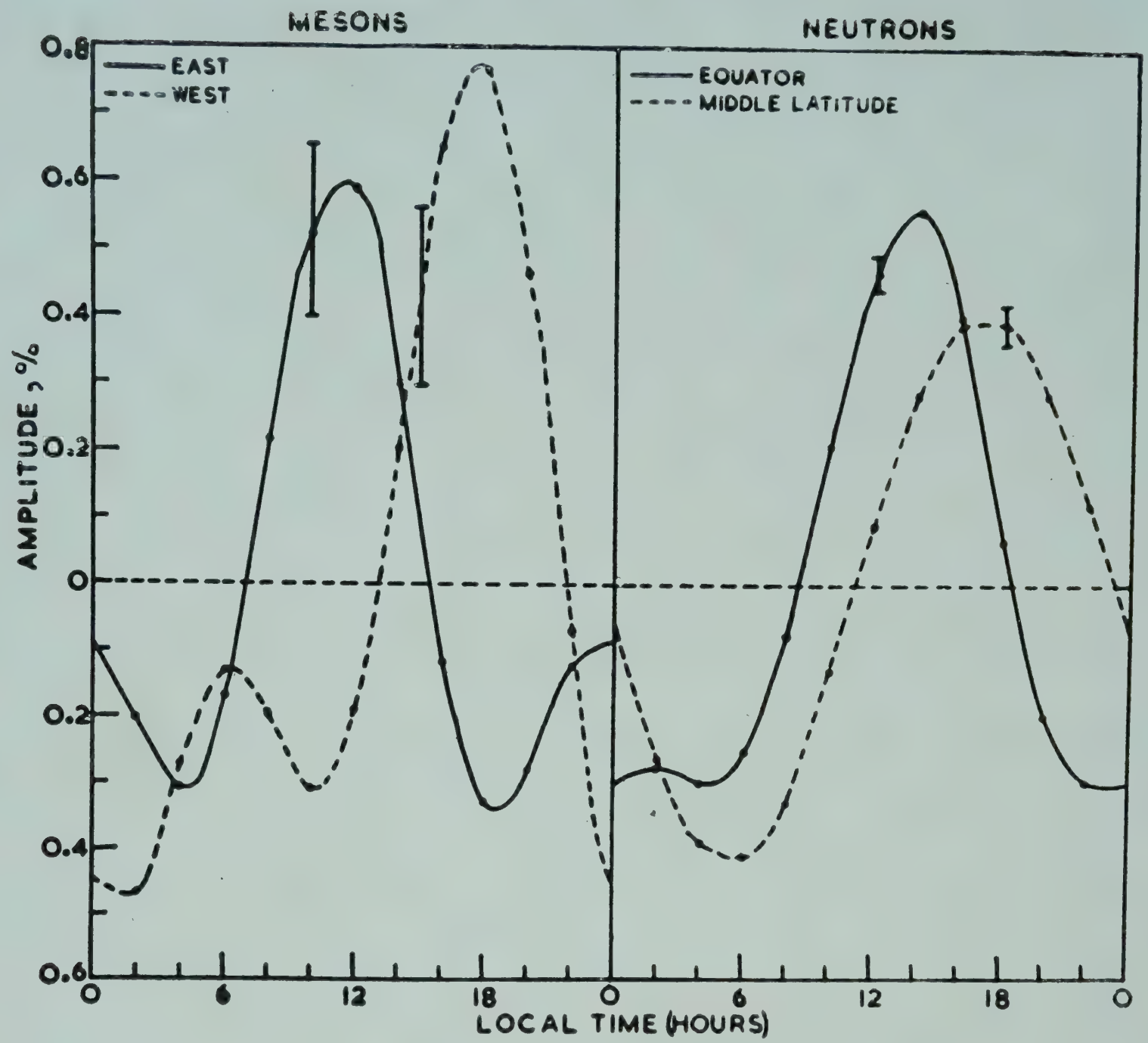

FIG. 1 — DAILY VARIATION OF MESON INTENSITY FOR EAST AND WEST AND OF NEUTRON INTENSITY AT STATIONS IN MIDDLE AND EQUATORIAL LATITUDE BELTS ON DAYS OF HIGH ASYMMETRY

Katzman and Venkatesan[2] and Forbush and Venkatesan[3] on the existence of a non-meteorological semidiurnal component associated with an anisotropy of primary radiation is not really valid.

CHANGES OF NEUTRON INTENSITY AND GEOMAGNETISM ASSOCIATED WITH EAST-WEST ASYMMETRY

Fig. 2 shows the changes associated with epochs of low and high asymmetry through Chree analysis of (i) daily mean neutron intensity in middle and equatorial latitude belts, (ii) C_p, and (iii) H, the daily mean intensity of the horizontal component of the geomagnetic field at Kodaikanal, for ten days prior to and following the two types of epochs. An examination of the figure leads to the following conclusions:

(i) Days of low asymmetry are associated with depressed mean intensity of neutrons at all the stations and days of high asymmetry with enhanced

TABLE 1 — PARTICULARS OF COSMIC RAY NEUTRON MONITOR STATIONS USED IN THE ANALYSIS

Station	Altitude *m.*	Geographic coordinates	Geomagnetic coordinates		Investigator
			Latitude	Longitude	
Equatorial:					
Ahmedabad	S.L.	23°01′N: 72°36′E	13°·9	143°·9	Dr V. Sarabhai, India
Huancayo	3400	12°02′S: 75°20′W	−0°·6	353°·8	Dr J. A. Simpson, Chicago
Kodaikanal	2343	10°14′N: 77°28′E	0°·6	147°·1	Dr V. Sarabhai, India
Lae	S.L.	6°44′S: 147°0′E	−16°·0	217°·4	Dr A. G. Fenton, Hobart
Makerere College	1196	0°20′N: 32°34′E	−2°·0	101°·4	Dr D. M. Thomson, Uganda
Middle latitude:					
Churchill	39	58°45′N: 94°05′W	68°·7	322°·9	Dr D. C. Rose, Canada
Ottawa	101	45°24′N: 75°54′W	56°·8	351°·1	Dr D. C. Rose, Canada
Murchison Bay	S.L.	80°03′N: 18°15′E	72°·2	137°·2	Dr A. E. Sandstrom, Sweden
Resolute	17	74°41′N: 94°54′W	82°·9	289°·3	Dr D. C. Rose, Canada
Mawson	S.L.	67°36′S: 62°53′E	−73°·1	103°·8	Dr A. G. Fenton, Hobart
Mt Wellington	725	42°55′S: 147°14′E	−51°·5	224°·5	Dr A. G. Fenton, Hobart

TABLE 2 — CHARACTERISTICS OF THE AVERAGE DAILY VARIATION OF MESON AND NEUTRON INTENSITIES ON DAYS OF HIGH ASYMMETRY

Particle	Location of station	$\bar{r}_1$	$\bar{\phi}_1$	$\bar{r}_2$	$\bar{\phi}_2$
Meson	East of Ahmedabad	0·35±0·12	167°	0·26±0·12	−20°
Meson	West of Ahmedabad	0·46±0·11	π+76°	0·32±0·11	175°
Neutron	Equatorial	0·42±0·02	π+17°	0·14±0·02	48°
Neutron	Middle latitude	0·41±0·02	π+79°	0·02±0·02	63°

mean intensity, the change in both the cases being lower at equatorial stations than at middle latitude stations.

(ii) The horizontal component of the earth's magnetic field having a high value 6 days prior to low asymmetry epochs reaches a minimum coincident with an enhanced C_p, 3 days prior to the epochs. The changes of daily mean cosmic ray intensity and the associated changes of geomagnetism make

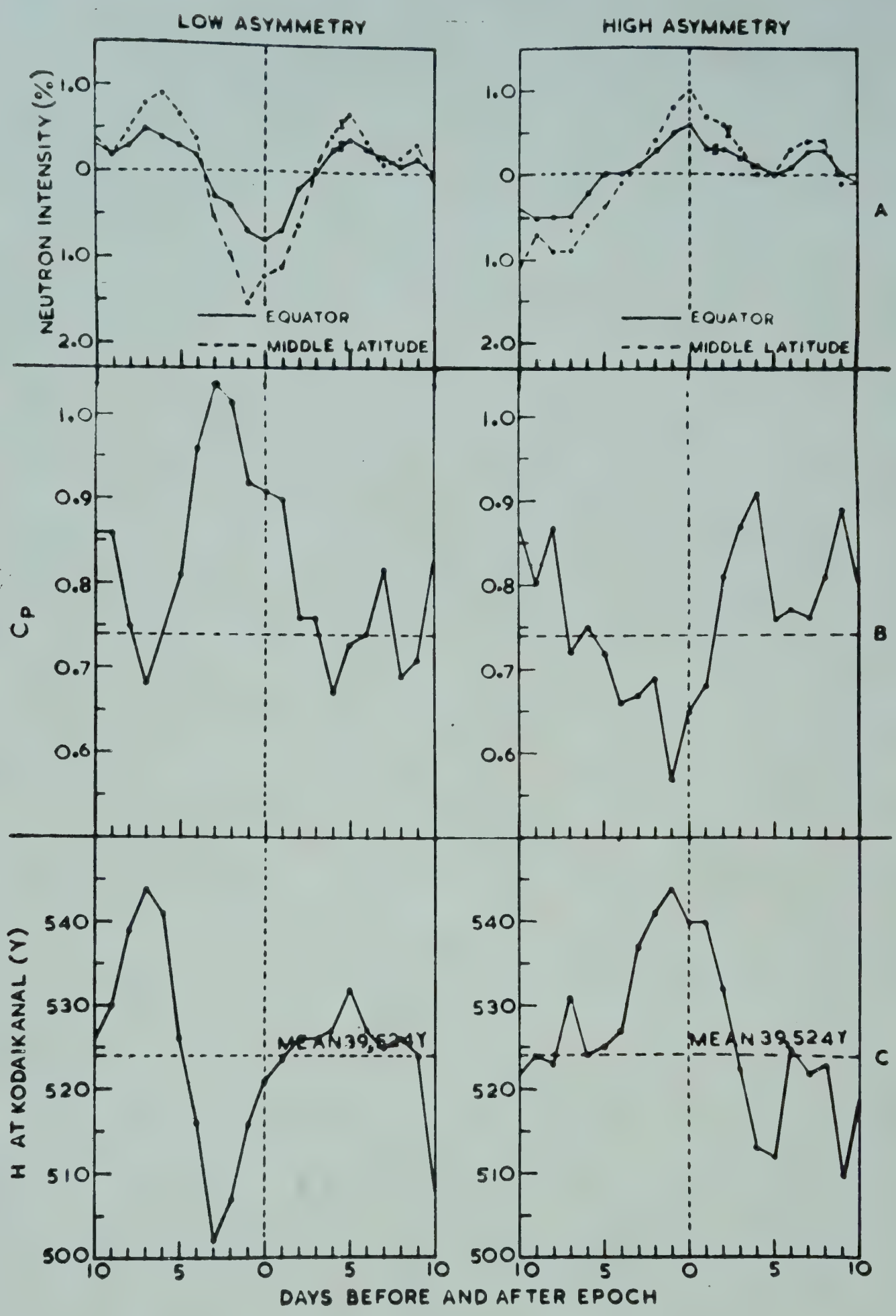

FIG. 2 — CHREE ANALYSIS OF (i) DAILY MEAN NEUTRON INTENSITY IN MIDDLE AND EQUATORIAL LATITUDE BELTS, (ii) C_p, AND (iii) H, THE DAILY MEAN INTENSITY OF HORIZONTAL COMPONENT OF THE GEOMAGNETIC FIELD AT KODAIKANAL FOR EPOCHS OF LOW AND HIGH EAST-WEST ASYMMETRY

it clear that low asymmetry epochs occur 3-5 days after the onset of cosmic ray storms generally associated with SC magnetic storms.

(iii) High asymmetry epochs occur with relatively undisturbed geomagnetic conditions. However, during the 4 days following epochs, C_p continuously

rises and H decreases indicating that high asymmetry occurs 3-5 days prior to the arrival of solar corpuscular beams which envelop the earth.

Changes in asymmetry can be caused due to the change in geomagnetic cut-off energy or due to the change of primary energy spectrum. Rothwell's[4] calculations show that ionized clouds from the sun emitted with high velocities can modify geomagnetic cut-off energies even at equatorial latitudes. Following Alpher[5] it can be shown that the cut-off energies in directions pointing 45°E and 45°W at Ahmedabad are

$$\epsilon^{E}_{\text{min.}} = \cos^4 \lambda/2{\cdot}52$$

and

$$\epsilon^{W}_{\text{min.}} = \cos^4 \lambda/5{\cdot}23 \qquad (1)$$

If the geomagnetic field varies such that the cut-off is changed in all directions, then

$$\delta\epsilon^{W}_{\text{min.}} = \frac{2{\cdot}52}{5{\cdot}23}\,\delta\epsilon^{E}_{\text{min.}} \qquad (2)$$

An examination of the formula reveals that high asymmetry can be produced only by a decrease in intensity in all directions, the decrease being smaller for west than for east and low asymmetry by an increase of intensity in all directions, increase in west being smaller than in east. On the other hand, it has been shown in Fig. 2, that high east-west asymmetry is associated with a world-wide increase of neutron intensity and low asymmetry by a decrease of neutron intensity. Thus the observed changes of intensity cannot be explained through changes in cut-off.

Interpretation of Changes of Asymmetry and Daily Variation

High Asymmetry. With a knowledge of the cut-off energy $\epsilon_{\text{min.}}$ for east and west directions derived by using Quenby and Webber's[6] method (23·1 and 11·2 BeV. respectively) and from the coupling coefficients derived for the two directions, the energy spectrum $\delta D(\epsilon)/D(\epsilon)$ of daily variation can be estimated by using the formula

$$\frac{\delta N^i}{N^i} = \int_{\epsilon_{\text{min.}}}^{\infty} \frac{\delta D(\epsilon)}{D(\epsilon)}\, W d\epsilon \qquad (3)$$

where $\delta N^i/N^i$ is the per cent change of intensity and W is the coupling coefficient in the appropriate direction. The coupling coefficients for east and west have been calculated by utilizing the experimental curves of Johnson and Read[7] showing the latitude effect of cosmic rays in these directions and using the method of extrapolation suggested by Dorman[8].

On days of high asymmetry, the daily variation has an energy spectrum of the type $a\epsilon^{-0{\cdot}8\pm0{\cdot}3}$, where $a = 0{\cdot}10$ and is consistent with an external source

situated at an angle of $112° \pm 10°$ to the left of the earth-sun line. Assuming the daily variation to be caused due to the acceleration of cosmic ray particles passing through solar plasma with frozen-in magnetic fields, it can be shown that the increase in intensity for east for telescopes looking at the beam for (24-x) hours is

$$\Delta N_E \approx \bar{N}_E \int_{\epsilon_{\text{min.}}}^{\infty} \left(1 - \frac{x}{24}\right) \frac{er}{\epsilon^2} \int W_E d\epsilon \qquad (4)$$

where $\bar{N}_E$ is the normal intensity, W_E is the coupling coefficient in east and e is the energy increment suffered by particles crossing the beam. The expression for increase in west intensity is the same as Equation (4) when the appropriate coupling coefficient and cut-off are used.

For telescopes looking at the beam for 12 hr, it is found that the energy increment required to explain the observed increase in asymmetry is 3·4 MeV. For a beam of width 3×10^{12} cm. and an intensity of trapped magnetic field of 10^{-6} gauss, the radial velocity would be about 10^8 cm./sec. The width of the beam is of sufficient magnitude to keep the earth in it for a day and the radial velocity of the beam which is about 36 hr agrees well with the value derived from the delay in onset time of Forbush decreases. From the associated changes of geomagnetism it is clear that high asymmetry occurs 3–4 days prior to the solar corpuscular streams enveloping the earth. A fairly satisfactory explanation of the increase in asymmetry and associated daily variation by a common mechanism involving the acceleration of cosmic ray particles crossing beams of solar plasma supports some of the basic concepts underlying the theory developed by Alfven[9], Brunberg and Dattner[10], Nagashima[11], Nerurkar[12] and Dorman[8]. A significant fact which emerges from this work is the evidence for the existence of streams with trapped magnetic fields and presenting an electric polarization as viewed from the earth even during a period of maximum solar activity. The process is possible only if the ejection of beams takes place in rarefied regions of interplanetary space which extend radially over active solar regions. The evidence presented by Fan *et al.*[13], relating to the observation of cosmic ray decrease at large distances from the earth coinciding with Forbush decrease on the surface of the earth, also requires the extension of great distances from the sun, of plasma clouds with trapped magnetic fields.

Low Asymmetry. Three to five days after the onset of cosmic ray storms associated with SC-type magnetic storms, low asymmetry is found to occur. The daily variation on geomagnetically disturbed days has the same exponent as the background cosmic ray intensity. Qualitatively, therefore, it appears that low asymmetry is caused by the screening or scattering of low energy particles due to magnetic fields in plasma clouds.

Acknowledgement

The author is grateful to Dr V. Sarabhai and Prof. K. R. Ramanathan for many valuable discussions and suggestions. The project was supported by the Department of Atomic Energy, Government of India.

References

1. Sarabhai, V. & Rao, U. R., *Proc. roy. Soc.*, **263A** (1961), 101–35.
2. Katzman, J. & Venkatesan, D., *Canad. J. Phys.*, **38** (1960), 1011.
3. Forbush, S. E. & Venkatesan, D., *J. geophys. Res.*, **65** (1960), 2213.
4. Rothwell, P., *J. geophys. Res.*, **64** (1954), 2026.
5. Alpher, R. A., *J. geophys. Res.*, **55** (1950), 437.
6. Quenby, J. J. & Webber, W. R., *Phil. Mag.*, **4** (1959), 90.
7. Johnson, T. H. & Read, D. N., *Phys. Rev.*, **51** (1937), 557.
8. Dorman, L. I., *Cosmic Ray Variations* (State Publishing House, Moscow), 1957.
9. Alfven, H., *Tellus*, **6** (1954), 232.
10. Brunberg, E. A. & Dattner, A., *Tellus*, **6** (1954), 73.
11. Nagashima, K., *J. Geomag. Geoelectr.*, **7** (1958), 51.
12. Nerurkar, N. W., *Proc. Indian. Acad. Sci.*, **45A** (1957), 341.
13. Fan, C. Y., Meyer, P. & Simpson, J. A., *J. geophys. Res.*, **65** (1960), 1862.

* * *

Semidiurnal Variation of Cosmic Rays on Magnetically Disturbed Days. H. S. Ahluwalia, Physical Research Laboratory, Ahmedabad.

A statistical study has been made of the semidiurnal variation of the intensity of cosmic rays on geomagnetically disturbed days using the data on nucleonic component obtained at the equatorial stations of Ahmedabad and Huancayo during 1957 and 1958 and assuming the interplanetary character figure C_p as an index of geomagnetic activity.

The study reveals that the low average amplitude of the semidiurnal variation observed on geomagnetically disturbed days, compared to geomagnetically quiet days, is primarily due to the large variability of the time of maximum of the semidiurnal variation on disturbed days. The individual amplitudes of the semidiurnal variation on geomagnetically disturbed days are comparable in magnitude to those obtained on geomagnetically quiet days.

This result constitutes one more evidence to show that the semidiurnal variation of the intensity of cosmic rays at equatorial stations is of extra-terrestrial origin. A theory of the daily variation has, therefore, to take into account the semidiurnal as well as the diurnal component. (*Abstract*)

Latitude variation and earth tide at Dehra Dun

R. S. CHUGH*

Survey of India
Dehra Dun

The paper briefly presents the astronomical theory of the motion of the earth's pole based on Euler's differential equations governing the motion of a solid about a fixed point and how this motion affects the latitude of an observatory, causes of earth tides and measurement both of polar variation and earth tides.

Latitude observations made at the Dehra Dun Astronomical Observatory commencing from June 20, 1957 using Talcott's method have been described. The mean latitude of Dehra Dun, as computed from Orlov's formula, has been found to be $30^\circ : 18' : 51''{\cdot}759$.

The curve plotted from observed monthly mean values of latitudes used for analysing 14-monthly, annual and semi-annual periodic terms of latitude variation and that plotted for latitude variation from coordinates X, Y of the pole, published at 10 days' intervals by the International Latitude Service, have been found to run closely parallel.

After eliminating the large change of latitude of semi-annual, annual and 14-monthly periods from the observational data, the residuals have been analysed for the constituents M_2, S_2, K_1 and O_1 of the earth tide. The theoretical values of these components have also been computed from the tide-generating potential. The ratio of observed tilt to the equilibrium tilt for the lunar semi-diurnal constituent M_2 has been found to be 1·81 which is very close to an expected value of 1·49 for the continental stations considering the short series of observations used for analysis.

General Remarks on Polar Motion and Earth Tides

The existence of the motion of the pole is an established fact, the causes being periodic circulations of winds, distribution of atmospheric pressure,

*Present address: Survey of India, Training Directorate, Bangalore

non-identity of axes of rotation and inertia of the elastic earth, bodily attraction of the earth by sun and moon and some other local causes.

The astronomical theory of the motion of the pole is based on Euler's differential equations governing the motion of a solid about a fixed point. He showed that a rigid body under no forces could rotate permanently about any of its principal axes of inertia, the motion being stable about the axis of either greatest moment or least moment. The shape of the earth is very close to that of an ellipsoid of revolution and if we put two least moments as equal ($A = B$), there is one stable rotation about the axis of the greatest moment. The moments being (A, A, C), a small disturbance from rotation about axis of greatest moment makes the axis of rotation move in a cone about the axis of greatest moment, completing its revolution within the body in a period $A/(C-A)$ times the period of rotation. In the case of earth, the value of $A/(C-A)$ given by the theory and observation of precession of the equinoxes is about 305 days. If the earth were an ellipsoid with three unequal axis ($A \neq B$), this cone would be elliptical.

This displacement of the pole of rotation within the earth can be detected by astronomical observations since they affect the observed latitudes of observatories, the colatitude of the station being the angle between local gravity and the earth's instantaneous axis of rotation and a motion of the instantaneous axis of rotation affects observed latitudes of all stations. Systematic observations of the variations at some six stations in as nearly as possible the same latitude give the displacement of the pole in two perpendicular directions at intervals of, say, one-tenth of a year.

The period of 305 days was based on the hypothesis that the earth is a completely rigid body. With the development of the theory of elastic deformation of the earth, the period is lengthened from 10 to 14 months and the 14-monthly motion is really the Eulerian nutation, and conversely the period of free oscillation in latitude gives a measure of the elastic strain.

There is a further forced variation of latitude of 12 months' period caused by periodic variations of the products of inertia with changes in mass distribution. The chief cause is the annual change in the distribution of air, which is shown by the great variations of pressure in Central Asia, with monsoons as the by-product. There are possible contributions from the accumulation of snow in winter and an almost negligible one from annual changes of vegetation. The theory of forced motion shows that the pole of rotation describes an ellipse whose amplitude depends on that of the motion of the pole of inertia and on the period of free motion.

The curves described by the instantaneous pole develop regularly in a clockwise spiral, alternately moving outwards and inwards, while at certain times they exhibit nodes and reversal of direction (Fig. 1). The maximum diameter of the spiral observed since 1900 is about 0·7 seconds of arc

corresponding to a displacement of $R \tan 0{\cdot}7'' = 21$ m. on the earth's surface. By the interference of the two components, 14- and 12-monthly, the amplitude of the spiral is a minimum about every seven years.

The attraction of the sun and moon on the body of the earth produces elastic deformations analogous to tides in oceans. The attraction produces a tilting of the surface which can be measured in favourable conditions. Love has introduced two dimensionless constants, known as Love numbers h and k, to characterize the various aspects of deformation of an elastic body subjected to a perturbing potential. Any type of deformation can be represented by a combination of these numbers which are in turn

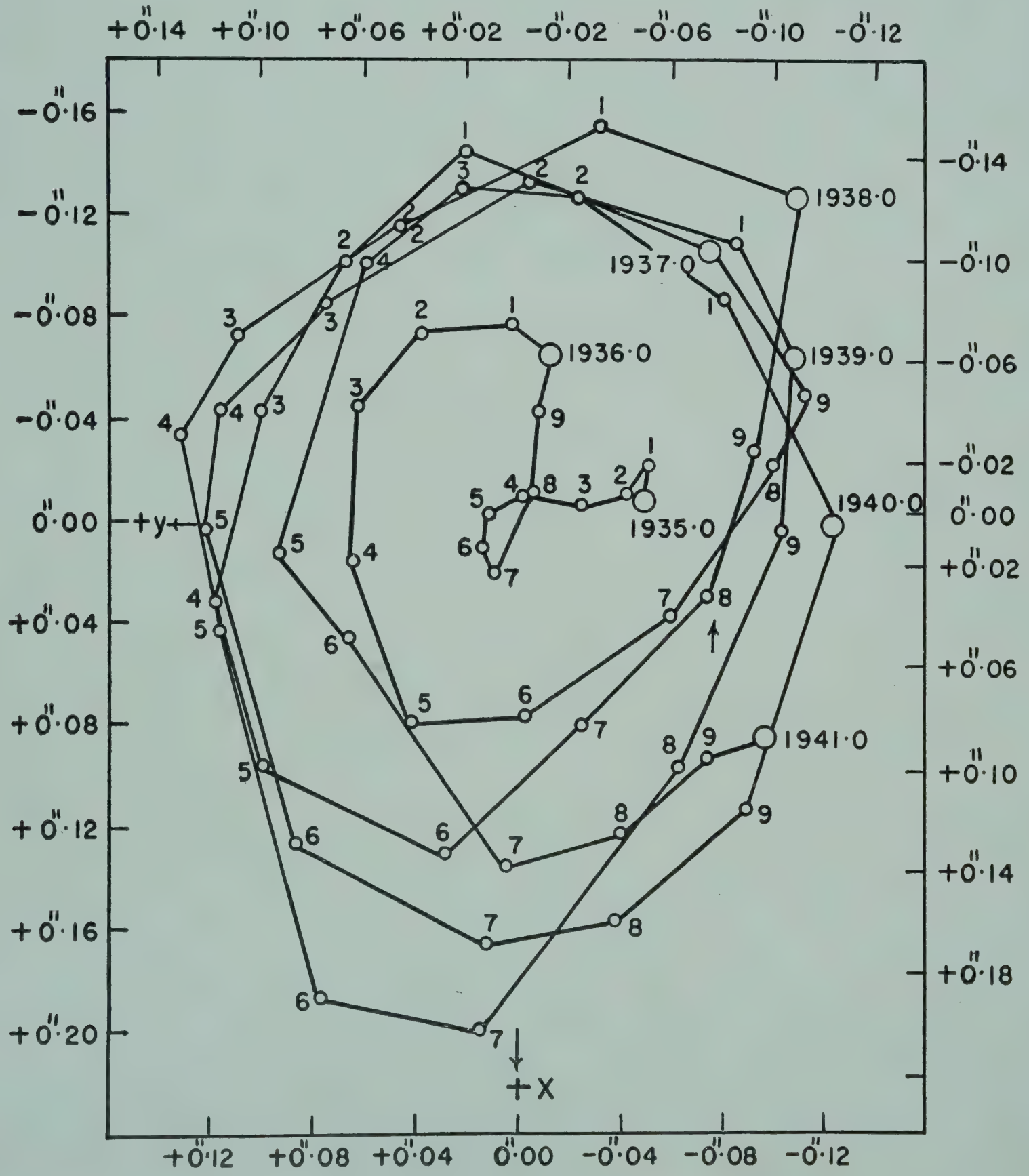

FIG. 1 — POLAR MOVEMENT DURING 1935·0–1941·0

related by fairly complex differential equations, to the distributions of modulus of rigidity and density in the earth. Another notation l was introduced by Toshi Shida in 1912; this is a quantity dependent on the linear elastic displacement along the meridian of the place of observations.

The tides of the so-called solid earth have been measured by means of (i) tidal deflection of the vertical referred to the adjacent ground measurements made with horizontal pendulums or with long water levels, (ii) tidal deflection of the vertical referred to the axis of the earth (calculated by analysis of astronomical observations for latitude), and (iii) tidal variation in gravity (measured by sensitive gravimeters).

The effect of tide-producing forces on an ideal unyielding earth can be theoretically computed and the ratios of the observed effect to the theoretical effect are of interest. These ratios can be expressed theoretically in terms of the numbers h, k and l. These numbers are applicable only in connection with those second degree spherical harmonics that represent the tidal forces and deformations of like kind produced by these forces. They do not apply to the actual tidal deformation of the earth as this is affected by the gravitational action of the oceanic tides and by the surface tractions produced by the shifting load of tidal water. The actual oceanic tide is very irregular as compared to the regularity of a second degree spherical harmonic. If we assume that the observations are so remote from the sea that the influence of oceanic tide is negligible and that other local effects are absent, then the factors for reducing, from the predicted effect for an unyielding earth, to the effect for the yielding earth, for the three cases mentioned above are $(1+k-b)$, $(1+k-l)$ and $(1+h-3/2k)$. These quantities should have numerical values near 0·72, 1·20 and between 1·15 and 1·22 respectively.

For the study of latitude variation and earth tides from observations of latitude, three methods are available: (i) Talcott's method used by the International Latitude Service (ILS) for the last 60 years (the method using the photo zenith tubes may be regarded as a derivative of it), (ii) the method of prime vertical which has been employed at the Basel Observatory, and (iii) the method of equal altitudes recently used successfully by Danjon at the Paris Observatory with the aid of Impersonal Astrolabe.

The motion of the pole is represented by the coordinate axis through the mean pole, OX tangent to the Greenwich meridian, OY tangent to the meridian 90°W and with given values of X and Y at any instant, the latitude variation at a place P in longitude $L°$ west, is given by

$$\Delta\lambda = X \cos L + Y \sin L + Z$$

Z is called the Kimura term which includes errors in aberration and nutation constants, the local effects of refraction and oscillation of the vertical. Thus it includes a part common to all stations (using the same stars) and a

part which is different for each station. The Z term can be eliminated to some extent by observing the latitude variation at three stations, using the same stars and a well-synchronized programme.

The results of observations at the ILS stations have been used to study a possible secular drift of the pole. This involves methods of calculation of the mean latitude of a station. Orlov suggested that mean latitude should be calculated from the formula

$$\lambda m = \frac{1}{20}\sum_{t=0}^{4}(\lambda_t+\lambda_{t+5}+\lambda_{t+6}+\lambda_{t+11})$$

which eliminates the oscillations of the annual and 14-monthly components of the motion of the pole. Melchior has shown that Orlov's method does not filter out oscillations of short period, viz. 0·5 to 1 year, and has suggested a combination S_4, S_5, S_6, S_7 from 45 ordinates. He first applies S_4S_5 and on the results obtained, he applies S_6S_7. The coefficients K_i of these combinations are:

	i	0	1	2	3	4	5	6	7	8	9	10	11	12	13
K_i	S_4S_5	9	9	8	7	6	5	4	3	2	1				
	S_4S_7	13	13	12	11	10	9	8	7	6	5	4	3	2	1

with $K_{(-i)} = K_{(i)}$

He also shows that this selectivity is even better than the selectivity of combination S_{30} which corresponds to mean of 61 ordinates, i.e. practically 6 years. However, by taking the mean pole as a running mean at intervals of 6 years, and by the method of Melchior, displacement of the mean pole from 1906 to 1946 according to Sekiguchi and Melchior are shown in Fig. 2. Every change

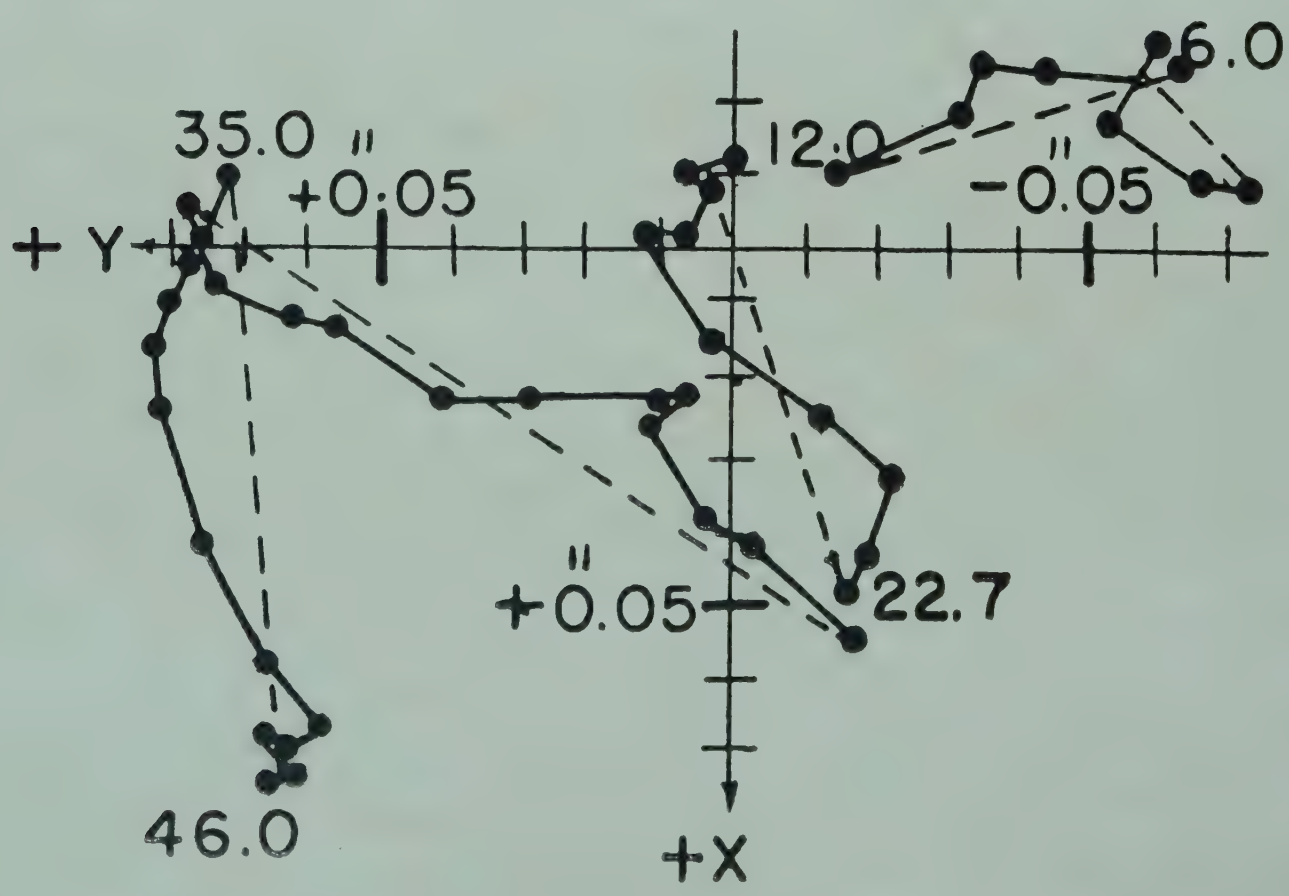

FIG. 2 — DISPLACEMENTS OF THE MEAN POLE DURING 1906–46

of the catalogue brings a change in the direction of drift of the mean pole, and for such studies the need of a homogeneous catalogue cannot be over-emphasized. Some oceanographers and geophysicists have tried to explain this drift as due to the melting of snow and ice and consequent rise in the level of the Atlantic. The study of large-scale drifting of the pole during geological eras is, however, beyond the scope of the present methods of instrumental astronomy.

Latitude Determinations at Dehra Dun

The observations were commenced on June 20, 1957 and those for study of latitude variation are still continuing.

The method adopted was that of Talcott's by making use of a Zenith Telescope and a Wild T_4 Universal Instrument. If λ be the latitude of the place, δ_N, ζ_N be the declination and zenith distance of a star transitting towards north of the zenith, and δ_S, ζ_S the values for a star transitting south, then $\lambda = \frac{1}{2}(\delta_N+\delta_S)+\frac{1}{2}(\zeta_S-\zeta_N)$. The first term is computed by the star places given in the catalogue, while the second term is so made, by the proper selection of stars, that it is measurable in terms of the micrometer screw only. The instrument is adjusted for level and setting of line of collimation in the meridian. Its various instrumental constants, viz. angular value of the micrometer drum, the interval between its outer meridional wires and the central wire in equatorial seconds of arc, the value of one division of the transit axis level and values of one division of Horrebow-Talcott levels have to be determined accurately by various methods available, in advance, and again periodically during the course of observations. After applying various corrections due to the axis tilt of the telescope, non-levelment of the instrument, collimation of different wires, curvature of the star's path, missing wire or pair, the instantaneous latitude of the place from each star pair is computed. This determination is burdened with accidental errors of observations, declination errors of the catalogue, and error in the adopted value of the run of the micrometer.

Considering the latitude of Dehra Dun and its peculiar weather conditions, the observation could be arranged only in six different groups, each consisting of seven to eight pairs of stars, so that two groups could be observed each night, including one more whenever it was found that the connection between the two morning and evening groups could not otherwise be sufficiently well determined.

The group results observed every night were reduced by the method of least squares, assuming that $d\Delta$ to be the correction to the mean colatitude of a group for a night and $d\mu$ to be the correction to the value of one division of the micrometer screw, observation equations were formed one for each

pair. Converting them into normal equations, they were solved for $d\Delta$ and $d\mu$. The weights given were 1 for a single pair and 0·7 to each of the two values obtained from a double pair. The value of $d\Delta$ being negligible, the values of $d\mu$ were utilized later in the computation of declination errors of individual star pairs as described below.

As the pair means generally differed from the group means, the differences were utilized in calculating the declination errors of the pairs and the corrections to the values of one division of micrometer, knowing that

$$\gamma_{im}-\gamma_m = [M_m-M_{im}]d\mu+d\delta i$$

where im denotes the pair, m the group mean, γ the colatitude, $d\mu$ correction to one division of micrometers, $d\delta i$ the declination error of the pair i, and M the semi-difference of the zenith distance for the same pair as obtained from micrometer readings to the stars of the pair (corrected for micrometer errors, refraction, level, etc.). The values of $d\mu$ and $d\delta i$ were determined by the method of successive approximations. For doing so, in the absence of observations with same stars at other observatories, the consideration kept in view was that as the same group was observed first in the morning for 2 months and then in the evening for subsequent 2 months, declination errors of the pairs in the two cases must be the same. Starting as a first approximation the value of $d\mu$ determined from least square adjustment, described above, separately for each group observed in the evenings and mornings, two values of $d\delta i$ of the same group corresponding to evening and morning means were obtained. Taking the mean as the declination error, a second approximation for $d\mu$ both for morning and evening values was computed. The process was repeated to get a second approximation to values of $d\delta i$, a third approximation to values of $d\mu$ and the process was continued until the $d\mu$'s could no more be refined. The values of declination errors of different star pairs observed with different instruments and different years are given in Table 1. The agreement between the different values of $d\delta i$ is an indication of the true errors of the catalogue.

The values of colatitudes from each pair were then corrected for the declination errors and the micrometer errors. The night means were then taken and a weight equal to the number of pairs observed in that night was given to it. The difference between the means on different faces gave the face correction separately for the various morning and evening groups and half of this quantity was added to or subtracted from the values of colatitudes observed on different faces.

Generally, the two group means of colatitudes for the same months of observations are not the same and the differences are attributed to residual declination errors of the groups. These group differences for the observations carried out with Wild T_4 from June 1957 to December 1958 are given in Table 2, with the number of nights of observations, which gives the weights

TABLE 1 — DECLINATION ERRORS

Group	Instrument	Year	Pair 1	2	3	4	5	6	7	8	9
II	T_4	1957	−0″·297	−0″·083	+0″·003	+0″·330	−0″·125	−0″·015	+0″·185		
		1958	−0″·053	+0″·138	−0″·082	+0″·178	−0″·116	+0″·028	−0″·096		
	Z.T.	1957	−0″·219	−0″·039	+0″·080	+0″·046	−0″·136	+0″·244	−0″·063		
		1958	+0″·028	+0″·028	+0″·198	−0″·056	+0″·006	−0″·031	−0″·174		
		1959	−0″·126	+0″·028	+0″·092	+0″·096	+0″·046	+0″·018	−0″·154		
		1960	−0″·076	−0″·070	+0″·064	+0″·224	−0″·040	+0″·188	−0″·288		
III	T_4	1957	+0″·086	−0″·119	−0″·077	−0″·084	+0″·220	−0″·070	+0″·043		
		1958	−0″·108	+0″·054	−0″·049	−0″·166	+0″·211	+0″·026	+0″·030		
	Z.T.	1957	−0″·129	+0″·070	−0″·044	−0″·145	+0″·133	+0″·156	−0″·042		
		1958	−0″·084	−0″·044	+0″·078	−0″·183	+0″·153	+0″·132	−0″·052		
		1959	−0″·292	−0″·118	+0″·176	−0″·014	+0″·357	−0″·003	−0″·106		
IV	T_4	1957	−0″·100	−0″·021	+0″·000	−0″·078	+0″·005	+0″·212	−0″·078	+0″·057	
		1958	−0″·262	−0″·004	+0″·008	−0″·099	+0″·084	+0″·208	−0″·037	+0″·104	
	Z.T.	1957	−0″·078	+0″·041	+0″·041	−0″·008	−0″·202	+0″·222	−0″·026	+0″·008	
		1958	−0″·128	+0″·016	+0″·145	−0″·086	−0″·206	+0″·171	−0″·058	+0″·140	
		1959	+0″·010	+0″·042	+0″·173	−0″·040	−0″·204	+0″·079	+0″·075	−0″·134	
V	T_4	1957-58	+0″·034	−0″·152	−0″·028	−0″·016	+0″·152	+0″·054	+0″·084	−0″·122	−0″·004
	Z.T.	1958	+0″·173	−0″·074	−0″·238	−0″·143	+0″·144	+0″·030	+0″·014	−0″·132	+0″·234
		1959	+0″·028	−0″·042	−0″·266	+0″·198	+0″·306	−0″·096	+0″·137	−0″·010	−0″·255
		1960	−0″·004	−0″·060	−0″·119	+0″·040	+0″·220	+0″·028	−0″·092	+0″·134	−0″·146
VI	T_4	1958	+0″·138	+0″·022	−0″·148	+0″·044	+0″·029	−0″·030	+0″·114	−0″·170	
	Z.T.	1958	+0″·172	−0″·142	−0″·144	−0″·052	−0″·098	+0″·274	+0″·016	−0″·025	
		1959	−0″·035	+0″·066	−0″·179	−0″·052	+0″·038	+0″·414	0″·000	−0″·252	
		1960	−0″·152	+0″·056	−0″·092	−0″·050	+0″·102	+0″·338	+0″·140	−0″·338	
I	T_4	1958	+0″·102	+0″·030	−0″·009	+0″·166	+0″·058	−0″·082	−0″·296	+0″·030	
	Z.T.	1958	+0″·116	+0″·099	+0″·119	+0″·090	+0″·085	−0″·224	−0″·305	+0″·020	
		1959	+0″·206	+0″·042	+0″·104	−0″·112	−0″·044	−0″·108	−0″·294	+0″·206	
		1960	+0″·154	+0″·121	+0″·048	+0″·002	−0″·014	−0″·210	−0″·364	+0″·262	

TABLE 2 — DEFINITIVE GROUP CORRECTIONS TO COLATITUDES

Group		No. of observations	Date	γ_E-γ_M	Correction	γ_E-γ_M Corrected	Corrections to reduce to	
							Group II/IV	Main groups
II	E	10	20/21-8-57 to 5/6-10-57	−0″·011	−0″·039	−0″·050	0″·000	+0″·042
III	M	9	20/21-8-57 to 5/6-10-57				−0″·050	−0″·008
	E	16	11/12-10-57 to 27/28-11-57	−0″·001	−0″·039	−0″·040	−0″·050	−0″·008
IV	M	12	4/5-10-57 to 26/27-11-57				−0″·090	−0″·049
	E	9	19/20-12-57 to 7/8-2-58	+0″·026	−0″·038	−0″·012	−0″·090	−0″·049
V	M	10	19/20-12-57 to 7/8-2-58				−0″·102	−0″·060
	E	14	15/16-2-58 to 31/1-4-58	+0″·136	−0″·039	+0″·097	−0″·102	−0″·060
VI	M	13	15/16-2-58 to 31/1-4-58				−0″·005	+0″·037
	E	19	3/4-4-58 to 27/28-5-58	+0″·041	−0″·039	+0″·002	−0″·005	+0″·037
I	M	18	3/4-4-58 to 27/28-5-58				−0″·003	+0″·038
	E	13	3/4-6-58 to 21/22-7-58	+0″·041	−0″·038	+0″·003	−0″·003	+0″·038
II	M	10	24/25-5-58 to 4/5-7-58				0″·000	+0″·042
			Sum	+0″·232	−0″·232	0″·000	−0″·250	0″·000
IV	E	9	19/20-12-57 to 7/8-2-58	+0″·026	−0″·040	−0″·014	0″·000	−0″·051
V	M	10	19/20-12-57 to 7/8-2-58				−0″·014	−0″·065
	E	14	15/16-2-58 to 31/1-4-58	+0″·136	−0″·040	+0″·096	−0″·014	−0″·065
VI	M	13	15/16-2-58 to 31/1-4-58				+0″·082	+0″·031
	E	19	3/4-4-58 to 27/28-5-58	+0″·041	−0″·040	+0″·001	+0″·082	+0″·031
I	M	18	3/4-4-58 to 27/28-5-58				+0″·083	+0″·032
	E	13	3/4-6-58 to 21/22-7-58	+0″·041	−0″·040	+0″·001	+0″·083	+0″·032
II	M	10	24/25-5-58 to 4/5-7-58				+0″·084	+0″·033
	E	16	12/13-8-58 to 29/30-10-58	+0″·026	−0″·040	−0″·014	+0″·084	+0″·033
III	M	19	8/9-8-58 to 29/30-10-58				+0″·070	+0″·020
	E	8	3/4-11-58 to 29/30-11-58	−0″·031	−0″·039	−0″·070	+0″·070	+0″·020
IV	M	24	9/10-10-58 to 29/30-11-58				0″·000	−0″·051
			Sum	+0″·239	−0″·239	0″·000	+0″·305	0″·000

TABLE 3 — CORRECTED MONTHLY MEAN VALUES OF LATITUDE

Epoch	1957·647	·727	·781	·880	57·973	58·041	·132	·225	·282	·376	·463	·507	·619	·797	·882	1958·956
Observed latitude	30°18′															
λ	51″·865	·882	·984	·950	·988	·793	·600	·530	·497	·490	·590	·575	·722	·970	51″·999	52″·122

(n_1n_2/n_1+n_2), and according to which the closing error was distributed. Closing error was found to be of the same sign as that of all the stations of ILS in northern hemisphere.

In order to reduce all the observations to the same group, the group correction for the declinations of group II was assumed as 0″·000 and the values for other groups were deduced. As these values would give an alteration in the mean of the latitudes, the starting value of group II was modified, thus obtaining definitive group corrections. These values are also given in Table 2.

The values of colatitude from each star pair were corrected for declination, micrometer errors, face and group differences. From these, corrected monthly mean values of latitude were worked out (Table 3). The mean latitude of the observatory, calculated by Orlov's formula, came out as 30°: 18′: 51″·759. Since long-period data were not available, Melchior's formula could not be used to find the mean latitude of the observatory.

Results of Latitude Variation

The latitude variation from monthly mean values obtained from observations with Wild T_4 from August 1957 to December 1958 is plotted in Fig. 3 in which the variation curve as computed from coordinates X, Y of the pole, circulated by the ILS, with the formula $X\cos L+Y\sin L$, and corrected for $\Delta\lambda$ as computed from Orlov's formula, has also been drawn. The observational curve not only includes the local Z term but also is weak during the monsoon months when weather conditions do not permit sufficient observations to be taken. It has already been stated that from observations at one station alone, the annual component of the motion of the pole cannot be

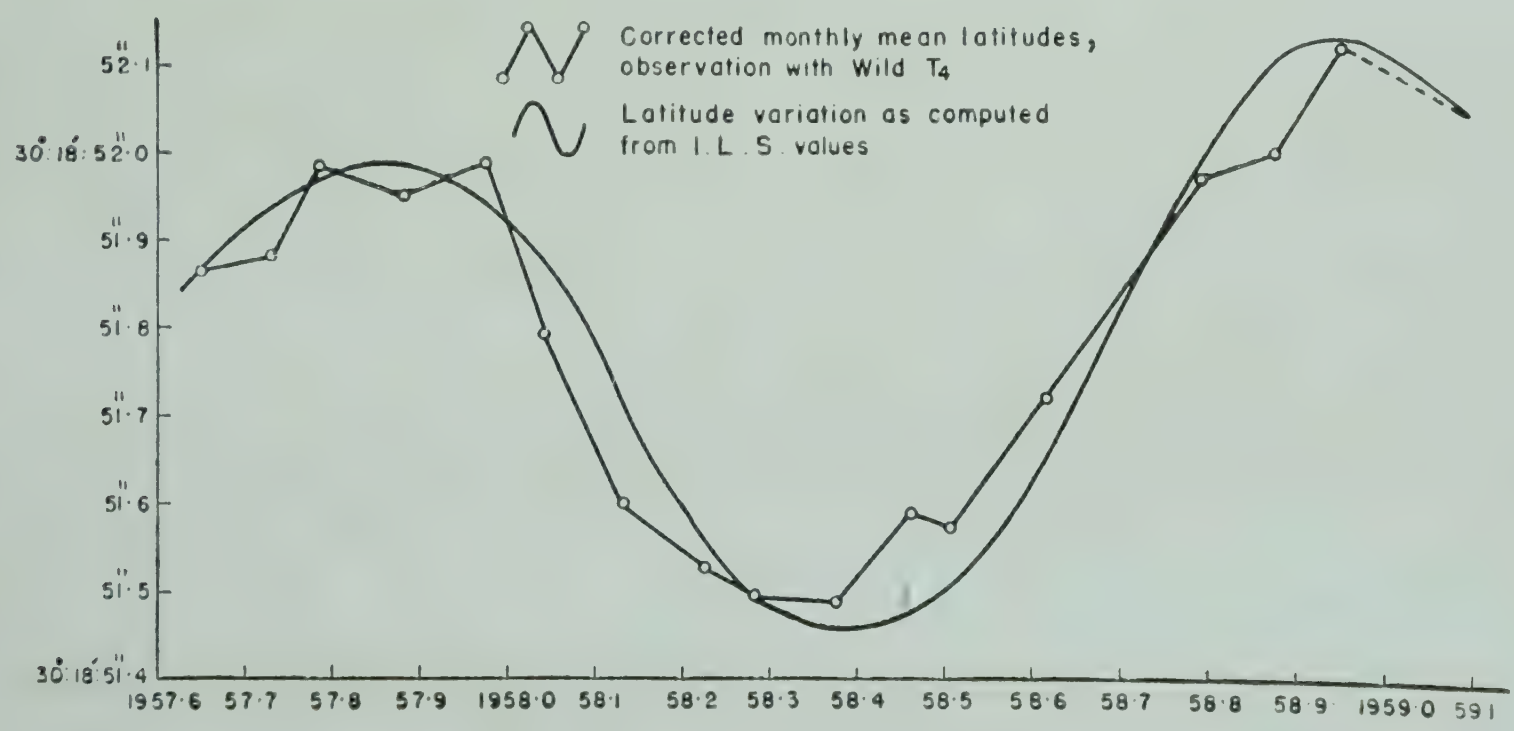

Fig. 3 — Latitude variation at Dehra Dun during 1957·6–1959·1

separated from the individual Kimura term of that station. However, the two curves are seen to run closely parallel.

Observational equations were formed for the two main periodic terms of latitude variation, viz. the annual and 14-monthly, at intervals of 0·05 of a year and were solved by least squares. The length of data taken for this purpose was 14-monthly from the epochs 1957·65 to 1958·83. It was realized that these two terms can be efficiently separated only if the data extend to 7 years, but such a length of the series was not available. The results are as follow, and in these equations m and n give speeds of 14-monthly and annual components, i.e. 36° and 30·5° per 0·1 year and origin of time is 1957·00:

(i) From the curve drawn with observed monthly mean values

$$\Delta\lambda = 0''\cdot1127 \cos (mt - 336^\circ\cdot4) + 0''\cdot1654 \cos (nt - 215^\circ\cdot9)$$

The first term includes the Z term.

(ii) From the curve drawn from ILS values for the same period

$$\Delta\lambda = 0''\cdot1623 \cos (mt - 13^\circ\cdot9) + 0''\cdot2486 \cos (nt - 212^\circ\cdot6)$$

The first term does not include the Z term.

The effect of polar motion as deduced in (i) was removed from the monthly values and the residuals were subjected to harmonic analysis for a semi-annual term and it was calculated to be $0''\cdot056 \cos (lt - 348^\circ\cdot1)$.

A similar semi-annual term was, however, not calculated from the ILS curve for the same period.

Influence of Earth Tides. To extract the tidal effect from the observational data of latitude, the large change of latitude of annual and 14-monthly periods was eliminated by subtracting a general smoothed value of these changes from the latitudes given by individual star pairs and the residuals thus remaining, viz. *li* from September 30, 1957 to October 30, 1958 were analysed for M_2, S_2, K_1 and O_1 terms of the tide. An equation was formed for each of such residuals from a star pair in the following manner:

$$M_2 \cos [(v_0+u)_{M_2} - m_2^\circ] + S_2 \cos [(v_0+u)_{S_2} - s_2^\circ] + K_1 \cos [(v_0+u)_{K_1} - k_1^\circ] + O_1 \cos [(v_0+u)_{O_1} - o_1^\circ] - l_1 = 0$$

There were 1254 such equations which were solved by the method of least squares. The resulting amplitudes and phase lags are given in Table 4.

It is clear that amplitudes of constituents are not in the equilibrium ratios, particularly the term S_2 cannot be analysed effectively from latitude observations which are done always at night. Similarly, diurnal constituents, in the tilt, are also unreliable as they are burdened with thermal effects, etc. Reliance can be placed only on the M_2 constituent.

TABLE 4 — AMPLITUDES AND PHASE LAGS OF TIDAL CONSTITUENTS FROM OBSERVATIONS

	M_2	S_2	K_1	O_1
R	0″·013722	0″·045182	0″·013680	0″·029142
H = R/f	0·013293	0·045182	0·015124	0·034548
g	17°·5	129°·3	247°·5	273°·2
k	14°·2	120°·4	242°·8	273°·6

The theoretical earth tilt was calculated from Doodson's development of the tide-generating potential. Using his notations, the tide-generating potential, V, can be expressed as

E = mass of the earth
M = mass of the moon
r = distances between centres of earth and moon
i/c = mean value of $1/r$
ρ = radius of earth at a given point P
λ = latitude of P
a = mean radius of earth
g = mean value of acceleration due to gravity
V = tide-generating potential due to moon

$$V = \mu\frac{M\rho^2}{r^3}\left(P_2+\frac{\rho}{r}P_3+\frac{\rho^2}{r^2}P_4+\ldots\right)$$

$$= V_2+V_3+V_4+\ldots$$

where $P_2 = \frac{1}{2}(3\cos^2\theta-1)$, etc.
θ = geocentric zenith distance of moon from P
μ = attraction between unit masses at unit distance apart
$= g\cdot\frac{a^2}{E}$

The development of the potential is a series of terms, harmonic in time, and for a typical constituent the mean value of the expression for V takes the form

$$V = CG.f(\lambda)\cos A$$

where A = phase of the constituent referred to the local meridian
$f(\lambda)$ = a function of latitude
C = numerical coefficient of the harmonic constituent as given by Doodson
$G = \frac{3Mga^2\rho^2}{4Ec^3}$

The expression for solar tide-generating potential is similar in form to the above except that G is replaced by

$$G_1 = \tfrac{3}{4} \times \frac{S}{E} \times \frac{ga^2\rho^2}{c_1^3} = 0{\cdot}4604G$$

In the development, G is retained as a common coefficient for both lunar and solar constituents and necessary adjustments are made in the numerical coefficients. Considering terms arising from V_2 alone, $f(\lambda)$ has the values $\sin 2\lambda$ for the diurnal tides and $\cos^2\lambda$ for the semidiurnal tides.

The equilibrium earth tide, which is the equipotential surface arising from the potential of gravity $\overline{V}$ and the tide-generating potential V is given by

$$\overline{V} + \zeta \frac{\partial \overline{V}}{\partial r_1} + V = \text{constant}$$

where ζ is the surface elevation above mean.

Assuming $\overline{V}$ to be constant on earth's surface and because

$$\frac{\partial \overline{V}}{\partial r_1} = -g, \; \zeta = \frac{V}{g} = \frac{CGf(\lambda)\cos A}{g}$$

If $\Delta\zeta$ is the increment in ζ corresponding to an increment in λ of $\Delta\lambda$, then

$$\Delta\zeta = \frac{\partial\zeta}{a\partial\lambda} a\Delta\lambda$$

and the equilibrium earth tilt in the meridian is given by

$$Lt \frac{\Delta\zeta}{a\Delta\lambda} = \frac{1}{a} \frac{\partial\zeta}{\partial\lambda} = \frac{CGf'(\lambda)\cos A}{ag}$$

where $f'(\lambda)$ is equal to $2\cos 2\lambda$ for diurnal tides and $-2\sin\lambda\cos\lambda$ for semidiurnal tides.

Taking $a = 6{\cdot}3712 \times 10^3$ km., $c = 3{\cdot}8440 \times 10^5$ km., $M/E = 1/81{\cdot}53$, $\lambda = 30°19'24''$, $C =$ coefficients given by Doodson, the values of equilibrium earth tilt have been worked out as under

M_2	S_2	K_1	O_1
0″·006841	0″·003186	0″·004443	0″·003156

Therefore, the ratio of observed tilt to equilibrium tilt $= 1+k-l$ works out to 1·94 for M_2.

The agreement between this and the expected value, 1·20, is very close, considering the short series of observations used for analysis.

Next, the semi-annual term of latitude variation was also eliminated from the residuals l_1, giving new residuals l_2, and these also were analysed for M_2, S_2, K_1 and O_1 and the values of amplitude and phase lag of M_2 were obtained as $0''{\cdot}012400$ and $22°{\cdot}3$ which gave a better value of $1+k-l = 1{\cdot}81$.

The lunar effect of earth tilt was also evaluated from the mean values of l_1 classified at 10 min. and 1 hr intervals, of lunar hour angles, separately, by the method of least squares. The results of these analyses were expressed in the following forms respectively, in which θ is the lunar hour angle:

$$\Delta\lambda = -0''{\cdot}0217+0''{\cdot}0202\cos(\theta-178°)+0''{\cdot}0187\cos(2\theta-66°)$$
$$\Delta\lambda = +0''{\cdot}0075+0''{\cdot}0362\cos(\theta-146°)+0''{\cdot}0174\cos(2\theta-327°)$$

In both cases, the amplitudes of M_2, more or less, agree with each other and also with the values analysed earlier. Data used for this analysis are also of short duration.

In observations for the latitude, the plumb line is referred to the earth's axis, not to the adjacent ground as is the case with observations with the horizontal pendulum. No correction, therefore, is needed for the deformation of the ground by the tidal load. A correction is, however, necessary in general for the gravitational effect on the plumb line of oceanic tides, but as the astronomical observatory at Dehra Dun is far away from the sea, no correction appears necessary for the attraction of the tidal water also.

While discussing the earth tides, Nishimura stated that discriminating between continental and coastal stations, the values $(1+k-l)$ for continental and coastal stations would be 1·49 and 1·07 respectively. The continental value of 1·49 is very close to the value 1·81 as obtained from Dehra Dun observations.

Acknowledgement

The author's thanks are due to Sarvashri S. K. Sharma, J. C. Bhattacharji and A. K. Bhattacharji and computers of the astronomical section of the Tidal Party for carrying out the computations, and all the observers who took part in the programme. Thanks are also due to Col. S. K. S. Mudaliar, Director, Survey of India, for his valuable guidance and advice in the execution of this project.

Literature

1. Carnera, L., *Results of International Latitude Service*, Vol. IX (International Latitude Service), 1957.
2. Melchior, P. J., *Latitude Variation* (Communications de l'Observatoire Royal de Belgique, No. 130, Bruxelles), 1957.
3. Doodson, A. T., *Int. hydr. Rev.*, **31** (1954), 37–62, 63–93.
4. Corkan, R. H., *Analysis of Tilt Records at Bidston*, Geographical Supplement, Vol. IV, 1937–40 (Royal Astronomical Society, London), 1940.

The Indian mean sea level

R. S. CHUGH*

Survey of India
Dehra Dun

The mean sea level as the surface of reference for basing precise elevations of points has been defined in detail. For the determination of the mean sea level, methods have been discussed for elimination of oscillations and surface gradients due to waves and tides, variations of atmospheric pressure and winds, effects of temperature and salinity, the 19-yearly tide, effect of eustatic factors, etc. Variations and eustatic changes in sea level in other parts of the world have been discussed in brief. The annual and secular variations of sea level in the Arabian Sea and Bay of Bengal have been presented graphically. The secular variation and amplitudes and phase lags of the 19-yearly tide, for four representative ports, for different epochs, have also been computed. Some results of local coastal subsidence have been given. It has been recommended that in the adjustment of Second Level Net of India, it will be necessary to confine to mean sea level values adjusted to a specified epoch.

A knowledge of precise elevations of points in a country is indispensable for all survey and engineering operations. The height datum is the geoid which is defined as ' an equipotential surface coinciding with the surface of the waters of the ocean, if they were free from the periodic disturbing effects of the sun and moon, the wind, the varying barometric pressure, and differences of temperature and density of the water and under land areas the geoid surface is that which would coincide with the water surfaces in narrow sea level canals if they were extended inland through the continents '. For the determination of the mean sea level in the open oceans, tidal observations are made with automatic tide gauges on coastal stations on the open sea but not within estuaries, gulfs or tidal rivers where the waters may be shallow. From the tidal observations the oscillations by the sea surface due to waves and tides, the surface gradients along the coasts due to variations of atmospheric pressure and to wind, the effects of other currents and of temperature and salinity have to be eliminated. It is necessary to take

*Present address: Survey of India, Training Directorate, Bangalore

the values over a number of complete years so that nodal and seasonal variations can be eliminated, but where data of a long period are being subjected to this analysis, the effects of the eustatic factors, i.e. increase of the mean sea level due to melting of polar ice, and land uplifts and subsidence have also to be considered. It is also incumbent to determine how far mean sea levels at various ports deviate from an equipotential surface.

Indian Levelling Adjustment of 1909. A simultaneous reduction of the level net was carried out in 1909–10 on the basis of height datum as the determination of mean sea level at nine selected tidal observatories. The following are the names of the tidal stations and the years of observations from which mean sea levels were determined:

Karachi, 1868–1910 (40 years); Bombay, 1878–1910 (30 years); Karwar, 1878–83; Beypore, 1878–84; Cochin, 1886–92; Nagappattinam, 1881–88; Madras, 1880–90; 1895–1910 (23 years); Vishakhapatnam, 1879–85; and False Point, 1881–85. Only the direct means of the annual values of the mean sea level were accepted and no attempt was made to refine them for the effect mentioned earlier.

The probable error of a final determination of mean sea level from 6 years' observations at any one port was calculated to be generally about 0·02 ft and as the probable errors of levelling are apparently larger than this, the mean surface of the oceans around these tidal stations was made the surface of reference. During these studies it was noticed that variations in the sea level with time in the Arabian Sea—Maskat to Cochin—was uniformly less than variations in the Bay of Bengal. Next, differences in the height of the mean sea at different places were investigated. Some lines indicated that the Bay of Bengal was 1 ft higher than the Arabian Sea and the sea level at Karachi was 1 ft higher than that at Bombay, but the accuracy of levelling was soon found not enough to warrant such definite conclusions.

Sea Level Variation in North America. The United States Coast and Geodetic Survey (USCGS) have reached certain conclusions from their study of variations of mean sea level from tidal records and a least square solution of levelling circuits based on the sea level of Galveston, Tex. They have found that there is a distinct tendency for the plane of mean sea level (MSL) to slope downwards in an easterly direction along the Gulf Coast of the United States and upwards in a northerly direction along both the Atlantic and Pacific Coasts of the continent of North America, and that the general elevation of the MSL plane on the Pacific Coast is higher by 206 mm. than that on the Atlantic Coast and this has been confirmed by accurate levelling carried across the Isthmus of Panama. The cause of the origin of the Gulf Stream is stated to be the difference in sea level in the Gulf of Mexico.

The reports of the USCGS state that over the past fifty years, sea level has been rising along the Atlantic Coast at an average of 1 ft per century. There have been ups and downs, but the net change has been an increase in sea level that is probably related to the gradual melting of the polar ice caps. On the Pacific Coast the rate has been only half of that on the Atlantic. An investigation was conducted in SE Alaska during the summer of 1959 where the land as measured from sea level appears to have risen as much as 5 ft in sixty years.

Reports of Unified European Levelling Network (UELN) Adjustments and 1959 Symposium at Liverpool. A preliminary report of UELN Commission of the International Association of Geodesy (IAG) indicated that the MSL, as shown by levelling and tidal reductions, was roughly −25 cm. in the Mediterranean, 0 at Amsterdam (and Atlantic), +15 cm. on North Sea and +25 cm. on Baltic, but these showed some apparent discrepancies from the geoid. The adjustment of UELN was later executed at Delft (1959) and the summarizing remarks made with reference to MSL are as follow:

(i) " It is thought, it is not now possible to arrive at a reliable conclusion about the behaviour of MSL along the Atlantic Coast.

(ii) " Without an improvement of the levellings on the Scandinavian peninsula, it is not possible to draw a reliable conclusion about the difference in level between the Gulf of Bothnia and the Atlantic.

(iii) " Great care should be taken in drawing conclusions from the observed difference in level between the Atlantic and the Mediterranean.

(iv) " Although the matter belongs to the competence of oceanographers, attention is drawn to the importance of getting a better insight into the definition of MSL, and into the accuracy of that definition at the mareographs."

Geodetic levelling has been carried out three times in Great Britain, first between 1840 and 1860, second between 1912 and 1952, and third between 1951 and 1959. When the work of the third geodetic levelling was computed and compared with the second, some disturbing differences were disclosed, the most disturbing being the relative values of MSL at Newlyn, Felixstowe and Dunbar for the epochs 1918 and 1950. The records for Felixstowe and Dunbar were not unfortunately very satisfactory, and definite conclusions could not be reached regarding causes of these differences.

Doodson has shown that the variation due to local barometer and its north and east gradients between Newlyn and Liverpool account for a difference of 0·25 ft in the mean sea level at the two places provided there were no wind and there was a uniform field of pressure. Under these conditions he

has used the simple formula

$$Z-\bar{Z} = b(B-\bar{B})+e(E-\bar{E})+n(N-\bar{N})$$

where Z is the daily MSL, B the barometric pressure at the place, E the increase of pressure 500 km. east over pressure 500 km. west of place, N for the north over south, the mean values of B, E, N, being $\bar{B}$, $\bar{E}$, $\bar{N}$, and b, e, n constants to be determined from equations. He has also shown that the range of secular change in MSL at ports is considerably reduced after meteorological effects from the annual values of mean sea level are removed. The mean sea level variations at Newlyn, Den Helder, Esbjerg and Dunbar were expressed in terms of four barometric pressures covering the North Sea and English Channel by using long series of annual values by the following formula:

$$Z-\bar{Z} = a_1(B_1-\bar{B}_1)+a_2(B_2-\bar{B}_2)+a_3(B_3-\bar{B}_3)+a_4(B_4-\bar{B}_4)$$

where the values of B for the stations at the extreme boundaries of the area are known from meteorological summaries, the mean values of B are indicated by $\bar{B}$, the values of a are constants to be determined, and Z is the annual value of mean sea level. The values of $Z-\bar{Z}$ were modified to eliminate what appeared to be a reasonable value of the secular variation centred on the middle year.

Lisitzin has shown that in the Gulf of Bothnia, the existence of a predominant distribution of atmospheric pressure, the prevailing winds and the regional differences in the mean vertical density of the sea water affect the surface of the sea with the mean amounts of 1·8, 3·0 and 4·7 cm. respectively, resulting thus in an average total annual height difference of 9·5 cm. between the innermost and the outermost parts of the gulf. It is, therefore, by no means insignificant whether the mean surface in the interior area or at a place near the approaches to the gulf is chosen as a reference level.

The effect of water density on the mean slope of the sea surface in the English Channel, North Sea, Baltic Sea and Western Mediterranean has been studied by Bowden. Expressing the slope of the sea surface due to the variation of density with position by

$$\frac{\partial \zeta}{\partial x} = -\frac{1}{\bar{\rho} h}\int_0^h \frac{\partial \bar{\rho}_z}{\partial x} z\, dz \qquad (1)$$

where ζ is the elevation above a standard level surface, near the free surface of the sea, Z is measured vertically downwards, $\bar{\rho}$ is the mean density, h is the depth of water and $\bar{\rho} z = \frac{1}{z}\int_0^z \rho\, dz$.

If $\partial\bar{\rho}z/\partial x$ is taken as independent of z, Equation (1) can be simplified to

$$\frac{\partial\zeta}{\partial x} = -\frac{1}{z}\frac{h}{\bar{\rho}}\frac{\partial\bar{\rho}h}{\partial x} \tag{2}$$

and if h is constant over a limited distance x_1 to x_2, Equation (2) can be written as

$$\zeta_2 - \zeta_1 = \frac{1}{z}\frac{h}{\bar{\rho}}(\bar{\rho}_1 - \bar{\rho}_2) \tag{3}$$

If the density variation is confined to a layer extending from surface to a depth h' which is small compared with depth h, then Equation (3) takes the form

$$\zeta_2 - \zeta_1 = \frac{h'}{\bar{\rho}}(\bar{\rho}_1 - \bar{\rho}_2) \tag{4}$$

Bowden has shown by calculation that the variations of density causes:
(i) a small change (*c.* 3 cm.) in the English Channel and North Sea;
(ii) a large rise (*c.* 18 cm.) in passing through the Danish passages;
(iii) a significant rise (*c.* 11 cm.) in the main basin of the Baltic Sea; and
(iv) a fall of sea level (16 cm.) from near east of Gibraltar to south of Toulan.

It is also known that the mean sea level at the Red Sea end of Suez Canal is about 24 cm. higher than that at the Mediterranean end. All these factors give the indication that the problem is not simple.

Annual Variation of Sea Level in Indian Waters. Fig. 1 shows the annual variations of the sea level at Sagar, Vishakhapatnam, Madras, Colombo and Port Blair in the Bay of Bengal and at Karachi, Bombay and Cochin in the Arabian Sea. The annual variations at Vishakhapatnam, situated a great distance away from Sagar, are closely parallel to those at Sagar. The mean sea levels on these ports begin to rise long before the onset of monsoons. The annual variations in sea level at Vishakhapatnam according to La Fond and Prasad Rao are due to (i) vertical distributions of the density of sea water (*c.* 90 per cent), (ii) atmospheric pressure difference (*c.* 10 per cent), (iii) rainfall and drainage (small per cent), and (iv) wind speed and direction (small per cent).

Secular Variations of Sea Level in Indian Waters. Fig. 2 shows the secular variations of the sea level at Vishakhapatnam, Madras, Port Blair in the Bay of Bengal and at Aden, Karachi, Bombay in the Arabian Sea. All these curves show a general rise in sea level. The values of secular variation in ft per 100 years and the amplitudes and phase lags of 19-yearly tide after removing the secular variation are given in Table 1. These show that the phase lags are different from zero, and therefore not in accord with the equilibrium tide, and the variations in the amplitude are also large. Both Aden and Bombay show different trends for different periods.

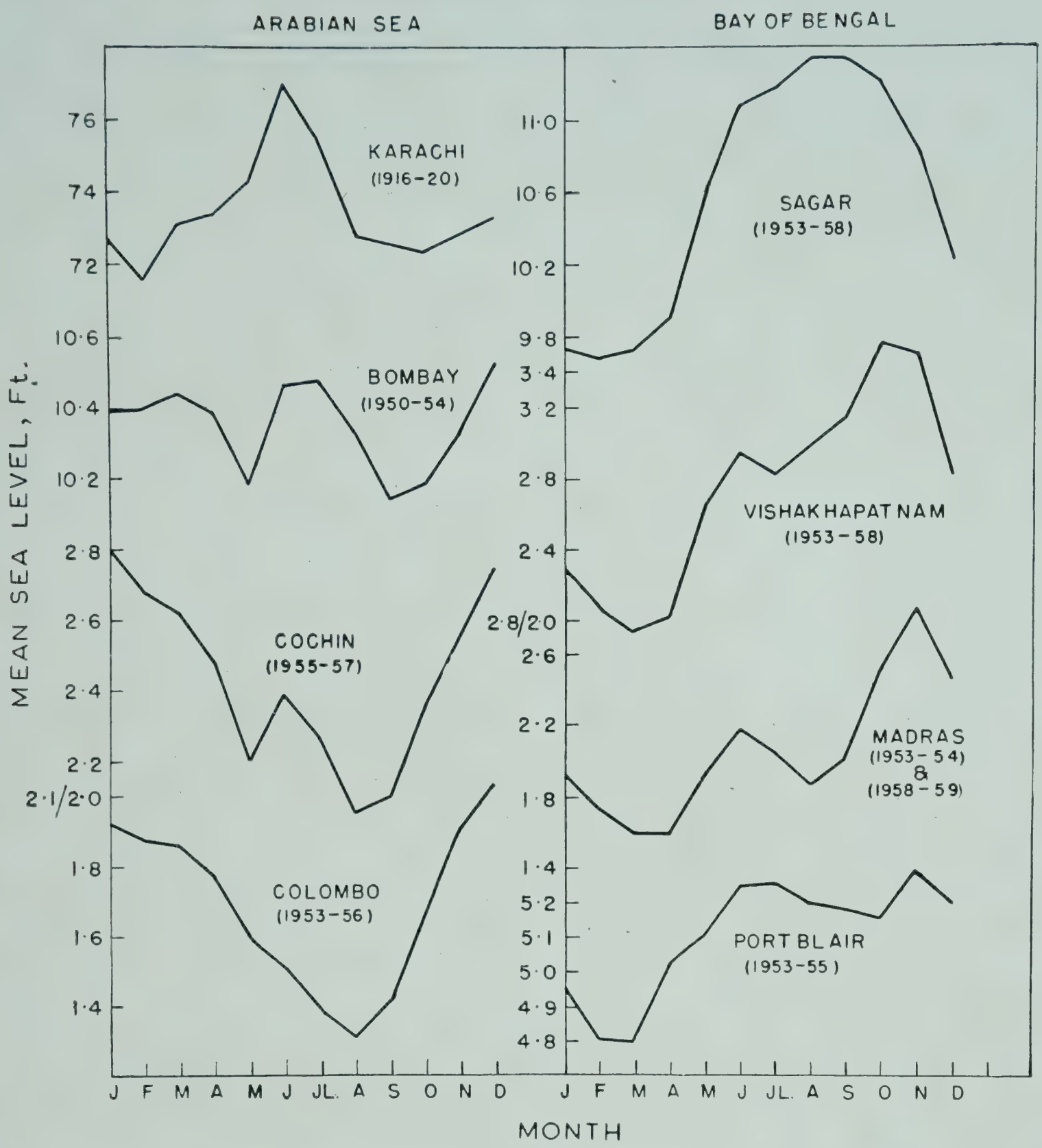

FIG. 1 — AVERAGE MONTHLY MEAN SEA LEVELS FOR DIFFERENT STATIONS IN DIFFERENT MONTHS IN THE BAY OF BENGAL AND ARABIAN SEA

Effects of Wind and Pressure. Neither the mean sea level of any port has been corrected so far for variations due to local barometer and its north and east gradients, nor mean sea level variations have been expressed in terms of barometric pressures at places covering the Bay of Bengal and Arabian Sea covering long series of annual means. It has, however, been seen that if a curve is drawn of mean monthly pressures and sea levels for places in the Bay of Bengal, a correlation between the two is obvious, for as the pressures decrease the height of the sea level increases and vice versa. In the months October–January, the winds are northerly and the pressures are high. Both these factors lower the heights of the sea level. During the south-west monsoon the pressures are low and give augmented sea level.

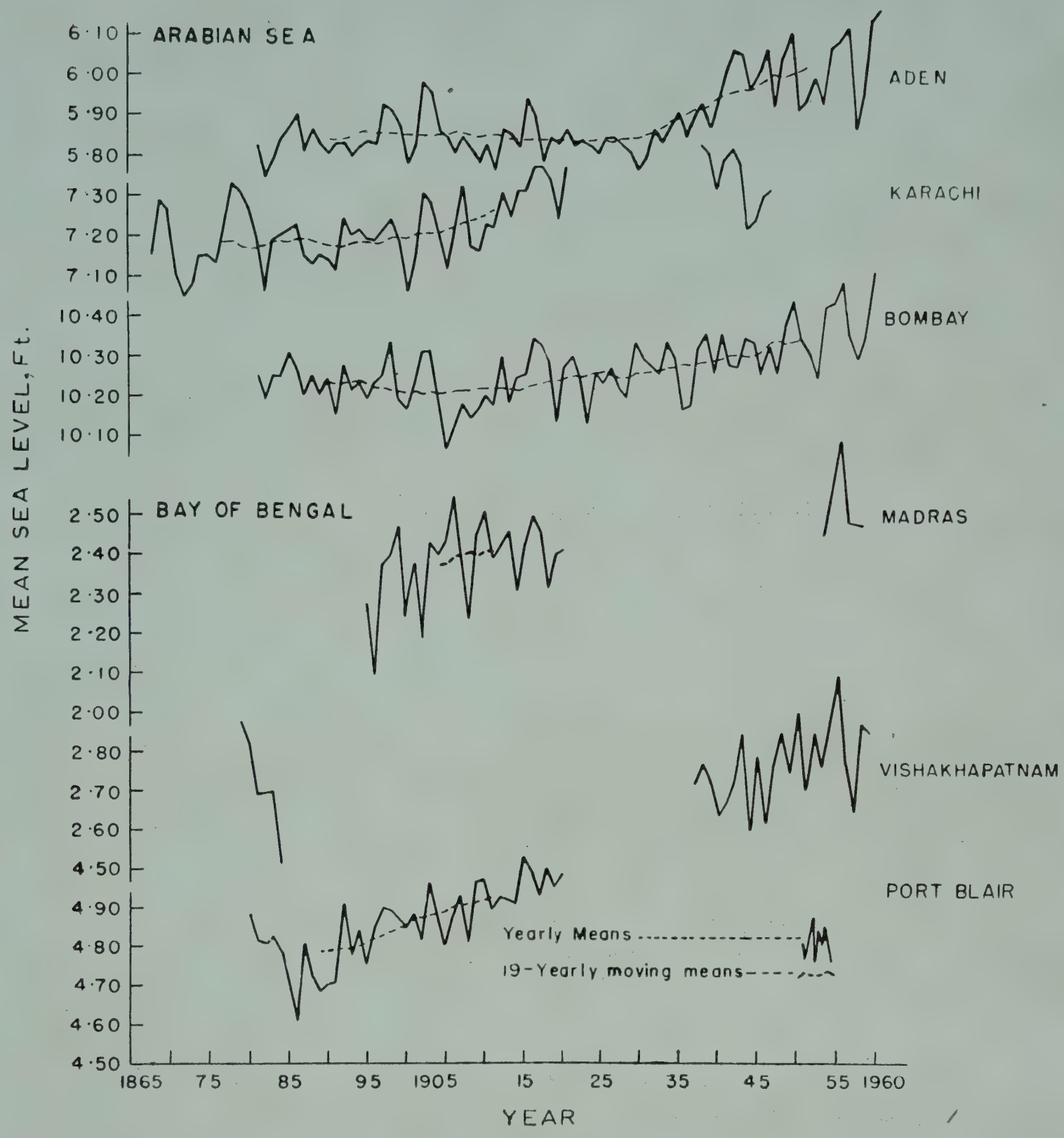

FIG. 2 — YEARLY AND 19-YEARLY MEAN VALUES OF MEAN SEA LEVELS FOR DIFFERENT STATIONS IN THE BAY OF BENGAL AND ARABIAN SEA DURING 1865–1960

Seasonal range of the barometer is greater at Sagar at the head of the bay than over southern portion (Port Blair) — the relative difference decreases by 0·3 in. between December and January giving rise to heaping up of water at the head of the bay. The sea level in the bay begins to rise in February itself before the onset of south-west monsoon.

Effects of Surface Temperature and Water Density. Detailed studies of the effect of surface temperatures and water densities on the mean slope of the sea surface have not been made for the Indian coastal stations. Some work has been done by La Fond on the relation of these data to the water masses and circulation. Table 2 taken from La Fond's paper gives monthly average surface temperatures and salinity at four stations on the east

TABLE 1 — SECULAR VARIATION OF SEA LEVEL AND 19-YEARLY TIDE IN SOME PORTS IN INDIAN WATERS

Ports	Period	Secular variation *ft*/100 *years*	19-Yearly tide	
			Amplitude *ft*	Phase lag *deg.*
Vishakhapatnam	1938–1956	nil	0·074	110
Madras	1900–1918	nil	0·042	29
Bombay	1881–1899	nil	0·018	212
	1900–1918	nil	0·069	145
	1919–1937	+0·30	0·017	20
	1938–1956	+0·30	0·030	138
Aden	1881–1899	nil	0·012	150
	1900–1918	nil	0·030	205
	1919–1937	+0·37	0·019	219
	1938–1956	+0·42	0·028	259

TABLE 2 — MONTHLY AVERAGE SURFACE TEMPERATURE AND SALINITY AT FOUR LOCATIONS ON EAST COAST OF INDIA

Months	Waltair half mile out in sea (Oct. 1951–Apr. 1953)		Sagar Island Tidal Observatory (Sept. 1950–Dec. 1953)		Madras harbour offshore in 8 fathoms of water (15 months)		Mandapam shallow western approach to Adams Bridge (Jan. 1950–Dec. 1953)	
	Temp. (°C.)	Salinity (°/₀₀)	Temp. (°C.)	Salinity (°/₀₀)	Temp. (°C.)	Salinity (°/₀₀)	Temp. (°C.)	Salinity (°/₀₀)
Jan.	25·06	29·20	23·20	31·11	27·2	30·06	25·17	28·87
Feb.	25·72	31·45	23·18	32·36	27·6	30·68	25·98	30·16
Mar.	26·28	33·72	23·33	34·72	28·5	34·10	27·82	31·89
Apr.	26·56	34·20	23·78	37·03*	29·6	34·39	29·66	33·26
May	27·00	34·08	23·78	37·54*	29·2	34·68	29·09	35·10
June	28·72	33·41	24·22	36·92*	28·0	34·32	27·62	35·56†
July	28·22	33·20	27·39	34·04	28·3	34·44	27·58	35·55†
Aug.	27·61	32·68	28·94	27·65	28·0	34·12	28·13	36·09†
Sept.	28·44	31·62	29·33	19·40	29·4	33·53	27·83	36·22†
Oct.	28·94	25·10	29·11	17·47	30·1	32·39	28·06	36·13†
Nov.	27·67	24·40	27·22	22·79	28·5	26·24	27·42	33·02
Dec.	26·33	26·14	24·72	29·04	27·4	28·80	25·67	28·83
Mean	27·21	30·77	25·68	30·01	28·48	32·31	27·50	33·39

*High values are questionable
†High values are due to near-shore evaporation effects

coast of India. This clearly shows that the density structure would cause a slope of the sea surface.

Land Uplift or Subsidence in Relation to Mean Sea Level on Indian Coastline. Tidal observations were originally commenced in India in 1873 with a view to investigating the secular changes, which were believed to be occurring, more particularly on the coast of Kathiawar, in the relative level of land and sea. This requirement has always been kept in mind in the study of tidal records.

No uplift or subsidence has been found on Indian coasts except local subsidence at Cochin harbour of 0·3 ft from 1890 to 1954, at Pamban Pass of 0·3 ft from 1880 to 1955.

The stability of the coastal region of Calcutta has been under study in the past and the 1955–56 levelling from Kidderpore to Dublat revealed that either the old levelling of 1948–49 or the new levelling was discrepant or that the Sagar Island had sunk by about 0·5 ft in 7 years.

There have been also some doubts on the sinkage of Ross Island in the Andaman group of about 0·3 ft from 1900 to 1955; this is under investigation.

The New Level Net of India and its Adjustment. A new network of levelling of High Precision Standards was commenced in India in 1914. This is now almost complete, with frequent ties to the 1909 net, and the tidal observatories which are functioning on the coastline. Before it can be adjusted, the mean sea level around the Indian waters will have to be accurately determined and defined. It will be necessary to subject the sea level recordings to the methods of ' Oceanographic Levelling ' described earlier. The accuracies of the tidal records, particularly connections to benchmarks of reference, will have to be carefully checked before using the values in further reductions. Continuous simultaneous observations of tides over long periods on Indian coastal stations have not been taken so far. It will be necessary to convert the observed data to mean sea level values adjusted to a specified epoch and to eliminate the larger anomalies in the data of mean sea level before calculating secular variations. For many places there are a few years of observations and values have to be corrected with the help of anomalies obtained from longer years of observations at a nearby port. It has been shown earlier that nodal variations in amplitudes and phase lags are not constant over large areas of the Indian waters; yet it appears to be the only method available for corrections to be made to the shorter period data for other ports in the area.

Therefore the choice of appropriate places as starting points for altitude measurements, and the exact computation of the mutual height differences between these places, will be the most essential task.

Acknowledgement

Thanks of the author are due to Sarvashri S. K. Bose and H. R. Ghildiyal and computers of Tidal Party for carrying out the computations and drawing of the figures. Thanks are also due to Col. S. K. S. Mudaliar, Director, Survey of India, for permission and guidance in carrying out this work.

Literature

1. Doodson, A. T., *Bull. géod. int.*, **55** (1960), 69–88.
2. Lisitzin, E., *Bull. géod. int.*, **55** (1960), 91–92.
3. Bowden, K. F., *Bull. géod. int.*, **55** (1960), 93–96.
4. *Andhra University Memoirs in Oceanography* (Andhra Universiy, Waltair), 1954.

Elasticity of Indian rocks

M. HAYAKAWA*
S. BALAKRISHNA

Geology Department, Osmania University
Hyderabad

The ultrasonic velocity in Indian granites is found to be higher than that of granites from other countries. To explain this peculiar behaviour of Indian granites, the authors had offered explanations based on theoretical considerations such as internal pressure, depth of formation and age. These values have already been measured in the case of some granites. Additional laboratory measurements which have been made for Mysore, Hyderabad and Rajasthan granites are presented. The results show that (i) there is considerable scatter in the values, and (ii) Indian granites have higher velocities than granites from Japan, America and Russia. The scatter has been explained as being due to variation in mineralogical composition, grain size, deformation and petrogenic history. The experimental data have also been analysed to examine if they throw new light on their petrogenic history as well as elastic behaviour.

Rocks are polycrystalline aggregates. When the microcrystals composing the aggregate are distributed in all possible random orientations in space (having no preferred orientation), they will be elastically isotropic and exhibit only two elastic constants. On the other hand, an orderly arrangement of the crystallites (preferred orientation) will result in a fibrous structure and will consequently be elastically anisotropic. Granites whose origin is still controversial present a complex picture regarding their elastic properties. Some granites exhibit perfect elastic isotropy while others exhibit marked variations in ultrasonic velocities with reference to definite directions, viz. lineation and foliation. Indian granites show higher velocity than similar rocks from different countries. Further, their elastic behaviour with pressure presents some special features which make them distinctive and hence can be classed as peculiar. Recently, the authors[1] offered an explanation for the high ultrasonic velocities in Indian granites on the basis of theoretical considerations like the initial internal pressure conditions and the particular depth at which the granite was originally formed as well as the age

---

*Present address: Geological Survey of Japan, Tokyo, Japan

that had lapsed since its formation. With a view to substantiating this explanation, the ultrasonic velocities of granites from Mysore, Hyderabad and Rajasthan have been measured. The grain size, longitudinal and transverse velocity of three typical granites, elastic anisotropy and elastic behaviour under pressure of some Indian granites have also been determined. These data have been examined in the light of the explanation and also to find out if they throw new light on the petrogenic history and elastic behaviour of rocks.

Results

Granites from Mysore (Closepet) and Hyderabad (Osmania University area) have been examined. They are broadly classified as pink and grey granites. The modal analysis of ten pink and grey granites (Table 1) gives the general nature and mineralogical composition.

Elastic Constants. By employing the Wedge method[2] the ultrasonic velocities (V_L and V_T) in a number of granites were determined; the elastic constants — Young's modulus (Y), rigidity modulus (n) and Poisson's ratio (σ) — were calculated with the help of density (ρ). The results are tabulated in Table 2.

The range of Poisson's ratio in the granites of almost equal density is plotted in Fig. 1. It is interesting to note that Poisson's ratio ranges from 0·30 to 0·39 in case of granites of density 2·60–2·70 g./cu. cm.

TABLE 1 — MODAL ANALYSIS OF GRANITES

Minerals %	Pink granites										
	P_1	P_2	P_3	P_4	P_5	P_6	P_7	P_8	P_9	P_{10}	Av. %
Quartz	35·5	31·8	29·7	22·5	20·4	34·0	38·0	29·0	26·0	26·0	30·2
Potash felspars	43·8	46·8	35·2	51·7	57·2	58·0	58·0	59·0	59·0	57·0	56·3
Plagioclase	15·0	16·0	22·0	19·1	20·4	2·0	2·0	3·0	13·0	9·0	7·0
Mafics	5·7	5·1	13·5	6·6	1·8	4·0	2·0	9·0	2·0	8·0	5·3
	Grey granites										
	G_1	G_2	G_3	G_4	G_5	G_6	G_7	G_8	G_9	G_{10}	Av. %
Quartz	45·5	45·3	41·6	46·3	51·6	28·7	31·0	31·0	32·0	22·0	31·8
Potash felspars	21·5	23·4	20·3	18·2	16·7	48·0	36·0	35·0	48·0	44·0	37·0
Plagioclase	25·6	26·1	29·7	35·4	20·4	6·0	14·0	19·0	5·0	19·0	15·0
Mafics	8·4	5·1	7·9	0·2	11·9	16·0	19·0	15·0	15·0	15·0	14·4

TABLE 2 — ULTRASONIC VELOCITIES AND ELASTIC CONSTANTS OF GRANITES

Specimen No.	ρ *g./cu. cm.*	V_L *km./sec.*	V_T *km./sec.*	Y 10 *dynes/ sq. cm.*	n 10 *dynes/ sq. cm.*	σ
1	2·67	6·25	3·40	8·00	3·10	0·29
2	2·68	6·39	3·36	7·93	3·03	0·31
3	2·66	6·15	3·15	6·97	2·63	0·32
4	2·65	6·32	3·26	7·31	2·81	0·32
5	2·68	6·87	3·47	8·58	3·23	0·33
6	2·64	6·42	3·07	6·74	2·49	0·35
7	2·60	6·08	3·06	6·81	2·52	0·33
8	2·69	6·67	2·71	5·54	1·97	0·39
9	2·60	6·11	3·02	6·63	2·46	0·34
10	2·62	6·20	2·96	6·17	2·28	0·35
11	2·60	6·16	2·75	5·42	1·97	0·37
12	2·68	6·40	3·41	8·11	3·12	0·30
13	2·68	6·15	3·20	7·21	2·74	0·31
14	2·65	6·32	3·20	6·95	2·71	0·33
15	2·69	6·37	3·31	7·63	2·90	0·32
16	2·70	6·90	3·00	6·72	2·43	0·38
17	2·68	6·40	2·90	6·20	2·25	0·37
18	2·70	6·90	3·50	8·77	3·31	0·33
19	2·67	6·21	2·60	5·03	1·81	0·39
20	2·63	6·13	2·60	4·95	1·78	0·39
21	2·67	6·20	3·30	7·62	2·90	0·30
22	2·66	6·08	3·05	6·83	2·56	0·33
23	2·70	6·23	2·95	6·37	2·35	0·35
24	2·61	6·54	3·15	6·93	2·56	0·34
25	2·65	5·96	2·85	6·54	2·42	0·35

TABLE 3 — DENSITY, GRAIN SIZE AND VELOCITIES IN DIFFERENT GRANITES

Type	Specimen No.	Density *g./cu. cm.*	Grain size *mm.*	V_l *m./sec.*	V_t *m./sec.*
Fine grained	1	2·68	0·4	6·87	3·47
	2	2·70	0·6	6·37	3·36
	3	2·75	1·5	6·08	3·05
Medium grained	4	2·67	0·3	6·77	3·41
	5	2·68	0·5	6·54	3·24
	6	2·68	0·8	6·34	3·00
Coarse grained	7	2·68	0·3	6·20	3·05
	8	2·66	0·4	6·40	3·17
	9	2·68	0·5	6·60	3·25

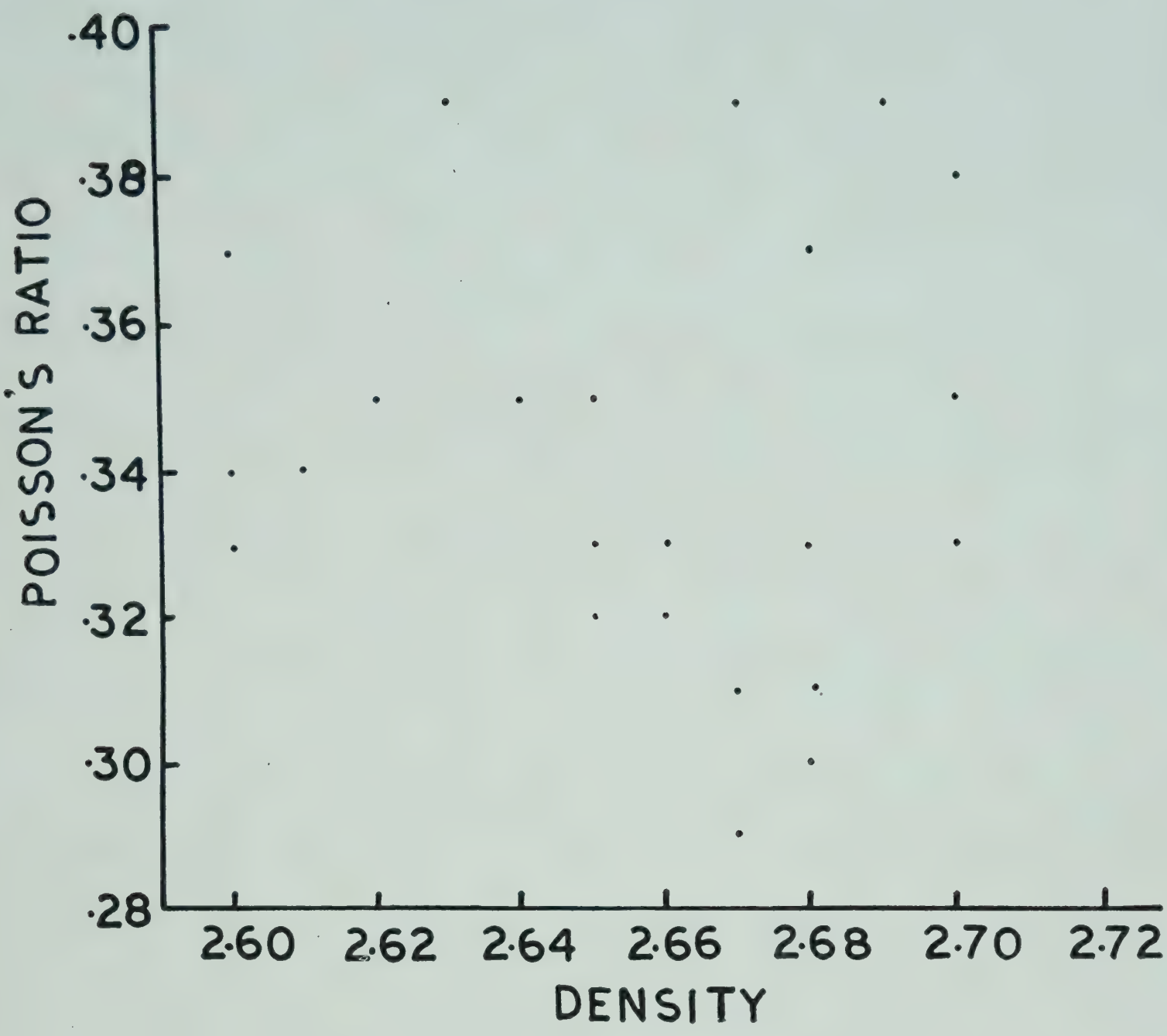

FIG. 1 — DISTRIBUTION OF POISSON'S RATIO IN GRANITES

Grain Size and Velocity Values. Another aspect of study in granites relates to the grain size. One of the authors[3] has shown that there is a difference in transmission of sound through different rocks and that this is intimately connected with their grain size. It has also been shown that the velocities in coarse-grained rocks are lower than those in fine-grained rocks. Both longitudinal (V_l) and transverse (V_t) velocities together with the density and average grain size for three typical granites were determined (Table 3).

It can be seen from the above table that, for each type, as the grain size increases velocity decreases. However, this conclusion on the basis of grain size alone is not justifiable because other factors such as polycrystallinity and modal composition associated with granites may have influence.

Elastic Anisotropy of Granites. Specimens of similar orientation and a few other granites in which no lineation or foliation directions were visible (probably batholithic) were chosen for determining the ultrasonic velocities and studying the elastic anisotropy. Three plates were cut from each specimen

TABLE 4 — ULTRASONIC VELOCITIES IN GRANITES IN DIFFERENT DIRECTIONS

Specimen No.	V_L (km./sec.) along		
	a	b	c
1	6·27	6·14	6·20
2	5·90	6·00	5·84
3	6·08	5·80	6·20
4	6·02	6·23	6·24
5	6·54	6·48	6·62
6	6·61	6·58	6·49
7	6·93	6·13	—
8	6·66	6·08	—
9	6·82	6·21	—
10	6·75	6·12	—

mutually perpendicular to one another (a, b and c) in order to study the variation of ultrasonic velocities with direction. In granites in which dimensional orientation was noticed, one section was cut parallel to the reference direction and velocities were measured in a direction perpendicular to reference (a), while the other was cut perpendicular to reference (b). In both cases, plates of about 2·5 cm. square and 4·0 mm. thickness were cut with a machine, strictly adhering to the reference directions and were ground to uniform thickness. Table 4 gives ultrasonic velocities (compressional) in these three directions.

It can be seen from the table that the velocities in granites are rather high and range from 5·8 to 6·9 km./sec. for the compressional wave velocities. It is interesting to note that in specimens 1–6 (no dimensional orientation, possibly of batholithic) there is not much variation of ultrasonic velocities with direction, while in the other specimens variation is marked.

Elastic Behaviour of Rocks with Pressure. In Table 5 the ultrasonic velocities of some Indian granites obtained by the author, those of American granites by Birch[4] and those of Japanese granites (Shimozuru) at atmospheric pressure and also at high pressure (of the order of 10,000 bars) are given.

The velocity generally increases rapidly at low pressures and slowly at higher pressures[5]. This effect is pronounced in the American granites and more so in the Japanese granites when compared to Indian granites. The gradient in the case of the Japanese rock is less when compared to American granites and this is of some interest. It can be further seen that Indian granites exhibit comparatively high values of velocity at low pressures and

TABLE 5 — ULTRASONIC VELOCITIES IN INDIAN, AMERICAN AND JAPANESE GRANITES

Locality	Density *g./cu. cm.*	V_P (0) *km./sec.*	V_P (10,000) *km./sec.*
Rock port	2·62	5·00	6·51
Quincy	2·62	5·00	6·42
Barre	2·65	5·10	6·39
Chelmsford	2·63	4·20	6·36
Minnesota	2·67	6·00	6·48
India	2·66	6·15	6·66
India	2·65	6·32	6·68
India	2·74	6·00	6·39
Japan	2·69	4·70	—
Japan	2·54	4·32	—

relatively small rise at high pressures. The variation of elasticity of tropical granites with pressure is given in Fig. 2. It can be seen that the behaviour of Indian rocks is different from those of other countries in regard to their ultrasonic velocities.

Theoretical Considerations

Initial Internal Pressure. The effect of external pressure on the elastic properties of a granular substance has been discussed by Takahashi and Sato[6,7]. However, the high velocity in a rock could not be explained on the score of its being granular, and hence a modification was made by Nagumo[8,9] by introducing the factor, internal pressure. According to him the longitudinal wave velocity, V_P, through the granular substance is given by

$$V_P^* = \sqrt{A(P_{01}+I_P)^{1/3}+V_0^2} \qquad (1)$$

where V_P^* = longitudinal wave velocity at any pressure through the granular substance;
V_0 = longitudinal wave velocity when $P = 0$;
V_P = longitudinal wave velocity in particle;
P_{01} = external pressure; and
I_P = internal pressure.

In the above equation, V_P and P_{01} are known, while I_P and V_0 are unknown. Therefore, if we consider A as a constant, I_P and V_0 can be calculated by the method of least squares by treating them as simultaneous equations. However, this method involves laborious calculation. Hence, Equation (1) was

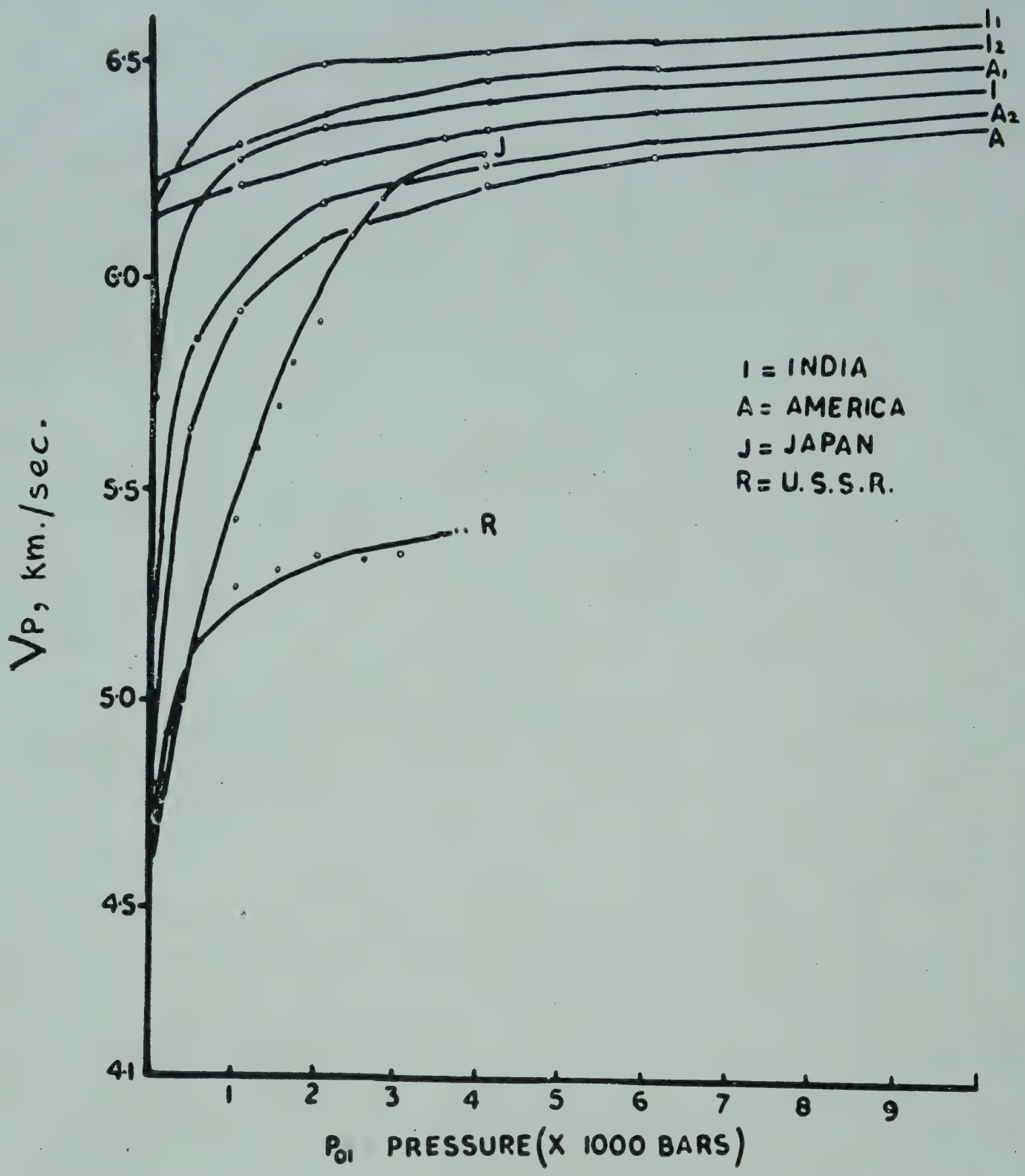

FIG. 2 — VARIATION OF ULTRASONIC VELOCITIES IN GRANITE WITH PRESSURE

solved directly by giving different values to the parameters. The combinations chosen for getting standard curves are given in Table 6.

It may be mentioned that it is easier to find the suitable theoretical curves at comparatively low pressures than at pressures higher than 4000 bars (Fig. 2). The theoretical curves for a value of $V_0 = 6{\cdot}5$ are presented in Fig. 3. Using these data and the standard curves, the values of different parameters have been calculated (Table 7).

These values and the variation of elastic stress with depth and the effect of time on elasticity after the formation of the rock are taken into account for discussion.

TABLE 6 — PARAMETERS USED IN THE STANDARD CURVE

A	0	0·1	0·2	0·3	0·6	1·0	1·5	2·0	2·5
V_0, *cm./sec.*	2·0	3·0	4·0	4·5	5·0	5·5	6·0	6·5	7·0
P_{01}, *bars*	0	1000	2000	3000	4000	6000	8000	10,000	—
I_P, *bars*	0	250	500	1000	2000	3000	—	—	—

TABLE 7 — VALUES OF DIFFERENT PARAMETERS FOR GRANITES OF DIFFERENT ORIGIN

Granite origin	ρ	A	V_P	V_0		I_P		Age of rock
				Standard curve	Least square method	Standard curve	Least square method	
India	2·65	0·25	6·15	6·05	6·00	250	250	Pre-Cambrian
	2·65	0·20	6·20	6·00	6·02	500	650	Pre-Cambrian
	2·66	0·20	6·15	6·05	6·05	1100	1300	Pre-Cambrian
America	2·67	0·40	5·80	5·50	5·50	250	250	Pre-Cambrian
	2·65	0·50	5·30	5·25	5·20	50	50	Pre-Cambrian
	2·65	0·70	4·80	4·00	—	50	—	Pre-Cambrian
Japan	2·69	0·70	4·60	2·00	2·00	700	800	Recent
Russia	—	0·20	4·50	2·00	—	500	—	—

Discussion and Conclusion

Effect of Depth, Stress and Time on Velocity. The true meaning of V_P can be obtained by considering how much of stress energy can be stored by time elapse under a certain depth.

Biot[10] has already obtained the general solution of consolidation of porous material under stress and strain. According to him, in one-dimensional consolidation problem where a column of height h under a vertical load γ/unit area, the time dependent part ϕ of the strain satisfied the equation

$$\phi = \cos \sqrt{\frac{\alpha}{a}}\, ze^{-\alpha t}$$

By integrating this with time, stress E can be obtained as

$$E \propto -\frac{1}{\alpha^n} \cos \sqrt{\frac{\alpha_n}{a}}\, ze^{-\alpha_n t}$$

Therefore, the stress quantity E with depth and time can be obtained under the assumption of a constant value for a.

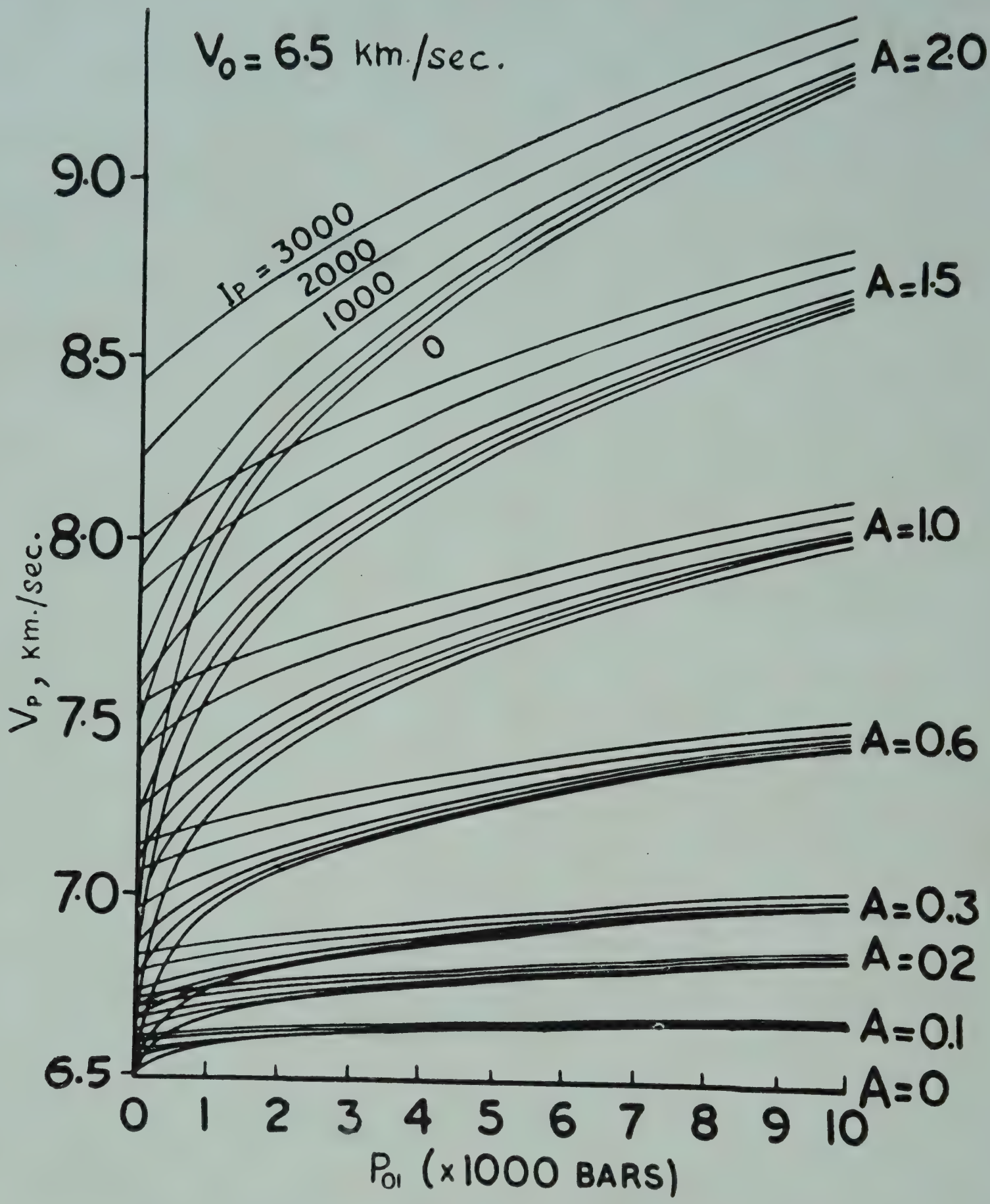

FIG. 3 — STANDARD CURVES FOR VELOCITY VERSUS PRESSURE

It requires longer time to complete the process of formation of the rock under higher pressure (deeper depths) than under lower pressure (lower depths). Further, considerable amount of stress energy can be stored under higher pressure, i.e. the initial velocity becomes high when the rock is formed at great depths, while at shallow depths less stress energy can be stored and consequently lower velocity values are obtained.

The following conclusions may be drawn from these considerations:

(i) High velocities in granites can be expected if their formation was initiated at great depths and their age is high, and vice versa. There are bound to be

intermediate cases with either of the parameters or both taking intermediate values.

(ii) The effect of petrogenetic history, if any, should also be taken into account in explaining special anomalies. For example, the comparatively large torsional velocities exhibited by the Japanese granites which are of recent origin constitute one such anomaly. This should be attributed to the complex shearing stresses to which these rocks are known to be subjected to.

References

1. Hayakawa, M. & Balakrishna, S., *Europ. Ass. explor. Geol.*, **9** (1961), No. 1.
2. Bhagavantam, S. & Bhimasenachar, J., *Proc. Indian Acad. Sci.*, **20A** (1944), 298.
3. Balakrishna, S., *Proc. Indian Acad. Sci.*, **39A** (1954), 223.
4. Birch, F., *J. geophys. Res.*, **65** (1960), 1083.
5. Balakrishna, S., *Bull. nat. Inst. Sci. India*, No. 11 (1958), 50.
6. Takahashi, T. & Sato, Y., *Bull. Earthq. Res. Inst. Tokyo*, **27** (1949).
7. Takahashi, T. & Sato, Y., *Bull. Earthq. Res. Inst. Tokyo*, **28** (1950).
8. Nagumo, S., *Rep. geol. Surv. Japan*, **8** (1958).
9. Nagumo, S., *Rep. geol. Surv. Japan*, **9** (1959).
10. Biot, M. A., *J. appl. Mech.*, **3** (1956), 91.

Study of earth tide at Hyderabad

S. BALAKRISHNA
M. HAYAKAWA

Geology Department, Osmania University
Hyderabad

The earth tide at Hyderabad (an ideal place for eliminating the effect due to oceanic tides) has been measured during June 29-September 1, 1960 making use of the Askania gravimeter GS-11. The data have been analysed theoretically by least square method and by modified Fourier method. The last method has been used for the data obtained from June 29 to August 1, 1960. As a first trial, the analysis has been carried out only for three tidal components, M_2, S_2 and K_1. Some interesting results have been obtained. One of them is that the gravimetric factor for M_2, S_2 and K_1 is 1·18, 0·77 and 0·90 respectively probably suggesting that the part of the earth at Hyderabad is well compacted.

Tide-generating forces are acting on every part of the earth's surface. As the earth itself is an elastic yielding body, not only the marine surface but also the earth's surface is deformed due to the gravitational attractions of the sun and moon. This deformation independent of the oceanic surface is called an earth tide. Though the theoretical study of earth tides is sufficiently old, their experimental study has been rather of recent origin as it involves precise observations of variation of normal gravity with time.

By using gravimeters with high sensitivity and accuracy the vertical component of earth tide whose amplitude is some 10^{-7} of the normal gravity values can be observed. From the data of gravity change with time, the gravimetric factor of the earth tide can be calculated by comparison with corresponding theoretical values. The elasticity of the earth can be calculated from the gravimetric factor. However, there exist additional influences which bring about elastic deformations of the earth's crust. One of these is the indirect effect of maritime tides, which is similar to the primary tidal force. Other influences have time variations comparable with the periods of the tidal forces and often attain considerable amplitudes. They are

mainly of meteorological origin, but geological or tectonic conditions also play a part.

The location of Hyderabad [long. 78°33′E: lat. 17°26′43″N (geog.): 17°19′24″ (geom. lat.)] is such that the oceanic tidal effects are minimum. Besides, there have been only a few data of earth tide south of 20° latitude. Therefore, the data of earth tide at Hyderabad will be of great interest and importance. With this background the study of the earth tide was taken up and a preliminary report of the study using the first month's data from June 29 to August 1, 1960 is presented in this paper.

Observations

The variation of gravity at different times of all the dates has been measured using the Askania gravimeter GS-11. The radius of the earth at observation point is 6375+0·567 km. The records of observations are shown in Fig. 1.

As the direction of the vertical component of the tidal forces is taken as positive in the direction opposite to the normal gravitational field, the maximum of the tidal action corresponds to a measured minimum of gravity. One can see the good correspondence of this by noting the observation at the full moon position.

Besides, the amplitudes of periodic tidal actions are larger in full moon or new moon than those in other days of the month. The drift of the gravimeter, fortunately, does not affect the observations very much.

Method of Analysis

Theoretical Analysis. Fig. 2 represents the deformation of the equipotential surface of the earth on account of tidal forces[1]. If the tidal forces are due to an ideal liquid of zero density, the equipotential surface will be at C. On account of the elastic properties of the earth and its density, the equipotential surface attains an intermediate position B. But due to the different distribution of the yielding mass of the earth the equipotential surface corresponds to another shape D. Consequently, the position of the observer shifts from A to B.

The potential W_{el} at a station on the surface of the yielding earth can therefore be expressed as

$$W_{el} = W_0 + W_2 + V_2 - gu_r \qquad (1)$$

where W_0 is the potential due to gravity, W_2 is the tidal potential, and V_2 is the potential due to changed mass distribution. The last term gu_r accounts for the displacement of the observed data.

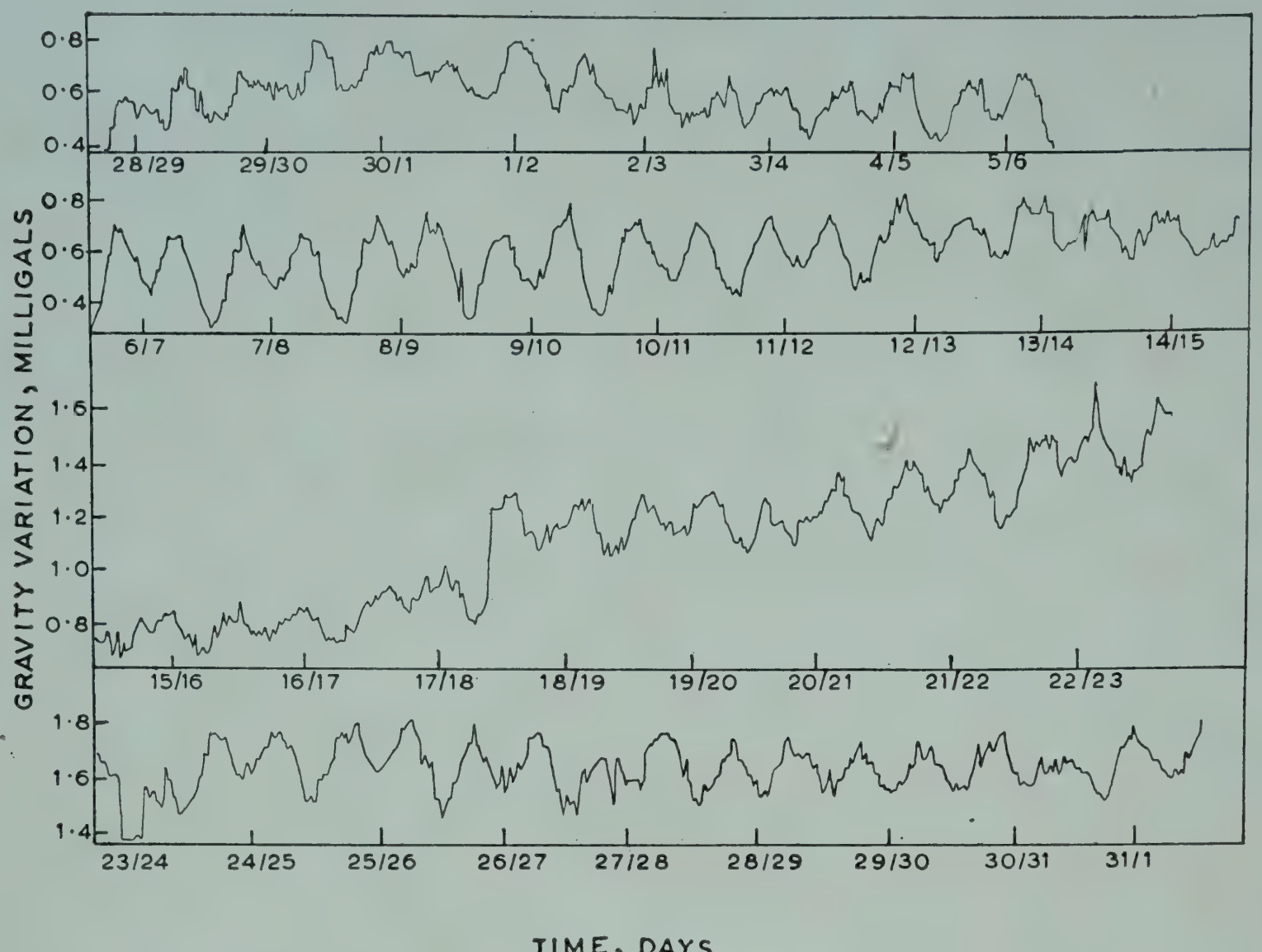

FIG. 1 — VARIATION OF GRAVITY WITH TIME

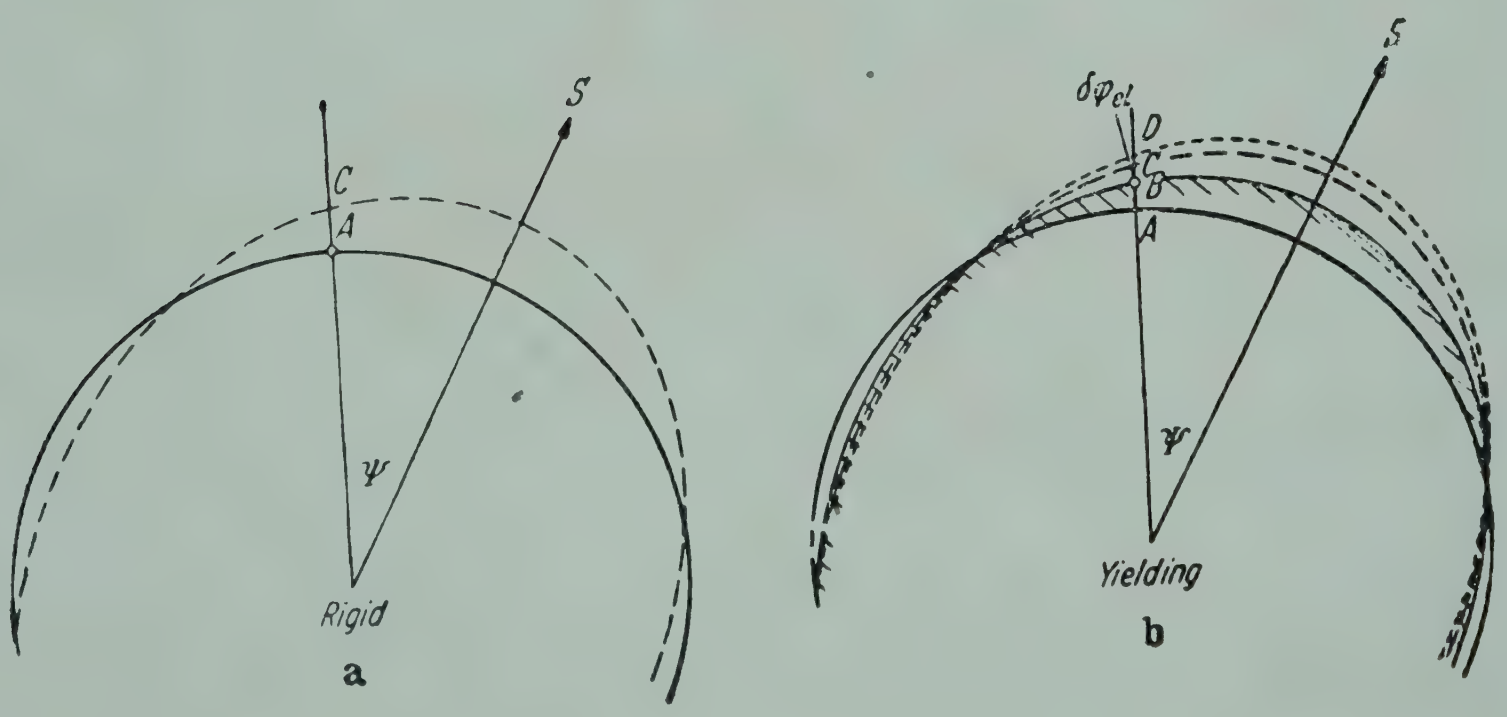

FIG. 2 — DEFORMATION OF EQUIPOTENTIAL SURFACE: (a) RIGID EARTH, AND (b) YIELDING EARTH

Using Love and Clairant's theorem and putting $V^2W_0 = 0$, Equation (1) can be written as

$$W_{el} = W_0 + W_2(1 + h - \tfrac{3}{2}k) \qquad (2)$$

Therefore the change of gravitational force due to celestial bodies with time becomes

$$\Delta g = \left[\frac{\hat{c}}{\hat{c}r} (\overline{W}_{el} - \overline{W}_0) \right]_{r=\rho} = \left(1 + h - \frac{3}{2}k\right) \left(\frac{\hat{c}\overline{W}_2}{\hat{c}r}\right)_{r=\rho} \tag{3}$$

where ρ is earth's radius, h is the ratio between the height of the tide of the solid earth to the theoretical equilibrium height, and k represents the ratio of the additional potential due to the tidal deformation of the yielding earth to the tidal potential. Now, $\left(\frac{\hat{c}\overline{W}_2}{\hat{c}r}\right)_{r=\rho}$ can be expressed as follows by using the spherical harmonic functions:

$$\left(\frac{\hat{c}\overline{W}_2}{\hat{c}r}\right)_{r=\rho} = \frac{3}{2}\frac{M}{E}\, g\, \frac{\rho_1^2}{c^3}\, \rho \left[\left(\frac{c}{R}\right)^3 \left(\cos 2\theta + \frac{1}{3}\right) + \frac{1}{6}\frac{\rho}{c}\left(\frac{c}{R}\right)^4 \times (5 \cos 3\theta + 3 \cos \theta) + \ldots\ldots\ldots\right] \text{(ref. Fig. 3)} \tag{4}$$

where E = mass of the earth; M = mass of the moon; $E/M = 81{\cdot}53$;
g = gravitational acceleration at Hyderabad = 978·34 cm./sec.^{2};
ρ_1 = mediate earth's radius = 6371·221 km.;
ρ = earth's radius at the observation point = 6375·567 km. and $\sin \Psi = a/r$, $\sin \Psi_0 = a/c$, $\sin \Psi_0 = 0{\cdot}016593$;
Ψ = equatorial horizontal parallax of the moon;
Ψ_0 = average of Ψ;
a = equatorial radius of the earth = 6378·388 km.;
c = average of a;
r = distance between observation point and the centre of moon;
R = distance between earth's centre and the centre of the moon;
θ = angle between moon's centre and the observation point at the centre of the earth.

Similar expressions can be obtained with regard to the gravitational attraction due to the sun.

Though the gravitational attractions due to the sun and moon are expressed by such simple formulae, these tidal forces are divided into three main tidal components as shown in Table 1.

Of these, it is difficult to study the long-period tide from the present one-month's data. Therefore, as a trial, the main components including two main semidiurnal and one main diurnal components have been studied. Fig. 3 shows the geometric position of the observation point. Figs. 4 and 5 show the celestial triangle and its position in spring respectively. The tidal forces can be expressed by the following formulae.

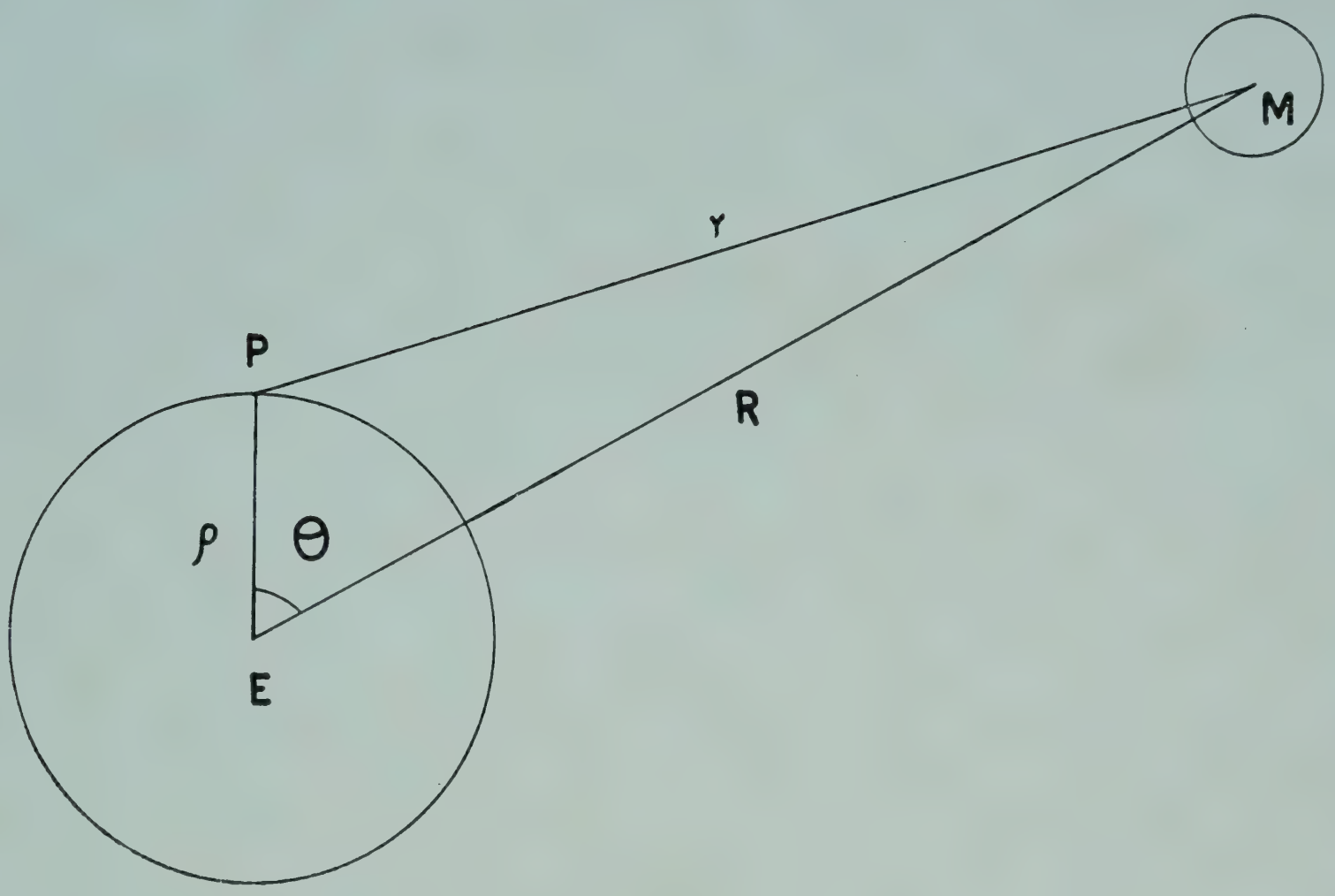

FIG. 3 — GEOMETRICAL POSITION OF OBSERVATION POINT

C

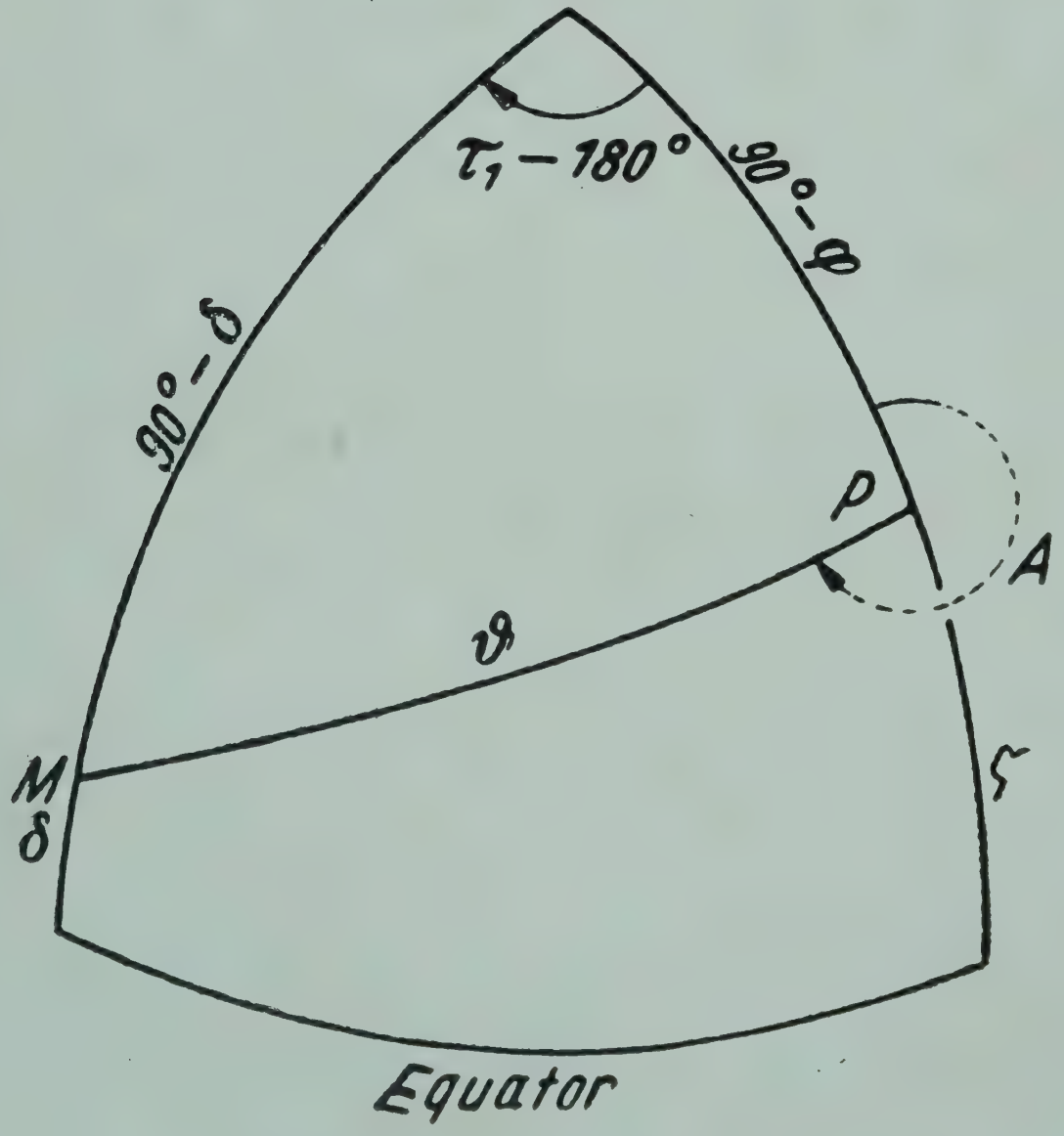

FIG. 4 — CELESTIAL TRIANGLE

Semidiurnal

From Fig. 4, it can be shown

$$M_2 = +G(\rho)\cos^2\varphi(c/R)^3\cos^2\delta_m\cos 2\tau_1 \tag{5}$$

(lun. princ)

$(c/R)^3 = 0{\cdot}9081$, $\tau_1 = \theta^* - \alpha$, α . . . Right ascension of moon

$\tau_1 = 24^h 50^m.47$ $\quad$ $(2\tau_1)$ = half = $12^h.42$

From Fig. 5 it can be shown

$$S_2 = +0{\cdot}4605G(\rho)\cos^2\varphi(c_s/R_s)^3\cos^2\delta_s\cos 2t_1 \tag{6}$$

(sol. princ)

$0{\cdot}4605 \times (c_s/R_s)^3 = 0{\cdot}4229$, $t_1 = \theta^* - \alpha_s$, α_s . . . Right ascension of sun

$t_1 = 24^h$ $\quad$ $(2t_1)$ = half = $12^h.00$

$$N_2 = +0{\cdot}1739G(\rho)\cos^2\varphi\cos^2\delta_m\cos[2\tau - (s-p)] \tag{7}$$

(lun. ellipt)

$2\tau = 12^h.66$

$K_2 = K_{2s} + K_{2m}$

$$\left.\begin{aligned} K_{2s} &= +0{\cdot}0365G(\rho)\cos^2\varphi\cos 2\theta^* \\ K_{2m} &= +0{\cdot}0786G(\rho)\cos^2\varphi\cos 2\theta^* \end{aligned}\right\} \tag{8}$$

period = $11^h.97$ = half a siderial day

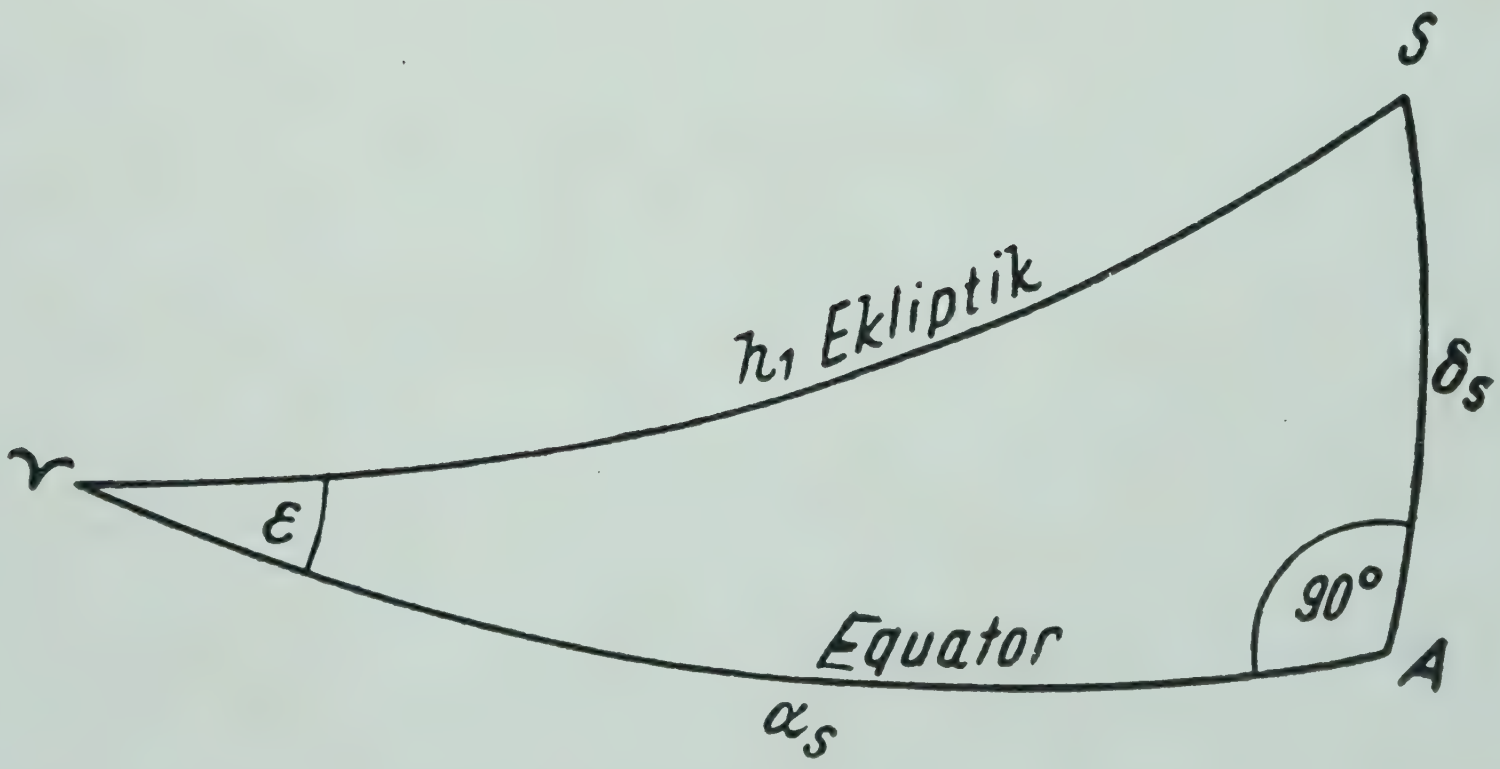

FIG. 5 — CELESTIAL TRIANGLE IN SPRING

Diurnal

$K_1 = K_{1s} + K_{1m}$

(lun. solar)

$$\left.\begin{aligned} K_{1s} &= -0{\cdot}4605G(\rho)\sin 2\varphi(c_s/R_s)^3\sin 2\delta_s\cos t_1 = -0{\cdot}1682\times G\sin 2\varphi\sin\theta^* \\ K_{1m} &= -G(\rho)\sin 2\varphi(c/R)^3\sin 2\delta_m\cos\tau_1 = -0{\cdot}3623\times G\sin 2\varphi\sin\theta^* \end{aligned}\right\} \quad (9)$$

$$\text{period} = 23^h.93 = \text{siderial day}$$

$$O_1 = +0{\cdot}3769G\sin 2\varphi\sin(\tau - s) \quad (10)$$

(luni decli)

$$\text{period} = 25^h.82$$

$$P_1 = +0{\cdot}1755G\sin 2\varphi\sin(t - h) \quad (11)$$

(sol decli)

$$\text{period} = 24^h.07$$

The two main tidal components which have been obtained by the above method are shown in Fig. 6.

These are the theoretical tidal forces.

Experimental Analysis. The data have been analysed using the least square method and a modified Fourier method.

Least Square Method — If the gravity values [Equation (4)] are given by

$$Z = Z_1\cos(\alpha t + \varphi_1) + Z_2\cos(\beta t + \varphi_2) + Z_3\cos(\gamma t + \varphi_3) + \ldots\ldots \quad (12)$$

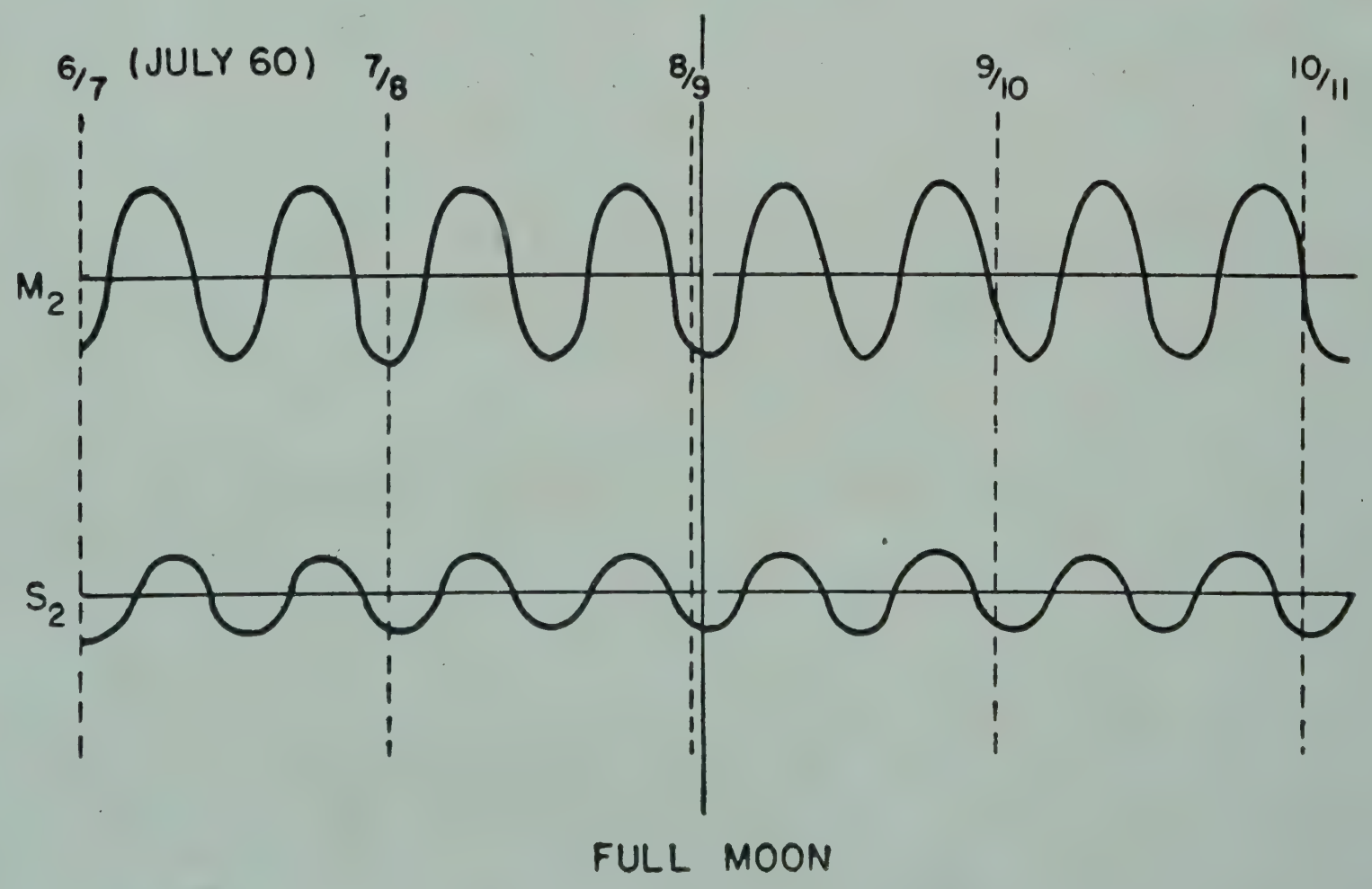

FIG. 6 — COMPONENTS M_2 AND S_2 OF TIDAL FORCES DURING FULL MOON

Z can be expressed as

$$Z = f_1(t)+f_2(t)+f_3(t)+. \ . \ . \ .+f_7(t) \tag{13}$$

where

$$\left.\begin{aligned} f_1(t) &= a_1\cos\alpha t+b_1\sin\alpha t \\ f_2(t) &= a_2\cos\beta t+b_2\sin\beta t \\ f_3(t) &= a_3\cos\gamma t+b_3\sin\gamma t \\ &\vdots \qquad\qquad \vdots \\ f_7(t) &= a_7\cos\lambda t+b_7\sin\lambda t \end{aligned}\right\} \tag{14}$$

therefore, Equation (12) can be expressed as

$$\left.\begin{aligned} Z = \cos\alpha t\ a_1+\sin\alpha t\ b_1 \\ +\ \cos\beta t\ a_2+\sin\beta t\ b_2 \\ +\ \cos\gamma t\ a_3+\sin\gamma t\ b_3 \\ \vdots \\ +\ \cos\lambda t\ a_7+\sin\lambda\ t b_7 \end{aligned}\right\} \tag{15}$$

This is a formula of one dimension with 14 unknown values. Suppose we have various values of Z with t as follow:

$$\left.\begin{aligned} (Z)_1 &= \cos\alpha t_1 a_1+\sin\alpha t_1 b_1+\cos\beta t_1 a_2+\sin\beta t_1 b_2+. \ . \ .+\cos\lambda t_1 a_7+\sin\lambda t_1 b_7 \\ (Z)_2 &= \cos\alpha t_2 a_1+\sin\alpha t_2 b_1+\cos\beta t_2 a_2+\sin\beta t_2 b_2+. \ . \ .+\cos\lambda t_2 a_7+\sin\lambda t_2 b_7 \\ &\cdots\cdots\cdots\cdots\cdots\cdots\cdots\cdots\cdots\cdots\cdots\cdots\cdots\cdots\cdots\cdots\cdots\cdots\cdots\cdots \\ &\vdots \\ (Z)_n &= \cos\alpha t_n a_1+\sin\alpha t_n b_1+\cos\beta t_n a_2+\sin\beta t_n b_2+. \ . \ .+\cos\lambda t_n a_7+\sin\lambda t_n b_7 \end{aligned}\right\} \tag{16}$$

Consequently, the orthogonal equation becomes

$$\left.\begin{aligned} &[\cos\alpha t_1\cos\alpha t_1]a_1+[\cos\alpha t_1\sin\alpha t_1]b_1+[\cos\alpha t_1\cos\beta t_1]a_2+. \ . \ .-[\cos\alpha t_1(Z)_1]=0 \\ &[\cos\alpha t_1\sin\alpha t_1]a_1+[\sin\alpha t_1\sin\alpha t_1]b_1+[\cos\beta t_1\sin\alpha t_1]a_2+. \ . \ .-[\sin\alpha t_1(Z)_2]=0 \\ &\cdots\cdots\cdots\cdots\cdots\cdots\cdots\cdots\cdots\cdots\cdots\cdots\cdots\cdots\cdots\cdots\cdots\cdots\cdots\cdots \\ &\vdots \\ &[\cos\alpha t_1\sin\lambda t_1]a_1+[\sin\alpha t_1\sin\lambda t_1]b_1+[\cos\beta t_1\sin\lambda t_1]a_2+. \ . \ .-[\sin\lambda t_1(Z)_{14}]=0 \end{aligned}\right\} \tag{17}$$

By solving these 14 simultaneous first order equations, the value of a_1, b_1, a_2, b_2, a_3, b_3, . . ., a_7, b_7 can be obtained.

Modified Fourier Method — Suppose the gravity values are given by Equations (13) and (14) as before and the values of Z are given, α, β, γ, . . . and λ are also given, the problem is to find the values of the coefficients a_1, b_1, a_2, b_2, . . . , a_7, b_7, where $\alpha-\beta$, $\beta-\gamma$, $\alpha-\gamma$, . . . , etc., are not integral multiples of π. If these are integral multiples of π, normal Fourier methods are available and in such a case the final results which are very similar to the normal ones are as follow:

$$a_1 = \frac{2}{n}\sum_1^n f(k)\cos k\alpha, \quad b_1 = \frac{2}{n}\sum_1^n f(k)\sin k\alpha$$

$$a_2 = \frac{2}{n}\sum_1^n f(k)\cos k\beta, \quad b_2 = \frac{2}{n}\sum_1^n f(k)\sin k\beta$$

$$\vdots \qquad\qquad \vdots$$

$$a_7 = \frac{2}{n}\sum_1^n f(k)\cos k\lambda, \quad b_7 = \frac{2}{n}\sum_1^n f(k)\sin k\lambda$$

Results and Discussion

In the case of practical analysis, first, it is necessary to eliminate the long-period tidal components and the effect of spring drift of the gravimeter, if any.

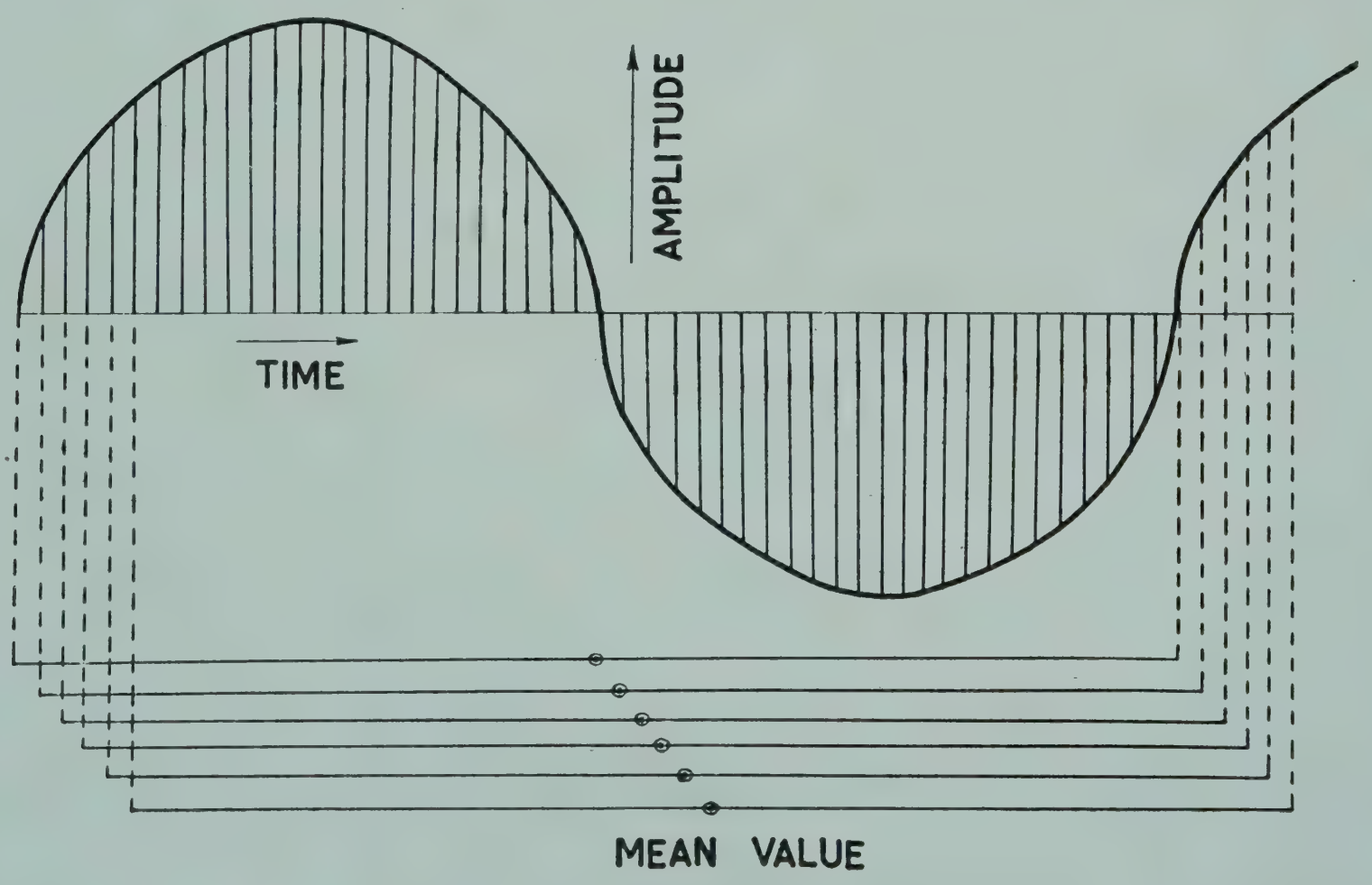

Fig. 7 — True mean curve

For this purpose, the 'running mean method' has been used, because it is very effective in eliminating these components. If the range (width) of running mean wavelength on a multiple integer of it is taken, these effects will be cancelled and the true mean curve (Fig. 7) can be obtained.

Even if the curve has the period a little longer or shorter than the original curves, its remaining near value is $\Sigma(\text{original} \pm \text{excess})/n$ and, therefore, in this case it is negligibly small.

TABLE 1 — TIDAL FORCES AND COMPONENTS

$$\left[G_0 = \tfrac{1}{2}G(1-3\ \sin^2\ \Psi);\ G_1 = G\ \sin\ 2\Psi,\ G_2 = \cos^2\ \Psi,\ G(\rho) = (\rho/\rho_1)^2\ G,\right.$$
$$\left. G(\rho) = \frac{3}{2}\ \frac{M}{E}\ \frac{g\rho_1^2}{c^3}\ \rho = \frac{3}{2}\ \frac{M}{E}\ g\ \frac{\rho_1^2\ \sin^3\ \Psi_0}{a^3}\ \rho\right]$$

Symbol	Coefficient $K\times10^5$	G_k	Argument	Period *hr*
		Long-period Tide		
M_0	+50458	G_0	cos (055·555)	20740*
S_0	+23411	G_0	cos (055·555)	
M_f	+15642	G_0	cos (095·555)	27, 321582†
		Diurnal Tide		
O_1	+37689	G_1	sin (145·555)	25.82
P_1	+17554	G_1	sin (163·555)	24.07
K_{1m}	−36233	G_1	sin (165·555)	23.93 (siderial day)
K_{1s}	−16817	G_1	sin (165·555)	
		Semidiurnal Tide		
N_2	+17387	G_2	cos (245·6555)	12.66
M_2	+90812	G_2	cos (255·555)	12.42
S_2	+42286	G_2	cos (273·555)	12.00
K_{2m}	+7854	G_2	cos (275·555)	11.97 (half a siderial day)
K_{2s}	+3648	G_2	cos (275·555)	

*years; †days

TABLE 2 — GRAVIMETRIC FACTORS

Symbol	Gravimetric factor	Phase lag
M_2	1·1833	$2^{ho}0^{m}.5$
S_2	0·7706	1 53′·0
K_1	0·8964	—

Considering the three main tidal periods (Table 1), the range of running mean 25 hr (51 readings) and each 30 min. reading have been taken. By applying this method, the gravity curves (Fig. 8) have been obtained after the elimination of the drift in Fig. 1.

As these two methods give identical results, the latter method has been used as a trial. The three main tidal curves obtained by this method are shown in Fig. 9.

By comparing Fig. 9 with Fig. 6, the phase lag between the original and practical values has been obtained and later the gravimetric factors $(1+h-\frac{3}{2}k)$ have been obtained (Table 2) by applying Equation (3).

Influence of the Ocean. As far as the oceanic tides are concerned it can be stated that as seven-elevenths of the earth's surface is covered with oceans, oceanic tides must exert an influence on continental stations also.

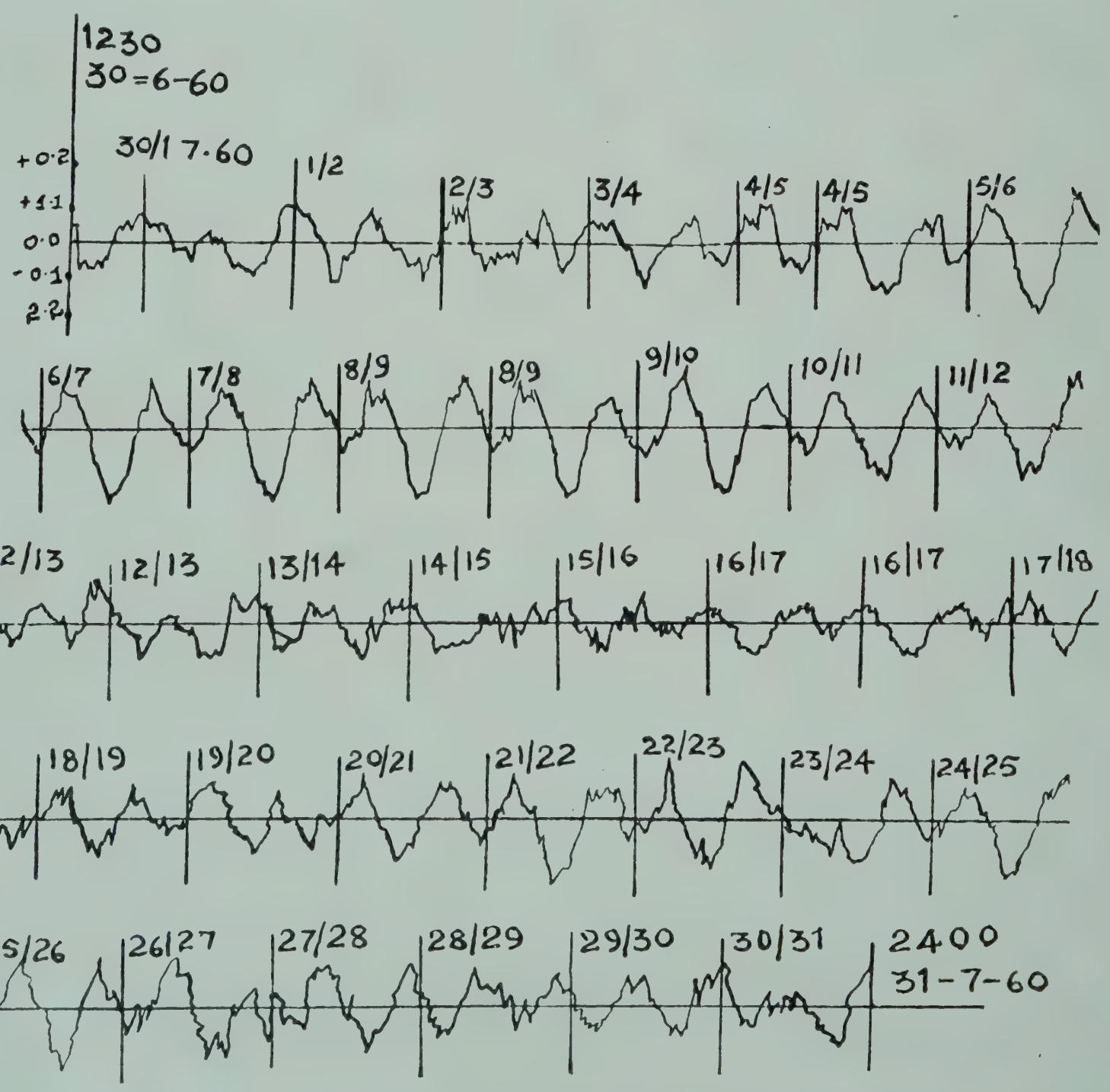

FIG. 8 — GRAVITY CURVE AFTER ELIMINATION OF DRIFT

According to Tomaschek, their effect consists of three components: (i) gravitational attraction of the shifted water masses on the point of observation; (ii) deformation of the solid earth due to the shift of the water masses (this deforms the whole globe of the earth in general and tilts or moves the observing station in particular); and (iii) change of potential due to the changed distribution of masses.

From Fig. 10 which shows the relationship between the distance from sea shore and oceanic effect, it can be seen that oceanic effect at Hyderabad is negligible, as it is situated 300 km. from the sea coast.

The values of gravimetric factor seem to be very interesting. The values compared with Tomaschek's data (Fig. 11) show that the value 1·18 of the gravimetric factor of M_2 is smaller than the average value obtained in the last 13 years. Considering the high theoretical value of the gravimetric factor of M_2 in low latitudes (Fig. 12), it is suggested that the crustal formations at Hyderabad are very compact and consist of hard material.

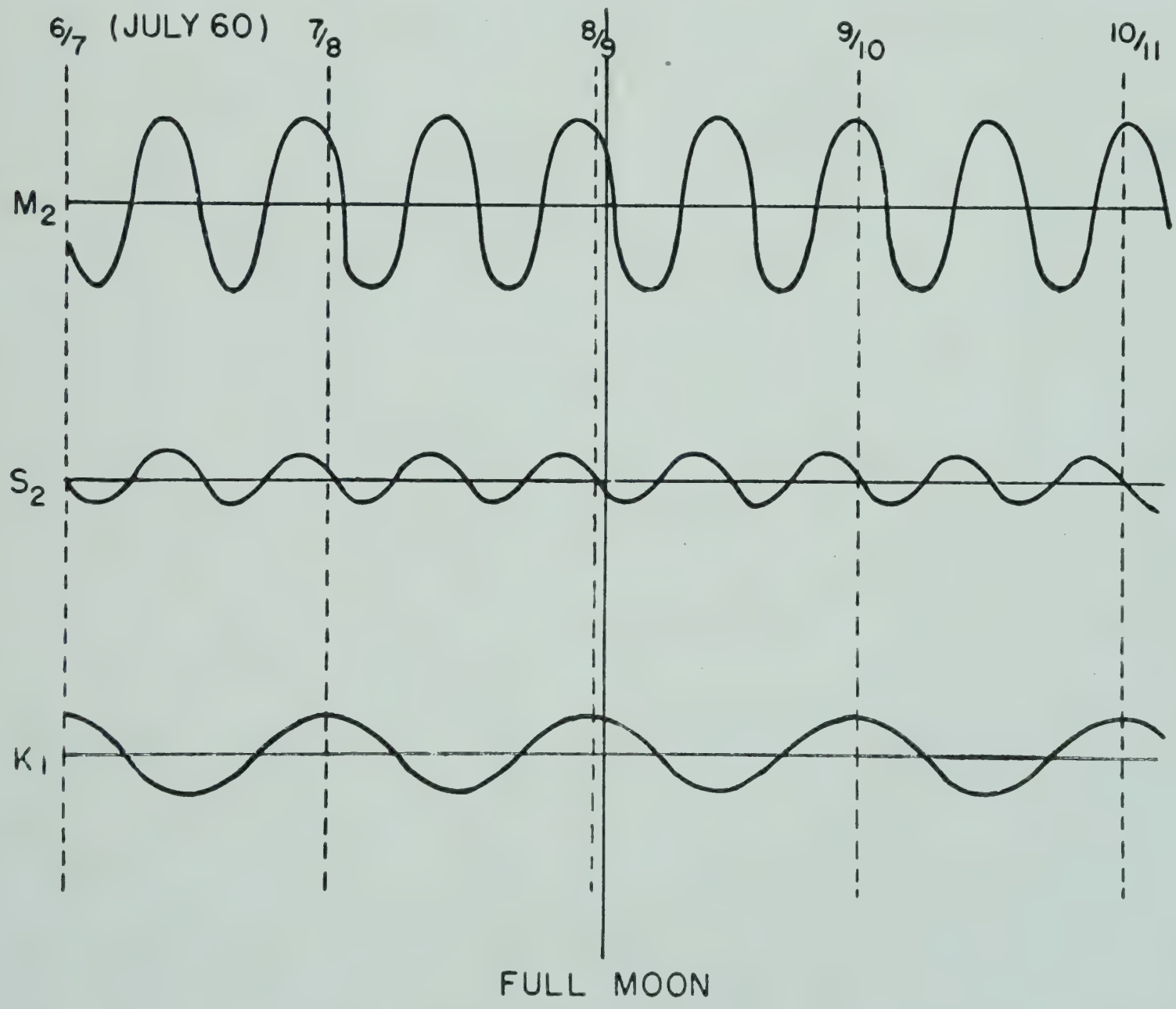

FIG. 9 — CURVES FOR TIDAL COMPONENTS M_2, S_2 AND K_1

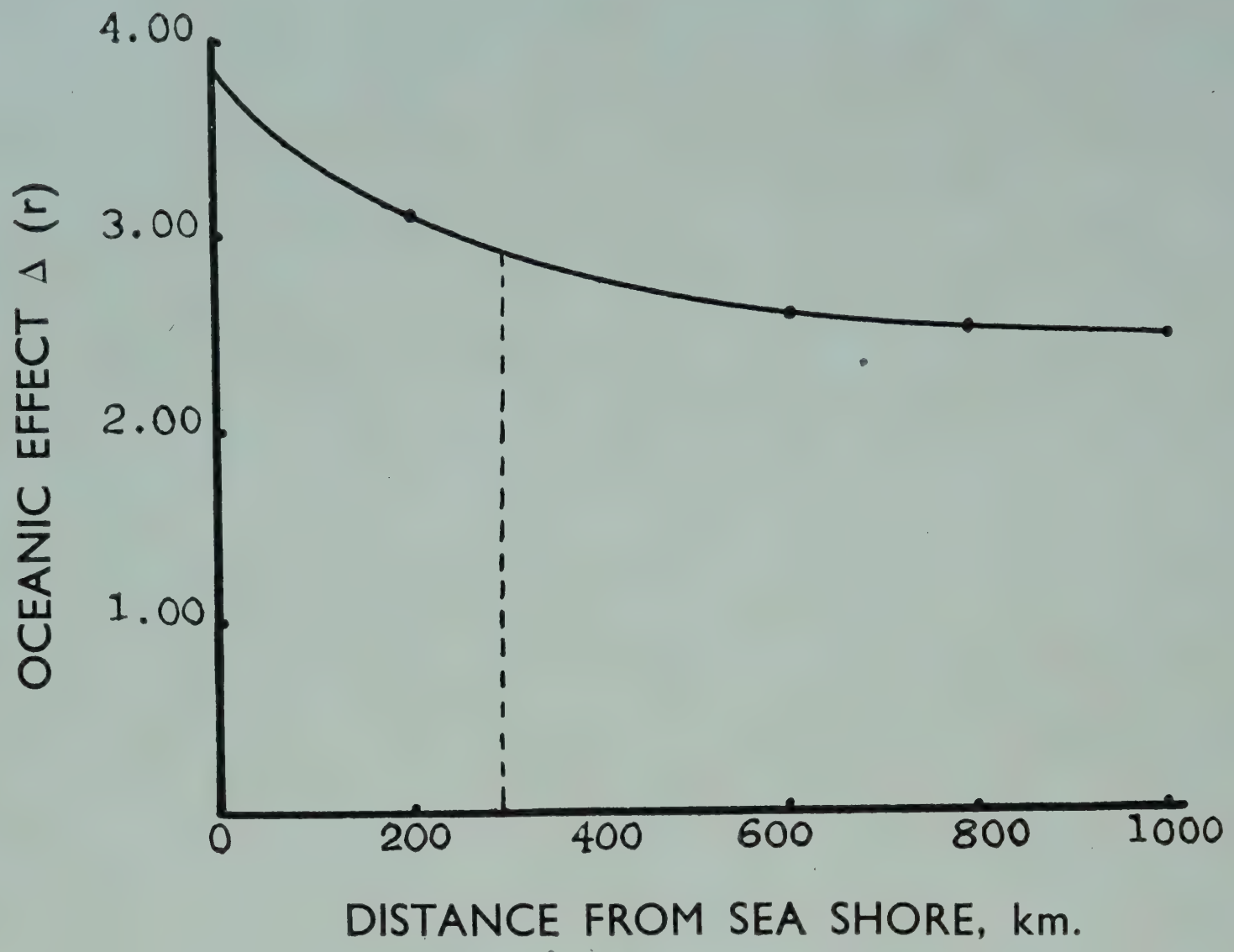

FIG. 10 — RELATION BETWEEN DISTANCE FROM SEA SHORE AND OCEANIC EFFECT

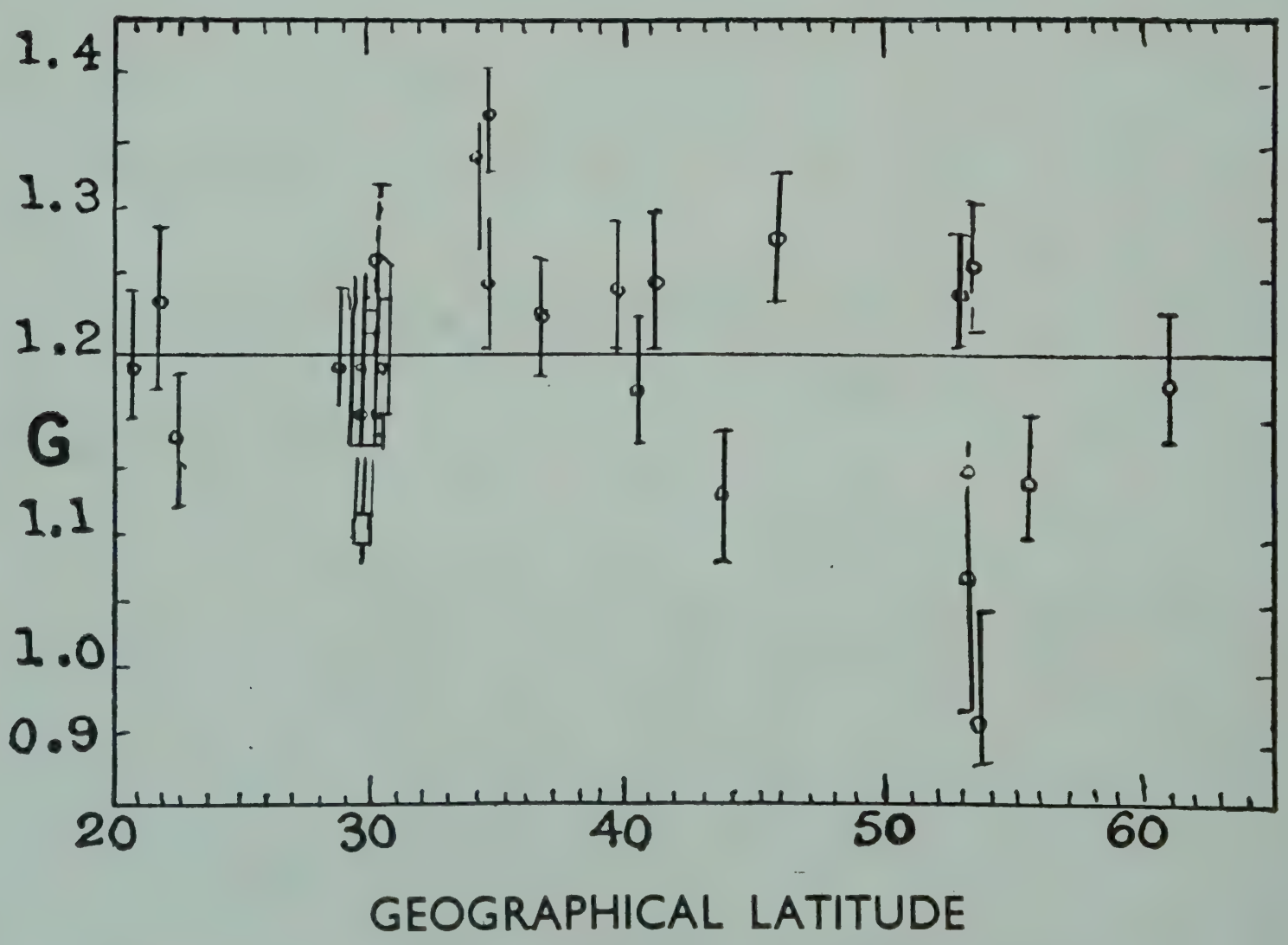

FIG. 11 — GRAVIMETRIC FACTOR FOR M_2 WITH LATITUDE

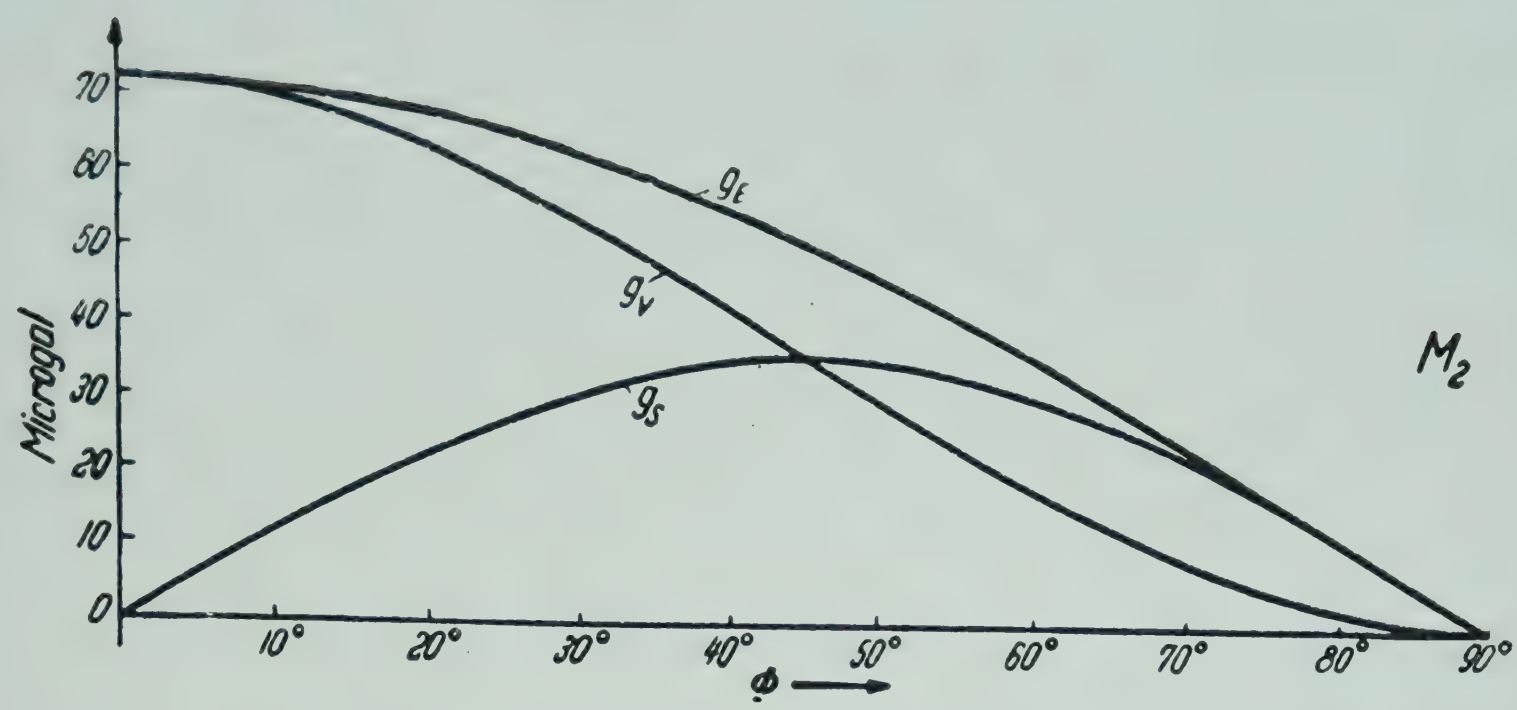

FIG. 12— COMPONENTS OF EQUILIBRIUM TIDAL GRAVITY VECTOR WITH LATITUDE [g_V = VERTICAL VECTOR OF GRAVITY, g_E = HORIZONTAL VECTOR OF GRAVITY EAST COMPONENT AND g_S = HORIZONTAL VECTOR OF GRAVITY SOUTH COMPONENT]

ACKNOWLEDGEMENT

The authors desire to express their grateful thanks to Messrs P. V. Johnson and G. Yazdani for their ungrudging help in calculating the tidal factors.

REFERENCE

1. *Encyclopaedia of Physics*, Vol. XVVIII, Geophysics II by R. TOMASCHEK (Springer Verlag), 1957, 775–845.

Palaeomagnetism and the continental drift

C. RADHAKRISHNAMURTY
P. W. SAHASRABUDHE

Tata Institute of Fundamental Research
Bombay

The various processes by which rocks acquire remanent magnetization and their relative importance in palaeomagnetic studies have been discussed. The results of extensive studies of several igneous rock formations in India have been presented. The data lead to some tentative conclusions regarding the continental drift of the Indian sub-continent during the last two hundred million years.

It is well known that palaeomagnetic measurements of certain rocks can be used to study the history of the geomagnetic field, continental drifting and polar wandering during geological periods. Sensitive instruments have been developed for measuring the direction and intensity of remanent magnetization of rocks. The two types of magnetometers generally used, the Spinner and the Astatitic types, have been described in detail by Johnson and McNish[1] and Blackett[2] respectively. A reasonable amount of data on remanent magnetization of most of the suitable geological horizons from all the continents has been made available during the last two decades.

The results obtained in India for the Rajmahal, Sylhet and Deccan traps and the various igneous intrusions associated with each of these are discussed in this paper. The data lead to a picture of continental drifting of the Indian land mass during the last two hundred million years which is consistent with indications based on some geological evidence.

Types of Magnetization

There are mainly three types of magnetization, namely thermoremanent magnetization (TRM), detrital remanent magnetization (DRM) and chemical remanent magnetization (CRM), which are useful for palaeomagnetic studies. There are others, such as isothermal remanent magnetization (IRM)

and viscous magnetization which induce secondary and unwanted effects on the natural remanent magnetization (NRM) of the rocks.

Thermoremanent Magnetization. TRM is acquired by a rock when its ferromagnetic constituents cool through their Curie temperature under the influence of the earth's magnetic field. This type is most suitable for palaeomagnetic studies and is retained by many rock types for geological periods[3]. The characteristics of TRM, such as its relation to the ambient field and its additive nature in the temperature range, have been established by Thellier[4] and Nagata[5].

A general theory for the TRM has been developed by Neel[6] who has also suggested some mechanisms by which a rock under suitable physico-chemical conditions could acquire a TRM in a direction opposite to that of the ambient field. One of these mechanisms has successfully explained the reverse TRM observed in some of the Japanese rocks studied by Nagata[7]. However, the number of reversely magnetized rocks observed in nature is very large and their adverse remanence cannot be explained by any of the mechanisms suggested by Neel. It has also been suggested that the earth's magnetic field probably underwent a number of reversals in past, having been in the reversed sense during the formation of the reversely magnetized rocks. Such a belief is strengthened by the fact that the reversely magnetized rocks are almost as many as the normal ones, and that the two types from the same formation and differing slightly in time interval do not exhibit any major chemical, mineralogical and structural differences.

Detrital Remanent Magnetization. This type of magnetization in sedimentary rocks originates, at the time of their deposition, due to the aligning effect of the geomagnetic field on the magnetic particles derived from parent rocks. The orientation of the particles on deposition depends on many factors such as the strength of the field, turbulence in water, the shape and size of the particles and the nature of the deposition floor. It is almost certain that it would be further affected during subsequent consolidation processes. The remanent magnetic direction acquired by sedimentary rocks would therefore only approximately correspond to that of the ambient field. Moreover, the rates of sedimentation vary over a wide range so that a centimetre thick layer may cover a period anywhere from a few decades (varve clays) up to several thousand years (deep sea sediments).

In spite of the above-mentioned problems associated with DRM their studies can be valuable, in the case of those rocks which have not been affected by disturbing effects, for studying field reversals in the past.

Chemical Remanent Magnetization. Chemical changes taking place in the magnetic constituents of a rock, in the presence of the magnetic field,

result in the rock acquiring a remanent polarization as has been demonstrated by Haigh[8]. Iron bearing solutions filling in the pores of sedimentary rocks may sometimes give them a remanent magnetization. Blackett[9] has described the effect of this process on the magnetization of the British red sandstones.

Rocks can acquire CRM at any time subsequent to their formation and the magnetic directions, in such cases, can be fully utilized only if the probable age of origin of the CRM can be ascertained.

Other Types of Magnetization. Other forms of isothermal induced magnetization, viz. viscous magnetization and those arising from lightning, are weak and unstable and can be removed easily. These effects often influence the observed magnetic directions in rocks and therefore have to be removed for obtaining the unmodified original magnetization in rocks.

Laboratory Stability Tests. The three types of magnetization are believed to be stable over periods of several million years if later modifications by chemical or mechanical agencies do not occur. The stability can be tested in the laboratory by demagnetizing the rocks in low alternating magnetic fields and by heating and cooling them in field-free space. The rocks having a stable remanence retain their directions even after the above tests although there is usually some decrease in the magnetic vector. On the other hand, rocks which acquire sufficient amounts of secondary components are affected both in intensity and direction. If the original magnetization in the rock is sufficiently strong and stable, it will stand out even after the removal of the secondary components by magnetic cleaning.

Consistency in magnetic directions among samples from a formation, particularly when these are different from that of the present earth's field, itself indicates their high magnetic stability. However, it is necessary to use both the tests mentioned above on some representative samples to ascertain if the overall magnetization is free from any disturbing effects.

Formations studied. Extensive palaeomagnetic measurements have been made on rocks from various igneous formations in India.

Deccan Traps — Deccan traps are believed to be of Cretaceous-Eocene epoch. They cover a total surface area of about 200,000 sq. miles.

Samples from the Deccan traps in different localities covering a varying number of flows have been analysed[10-13]. These traps are believed to be some 10,000 ft in total thickness, although the maximum thickness studied in these studies was only from 1600 to 1800 ft. At no place the entire thickness of traps is accessible and the relationship among flows in different localities is not definitely known.

FIG. 1 — EQUAL AREA PROJECTION PLOT OF THE MEAN VECTORS FOR THE WHOLE SERIES OF FLOWS: MAHABALESHWAR AREA

Therefore, it was felt that the study of a thicker section of trap flows in a single locality would yield very useful information. A 3500 ft thick section comprising about 26 (analysed) flows on the Mahad–Mahabaleshwar road has been studied in detail. The flows have an average thickness of 80–100 ft. The 20 lowermost flows sampled could be traced, whereas some flows (probably 5 or more) in the upper section could not be sampled due to lack of proper exposures. Out of the 26 flows studied, three had to be rejected since the rocks showed appreciable weathering effects. In all 200 samples giving a total of 1000 specimens have been studied. Fig. 1 shows the equal area projection plot of the mean vectors for the whole series of flows. The points represent projections of the north-seeking poles of vectors placed at the centre of the sphere.

Some dykes in the Deccan traps exposed near Poona, Khandala, Bombay and Nagpur have also been sampled and this work is now in progress. Test samples from a large number of localities covering most of the trap area have also been analysed from time to time for comparison of their remanent directions with those from the main areas studied.

Rajmahal Traps — These traps are believed to be Jurassic in age and cover an area of about 2–3 thousand sq. miles in Bihar.

A total of 110 samples from 17 sites, 5–10 miles apart and covering an area of over 1500 sq. miles of Rajmahal traps was collected in two trips. The first collection consisted of 50 samples from seven sites in the two uppermost flows and the results of this study have already been reported[14]. Samples from two of these sites were rejected since the specimens showed

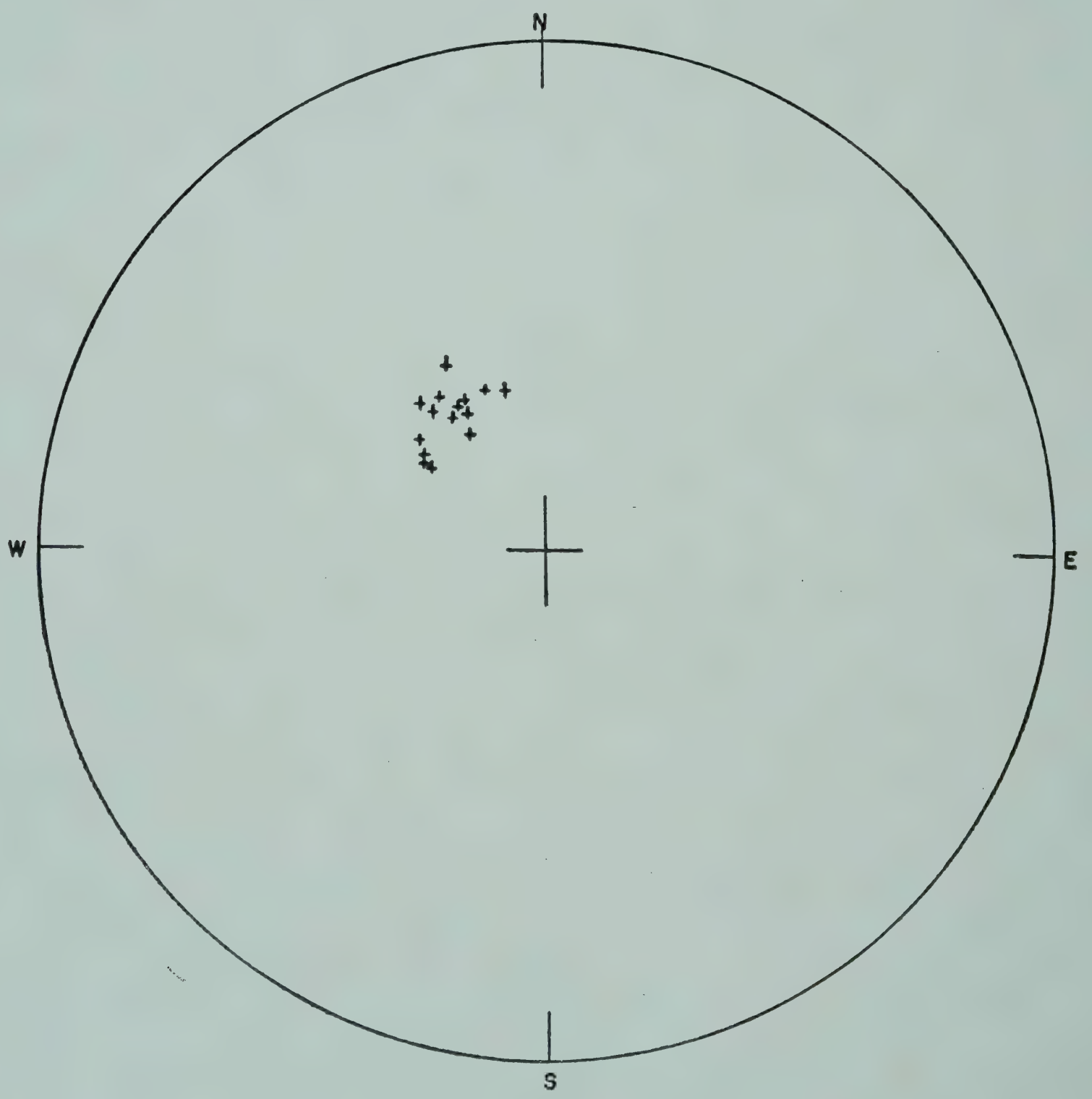

FIG. 2 — EQUAL AREA PROJECTION PLOT OF THE MEAN VECTORS REPRESENTING THE FIFTEEN SAMPLING SITES: RAJMAHAL AREA

considerable weathering. The second collection consisted of 60 samples from a total of 10 sites covering the entire Rajmahal area. Fig. 2 gives an equal area projection plot of the mean vectors representing the 15 sampling sites (probably flows).

Four dykes believed to be causally related to the Rajmahal traps have also been sampled. These have given directions similar to those of the traps.

Sylhet Traps — There is a controversy regarding the age of the Sylhet traps although they are often believed to be of nearly the same age as Rajmahal traps. Some 40 samples from seven sites in the Sylhet traps have very recently been analysed. Results from these are very similar to those obtained for the Rajmahals and since their formation period is closely the same as Rajmahals, this gives confidence in the results obtained.

Studies have also been made on oriented sandstone samples from Cretaceous, Gondwana and Vindhyan age groups. These, however, showed a lack of consistency and stability and no definite indications have so far been obtained.

Results and Discussion

The remanent magnetic directions of all the Indian igneous rocks ranging in age from Jurassic to Eocene have been found to be consistent among themselves but are widely different from the direction of the present earth's field at the corresponding sites of collection. In general the directions obtained are (i) normal (parallel to present earth's field) azimuth with a steep upward (negative) inclination or (ii) reversed (opposite in direction to present earth's field) azimuth and steep downward (positive) dip.

In the case of Rajmahal traps, from the close grouping of points in Fig. 2, it is clear that the variation in the direction from one site to another is very small. As the sites are supposed to cover at least ten flows and a sufficiently large interval of time, the mean of the sites $A = 320°$ and $D = -64°$ up can be safely taken to represent the mean remanent direction for the entire Rajmahal trap horizon.

In the case of Deccan traps, the flows 1–18 (Fig. 1) are magnetized reversely with a downward dip, whereas flows 19 and above have a normal declination and upward (negative) inclination. The grouping of points in this case is not so close and there is actually considerable variation in direction from one flow to another. Such a variation could have been caused by secular changes in the earth's field. However, since a large number of thick flows (18 in all) in succession have been sampled, their mean can be taken to represent the average values of A and D for the reversely magnetized flows. This mean azimuth $A = 157°$ and inclination $D = +52°$ down compare well with the means obtained in other localities[10–13]. The same cannot be applied to the

normally magnetized flows since some of them have not been sampled; the mean would obviously depend on the number of flows studied especially where there is a large difference in direction among successive flows.

The Deccan trap flows at Linga which have been found to be reversely magnetized are believed to be the oldest ones[11]. At Mahabaleshwar, the border between normal and reversed groups of flows lies at about 2000 ft above MSL. The similar border at Nipani and Amba also lies approximately at the same height. It seems permissible, therefore, on palaeomagnetic basis, to divide the Deccan traps into upper and lower sub-groups having anti-parallel magnetic directions.

The observed deviation of the magnetic vectors in rocks from the direction of the present earth's field can be explained on the basis of (i) large-scale movements of magnetic poles relative to rotation axis, i.e. polar wandering, or (ii) large-scale movements of land masses relative to each other and, relative to the rotational axis, or a combination of both (i) and (ii). It is assumed, for this purpose, that averaged over periods of the order of secular variation (a few thousand years) the geomagnetic field corresponds to that of a dipole placed along the axis of rotation of the earth.

The ancient pole positions calculated for the Indian results are widely different from those obtained from other countries. In general the pole positions for rocks of the same age from different countries do not agree. It becomes necessary then to postulate the movements of continents.

At a point on the earth's surface with latitude, λ, the magnetic inclination (D) is given by

$$2 \tan \lambda = \tan D$$

From this, one can calculate the ancient latitudes for India for periods corresponding to the formation of the igneous rocks studied. The ancient longitudes cannot be uniquely calculated from palaeomagnetic results alone. The ancient latitudes for Nagpur calculated without any polar drift for Rajmahal and Lower Deccan traps are 49°S and 37°S respectively.

It is possible that both (i) and (ii) might have occurred, but information on this can be sought through comparing results from countries which are geologically known to have moved considerably relative to each other.

Attempts have also been made to explain the palaeomagnetic results on the basis of (iii) magnetostriction effects in rocks[15], (iv) magnetic anisotropy effects[16], and (v) plastic flow of rocks[17]. Results discussed herein are from rocks which have been subjected to varying natural stresses in different localities but are still consistent, and hence (iii) can be ruled out.

From the foregoing discussion, it is to be noted that the rocks analysed represent a variety of types (basalts, dolerites, rhyolities, etc.) and formations

(flows, sills and dykes) and cover a large time scale (Jurassic to Eocene) and almost the entire east-west surface of the sub-continent of India and, therefore, it seems to us that (iv) and (v) cannot seriously alter our conclusions.

Conclusion

(i) Palaeomagnetic studies in India show that this sub-continent occupied a position well south of equator between Jurassic and Eocene times.

(ii) During the eruption of the lower group of Deccan trap flows, the earth's magnetic field was reversed.

(iii) On the basis of palaeomagnetic results alone, the Deccan traps can be divided into two sub-groups, lower and upper traps, with the boundary lying at about 2000 ft above MSL in the high Western Ghats.

The assumed ages of the rocks studied are based on the stratigraphic evidence, and we can, therefore, only discuss the time scales involved in the movements on a crude basis.

The conclusions drawn herein should be regarded as tentative pending more results from India and also other countries. World-wide palaeomagnetic data have recently been reviewed, but the pictures drawn by the various authors are not yet satisfactory. More work is needed and particularly some of the horizons studied, on which the data are based, require a more detailed study. A comprehensive study of the world-wide palaeomagnetic data would be warranted when reliable mean remanent magnetic directions for formations covering most of the geological sequence from different land masses become available. This is often limited because of lack of existence of suitable formations and also to some extent of proper exposures of the existing formations.

Acknowledgement

We are grateful to Prof. J. A. Clegg, Prof. M. G. K. Menon and Prof. D. Lal from whom we have received valuable guidance throughout this work.

References

1. Johnson, E. A. & McNish, A. G., *Terr. Magn. atmos. Elect.*, **43** (1938), 393.
2. Blackett, P. M. S., *Phil. Trans.*, **245** (1952), 303.
3. Nagata, T., *Fundamental Basis of Rock Magnetism* (International Union of Geology & Geophysics), Helsinki, 1960.
4. Thellier, E., *J. Phys. Radium*, **12** (1951), 205.
5. Nagata, T., *Rock Magnetism* (Tokyo, Japan), 1953.
6. Neel, L., *Adv. Phys.*, **4** (1955), 191; *Ann. Geophys.*, **7** (1951), 90.
7. Nagata, T., *Nature, Lond.*, **169** (1951), 704; **172** (1953), 850.
8. Haigh, G., *Phil. Mag.*, **3** (1958), 267.

9. Blackett, P. M. S., Weizman Lectures on Rock Magnetism, Jerusalem, 1956.
10. Irving, E., *Geophysica*, **90** (1956), 23.
11. Clegg, J. A., Deutsch, E. R. & Griffiths, D. H., *Phil. Mag.*, **1** (1956), 419.
12. Deutsch, E. R., Radhakrishnamurty, C. & Sahasrabudhe, P. W., *Ann. Geophys.*, **15** (1959), 39.
13. Deutsch, E. R., Radhakrishnamurty, C. & Sahasrabudhe, P. W., *Phil. Mag.*, **3** (1958), 170.
14. Clegg, J. A., Radhakrishnamurty, C. & Sahasrabudhe, P. W., *Nature, Lond.*, **181** (1958), 830.
15. Graham, J. W., *Adv. Phys.*, **6** (1957), 392.
16. Girdler, R. W., *Geophys. J.*, **3** (1961), 197.
17. Evison, E. F., *Geophys. J.*, **4** (1961), 320.

* * *

Tidal Variations of Gravity in India. A. N. Ramanathan.

The results of harmonic analysis of gravity tide observations over a period of 31 consecutive days at each of 8 representative stations in India during the IGY period are presented. In the case of the primary lunar semi-diurnal wave M_2 a weight mean value of $1{\cdot}164 \pm 0{\cdot}009$ for the G-factor has been obtained. The value of this factor derived from the other main tidal constituents, especially that derived from the diurnal (lunar-solar declinational) wave K_1, is somewhat larger. This is probably due to the unavoidable temperature fluctuations in the observation rooms and imperfect temperature compensation of the gravimeters. (*Abstract*)

Standard Frequency and Time Transmission Centre, ATA, Delhi. C. S. Rangan*, National Physical Laboratory, New Delhi [*J. Instn Telecomm. Engrs*, **6** (1960), 67].

The set-up and method of transmission of standard time signals on a radio frequency carrier of 10 Mc/s. carried out by the laboratory have been described. Highly stable piezoelectric quartz crystal oscillators are used as the basic standards of time signals. The time signal pulses are derived electronically from the crystal oscillators by proper frequency division and switching mechanism. These signals are maintained with an accuracy of ± 2 parts in 10^8 of a nominal value. The methods by which the relative performance of clocks are assessed and corrected have been discussed. The error that is likely to be introduced in the accuracy due to propagation is also reviewed. (*Abstract*)

*Present address: National Aeronautical Laboratory, Bangalore

Water Masses of the Laccadive Sea. A. A. Rama Sastry, Meteorological Office, Poona.

During 1958, deep sea observations were made in the area between the Laccadive group of islands and Minicoy on the west and the depth countour corresponding to 1000 m. along the Indian coast on the east. Depending upon the depth of bottom these serial observations were extended up to 1500 m. or 2000 m.

From the temperature-salinity diagrams, the water masses of the Laccadive Sea have been identified. Below the tropical discontinuity layer the predominant water mass is the Indian equatorial water. The possible presence of the Antarctic Intermediate water has been examined. The influence of the Red Sea water and that of the 'I-Water' as defined by Thomson has been discussed.

The influence of the Nine Degree Channel and the other features of the bottom topography on the vertical distributions of temperature and salinity has also been studied. The general hydrography of the region is also presented. (*Abstract*)

Electron density in the exosphere from whistler data

S. N. GHOSH
M. S. BISHT

J.K. Institute of Applied Physics
University of Allahabad
Allahabad

A method which has been developed for determining the electron densities in the exosphere using spectrograms of whistlers has been described. A comparison of the values for the stations, Stanford, Seattle and Boulder, obtained by this method, with those of Allcock and Helliwell shows that the present values are higher than Helliwell's but lower than Allcock's. It has also been found that the electron densities are very much higher than those of neutral particle densities calculated by extrapolation of values given by Mathur and Mitra.

Electron densities at the higher altitudes can be obtained by the use of whistlers. Allcock[1] of New Zealand and Helliwell[2] of Stanford have used whistler data independently for finding out the electron density at different altitudes in the exosphere. Allcock has used the method of successive approximations for finding the variation of electron density with height in the outer atmosphere, when the variation of whistler dispersion with geomagnetic latitude is already known. For a period between January and May 1957, he has given the following empirical relation describing the distribution of electrons up to a height of 13,000 km.:

$$N \simeq 5{\cdot}75 \times 10^4 \exp\ (-h/2640)$$

where N = number of electrons/cu. cm. and h = height in km.

Helliwell has used nose whistler data with a certain proposed model for the exosphere. In fact he has used many model distributions for a well-defined

nose frequency. Three or four independent measurements of time delay at different frequencies are required to obtain a corresponding number of independent parameters describing the path and electron distribution. When these parameters are known, the electron density can be easily calculated. A two-parameter method applicable at frequencies less than about one-tenth of cut-off frequency has been developed by Smith and Helliwell[3].

A method for obtaining the electron densities at higher altitudes using the spectrograms of whistlers has been developed here. The values obtained are higher than those of Helliwell[2] but much lower than those of Allcock[1].

Derivation of Electron Density at High Altitudes from Whistler Data

According to Eckersley's dispersion formula, the group velocity (V_g) of a whistler propagation is given by

$$V_g = \frac{2C\sqrt{ff_H}}{f_p} \tag{1}$$

where f = wave frequency, f_H = gyrofrequency and f_p = plasma frequency.

It follows from this formula that the time delays between two consecutive echoes for a given whistler frequency is given by

$$T = \int_{\text{path}} \frac{ds}{V_g}$$

Substituting V_g from Equation (1), we have

$$T = \frac{1}{2C}\int_{\text{path}} \frac{f_p ds}{\sqrt{ff_H}} = \frac{D}{\sqrt{f}} \tag{2}$$

where $D = \frac{1}{2C}\int_{\text{path}} \frac{f_p}{\sqrt{f_H}}\, ds$ is the dispersion path.

For two close points A and B (Fig. 1) at different geomagnetic latitudes we obtain

$$\frac{dD}{ds} = \frac{D_2 - D_1}{S_2 - S_1} = \frac{1}{2C}\,\frac{f_p}{\sqrt{f_H}} \tag{3}$$

where D_2 and D_1 are dispersion paths for points A and B; and S_2 and S_1 are path lengths for magnetic lines of force from A and B.

Equation (3) can be utilized to find the plasma frequency at various altitudes along a whistler path provided we know (i) $(D_2 - D_1)$, (ii) $(S_2 - S_1)$ and

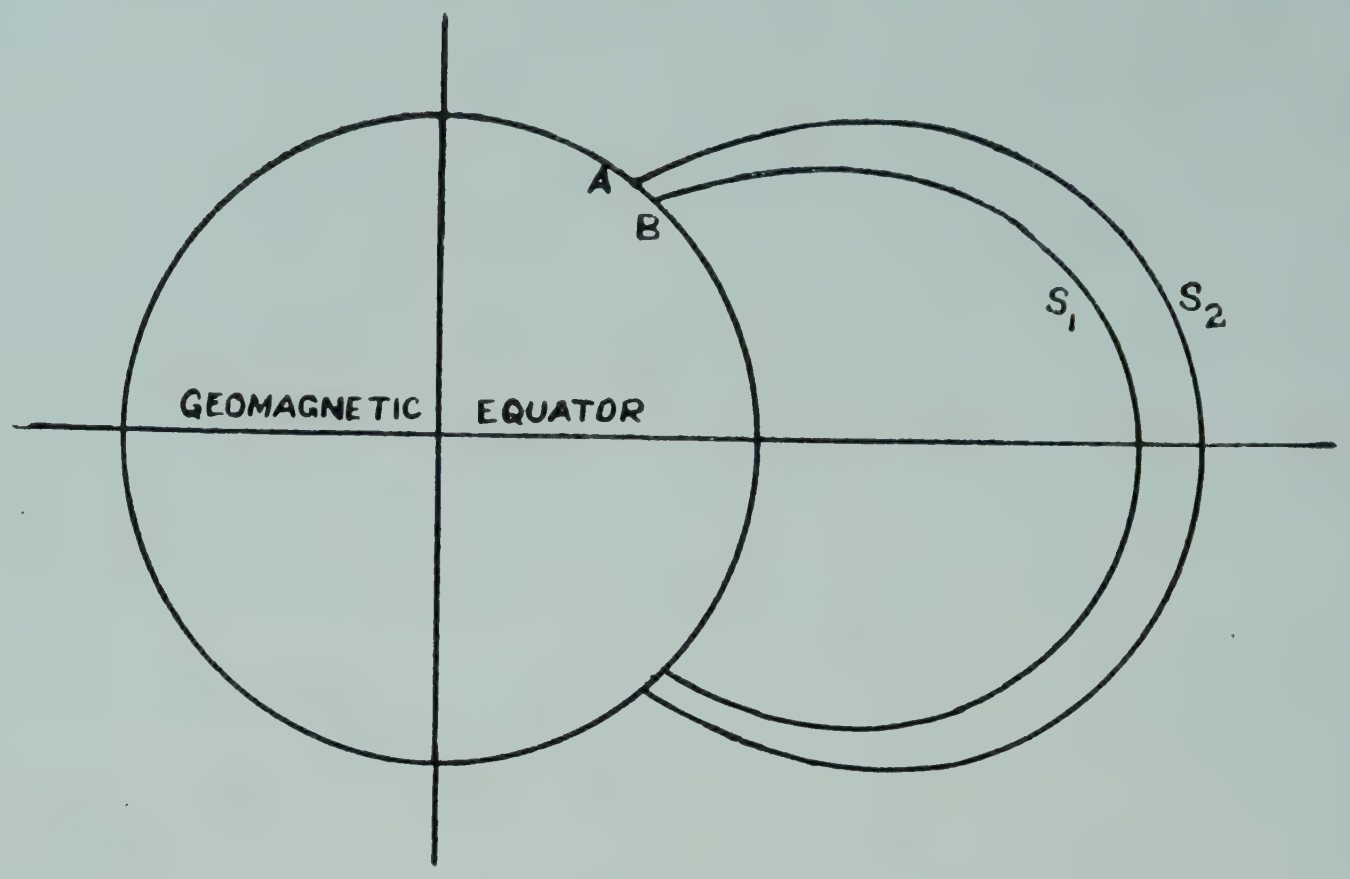

FIG. 1 — PATH LENGTHS S_1 AND S_2 OF TWO CLOSE MAGNETIC LINES OF FORCE ORIGINATING FROM THE EARTH'S SURFACE

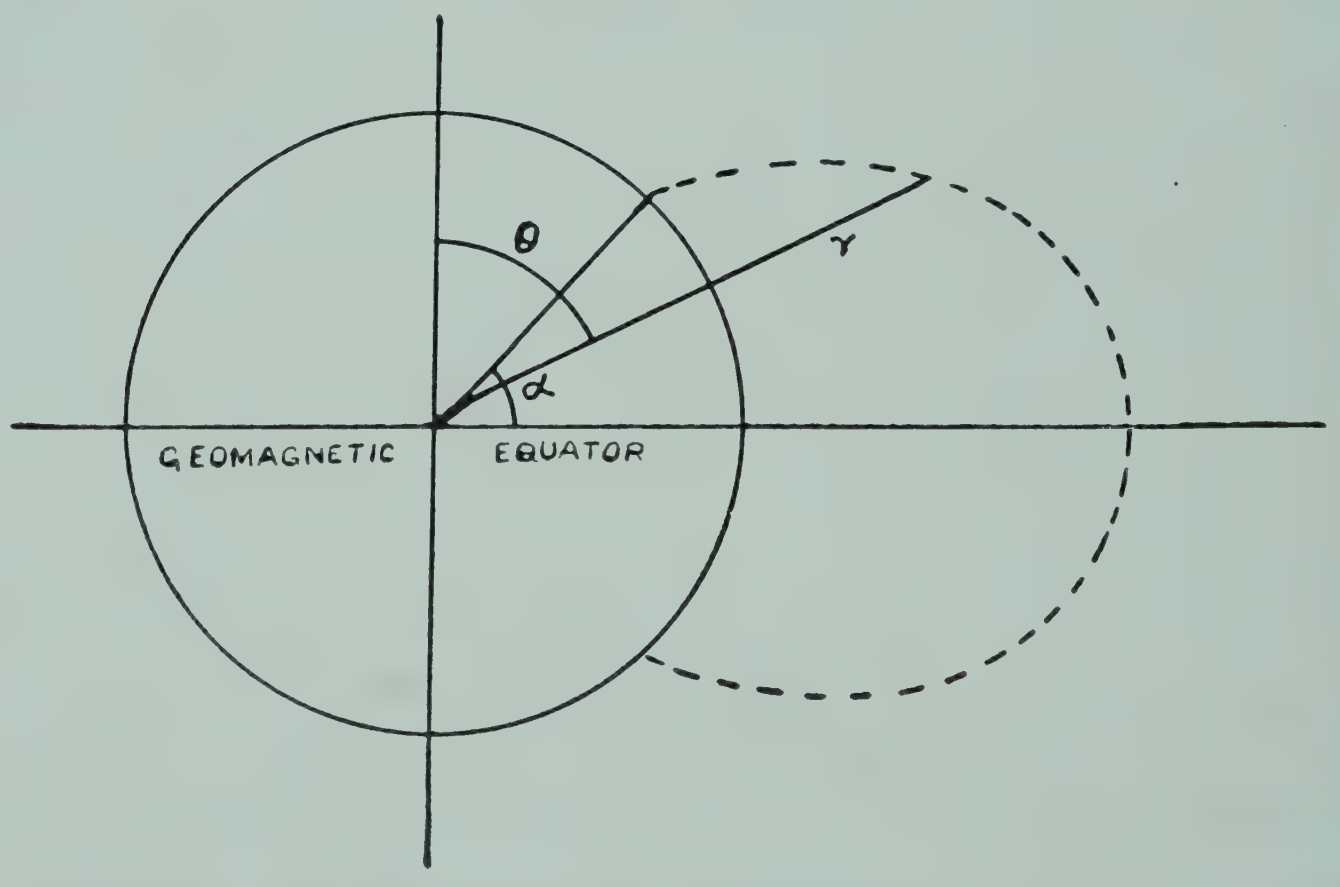

FIG. 2 — A MAGNETIC LINE OF FORCE FROM THE EARTH CONSIDERED TO BE A SIMPLE DIPOLE

(iii) f_H. The electron density in the exosphere can then be obtained by utilizing the relation

$$f_p = \sqrt{\frac{4\pi N e^2}{m}} \simeq 9{\cdot}0\sqrt{N} \text{ kc/s.}$$

where N is the number of electrons/cu. cm.

To obtain the value of $(D_2 - D_1)$ two nearby stations for which whistler spectrograms are available, like Stanford and Seattle, are taken. For a

particular frequency of propagation, the time delay T is measured from the spectrograms and the values of D_1 and D_2 for respective stations are obtained from Equation (2). The value of (S_2-S_1) is obtained after considering the earth as a magnetic dipole (Fig. 2), so that the equation of the line of force is given by

$$r = k/\sin^2\theta \tag{4}$$

where r is radial distance of a point on the path from the centre of the earth and k is a constant.

The value of f_H is calculated from the following relation:

$$f_H = f_{H_0}\,(1-X_0^2)^3 \tag{5}$$

where f_H is gyrofrequency at the top of a magnetic line of force, f_{H_0} gyrofrequency at the equator and $X_0 = \sin\alpha$ (α being the geomagnetic latitude where a magnetic line of force intercepts the earth's surface).

The value of f_{H_0} can be obtained from the data given by Gallet and Helliwell[4] who have shown that at the top of the magnetic line of force from 67° geomagnetic latitude $f_H = 3{\cdot}25$ kc/s. Using Equation (5) we obtain, $f_{H_0} = 360$ kc/s.; f_H can also be found from the relation

$$f_H = \frac{eH}{mc}$$

where H is the magnetic field intensity at a given point.

The above method gives the value of gyromagnetic frequency f_H at the top of the trajectories and hence from a number of such values one can obtain a variation of the gyrofrequency with altitude along a geomagnetic equatorial plane.

To obtain f_H at any point on a line of force, the points of interception of concentric circles with centre at the earth's centre passing through the trajectory tops of different lines of force are obtained (Fig. 3). The gyromagnetic frequencies at the point of interception are assumed to have the same values as of those at the respective trajectory tops.

Calculation of Electron Density

The spectrograms for only three close stations, Stanford, Seattle and Boulder, are available. The electron densities of exosphere are calculated from the data and are given below. It should be noted that the delay times can be measured only approximately from the spectrograms and hence the calculated values of the electron density will be very approximate.

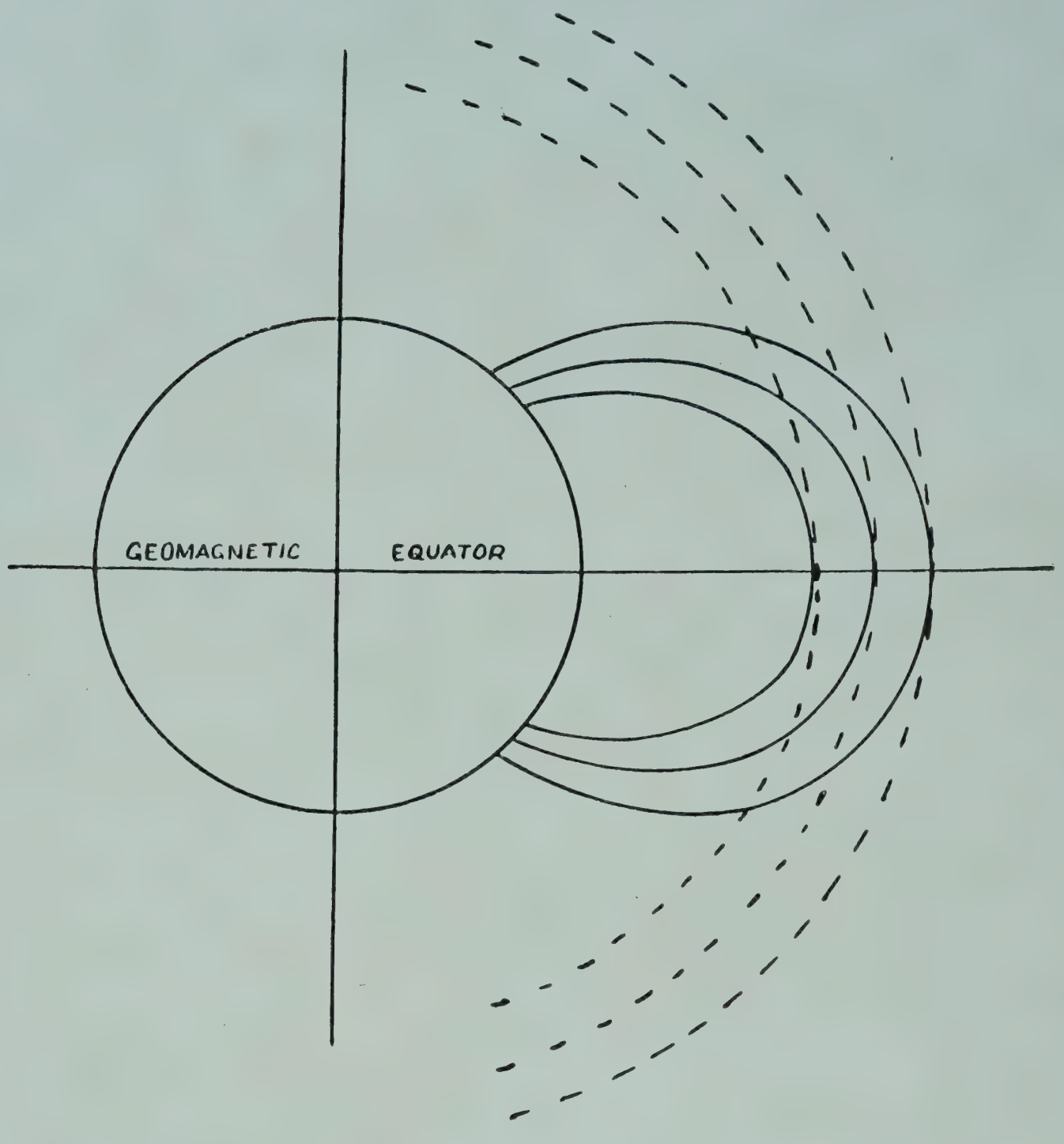

FIG. 3 — INTERCEPTION OF CONCENTRIC CIRCLES PASSING THROUGH THE TRAJECTORY TOPS OF DIFFERENT MAGNETIC LINES OF FORCE ORIGINATING FROM EARTH'S SURFACE

Helliwell *et al.*[5] have shown in their spectrograms that at 4 kc/s. the time delays for Stanford and Boulder are respectively 2·0 and 2·1 sec. From another set of spectrograms of Helliwell and Morgan[6], the time delay for Seattle is found to be 2·3 sec. The dispersion paths and time delays for these stations are given in Table 1. The path lengths for different geomagnetic latitudes have been calculated and are given in the same table. The variation of gyromagnetic frequency with altitude is given in Table 2. The values of (D_2-D_1) and (S_2-S_1) for Boulder-Stanford are 3·1 and 941·92; and those for Boulder-Seattle are 3·1 and 841 respectively. In Table 3 the electron density in the exosphere is calculated and the variation has been shown in Fig. 4.

RESULTS AND DISCUSSION

In Table 4, the distribution of electron densities obtained from whistler data by different workers are given.

TABLE 1 — DISPERSION PATHS AND TIME DELAYS FOR STANFORD, BOULDER AND SEATTLE

Station	Geomagnetic latitude (*approx.*)	Time delay at 4 kc/s. *sec.*	Dispersion path *sec.*$^{1/2}$	Path lengths*
Stanford	45°	2·0	126·4	2·570
Boulder	48°	2·1	132·62	2·848
Seattle	51°	2·3	145·36	3·350

*In terms of earth's radius 'a'

TABLE 2 — VARIATION OF GYROFREQUENCY WITH ALTITUDE

Altitude from earth's surface*	Altitude *km.*	Gyrofrequency *kc/s.*
1·5	10951	21·14
1·2	8088	32·40
1·0	6730	47·88
0·75	5047	64·80
0·50	3365	101·00
0·25	1682	180·00
0·125	841	253·80
0·0625	420	281·00

*In terms of earth's radius 'a'

TABLE 3 — ELECTRON DENSITY IN THE EXOSPHERE

Altitude from earth's surface*	Stanford-Boulder		Boulder-Seattle	
	Plasma frequency *kc/s.*	Electron density *no./cu. cm.*	Plasma frequency *kc/s.*	Electron density *no./cu. cm.*
0·0625	1062	13,950	1146·96	15,200
0·125	1008	12,600	1089·00	14,634
0·25	840	8,712	906·00	10,017
0·50	629	4,800	669·60	5,508
0·75	516	3,285	557·29	3,798
1·00	426	2,172	475·2	2,664
1·20	357	1,606	—	—
1·50	—	—	312·9	1,208·7

*In terms of earth's radius 'a'

TABLE 4 — DISTRIBUTION OF ELECTRON DENSITIES OBTAINED FROM WHISTLER DATA BY DIFFERENT WORKERS

(*Density of coronal electrons,* $4{\cdot}1\times10^3$*/cu. cm.*)[7]

Height *km.*	Electron density (*no./cu. cm.*) by		
	Present authors	Allcock	Helliwell
1125	12000	22×10^3	8000
1625	10020	20×10^3	6000
2875	4908	15×10^3	—
4000	4400	12×10^3	2500
5000	3798	8000	—
6000	2928	5000	1200
7000	2400	—	1000
8000	1600	3000	800
9000	1126	1800	500
10000	1208	400	400

TABLE 5 — NEUTRAL PARTICLE DENSITIES AT DIFFERENT ALTITUDES

Height *km.*	Neutral particle density (*no./cu. cm.*) by	
	Extrapolation of Mathur's table	Mitra
1125	$1{\cdot}3\times10^5$	$1{\cdot}0\times10^5$
1375	$1{\cdot}8\times10^4$	$3{\cdot}0\times10^4$
1625	$3{\cdot}1\times10^3$	$8{\cdot}0\times10^3$
1875	$6{\cdot}9\times10^2$	$4{\cdot}5\times10^2$
2125	$1{\cdot}7\times10^2$	$2{\cdot}3\times10$
2375	$5{\cdot}7\times10$	2·0
2625	$1{\cdot}9\times10$	$1{\cdot}0\times10^1$
2875	$7{\cdot}6\times10^{-1}$	—
4000	$3{\cdot}6\times10^{-1}$	—
5000	$9{\cdot}9\times10^{-2}$	—
6000	$4{\cdot}4\times10^{-2}$	—
7000	$2{\cdot}7\times10^{-2}$	—
8000	$1{\cdot}7\times10^{-1}$	—
9000	$1{\cdot}8\times10^{-2}$	—
10000	$2{\cdot}2\times10^{-2}$	—

The neutral particle densities at different altitudes obtained by extrapolation of values given by Mathur and Mitra[8], and Mitra[9] are given in Table 5. Since at high altitudes only atoms (oxygen) are present the recombination process is of radiative type. Assuming the radiative recombination coefficient to be $1{\cdot}15\times10^{-12}$ cu. cm./sec., it is found that above

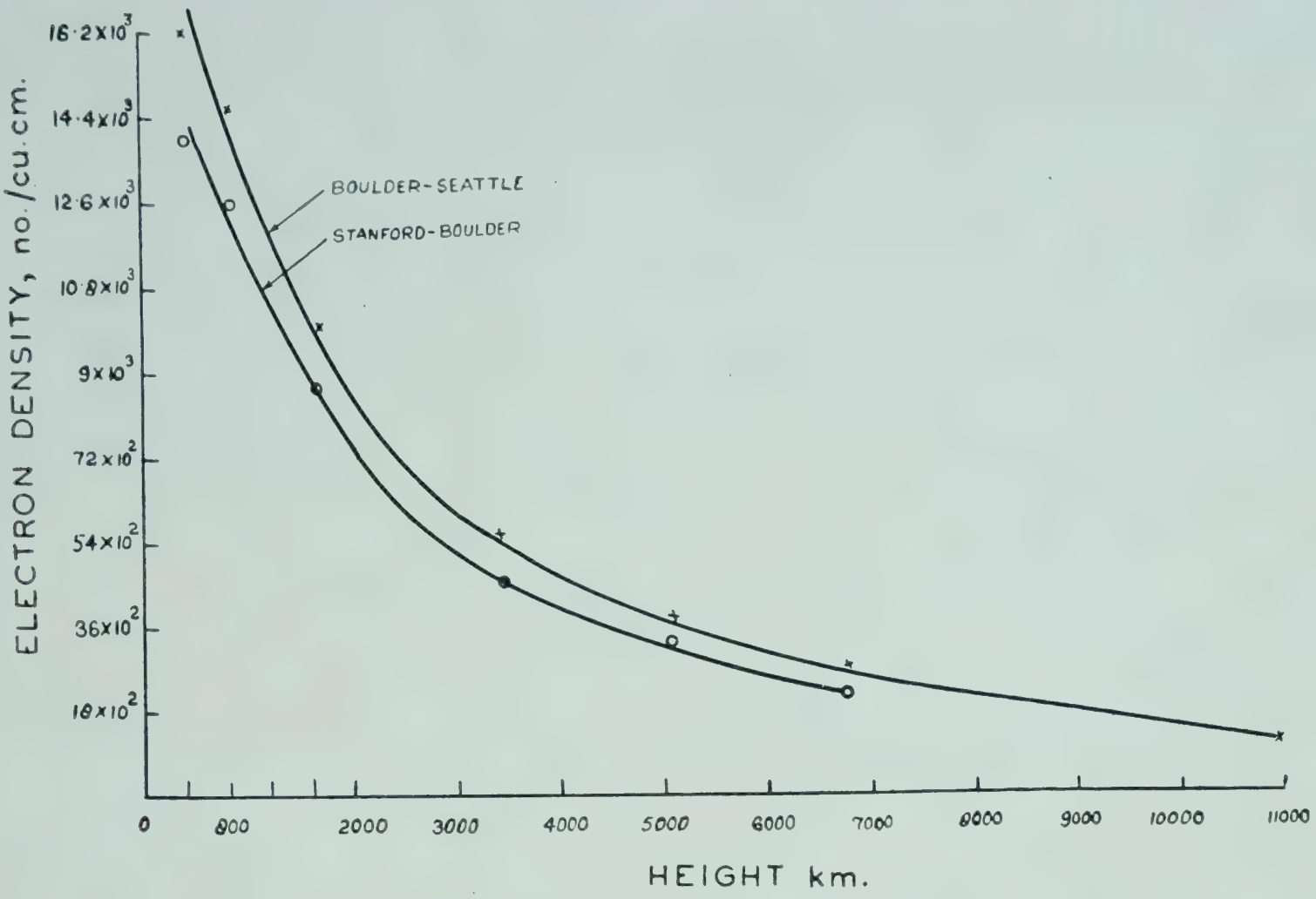

FIG. 4 — VARIATION OF ELECTRON DENSITY WITH HEIGHT OBTAINED FROM WHISTLER DATA

1000 km. all neutral particles are completely ionized by solar ultraviolet rays. The average time required for complete ionization at different altitudes is approximately $2{\cdot}2\times10^5$ sec. Comparing Tables 4 and 5, it is found that at high altitudes the particle density is many times lower than the electron density. Therefore, even assuming complete ionization of neutral particles one cannot account for the electron density from whistler data. From the electron density due to corona as given by Chapman[7] it may be concluded that electrons at high altitudes originate from corona.

It has been observed that whistler propagation is absent in the equatorial region approximately up to 30° geomagnetic latitude. Also, in the high latitude region between 55° and 60° geomagnetic latitude the whistler echoes are seldom observed. The absence of whistler propagation in these latitude regions may be due to the presence of Van Allen radiation belts which are situated at mean altitudes of about 1·5 and 3·5 earth radii. The magnetic lines of force originating from latitudes 25° to 35° intercept the lower belt and also those from 55° to 60° pass through the upper belt. As the whistler waves pass through these belts they may be heavily attenuated, so much so that they are not received at the conjugate points. Work in this direction is now being undertaken.

REFERENCES

1. ALLCOCK, G. M., *J. atmos. terr. Phys.*, **14** (1959), 185.
2. HELLIWELL, R. A., *J. geophys. Res.*, **65** (1960), 2583.

3. Smith, R. L. & Helliwell, R. A., *Calculation of the electron density of outer ionosphere using whistlers*, paper presented at the Symposium on Propagation of VLF Radio Waves, CRPL, NBS, Boulder, Colorado, January 1957.
4. Gallet, R. M. & Helliwell, R. A., *J. Res. nat. Bur. Stand.*, **63D** (1959), 21.
5. Helliwell, R. A. *et al.*, *Low Frequency Propagation Studies Rep.*, Part I, Radio Propagation Laboratory, Stanford, May 1958.
6. Helliwell, R. A. & Morgan, M. G., *Proc. Inst. Radio Engrs, N.Y.*, **47** (1959), 200.
7. Chapman, S., Notes on the solar corona and the terrestrial ionosphere, Smithsonian Contribution to Astrophysics, **2** (1959), 1.
8. Mathur, S. B. & Mitra, A. P., *J. sci. industr. Res.*, **19A** (1960), 311.
9. Mitra, S. K., *The Upper Atmosphere* (The Asiatic Society, Calcutta), 1952, 26.

* * *

Determination of the Electron Content of the Outer Ionosphere from Measurements of Cosmic Radio Noise Absorption. K. A. Sarada & A. P. Mitra, National Physical Laboratory, New Delhi [*J. atmos. terr. Phys.*, **23** (1962), 348].

Simultaneous use of ionograms obtained by a C-4 recorder and observations of cosmic radio noise made at Delhi at 22·4 Mc/s. have yielded approximate values of the electron content of the outer ionosphere. It has been assumed that the ionization decreases exponentially above h_mF_2 with an exponent x. The value of x is found to be, on the average, about $6{\cdot}6\times10^{-3}$ km.$^{-1}$, ranging from 5×10^{-2} to 3×10^{-3} km.$^{-1}$. With $x = 6{\cdot}6\times10^{-3}$ km.$^{-1}$, N decreases to about 30 per cent of its maximum value at 200 km above h_mF_2. These results are in agreement with deductions made in recent years using radio transmissions from satellites and rockets: values of x obtained by satellites range normally between $2{\cdot}5\times10^{-3}$ and $6{\cdot}0\times10^{-3}$ km.$^{-1}$.

Values of x given above are based on the atmospheric model given by Mitra and Mathur [*J. sci. industr. Res.*, **19A** (1960), 311] in which the atmospheric temperature increases rapidly from 1000°K. at 300 km. to 2000°K. at 700 km. and remains constant above this height. The exponent x has also been computed, for comparison, for two other models; both with a constant temperature above 300 km., and with (i) $T = 1500$°K. and (ii) $T = 1000$°K. The corresponding average values of the exponent x are $2{\cdot}7\times10^{-3}$ km.$^{-1}$ for model (i) and $4{\cdot}5\times10^{-3}$ km.$^{-1}$ for model (ii). (*Abstract*)

Microseisms and their studies during IGY

A. N. TANDON

Meteorological Office
New Delhi

The paper gives a brief review of the various viewpoints regarding the generation and propagation of microseisms. Data on microseisms due to cyclonic storms in the Bay of Bengal and the Arabian Sea recorded during the IGY period by the microseismograph stations in India have been analysed and studied. It has been shown that cyclonic storms of sufficient intensity in the Bay of Bengal are usually well recorded at all coastal and inland stations. This is not so for depressions and weaker cyclonic storms. Microseisms generated by cyclonic storms in the Arabian Sea outside the 0-200 m. depth are generally not transmitted with sufficient amplitudes to be of any operational value. A few suggestions for improving the present-day techniques of locating storms by microseismic methods have been made.

Ever since the introduction of sensitive seismographs in the beginning of the present century for recording earthquakes seismologists have observed that the ground actually is never at rest. Minute oscillations of earth caused either by traffic, explosions or by other natural causes are continuously recorded by sensitive seismographs. These vibrations have a large range of periods and amplitudes which vary from about one-tenth of a second to over two or three minutes. These minute observations have been given the name ' microseisms '. It has been found that highly sensitive instruments which have a peak magnification for shorter periods are required generally for recording vibrations of short periods, while sensitive instruments are necessary for recording vibrations of longer periods.

During the last thirty years, attention of seismologists and meteorologists has been drawn specially to a class of microseisms which range in periods from 2 to 10 sec. It was found by Banerjee[1] that the Milne-Shaw seismograph

installed at the Colaba Observatory, Bombay, recorded microseisms of considerable amplitude during the monsoon period and also during the passage of cyclonic storms in the Indian Seas. The intensity of microseisms generally varied with the intensity of the associated weather phenomenon. He classified the microseisms recorded by him into three types. The first type had periods ranging from 10 to 30 sec., were irregular in form and were mostly recorded during the winter months when gusty winds produced waves in shallow water. The second type recorded during May–September had a more regular and continuous wave trains and its period ranged from 4 to 10 sec. The origin of these was attributed to the generation of waves by monsoon winds in deep sea. The third type had periods varying from 4 to 6 sec. and were recorded generally during the pre- and post-monsoon periods when there was a cyclonic storm in the Indian Seas. This type could easily be distinguished by its form. These microseisms occurred in well-defined groups in which the amplitude changed in a characteristic manner. The origin of these microseisms was attributed to the formation of large waves in the storm area which caused pressure fluctuations on the sea bed.

In addition to these types, studies by Gilmore[2] and others in U.S.A. during the war years showed that cold fronts over the sea also cause microseisms having a period range of 1–4 sec. Chakravarti and Sirkar[3] have also observed similar microseisms during the passage of nor'-westers in the Bay of Bengal.

Since microseisms having a period range of 2–10 sec. are associated with adverse weather over the seas, their study has opened the possibility of their use in meteorological investigations. Microseismic research during recent years has been directed to find out whether this phenomenon could be used for tracking cyclones, hurricanes and extra tropical storms over the oceans. In regions of the world with large expanse of water, it is difficult to get meteorological observations for use in storm location. The only source of information from a storm with its centre far out in the ocean is the arrival of sea-swell on the coast which can be recorded by wave recorders. Since the swell-waves travel at the rate of only about 30 miles an hour, the detection of a storm by this method gets considerably delayed particularly when the storm is far away from the shore. Microseismic waves, on the other hand, travel very much faster (one to two miles per second) and can reveal the presence of a cyclone or hurricane much in advance of the arrival of the swell. This fact has been established by a number of research workers in U.S.A. and U.K. Mention may be made of the observations by Decon[4] of wave heights and periods at Paranforth, Cornwall, and comparison of these observations with those of recorded microseism periods and amplitudes at Kew. He found that the microseismic maxima were recorded much earlier than the maxima of the swell-waves.

Theories of Microseisms. Several theories to explain the origin of these microseismic waves have been proposed. The earliest was given by Gherzi[5] who attributed the microseisms to the pumping action of air on water in regions of lows caused by typhoons. Banerjee[1] gave a theoretical explanation of the origin of both storm and monsoon type microseisms. According to him, the pressure due to change in the wave heights in the region of the storm was communicated to the bottom of the sea and transmitted from there to the recording station as seismic surface waves. Normally the pressure effect due to water wave on the surface of the sea is reduced exponentially with the depth of water, but Banerjee showed that if the compressibility of water is taken into account the theory could explain how these pressures could be communicated to the sea bottom. According to this theory, the sea waves and microseismic waves should have the same periods. Another point of view which can also explain the origin of these microseism was given by Gutenberg[6,7] following an idea of Weichert. According to this theory, sea waves beating against a steep coast are responsible for generation of microseisms. Gutenberg was able to explain the energy associated with the microseisms by assuming that only 1/1000th part of the total energy of the beating waves is communicated for producing the vibrations on the coast. Observations, however, show that microseisms are recorded even when there is no steep coast near the recording station. It was also observed by Banerjee[1] that monsoon microseisms appear on seismograms much earlier than the arrival of monsoon air near the coast. In the case of cyclones also, the microseisms are generally detected much earlier than the arrival of the swell on the coast. This shows that the surf theory will not be able to account for these types of microseisms. It is, however, quite possible that records of microseisms on coastal stations have a considerable component which can be ascribed to local beating of surf. The periods of such microseisms are usually less than those of storm microseisms.

Longuet Higgins[8] attributed the generation of microseisms to the interference of sea-swell of the same period travelling in opposite directions. This interference caused the formation of standing waves and hence according to the theory of Miche the pressure due to these waves could be communicated to the sea bottom. Standing waves could be caused either by refraction from a sea coast or in the region of cyclones where waves travelling in opposite directions were formed. According to this theory, the periods of microseisms should be half the period of waves responsible for their generation. This fact has been corroborated by actual measurements and lends strong support to the theory.

Although the theory given by Longuet Higgins has been able to explain a number of observations relating to generation of microseisms, yet its acceptance by workers in U.S.A. has by no means been universal. While Carder[9]

and Kammer and Dinger[10] have given many examples supporting the theory, Gutenberg[11] and workers of the Lamont Geological Observatory have been very critical of it. According to the views of Press and Ewing[12], Donn[13] and other workers at Palisades, pulsations or oscillations in the air striking the sea surface are coupled to the surface and then transmitted to the sea bed as sound waves. Certain specific periods are set up between the sea surface and sea bed, depending upon the depth of the sea. This theory requires a homogeneous path between the source of origin and the recording station.

Storm Tracking by Microseisms. Studies of microseisms having a period range of 3–6 sec. have clearly shown that they are associated with the passage of storms over the seas. In order to utilize these observations for actually tracking the path followed by a cyclonic storm, it is necessary to find out the direction of approach of the microseismic waves. Many attempts have been made in the past to show that storms could be tracked by microseismic methods. The earliest attempt in this connection was made by Lee[14] who wanted to find out the direction of approach of microseisms by observing the relative amplitudes of the microseismic waves on two horizontal component seismographs. He showed that microseisms consisted mainly of Rayleigh type waves in which the particles of earth moved along a retrograde ellipse that is up and down, forward and backward but not sideways. By comparing the ratio of the amplitudes of the horizontal components to that of the vertical components, he was also able to show that a large part of the microseismic waves consisted of Rayleigh waves. His method of detecting the direction of approach of microseismic waves, however, did not meet with much success.

Another approach, which has been given considerable importance and on which a large amount of money was spent in America during the war years and later, uses a method known as ' tripartite method '. Although the principle of the method was well known, its application to the problem of studying microseisms was first conceived by Ramierez[15] who put three sensitive seismographs at the vertices of a triangle having sides of a few kilometres. By finding the accurate time of arrival of the same wave at these three stations, he was able to compute the direction from which the microseismic wave arrived. This method was adopted later by the U.S. Navy which established a number of such stations around the Carribbean Sea for tracking hurricanes. Gilmore[16] collected considerable data by this method and found that under suitable conditions the method proved successful, but in quite a number of cases, it failed to give correct bearings of the storms. At present, there seems to be a good deal of controversy about the feasibility of tracking storms with this method. There is difference of opinion amongst Japanese workers about the adequacy of the method. The conclusion that emerges

from many studies of this method is that it can only be applied under very limited conditions. One school of thought believes that the tripartite method intrinsically has large errors and so cannot be applied to tracking of storms. The accuracy of time measurement has to be of the order of a fraction of a second and a good amount of accuracy has to be expected from the instrument. However, recent studies in Russia have lent some support to the tripartite method.

The difficulties experienced with the working of the tripartite method by the U.S. Navy led Gilmore[17] to work out an empirical method for tracking of storms and assessing their intensities from microseismic record. This method has been given the name of 'micro-ratio technique'. In this method, microseismic data collected over a large number of years are used to prepare micro-ratio charts for indicating the location of the storm centre. Ratios of amplitudes of microseisms at two stations are plotted at the centre of cyclonic storm. This ratio is independent of the intensity of the storm because for any position of the storm the intensity of the generated microseisms will simultaneously rise or fall at both the locations. Since the path of microseismic waves also remains the same, any refraction of the seismic waves between the storm centre and the recording station is automatically taken into account. If a large number of such ratios and positions of storms are available it is possible to plot micro-ratio charts. Similar data from a number of pairs of such stations help in finding out the exact location of the storm centre. For finding out the intensity of the storm, data from a large number of storms with known winds and the corresponding microseismic amplitudes at any station are correlated for a large number of storms and ultimately used in the preparation of charts showing the intensity of the storm as correlated to microseismic amplitudes and distance of the storm from the recording station. It is necessary that the instruments are maintained in a standardized condition over a large number of years. This, however, becomes very difficult to realize in practice. The method also requires collection of data for a large number of years before it can be used.

In recent years a new technique for finding out the direction of approach of microseism has been used by Derbyshire and Iyer[18]. Their method uses a three-component seismograph for finding out the direction of approach. According to them, the method adopted by Lee did not succeed because it was presumed that microseisms consisted of pure Rayleigh waves. It is, however, well established that in addition to Rayleigh waves, microseisms contain an appreciable amount of Love waves. It is necessary to find out the proportion of Rayleigh to Love waves and to use a vertical component also along with the two horizontal components used by Lee. The vertical component only records Rayleigh waves while the horizontal components record both Rayleigh and Love waves. In the method adopted by

Derbyshire and Iyer, a comparison of the records of the vertical seismograph is made with each of the horizontal components in turn, and correlation coefficient between the different components is calculated mathematically. Instruments have been devised to give these correlation coefficients expeditiously.

Iyer[19] working at the National Institute of Oceanography, U.K., used the method given by Derbyshire in tracking a number of extra-tropical storms in the Atlantic and found fairly good agreement in the determination of the bearings of the position of storm centres compared to those given by the synoptic situation. The bearing of the storm centre with respect to north and the ratio L/R of Love waves to Rayleigh waves are calculated from the following formula:

$$\tan^2\theta = \frac{(r_{yz}^{-2}-1)^{\frac{1}{2}}}{(r_{xz}^{-2}-1)^{\frac{1}{2}}}$$

$$\frac{\bar{L}^2}{\bar{R}^2} = (r_{yz}^{-2}-1)^{\frac{1}{2}}(r_x^{-2}-1)^{\frac{1}{2}}$$

where r_{xz}, r_{yz} are the correlation coefficients between the vertical components and the E–W components and the N–S components respectively. These correlation coefficients are obtained experimentally using a correlation meter.

It was also found that the bearing of the storm centre as calculated by the above method did not always coincide with the actual position of the storm. This has been attributed to refraction of the seismic waves due to the variations in the velocity of propagation along with the path from the generating area to the recording station and also to the varying depth of the ocean along the path. They found it difficult to estimate the correction which could be applied to account for the variations in the geological conditions of the earth's crust but made some refraction diagrams which could take into account the effect due to ocean depth.

It has been claimed by Iyer[19] that the method of correlations along with the refraction diagrams could be used for tracking at least simple meteorological situations. The method becomes unreliable when the storm centre approaches coastal regions. Under these conditions microseisms are generated both at the storm centre and on coast due to surf. The error in the estimated bearings can be minimized by using long lengths of records for calculation of correlation coefficients. By using band pass filter in the recording mechanism, Iyer has been able to record microseismic spectra within a period range of 5–10 sec. He has shown that microseismic sources of the different periods can exist independently. The maxima of the microseismic spectrum has been found to follow the storm centre more closely

than the total spectrum. Iyer found that Love waves have the nature of noise in comparison to the Rayleigh waves. The ratio of Love waves to Rayleigh waves has a tendency to decrease as the storm intensifies. Records obtained by him show a tendency for a period of microseisms to shift when the swell arrives on coast. Iyer estimated the value of the ratio R/L for various periods of microseisms. He found that this ratio depended on the position of microseismic source and could be used to estimate the distance of the source from the recording station.

Need for Further Work. It has now been established that cyclonic storms, cold fronts and high winds which are responsible for large sea waves cause microseisms. Before, however, microseisms can actually be used for tracking of storms for operational purposes, a few fundamental facts still remain to be answered. It has not yet been established beyond doubt that microseisms are actually generated near the centre of a cyclonic storm. Many workers, particularly Kammer and Dinger[10] in U.S.A., are very sceptical on this point. They have shown that microseisms have sometimes their origin at places far away from the region of storm.

The exact manner in which microseismic amplitudes are transmitted over large distances of intercontinental proportions is not very clearly understood. It has been found in a large number of cases that microseisms are recorded without any appreciable attenuation at inland stations more than thousand miles away from the centre of storm. Apparently, this points out that microseismic waves are communicated in some sort of channel in the same way in which audible sounds are propagated in a whispering gallery. The geological factors which may cause refraction and modifications to the passage of microseisms are not fully known. How the periods of microseisms get modified from station to station is also not very clearly understood. All these problems point to a still greater effort to be put forth for microseismic research. Recognizing this necessity the IGY Committee of the International Union of Geodesy and Geophysics recommended to all participating countries to collect as much data as possible on the microseismic phenomena. They recommended the establishment of more stations to record microseisms, particularly on the islands. In spite of the indifferent results given by the tripartite method, the Committee recommended the establishment of more tripartite stations for calculation of bearings of storms.

Indian IGY Programme

In India, research on microseisms is carried on mainly by three organizations, the India Meteorological Department, the Naval Physical Observatory, Cochin, and the Geophysics Department of the Bengal Engineering College. Most of the seismograph stations in operation in the country work

under the technical supervision of the India Meteorological Department. The Bengal Engineering College has a three-component Benioff seismograph. The Naval Physical Observatory at Cochin also operates a three-component seismograph with electronic magnification. Before the IGY, Sprengnether microseismographs were operating at Madras, Bombay and Shillong. In addition to these, a few other stations where Milne-Shaw seismographs operated could also be used for recording microseisms. A new station equipped with a Milne-Shaw seismograph and Sprengnether microseismograph was started at Port Blair in the Andaman Islands for special studies during the IGY. It was intended to have tripartite stations at Madras and Bombay but due to difficulties in laying of cables at these stations, they could only be operated as single stations.

Collection of Microseismic Data. Microseismic data giving the average periods and amplitudes at synoptic hours of zero, 0600, 1200 and 1800 GMT were collected every month from all the six participating stations and were made available to the World Data Centre 'C' at Strasbourg. The observations were continued during the IGC and are still being continued. The Sprengnether seismograph at the stations participating during the IGY were maintained at a standard magnification of 5000 according to the method suggested by Gilmore. The microseismograph at Port Blair could not function continuously due to successive galvanometer failures as a result of action of atmospheric salt on the galvanometer coil and it became necessary to use the amplitudes and periods at this station from the records of Milne-Shaw seismograph. The amplitudes and periods were measured for five largest regular groups within 10 min. of the hour of observation and the average was taken.

Processing of Data. The day-to-day amplitudes and periods of microseisms recorded at Bombay, Shillong, Madras and Port Blair were graphically plotted for the entire IGY period. Out of the set of observations special study has been made of microseisms which were recorded at the stations mentioned above (functioning under the India Meteorological Department) for those occasions for which a depression or a cyclonic storm was formed in the Indian Seas. During the IGY period, 17 depressions and storms formed in the Bay of Bengal and the Arabian Sea and their tracks have been recorded (Fig. 1). Brief descriptions of the history of the depressions and cyclones under study along with the microseismic activity observed at these four stations are given below. Amplitudes and periods of microseisms observed during these periods for 13 depressions and storms are shown graphically in Figs. 2–14. No microseisms were recorded for the remaining four depressions at any of the stations. Positions of storms and brief description of synoptic situation are also indicated in the figures.

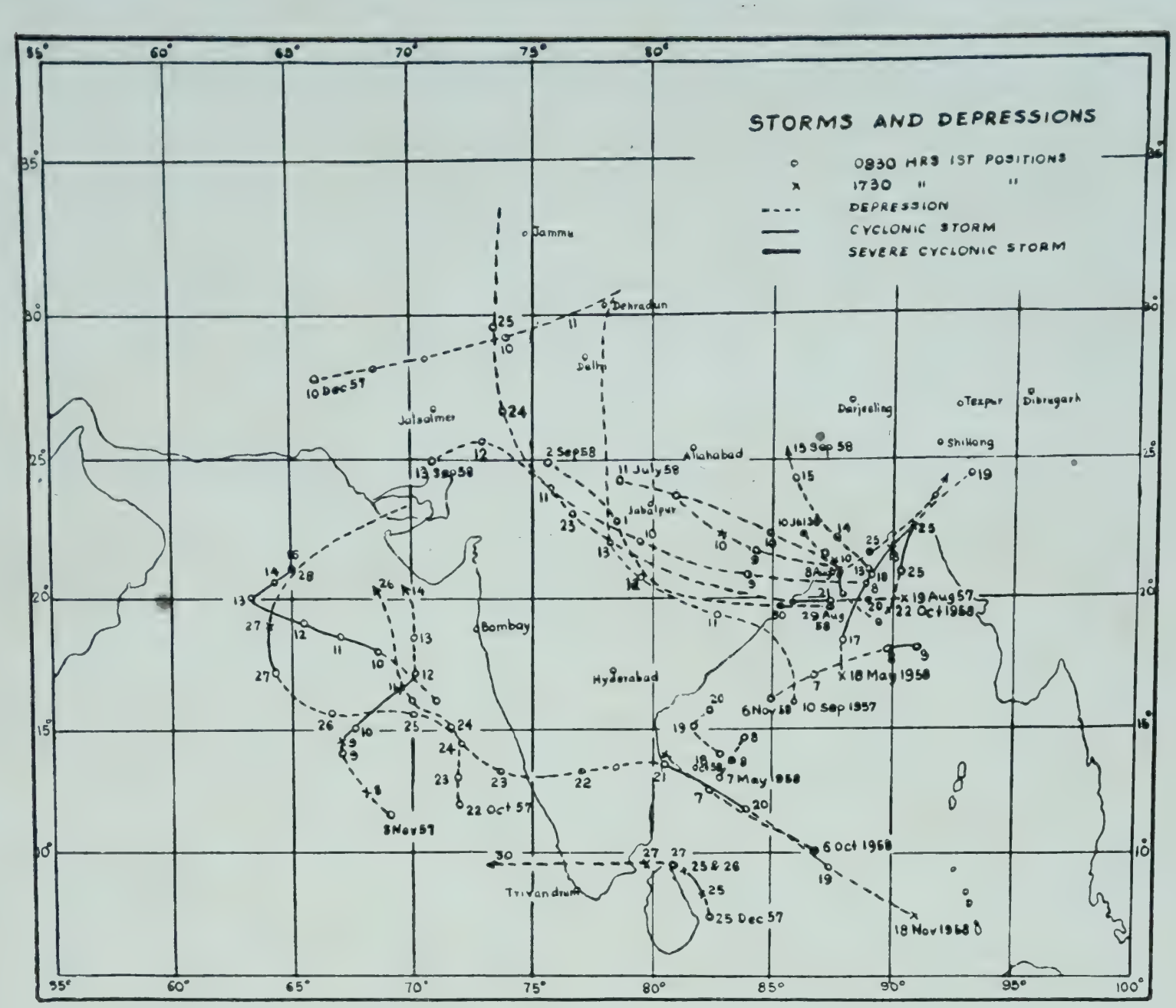

FIG. 1 — TRACKS OF DEPRESSIONS AND STORMS FORMED IN THE BAY OF BENGAL AND ARABIAN SEA

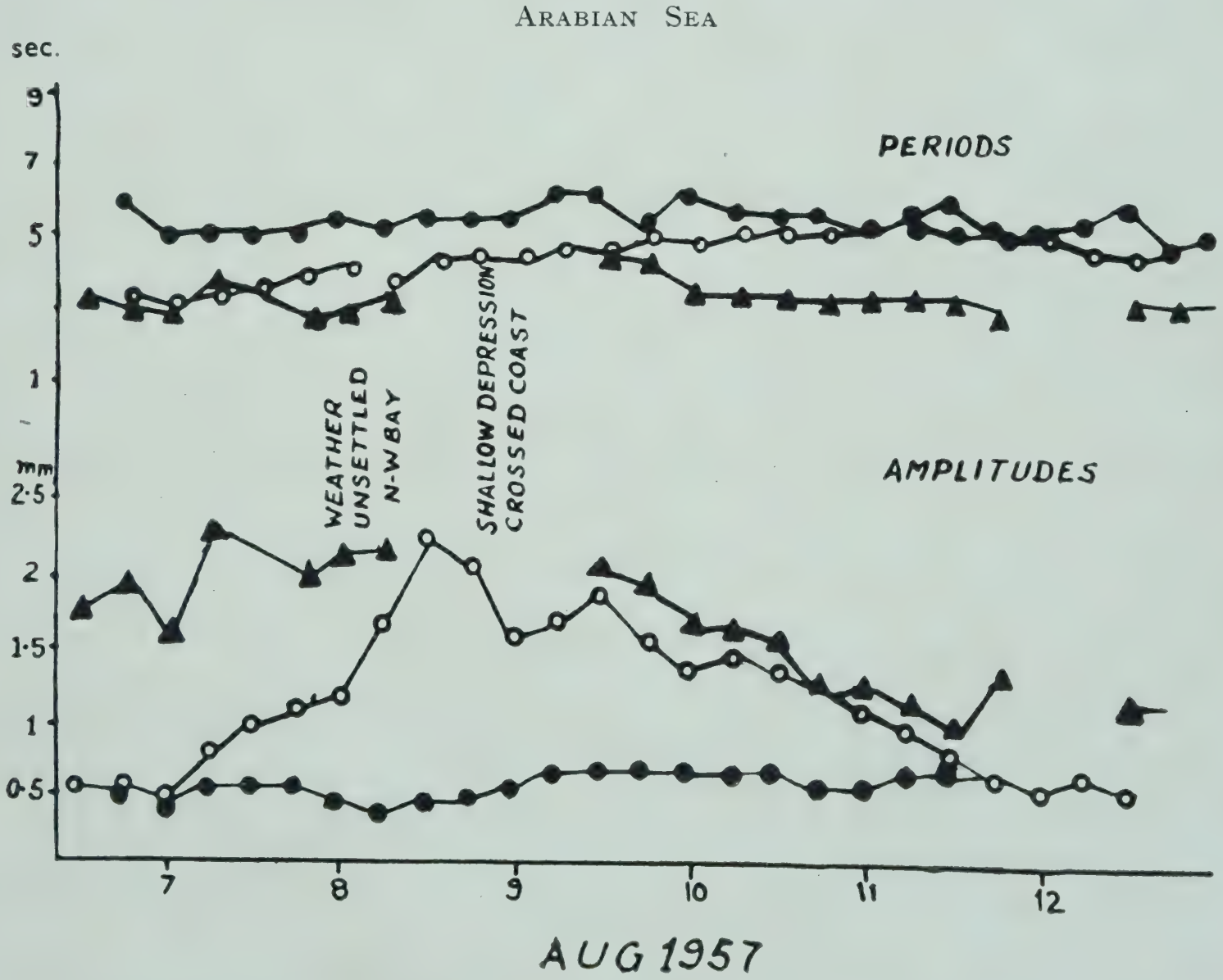

FIG. 2 — AMPLITUDES AND PERIODS OF MICROSEISMS: AUGUST 7–12, 1957

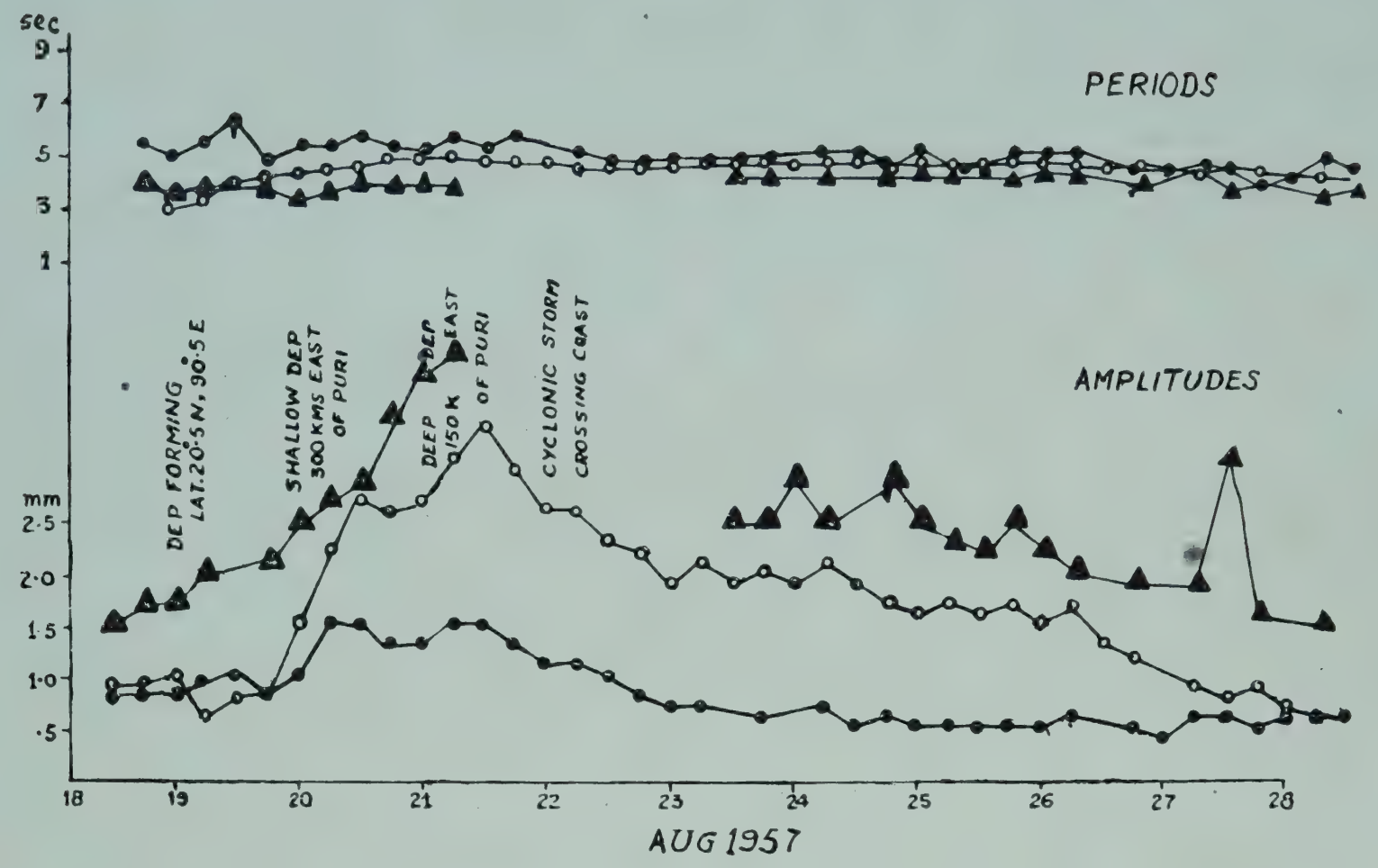

FIG. 3 — AMPLITUDES AND PERIODS OF MICROSEISMS: AUGUST 19–28, 1957

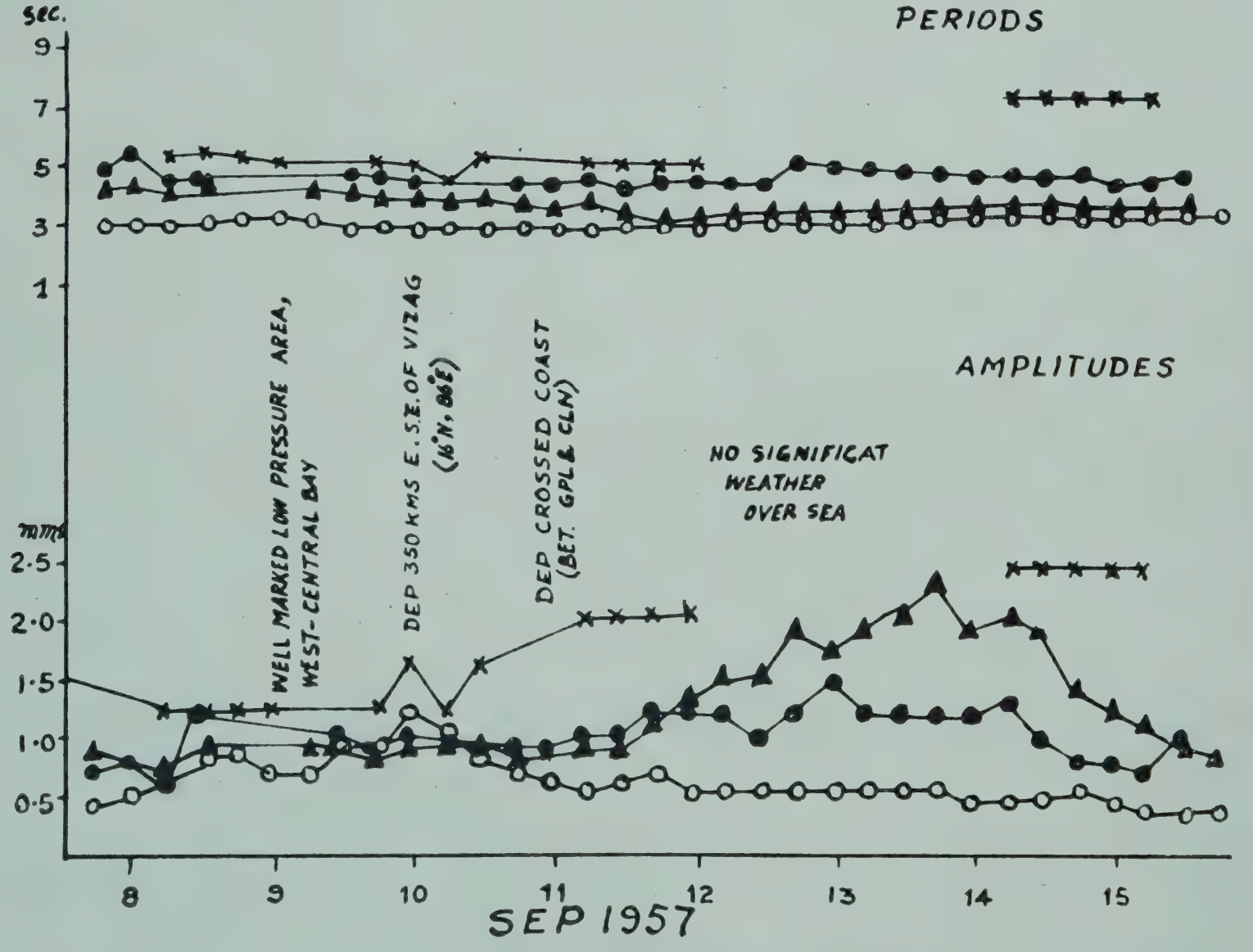

FIG. 4 — AMPLITUDES AND PERIODS OF MICROSEISMS: SEPTEMBER 8–15, 1957

August 7–12, 1957. According to the synoptic situation, weather became unsettled in the north-west Bay of Bengal on August 8, and a shallow depression was formed which crossed the coast before the next morning when it lay as a low pressure area over Orissa and adjoining Madhya Pradesh. The microseismic amplitudes started rising rather steeply at Madras from the morning of the seventh instant reaching a peak at 1200 hours GMT of August 8 after which they started declining. Microseismic amplitudes started rising at Bombay even before this date. They reached a peak about the morning of the eighth instant and then started decreasing gradually. There was no significant rise in the amplitudes recorded at Shillong. The period of microseisms rose slightly as the amplitudes increased at all the stations. The peak of microseismic activity was recorded at Madras near about the time storm was crossing the coast.

August 19–28, 1957. Unsettled conditions at the head of the Bay of Bengal concentrated into a depression which had its centre at latitude 20·5°N : 90·5°E on the morning of August 19. The depression started moving in a westerly direction, intensified into a cyclonic storm and according to weather reports crossed the coast on the morning of August 22. The microseismic amplitudes at Madras and Shillong started rising steeply from about 1200 hours GMT of August 19 reaching their maximum at 1200 hours GMT the day after, and thereafter decreased gradually becoming normal after several days.

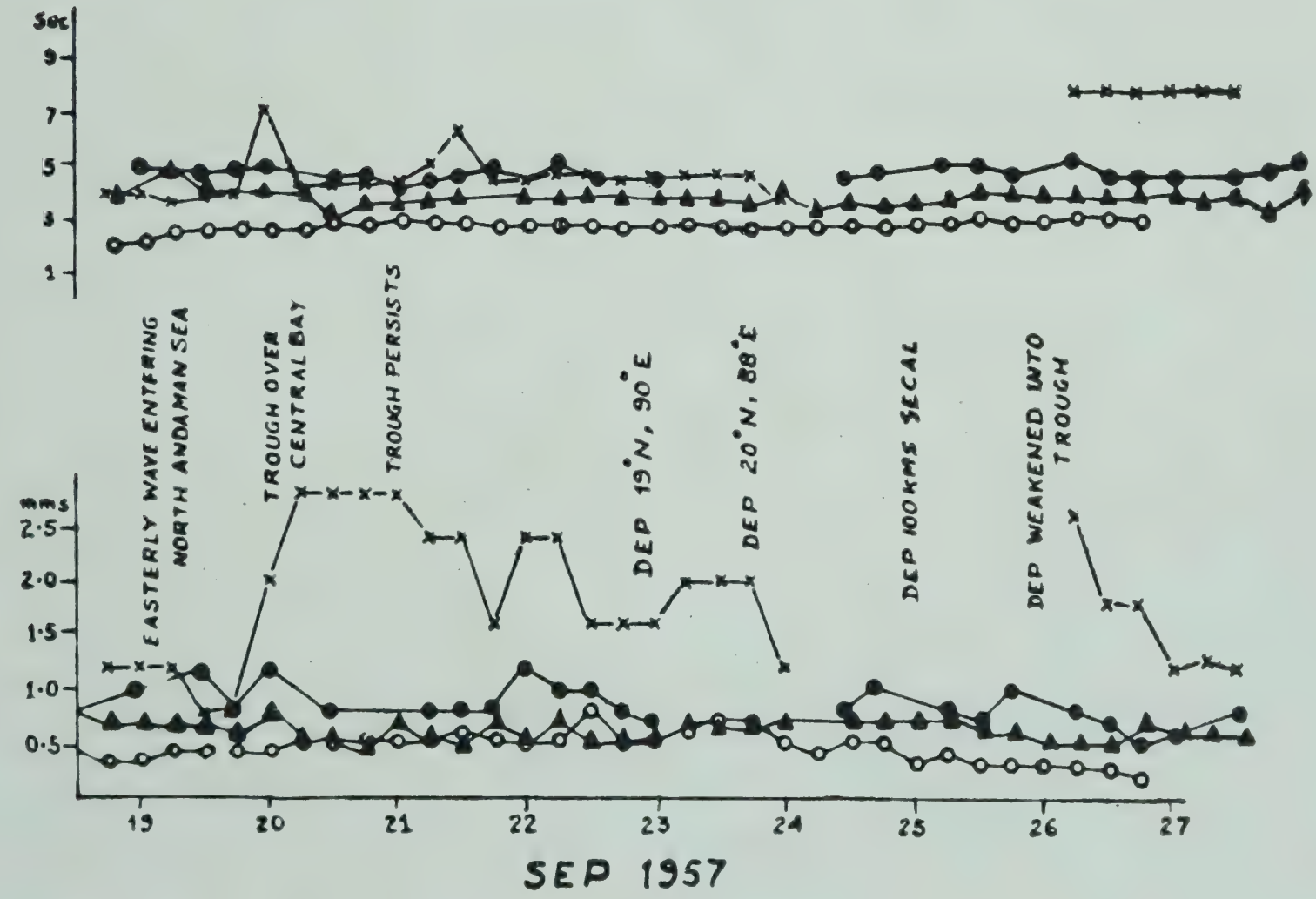

FIG. 5 — AMPLITUDES AND PERIODS OF MICROSEISMS: SEPTEMBER 19–27, 1957

The amplitudes at Bombay also followed a similar pattern except that the increase in amplitudes started about 12 hr earlier. It will be seen from the graph of amplitudes and periods that the maxima of the amplitudes at all the stations was recorded at about 1200 hours GMT on August 21, while according to weather reports, the storm crossed the coast the next morning. This would mean that before crossing the coast, the storm had already started weakening. Periods of microseisms showed an increase with amplitudes at all the three stations, more conspicuously at Madras.

September 8–13, 1957. A well-marked low pressure area was observed in the west-central Bay of Bengal on September 9. The next day it became a depression with its centre near latitude 16°N: 86°E. This depression crossed the coast between Gopalpur and Kalingapatam in the early hours of the next morning. There was no significant rise of amplitudes at Bombay and

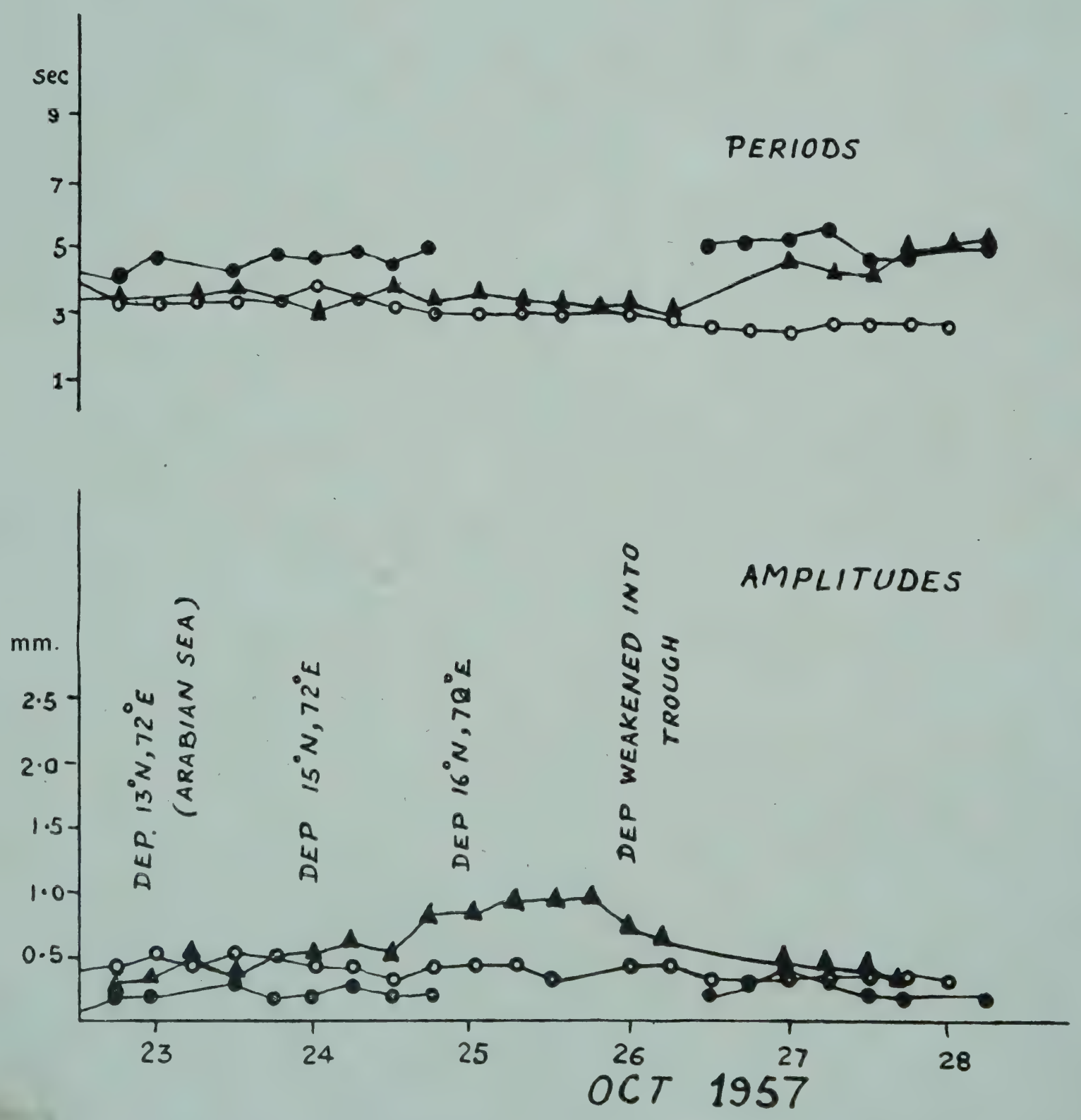

FIG. 6 — AMPLITUDES AND PERIODS OF MICROSEISMS: OCTOBER 23–28, 1957

Shillong. Madras seismograph showed a slight increase in the amplitudes which reached a peak on the morning of September 10 and thereafter started declining and becoming normal on the eleventh. The periods at all the stations remained nearly steady. The maxima was reached about 24 hr before the storm crossed the coast, showing that the depression must have started weakening much before it reached the coast. The amplitudes of microseisms show a significant rise from 1200 hours GMT of September 11 to 1400 hours GMT of September 13 at Bombay alone in spite of the fact that there was no significant weather either over the Arabian Sea or the Bay of Bengal. During this period, the amplitude of microseisms at Madras remained almost steady and at Shillong only a slight increase was noticed. This phenomenon could only be attributed to some unusual local surf activity.

September 19–25, 1957. An easterly wave moving across the North Andaman Sea on September 19 formed a depression with its centre near 20°N:88°E on the night of September 23. On the morning of September 25 this depression had its centre about 100 km. south-east of Calcutta and the next day it weakened into a trough of low pressure. The microseismic amplitudes

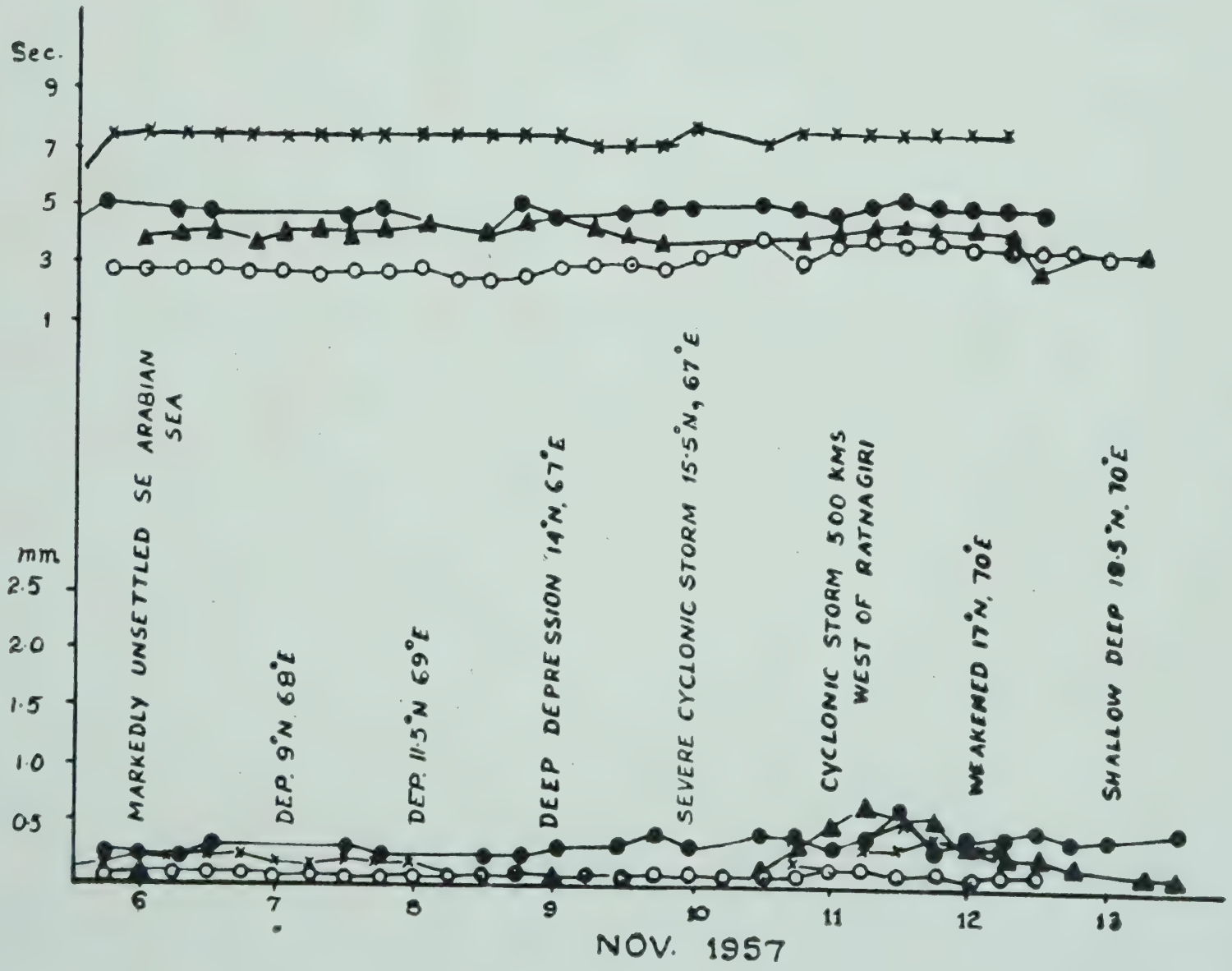

FIG. 7 — AMPLITUDES AND PERIODS OF MICROSEISMS: NOVEMBER 6–13, 1957

and periods at Madras, Bombay and Shillong did not show any significant change during this interval. The amplitudes at Port Blair, however, showed a sudden rise round about 1800 hours GMT on September 19, reached a peak at 1200 hours GMT the next day and then declined.

October 23–27, 1957. A depression was formed on October 22 with its centre near latitude 12°N: 72°E in Arabian Sea. The depression travelled in a N-NNW direction and weakened into a trough of low pressure four days later. The microseismic amplitudes at Madras and Shillong did not show any significant rise. The amplitudes at Bombay started rising slowly from 1200 hours GMT of October 23, reached a peak near about 1800 hours GMT two days later and then declined. Their periods of microseism at Bombay also showed a slight rise between October 24 and 25.

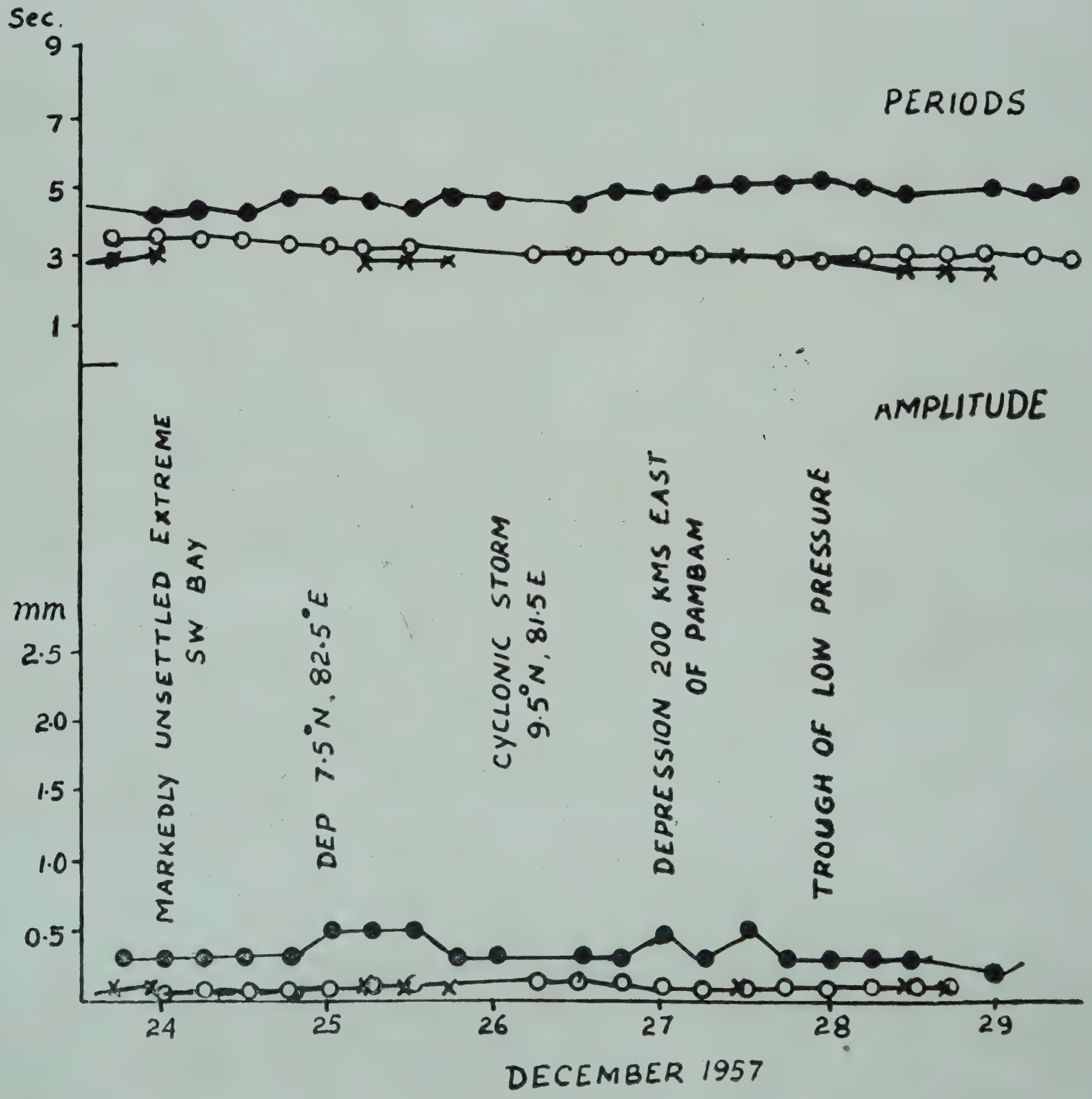

FIG. 8 — AMPLITUDES AND PERIODS OF MICROSEISMS: DECEMBER 24–29, 1957

November 10–13, 1957. A depression formed in the Arabian Sea on November 7 with its centre near 9°N: 68°E. It travelled in a north-westerly direction intensifying into a deep depression two days later. By the morning of November 10, it further intensified and became a severe cyclonic storm with its centre at latitude 15·5°N: 67·5°E. It travelled in a north-easterly direction and the next day its centre was about 500 km. west south-west of Ratnagiri. From November 12 onwards the storm weakened and travelled as a depression in a northerly direction and finally weakened into a trough of low pressure two days later. The microseismic amplitudes at Madras and Shillong showed a very slight rise just before November 11. The amplitudes at Bombay and Port Blair showed a significant rise from 1200 hours GMT of the previous day. At Bombay the maxima was reached at 0600 hours GMT of November 11 and at Port Blair at 1800 hours GMT of the same day. The amplitudes at these stations also returned to normal soon after two days. The period of the microseisms at Port Blair remained

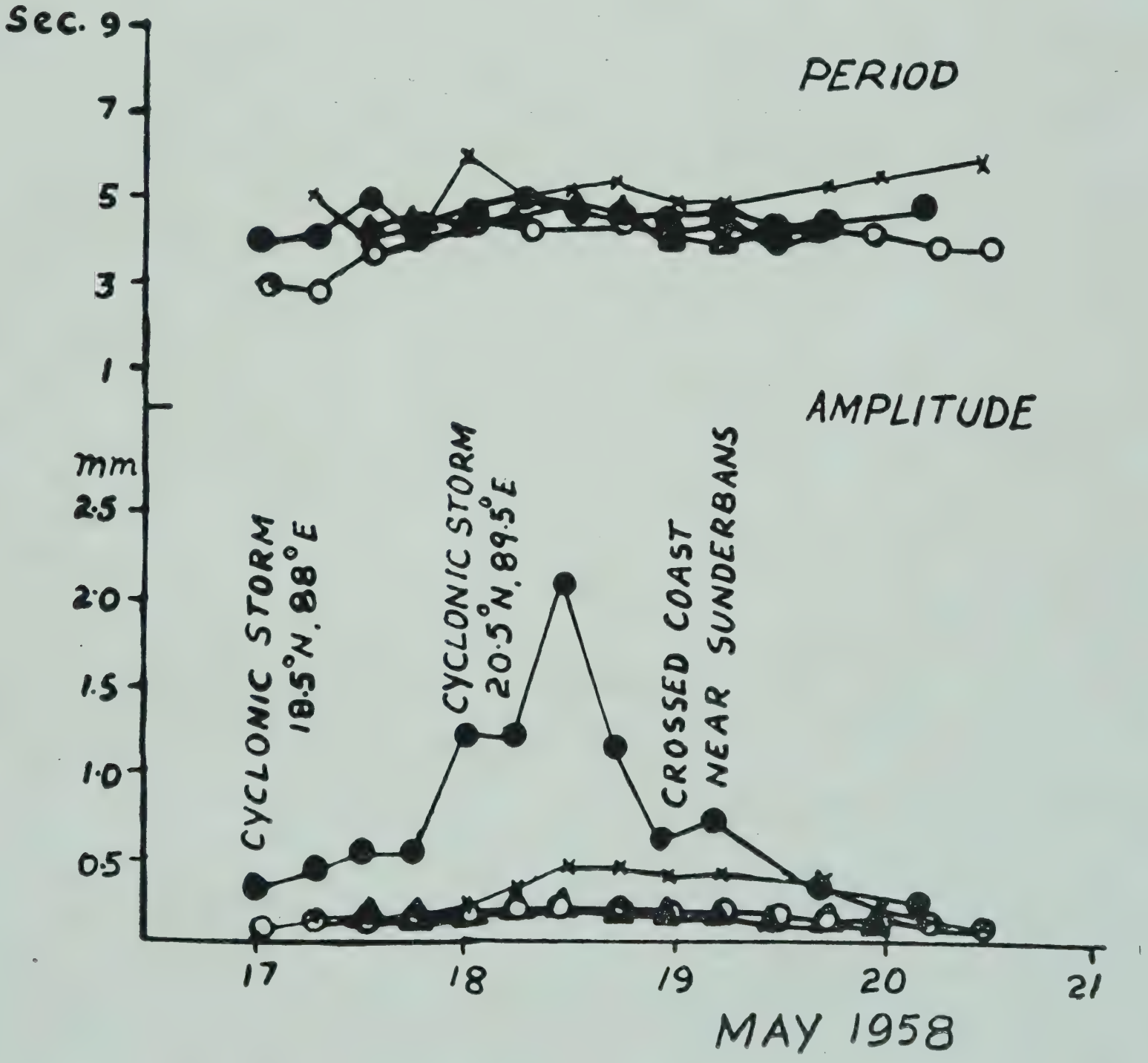

FIG. 9 — AMPLITUDES AND PERIODS OF MICROSEISMS: MAY 17–21, 1958

almost steady and at Bombay showed a very slight rise. It is significant to note that the amplitudes of microseisms at Bombay remained small until November 10 even after the depression had concentrated into a severe cyclonic storm.

December 25–28, 1957. Conditions became markedly unsettled in the extreme south-west Bay of Bengal on December 24. On the following morning, a depression was formed with its centre near 7·5°N: 82°E. The depression concentrated into a cyclonic storm on December 26 with its centre about 200 km. east of Panbam and finally became a trough of low pressure two days later. The amplitudes of microseisms at Port Blair and Madras were almost steady except for a very slight rise at Madras on December 25 which

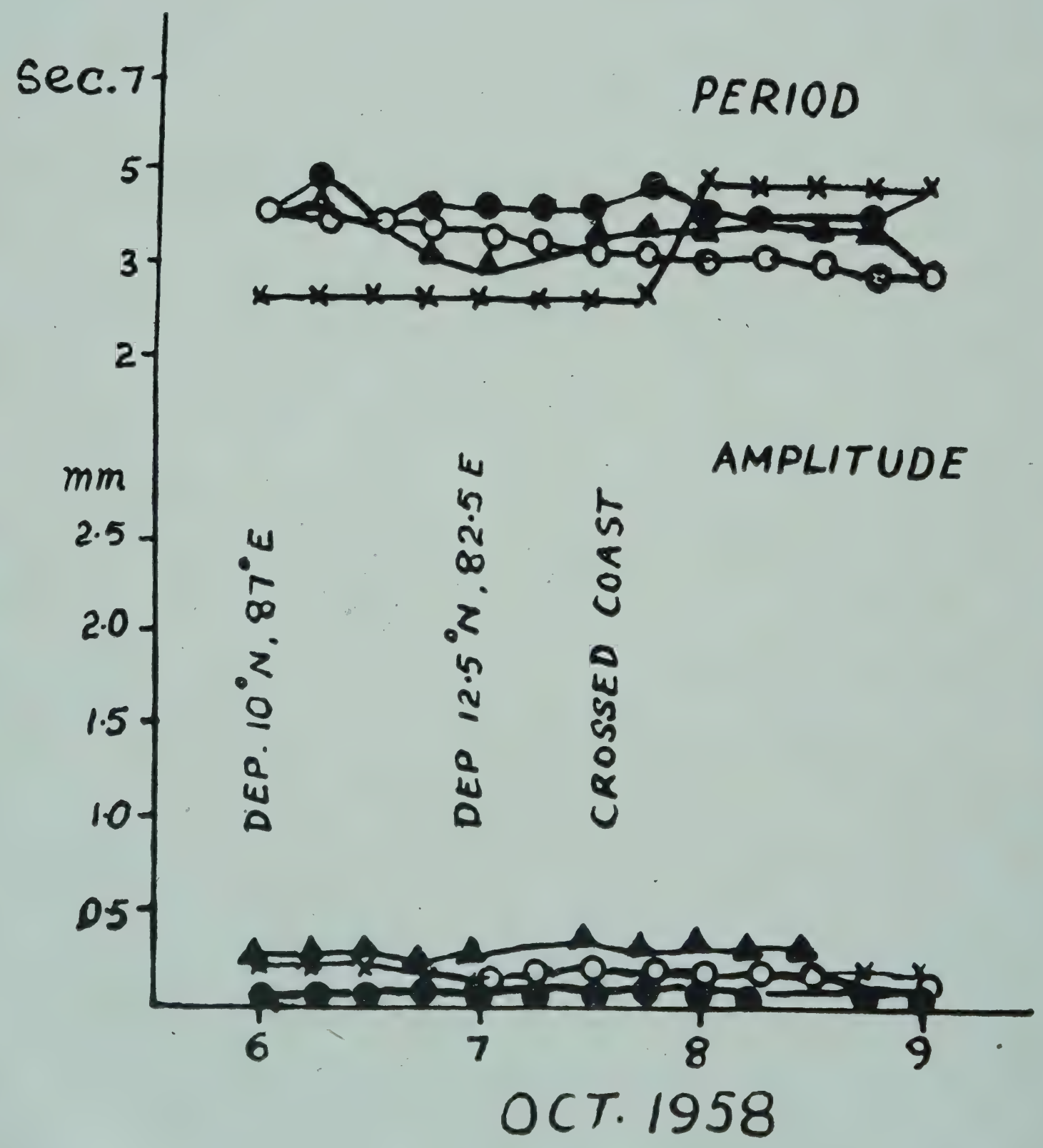

FIG. 10 — AMPLITUDES AND PERIODS OF MICROSEISMS: OCTOBER 6–9, 1958

reached its peak near about 0600 hours GMT next day and then declined gradually. It is interesting to note that the amplitudes at Shillong registered a significant increase at 1800 hours GMT of December 24. After registering a peak at 0600 hours GMT the next day they declined to their normal value by the morning of December 26. The rise in amplitudes at Shillong apparently does not correlate with the presence of this cyclonic storm on this day.

May 17–19, 1958. A trough of low pressure in the central Bay of Bengal concentrated into a depression during the night of May 16. It further intensified into a cyclonic storm of a small extent with centre at 18·5°N: 88°E the next morning. The storm moved in a north-easterly direction and was centred on the morning of May 18 at latitude 20·5°N: 89·5°E. It crossed the coast near Sunderbans the same night. The amplitudes of microseisms started rising slightly at Madras and Shillong from the morning of May 17. From 1800 hours on that date, the amplitude rose rather steeply at Madras and Port Blair and continued to rise slightly at Madras and Bombay. The peak of microseismic amplitudes was reached at 1200 hours GMT the next day. The amplitude at all the stations declined considerably by the morning of May 19 except at Port Blair where the decrease was more gradual. The periods at all the stations showed an increase with an increase in amplitude. The maximum microseismic activity was recorded a few hours before the storm crossed the coast.

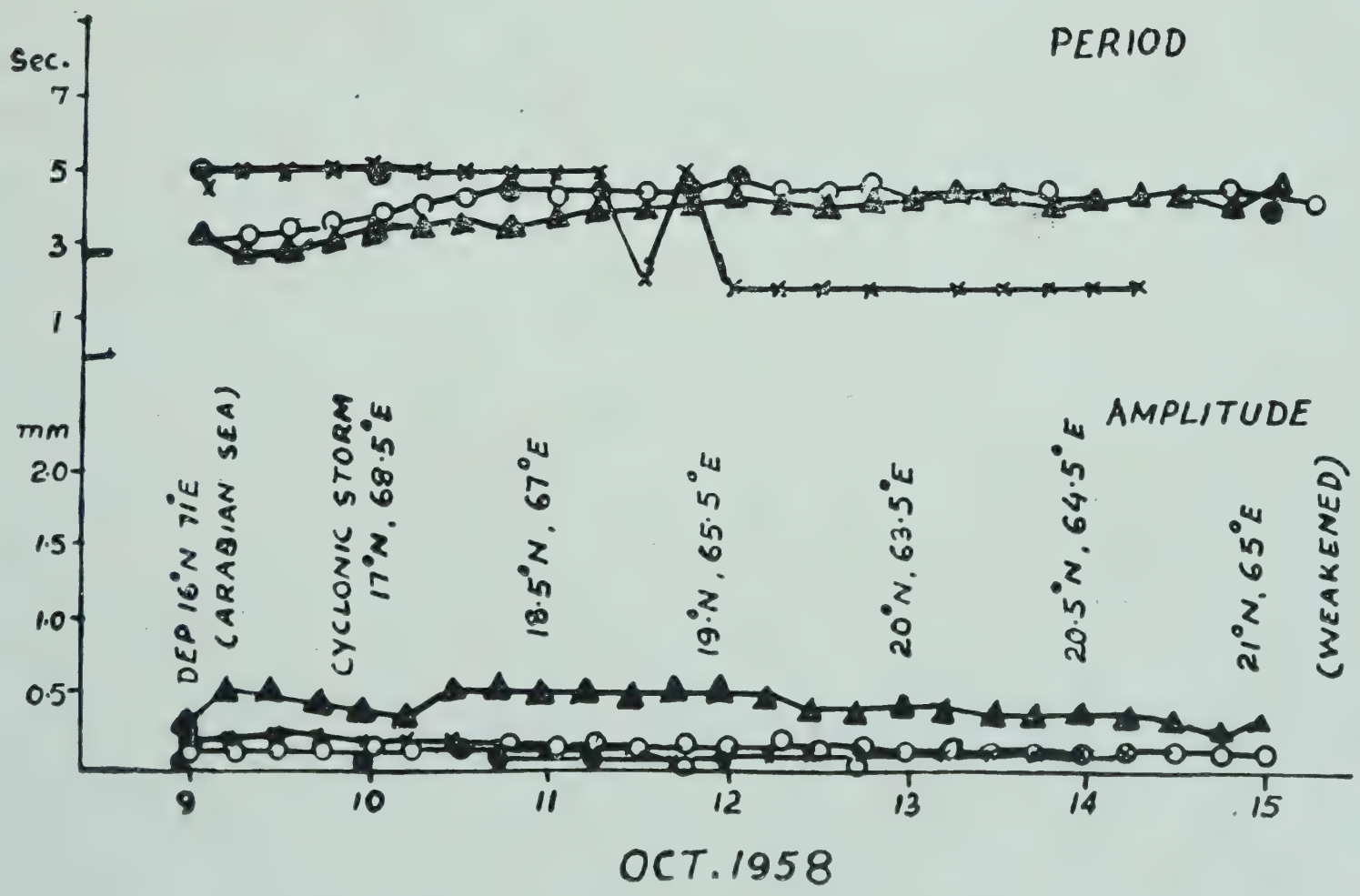

FIG. 11 — AMPLITUDES AND PERIODS OF MICROSEISMS: OCTOBER 9–15, 1958

October 6–9, 1958. The synoptic chart on morning of October 6 showed a depression with its centre at 10°N: 87°E. This moved in a north-westerly direction and crossed the coast near Nagapatnam about 1200 hours GMT the next day. None of the stations recorded any significant rise in amplitudes.

October 9–15, 1958. A depression formed in the Arabian Sea on October 9 with its centre near 16°N: 71°E. By the following morning it had intensified into a cyclonic storm and had its centre at 17°N: 68·5°E. The storm continued to travel in a north-westerly direction for 3 days when it recurved and travelled in a north-easterly direction and finally weakened by October 15. The microseisms at all the Indian stations did not show any significant rise, although the amplitude of microseisms at Bombay remained slightly above normal during this period. The periods of microseisms at Bombay and Madras increased for three days from October 9 after which they became almost steady.

October 21–23, 1958. A depression was formed on October 22 with its centre near latitude 19·5°N: 90°E. By the morning of the next day it intensified

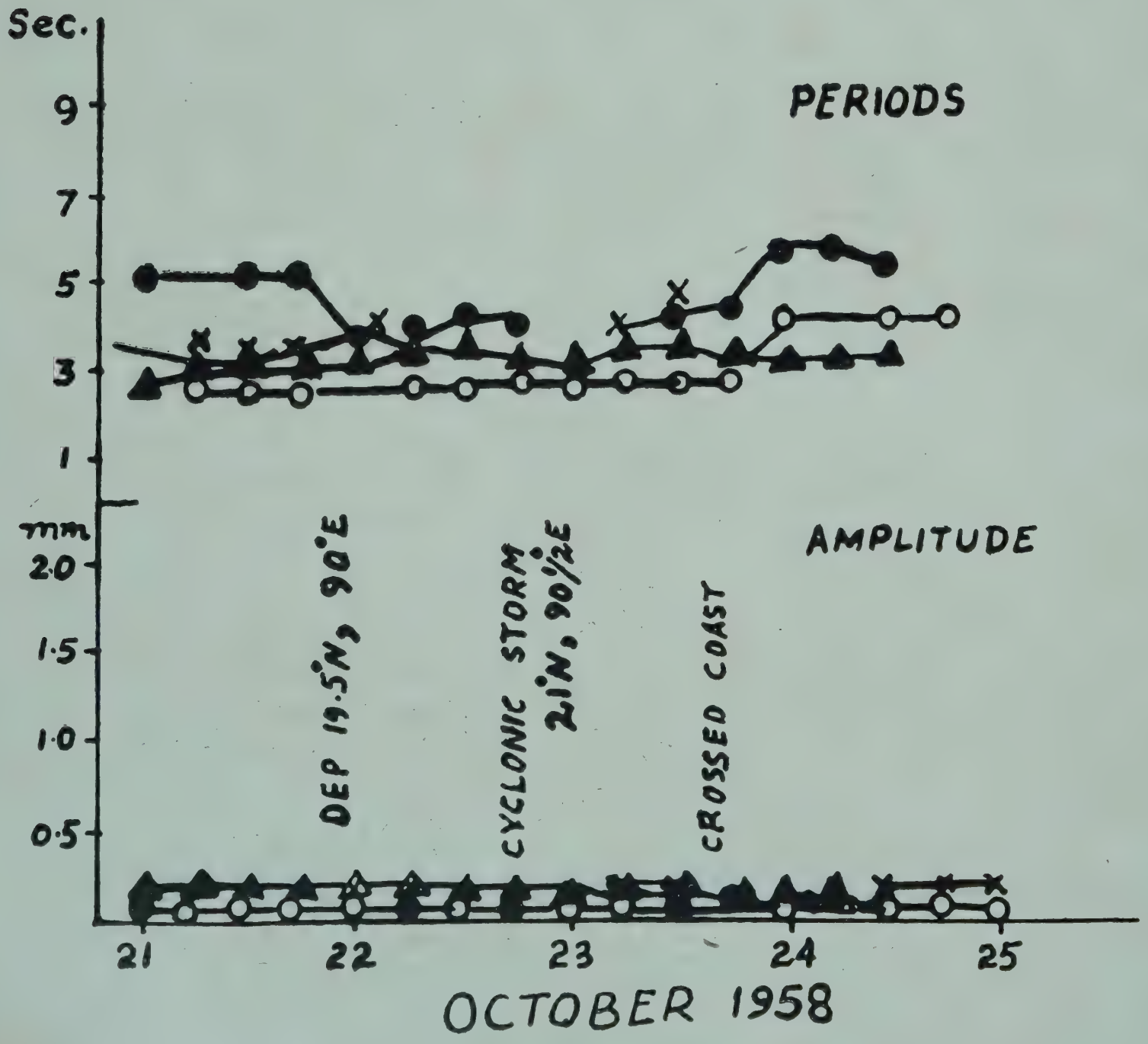

FIG. 12 — AMPLITUDES AND PERIODS OF MICROSEISMS: OCTOBER 21–25, 1958

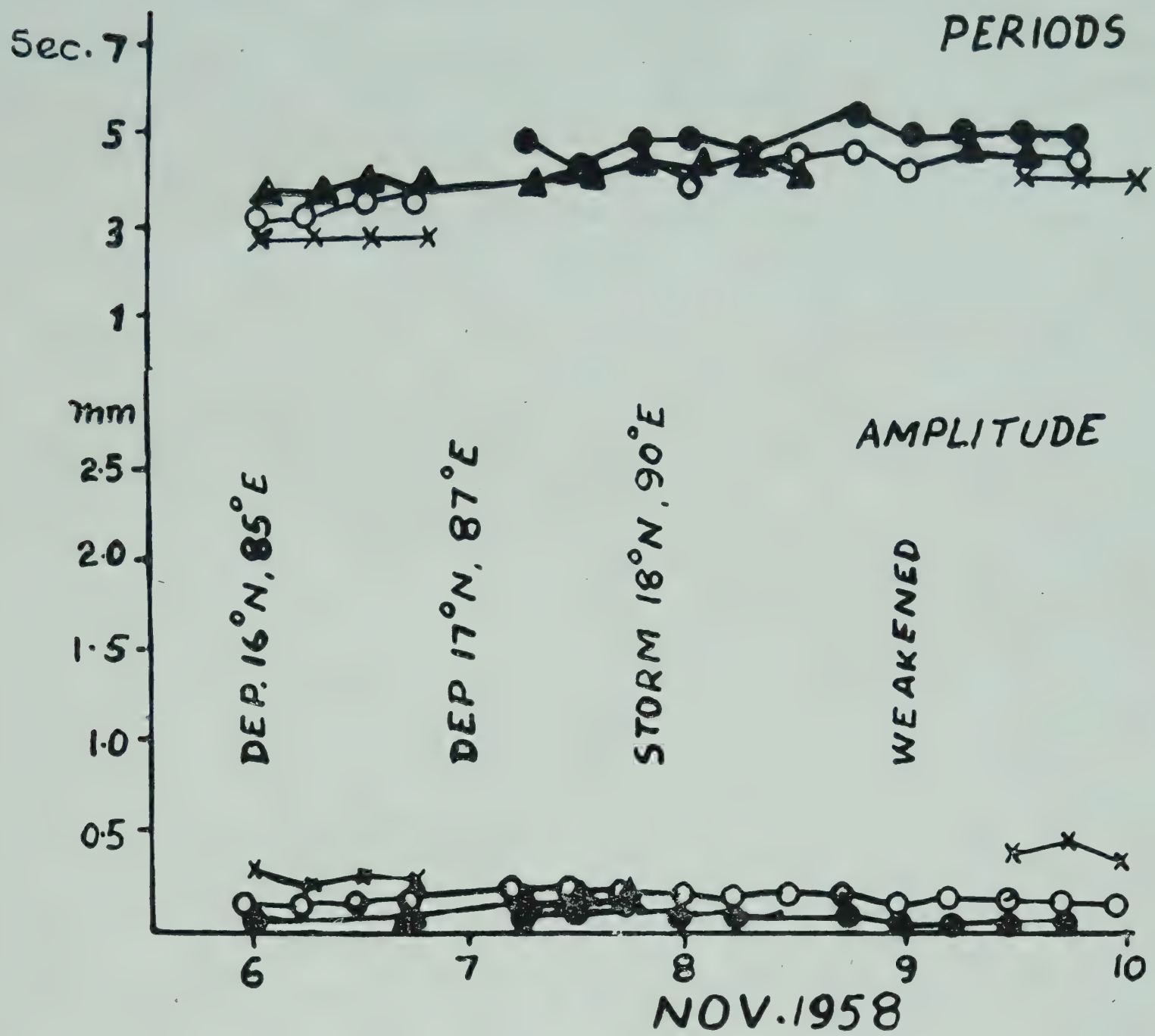

FIG. 13 — AMPLITUDES AND PERIODS OF MICROSEISMS: NOVEMBER 6–10, 1958

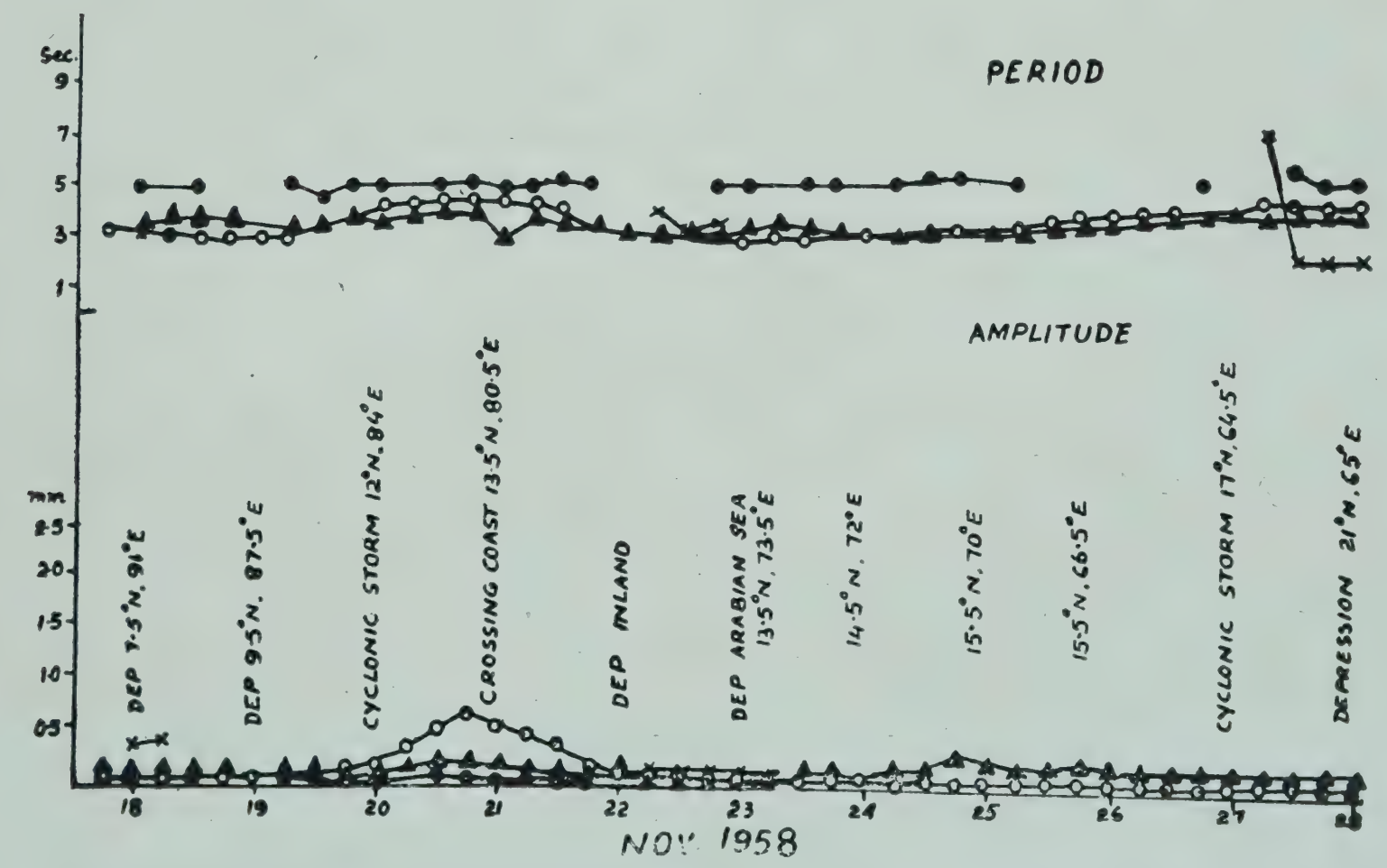

FIG. 14 — AMPLITUDES AND PERIODS OF MICROSEISMS: NOVEMBER 18–28, 1958

into a cyclonic storm and crossed the coast the same night. Except for a very slight rise in amplitudes of microseisms at Shillong, there was no significant rise of amplitudes at any of the Indian stations.

November 6–10, 1958. A depression formed in the Bay of Bengal on November 6 with its centre at latitude 16°N and longitude 85°E and started moving in the north-easterly direction. It intensified into a cyclonic storm by the morning of November 8, travelled eastwards and weakened on the next day. Microseismic amplitudes and periods at Bombay, Madras and Shillong started rising very slightly from 1800 hours GMT on November 6 reaching a peak at 0600 hours GMT the day after the next and thereafter declining slightly.

November 18–28, 1958. A depression formed in the south Bay of Bengal on November 18 with centre at 7·5°N and 91°E. It moved in a north-westerly direction, and on the morning of the day after lay as a cyclonic storm with its centre at 12°N : 84°E. The storm crossed the coast on the morning of November 21 near 13·5°N : 80·5°E. It travelled inland, emerged again as a depression in the Arabian Sea and on November 23 had its centre at 13·5°N : 73·5°E. The depression moved in westerly direction from November

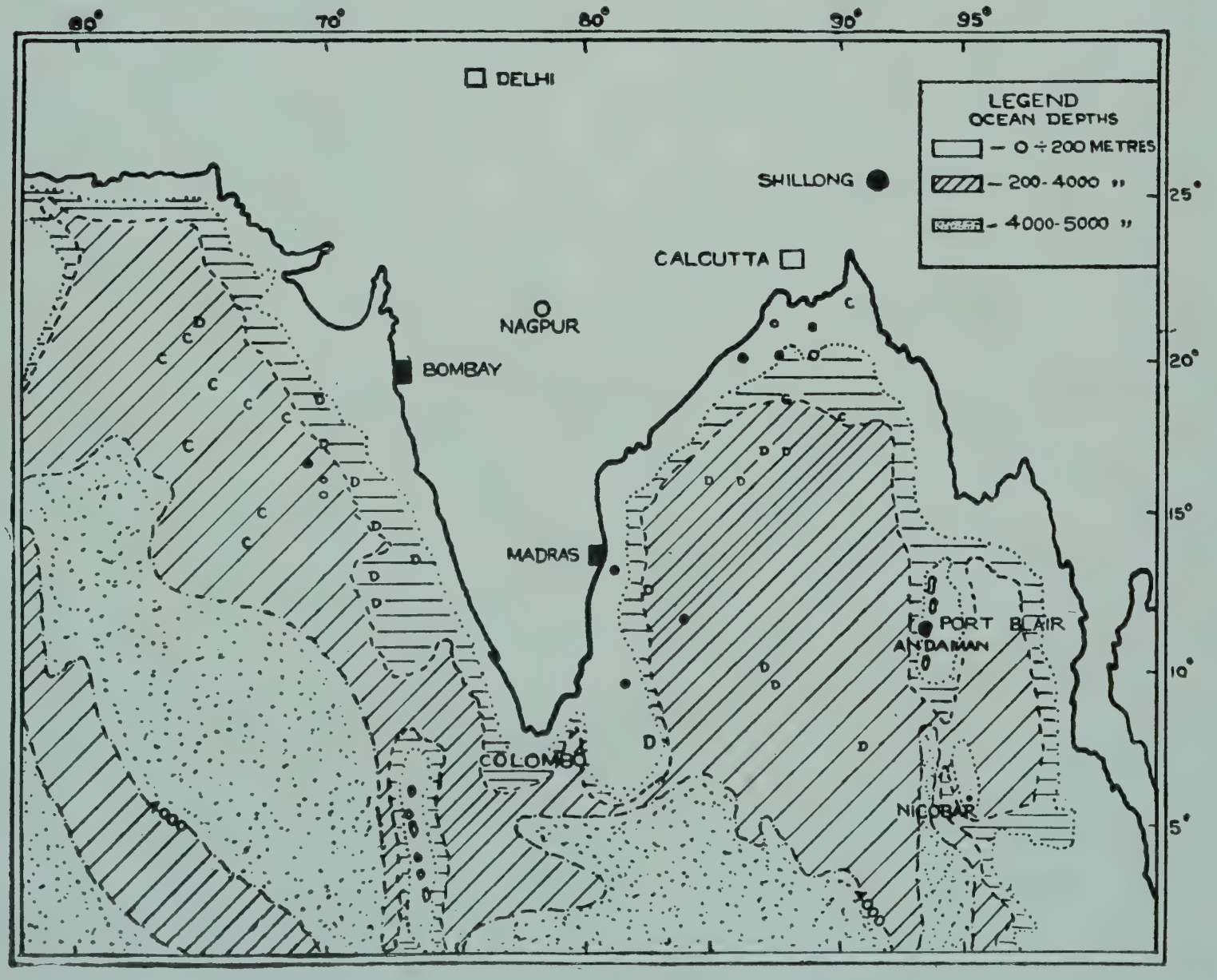

FIG. 15 — POSITION OF CENTRES OF CYCLONIC STORMS AND DEPRESSIONS

25 to 26 and then again north-westerly from November 26 to 27 when it intensified into a cyclone and recurved to north, then to north-east and finally weakened after the next day. There was a significant rise in the amplitude of microseisms at Madras, Bombay and Shillong near about zero hour GMT on November 20. The peak of this activity was recorded the same day at 1800 hours after which the activity started declining and returned to normal by the morning of the second day. During its passage in the Arabian Sea, there was no significant rise in the microseismic activity at the Indian stations except for a slight rise in amplitudes from zero hour GMT to 1000 hours on November 24 at Bombay. The periods of microseisms at Madras, Bombay and Shillong showed a slight increase from November 20 to 21 and at Madras and Bombay from November 24 to 27.

Discussion

Fig. 15 shows the position of centres of cyclonic storms and depression for which records of microseisms have been collected during the IGY period and plotted in Figs. 2–14. Depressions have been indicated by circles and letter D, and cyclonic storms by thick circles and letter C. The letters C and D indicate those cyclones and depressions for which no significant microseisms were recorded at any of the Indian stations. The map also shows contours for depths 0–200 m., 200–4000 m. and over 4000 m.

Although the number of positions of storms and depression centres are not very adequate, yet a few important inferences of a qualitative nature are obvious from an inspection of this map. It can be seen that nearly all the depressions and cyclonic storms located with the depth contours 0–200 m. have given rise to good microseismic build-ups at all the Indian stations. No significant microseisms due to depressions outside this belt were recorded at any of the Indian stations. Cyclonic storms having their centres at other locations in the Bay of Bengal, if they are sufficiently strong, do generate microseisms which can be recorded at Indian stations. This is not very evident from Fig. 15, as the number of cyclonic storms in the Bay of Bengal during the period under study was not sufficient. In an earlier paper[20], the case of a severe cyclonic storm which had its track right through the central Bay of Bengal from south to north was discussed, and it was found that microseisms with good build-ups and amplitudes were recorded at all the coastal and inland seismographs. The figure, however, indicates that there are certain regions in the Bay of Bengal which attenuate transmission of microseisms. One such region appears to be the extreme north-east angle of the Bay of Bengal and the other consists of the belt of deep water just outside the 0–200 m. depth contours.

In the Arabian Sea, the transmission of microseisms appears to take place only from locations confined to the 0–200 m. depth contour, except for a

small area about 500 km. to the west of Ratnagiri from where microseisms with attenuated amplitudes can be recorded at Bombay. No storm in the Arabian Sea within the belt 0–200 km. depth was located during the present study, but previous data indicate that microseisms from storms located within this belt are recorded at all the Indian stations. The data collected during the IGY seem to support the view that microseisms generated by storms located over deep waters can only be of operational value if the storm is fairly severe. It appears that deep sea bottom is not a good medium for transmission of microseisms.

Figs. 2–14 show that in nearly all cases when microseisms of significant amplitudes have been recorded, the amplitudes rise and fall almost simultaneously at all the stations. The microseismic maxima are recorded a few hours before the storm crosses the coast.

The effect of distance of the storm centre from the recording station on the amplitude of microseisms does not appear to be very straightforward. The amplitudes, as a rule, are not higher at stations nearest to the storm. It appears that the path of seismic rays from the storm to the station and the geology on which the station is located play an important role.

The variation of periods of microseisms has been attributed by various workers to a number of causes which include the distance of the recording station from the storm, intensity of the storm, depth of water below the storm, geology of the path and the recording station and type of seismograph used. The data presented in this paper show that the periods recorded at any station are not dependent upon the distance of the storm from the recording station. There is a distinct evidence from all the records presented here that the periods depend on the intensity of the storm. In nearly all the cases studied the periods show a rise with increase in amplitudes. The higher the period recorded, the more severe the storm. Periods of microseisms from cyclonic storms are seldom found below 4 sec. and in most cases are higher. Periods higher than 4 sec. are transmitted better through portion of the sea where the depth is large. Coastal stations like Madras and Bombay very often record periods of the order of 2–3 sec. These periods cannot be ascribed to microseisms due to cyclonic storms. Local surf activity is perhaps responsible for the generation of these periods. Whenever significant microseisms due to cyclonic storms have been recorded, it is found that the recorded period is generally higher than 4 sec. Sometimes even during the presence of a depression or storm near the station, the lower periods are recorded at coastal stations and the higher periods are eclipsed by them. Even in such cases the generation of short periods should be attributed to the increase in local surf activity caused by the neighbouring storm.

Microseismic periods recorded at Shillong are always higher than those recorded at Madras and Bombay, although the constants of seismographs operating at all the three stations are the same. The cause for these variations can only be attributed to local geology. The higher periods at Shillong may be due to greater depth of sediments as pointed out by Nag[21].

Conclusion

Data collected at the microseismic stations during the IGY indicate that operational use of microseisms for locating and tracking storms in the Indian Seas is feasible but with certain limitations. Microseisms generated by cyclonic storms of sufficient intensity in the Bay of Bengal are usually recorded at all coastal and inland stations. Microseismic storms generated in the Arabian Sea outside the 0–200 m. depth are not transmitted with sufficient amplitudes to seismographs to be of any operational value. Detection of cyclonic storms in the Arabian Sea can be done more expeditiously by conventional methods used in meteorology. In order to use microseismic data for operational use, it may be necessary to use highly sensitive seismographs having magnification of the order of 20,000 for the period range of the order of 4–6 sec. At coastal stations records of microseisms are vitiated by local surf activity which generates periods of the order of 2–3 sec. In order to make these stations more effective for storm detection and location, it will be necessary to use some technique to filter out these local microseisms. Techniques suggested and used by Derbyshire and Iyer may be useful for this purpose.

Empirical techniques such as those used by Gilmore can also be profitably used for storm tracking, but for this purpose data from standardized instruments will have to be collected for a large number of years. Collection of more data is also necessary to earmark areas in the sea from where microseisms are either not recorded or the amplitudes suffer considerable attenuation.

References

1. Banerjee, S. K., *Phil. Trans.*, **239** (1930), 287.
2. Gilmore, *Bull. Amer. met. Soc.*, **32** (1951), 346.
3. Chakravarti, S. K. & Sirkar, D., *Bull. seismol. Soc. Amer.*, **48** (1958), 181.
4. Decon, G. E. R., *Nature, Lond.*, **160** (1947), 419.
5. Gherzi, E., *Beitr. Geophys.*, **25** (1930), 145.
6. Gutenberg, B., *Bull. seismol. Soc. Amer.*, **26** (1936), 111.
7. Gutenberg, B., *J. Met.*, **4** (1947), 21.
8. Longuet Higgins, M. S. F., *Phil. Trans.*, **243A** (1950), 1.
9. Carder, D. S., *Trans. Amer. geophys. Un.*, **36** (1955), 838, 843.
10. Kammer, E. W. & Dinger, J. E., *J. Met.*, **8** (1951), 347.
11. Gutenberg, B., *Trans. Amer. geophys. Un.*, **30** (1953), 161.
12. Press, F. & Ewing, M., *Trans. Amer. geophys. Un.*, **29** (1948), 163.
13. Donn, W. L., *J. Met.*, **9** (1952), 61.
14. Lee, A. S., *Proc. roy. Soc.*, **149A** (1935), 183.

15. Ramierez, J. E., *Bull. seismol. Soc. Amer.*, **30** (1940), 139.
16. Gilmore, M. H., *Bull. seismol. Soc. Amer.*, **36** (1946), 89.
17. Gilmore, M. H., *Symposium on Microseisms*, Sept. 1952 (National Academy of Sciences, National Research Council, Ottawa), 1953.
18. Derbyshire, J. & Iyer, H. M., *Geophys. J. roy. astron. Soc.*, **1** (1958), 180.
19. Iyer, H. M., *Geophys. J. roy. astron. Soc.*, **1** (1958), 32.
20. Tandon, A. N., *Indian J. Met. Geophys.*, **8** (1957), 1.
21. Nag, K. R., *J. Technol.*, **4** (1959), 171.

* * *

A Preliminary Note on Short Period Microseisms recorded by Benioff Seismograph at Shillong. B. P. Saha, Central Seismological Observatory, Shillong [*Indian J. Met. Geophys.*, **13** (1962), 81].

The records of the short period vertical component Benioff seismograph at Shillong indicate that short period group microseisms of period very close to one second occur at Shillong on some occasions. According to Walsh, the great majority of the short period microseisms of period very near to 0·3 sec. are associated either with the approach or passage at the station of cold frontal type discontinuity or both, or with local non-frontal convective activity. But, a study of the microseism storms at Shillong indicates that these are not associated with each and every convective activity at the station. It is, however, believed that they are associated with the passage of cold fronts in association with the secondaries of the western disturbances which move from west to east during the pre-monsoon months. The probable mechanism of generation of these microseisms has been discussed. (*Abstract*)

Role of cosmic ray produced isotopes in the study of large scale atmospheric circulation and other geophysical phenomena

D. LAL

Tata Institute of Fundamental Research
Bombay

Several isotopes produced by cosmic rays in the atmosphere have proved to be suitable tracers for studying the nature and details of intricate geophysical and geochemical processes occurring in nature. The basis of this application principally rests on two facts. Firstly, the rate of production of the isotopes is continuous, constant and occurs at a measurable rate. The isotope production rates can be obtained accurately from a variety of cosmic ray and accelerator data and simulated irradiation studies by exposing suitable targets to cosmic rays. Secondly, the cosmic ray interactions lead to the production of a large number of isotopes having widely different half-lives. Their production rates are small, nevertheless their resulting concentrations in materials from the geospheres are often enough to permit measurements with the presently available low-level counting methods combined with proper chemical techniques.

The half-lives of the nine isotopes detected to date, which form ideal tracers for the investigations of geophysical problems, range from 15 days to $2{\cdot}7 \times 10^6$ years. These isotopes have already proved to be useful or are beginning to make important contributions in archaeology, geophysics, oceanography and meteorology.

The present status of this rapidly growing field has been briefly reviewed. The applications of the short-lived isotopes in meteorological studies and the information obtained to date from measurements of their concentrations in air and in rain water have been discussed.

Nuclear interactions of the primary and secondary particles of the cosmic radiation with the atmospheric nuclei lead to a continuous production of a

host of radio nuclides whose half-lives, though as long as up to a few million years, are sufficiently short that their original amounts created at the time of nucleosynthesis could not have survived till the present time. Cosmic rays are, therefore, solely responsible for their present abundance in nature.

As soon as the nuclear fragments are created, they are oxidized and get attached to aerosols. Except in the lower troposphere, the sizes of the aerosol particles are small enough not to be influenced by gravitational settling; the trajectories of the radio nuclides may be presumed to be identical with those of the surrounding air molecules. Isotopes having half-life periods comparable to the time scales involved in the meridional transport of air, stratosphere-troposphere exchange processes form suitable labels of air molecules to determine the details and the rates of such processes. Isotopes produced in the troposphere, and those entering the troposphere from the stratosphere, are removed to the surface of the earth by scavengings operative during condensations of moisture in time periods which are of short magnitude compared to those involved in their removal from the stratosphere by downward mixing of air. The removal of isotopes from the atmosphere, therefore, occurs from the lower troposphere by wet precipitations and is effective in the case of all isotopes studied so far except C^{14}. This isotope exists in the atmosphere in the form of CO_2; it enters the biosphere and also exchanges with the ocean bicarbonate as a result of molecular exchange reactions. The mean residence time of an isotope or of a contaminant introduced in the troposphere can be properly studied by observing the fall-out of cosmic ray produced isotopes having half-lives of the order of one month.

Isotopes produced in the atmosphere are thus introduced in the various geological domains, either by fall-out from the troposphere or by molecular exchange reactions. They reach the principal geospheres, the biosphere, lithosphere and the hydrosphere, and continue to play important roles as tracers. The internal circulation and mixing of material between these natural reservoirs can be studied using isotopes having adequate half-life periods. Some of the isotopes also prove valuable for a study of the chronology of the deep sea sediments. A knowledge of the chronology of slowly accumulating sediments in itself is very valuable since such sediments contain the historic and prehistoric records of the biological productivity in the oceans, climatological conditions, volcanic activity, rates of influx of extra-terrestrial material, and polar drift, to mention a few among the many geophysical events which can be studied from a careful examination of their constituents. The cosmic ray produced isotopes can introduce absolute time scales in these geophysically significant records up to periods of the order of ten million years in the past. The techniques based on the naturally occurring long-lived radio-isotopes K^{40}, Rb^{87}, and the radioactive series of the isotopes Th^{232}, U^{235}, U^{238} are not applicable to time periods in the interval 0·25–10 million years in the past.

The study of historic or geological events, or long-term geophysical processes essentially requires a knowledge of the time variations of cosmic ray intensity in the past. An investigation of events or processes, where some information is available by the use of other reliable methods, can in fact be used to determine the cosmic ray intensity variations in the past. The measurements of C^{14} activity in old archaeological samples of known ages agree very closely with those expected on the basis of the present-day cosmic ray intensity. This, by itself, cannot be taken to indicate that the cosmic ray intensity has been constant during the periods in question; it is hinged to several questions which produce effects in opposite directions, e.g. changes in the earth's magnetic field, climatological changes and prevalent rates of mixing between the ocean and the atmosphere. Most reliable indicators of cosmic ray intensity variations are the meteorites which contain well-preserved records of long-term cosmic ray irradiations received during their travel in the interplanetary space. Recent detailed investigations of isotopes in meteorites have shown that the cosmic ray intensity has been much the same during the past few millions of years except for the possible presence of any short-lived changes which may have occurred with frequencies so small as not to disturb the overall feature of constancy required by the observed data[1,2].

The only changes in cosmic ray intensity which are known to occur are of temporal nature and arise from two causes which are both of solar origin. The cosmic ray intensity varies inversely with the 11-year sunspot cycle, presumably due to modulations of the galactic cosmic ray flux by a solar cycle dependent plasma cloud emission from the sun. The second type of variation results from the acceleration and emission of charged particles during solar flares. Such events are rare, but may result in an appreciable influx of low energy protons for periods of the order of a few days at the polar regions. The magnitude of these time variations is nevertheless small on the effective isotope production rates and for all practical purposes, the cosmic ray intensity can be regarded to be constant for most isotope applications. In the polar stratosphere, the concentrations of isotopes having half-lives of the order of a few days will be appreciably modified during solar flares and in such investigations, one has to take into account the time variations of the cosmic ray intensity. The variations in the isotope production rates due to the two main solar effects have been discussed in detail by Lal and Peters[3].

Useful Cosmic Ray produced Isotopes and their Rates of Production

The various cosmic ray produced isotopes which are suitable for investigations of geophysical processes are listed in Table 1, in the order of decreasing half-lives. A complete bibliography and details of mechanisms responsible for their production in the atmosphere are given by Lal and Peters[3].

TABLE 1 — COSMIC RAY PRODUCED ISOTOPES

Isotope	Half-life *years*	Production rate (*atoms/cm.²* *sec.*)		Global inventory *g.*
		Troposphere	Total atmosphere	
Be^{10}	$2{\cdot}7\times10^{6}$	3×10^{-2}	9×10^{-2}	930†
C^{14}	5568	0·8	1·8	54†
Si^{32}	710	$5{\cdot}4\times10^{-5}$	$1{\cdot}6\times10^{-4}$	1400
H^{3}	12·5	$8{\cdot}4\times10^{-2}$	0·25	3500
Na^{22}	2·6	$1{\cdot}8\times10^{-5}$	$5{\cdot}6\times10^{-5}$	1200
S^{35}	87*	$4{\cdot}9\times10^{-4}$	$1{\cdot}4\times10^{-3}$	4·5
Be^{7}	53*	$2{\cdot}7\times10^{-2}$	$8{\cdot}1\times10^{-2}$	3·2
P^{33}	25*	$2{\cdot}2\times10^{-4}$	$6{\cdot}8\times10^{-4}$	0·6
P^{32}	14·3*	$2{\cdot}7\times10^{-4}$	$8{\cdot}1\times10^{-4}$	0·4

*Days; †Tons

Table 1 does not include the isotopes of chlorine Cl^{39} and Cl^{36}, which have also been detected. The half-life of Cl^{39} is only 55 min. and it will probably find applications in the study of very short-term atmospheric movements. The isotope Cl^{36} is produced both in the atmosphere and on the surface of the earth by the neutron capture reaction Cl^{35} (n, γ) Cl^{36}. Several other isotopes are also produced in the uppermost layers of the earth[4,5].

The production rates of the various isotopes have been calculated from the available cosmic ray and accelerator data as a function of latitude and altitude in the atmosphere. A direct measurement was made with a view to obtaining more accurate production values in the case of the isotopes Be^{7}, S^{35}, P^{33} and P^{32} by exposing oxygen and argon at mountain altitudes[6]. The useful methods of obtaining the isotope production rates are discussed by Lal and Peters[3]. The calculated average global production rates and the corresponding global inventories are given in Table 1.

In the case of isotopes Be^{10}, C^{14} and Si^{32} which are useful for oceanographic studies, it is probably quite sufficient to deal with their average global production rates (atoms/cm.²/sec.) since their half-lives are long compared to the atmospheric circulation periods. Their global fall-out must equal the average global production rates. Any departures from a uniform fall-out rate on the surface of the earth will probably be smoothened out due to the rapid mixing processes in the uppermost layers of the oceans.

The use of the short-lived isotopes P^{32}, P^{33}, Be^{7}, S^{35}, Na^{22} and H^{3} in meteorology and hydrology requires a more detailed knowledge of their source function in the atmosphere. Their dependence on altitude and latitude has been

derived by Lal *et al.*[7]. Fig. 1 gives the position of lines of equal isotope production rates (atoms/10^3 cu. ft/min.) as a function of latitude and altitude for the isotopes Be^7, S^{35}, P^{32} and Na^{22}. The production rates of H^3 and P^{33} are obtained if the Be^7 values are multiplied by 3·1 and $8{\cdot}4 \times 10^{-3}$ respectively. Isotope production rates are identical in the two hemispheres. The production rates at a given altitude are the same for all geographic coordinates having a given geomagnetic latitude. The strong zonal circulation of air makes it difficult to look for finer details by making a distinction between either the geographic or geomagnetic latitude, i.e. the longitudinal coordinate.

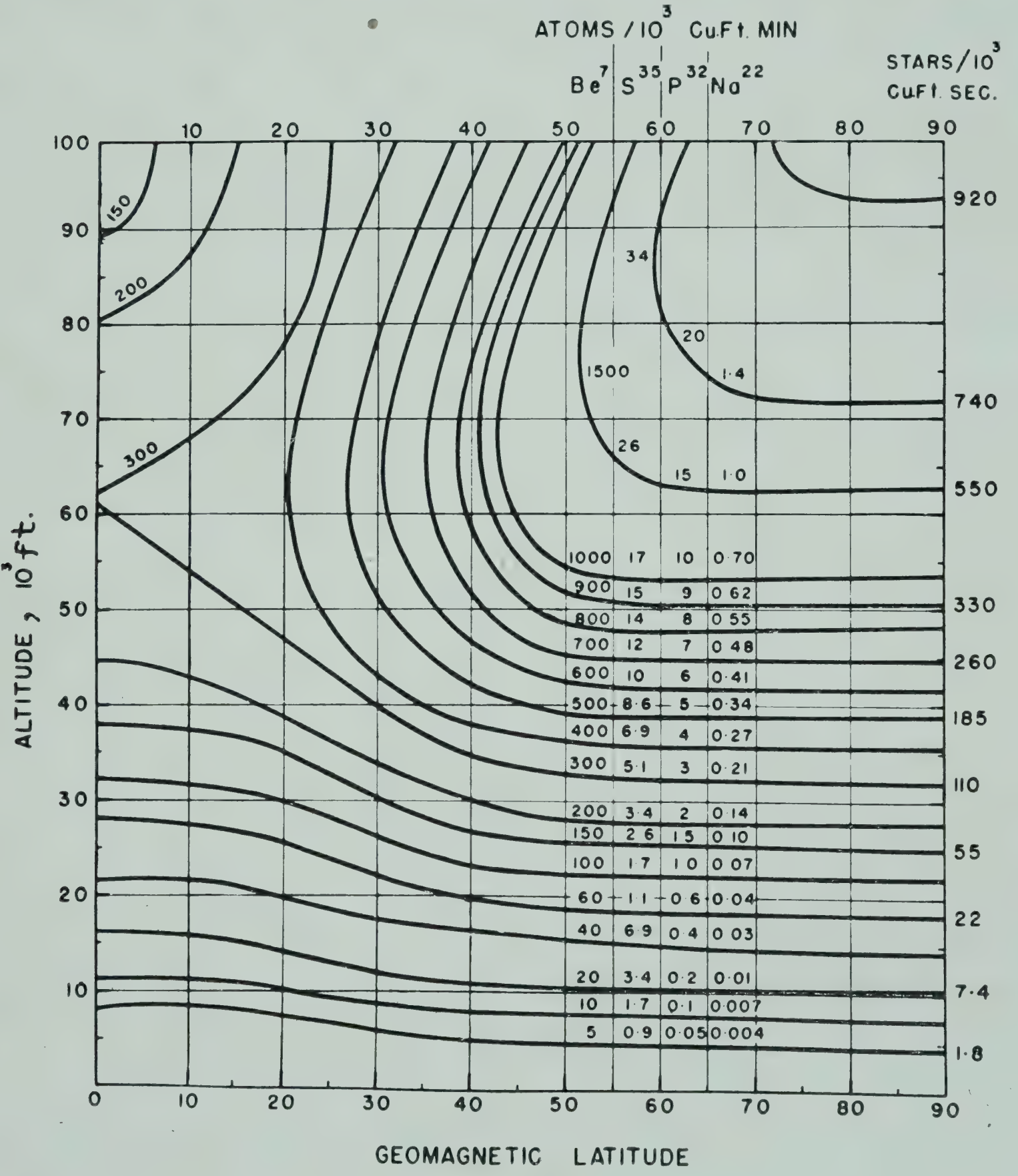

FIG. 1 — RATES OF PRODUCTION OF THE COSMIC RAY PRODUCED ISOTOPES Be^7, S^{35}, P^{32} AND Na^{22} IN THE ATMOSPHERE AS A FUNCTION OF LATITUDE AND ALTITUDE

It is seen from Fig. 1 that the relative production rates of isotopes are practically constant in all regions of the atmosphere. The absolute isotope production rates at a given altitude increase towards higher latitudes, especially in the stratosphere. The integrated isotope production rates in the troposphere, however, remain practically independent of latitude since the height of the tropopause decreases towards polar regions.

Circulation of Isotopes on the Earth

It was discussed qualitatively at the outset how the various isotopes get dispersed in the various geospheres. The circulation of isotopes can be conveniently discussed in greater detail by considering the geospheres as made up of a few significant zones or reservoirs which are more or less typical with respect to exchange or mixing of material within and with the neighbouring reservoirs in communication. Such subdivisions aim to derive geophysical information from over-simplified models but are very meaningful and instructive because of two reasons: firstly, the physical properties of these reservoirs are typical so that for all practical purposes, the flow of matter can be considered to occur across the surfaces of discontinuity between two communicating reservoirs which are assumed to be individually well mixed; secondly, when the number of isotope measurements are not very large, some useful information can still be derived using such simplified models. The purpose of isotope studies is to determine the rates of exchange of matter between these reservoirs, and the sizes of these reservoirs, when the latter are not known *a priori*.

A schematic diagram showing such natural reservoirs and the surfaces of discontinuity is shown in Fig. 2. The size of the reservoirs and the average time of residence of molecules following the bulk movements of matter in the reservoirs, against removal to adjacent reservoirs, are also given. The inventories of isotopes in the various reservoirs depend on their half-lives, rates of flow of matter across the surfaces and their geochemical behaviour in the media constituting the reservoirs. One can regard three principal modes of circulation applicable to the various cosmic ray produced isotopes. These are schematically shown in Fig. 3.

The information which can be derived from such models has been reviewed by Lal and Peters[3]. This will be briefly discussed here. Some of the experimental data in air and in wet precipitations and the implications of the results to large-scale atmospheric circulation will be discussed in some detail.

Meteorological Studies using Cosmic Ray produced Isotopes

Several techniques have been employed for studying the characteristics of the large-scale atmospheric circulation. Water vapour, ozone and radio-isotopes

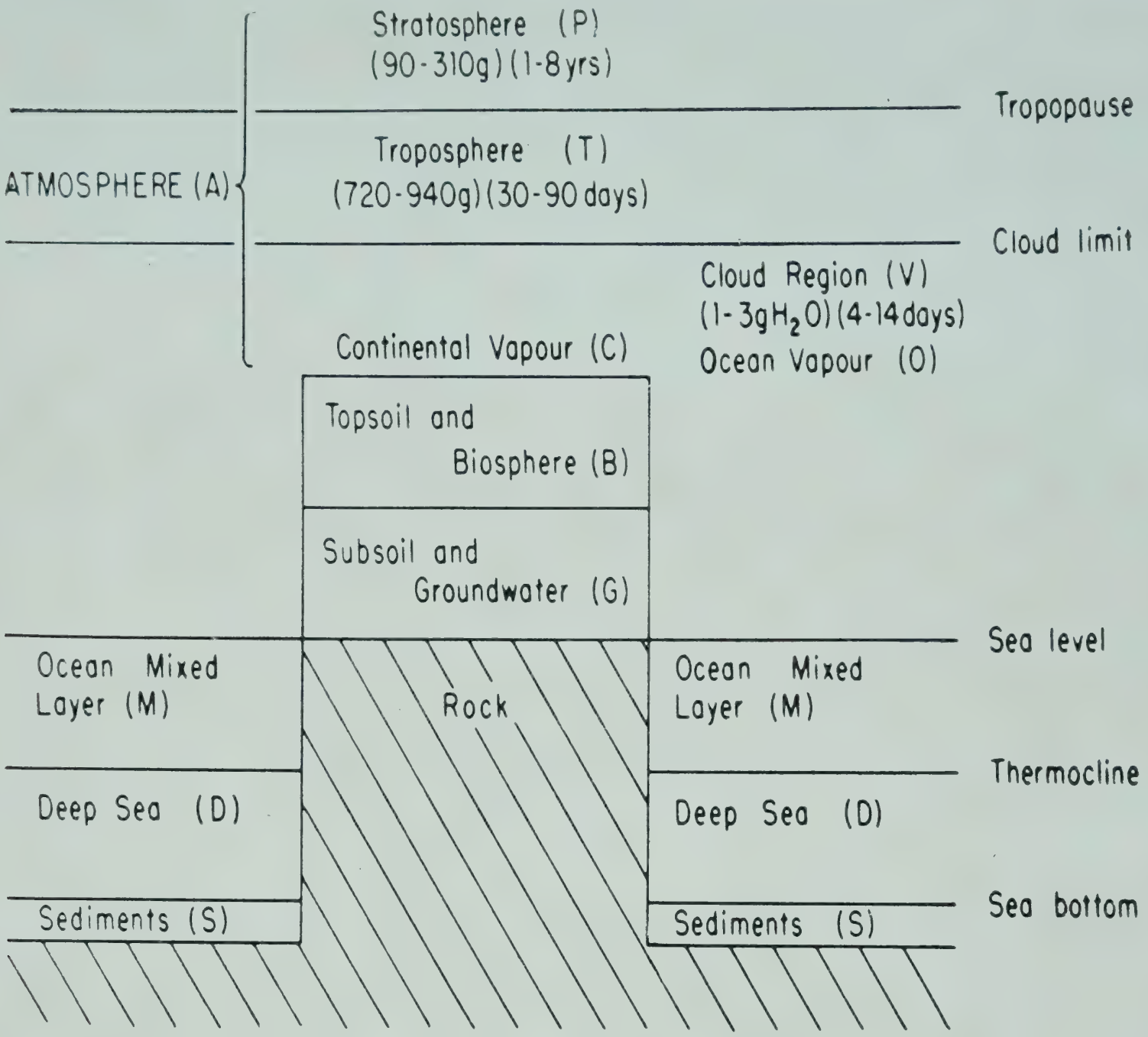

FIG. 2 — GEOPHYSICALLY SIGNIFICANT SUBDIVISIONS OF THE GEOSPHERES

produced by nuclear detonations have been used as tracers. Observations of potential temperatures, wind velocities and smoke trials are examples of other useful methods. Most of the information available to date is obtained from these different methods. Cosmic ray produced isotope studies have begun only recently; these studies not only complement the information available from other methods, but promise to be unique for answering certain questions which cannot be tackled properly otherwise. This is due to the fact that they form the only tracers whose source functions are known accurately. The properties of the source function are also ideal in many respects. The production rates at a given altitude are, to a first approximation, only dependent on the latitude but not the longitude. The production rates are strongly latitude- and altitude-sensitive (Fig. 1). These properties make it possible to measure the much smaller vertical and meridional transport rates prevalent in the stratosphere in the presence of much larger zonal components.

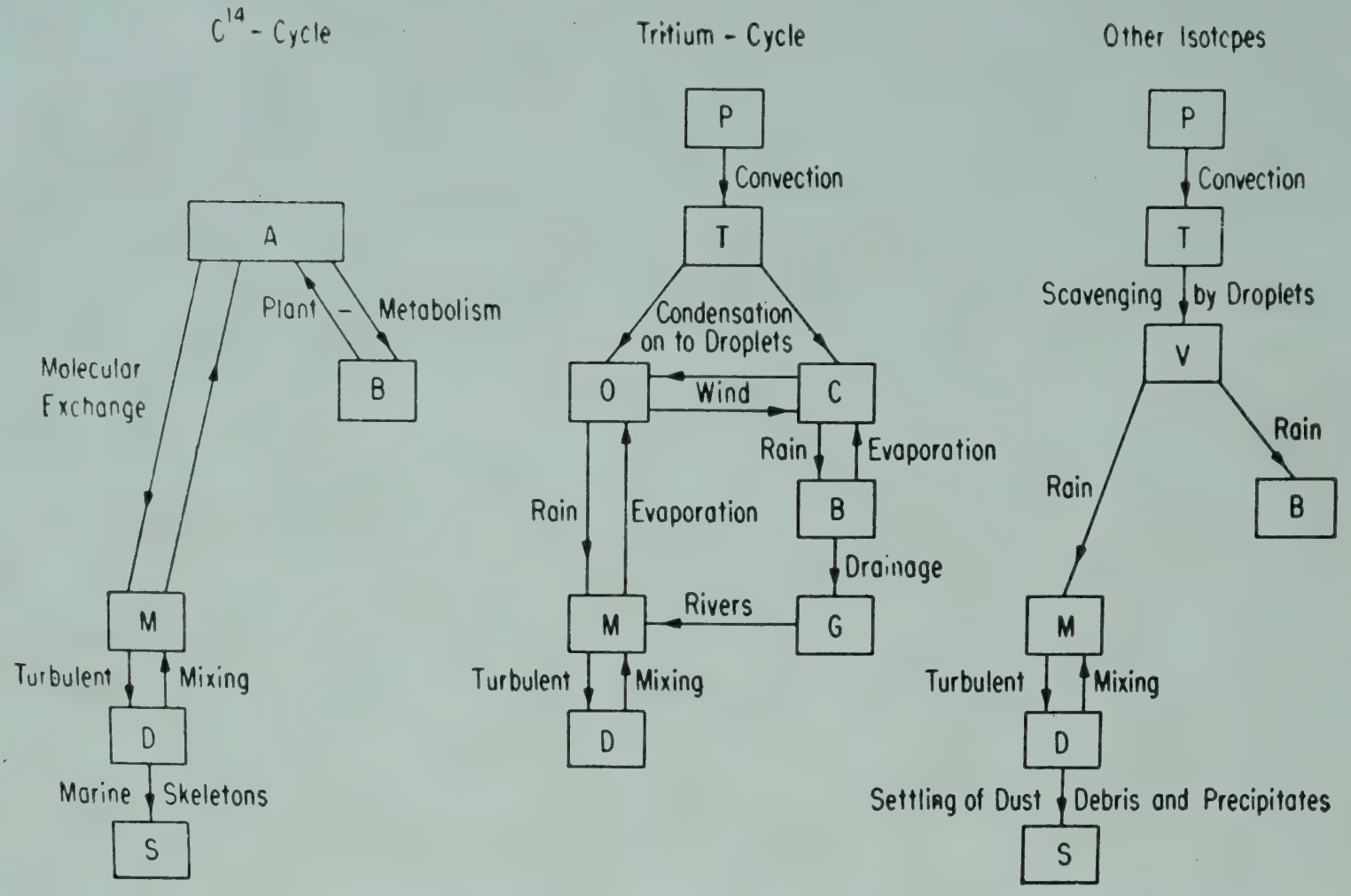

FIG. 3 — SIMPLIFIED CIRCULATION PATTERNS OF THE COSMIC RAY PRODUCED ISOTOPES

It has recently been shown[3,8] that the displacement of the isoproduction surfaces in the stratosphere, resulting from a circulation pattern governed by transport lasting over periods long enough to allow a steady state concentration of isotopes to reach in the atmosphere, can be used to measure the transport velocity vectors. If the rate of production of an isotope of mean life, τ, at a given point in the atmosphere is P (atoms/g.), the observed concentration of the isotope, C (atoms/g. air) is related to the velocity, $\vec{v}$, by the relation:

$$\tau P - C = \tau \vec{v} . \overrightarrow{\text{grad}}\ C$$

Since several isotopes of widely different half-lives are available, the non-zonal vector components of the transport velocity can be determined accurately.

EXPERIMENTAL DATA ON SHORT-LIVED ISOTOPES

Isotope concentrations in rain water (and snow) have been measured in Sweden, Chicago and India[9–14]. The concentration values for the isotopes Be^7, P^{32} and S^{35} in rain water for the Indian stations[9,10,13,14] are summarized in Tables 2, 3 and 4. The errors in individual measurements are ± 20 per cent in most cases.

TABLE 2 — COSMIC RAY PRODUCED ISOTOPE CONCENTRATION IN RAIN WATER AT KODAIKANAL: 1956-59

Date of rainfall	Atoms/ml. rain water			Date of rainfall	Atoms/ml. rain water		
	Be^7	P^{32}	S^{35}		Be^7	P^{32}	S^{35}
30-1-56	1750	—	—	6-11-56	500	—	—
25-2-56	6200	—	—	8-11-56	1100	—	—
10-3-56	5100	—	—	11-11-56	200	—	—
4-4-56	6400	—	—	16-11-56	1200	—	—
7-4-56	10000	—	—	19-11-56	300	—	—
18-4-56	2800	—	—	21-11-56	400	—	—
20-4-56	4800	—	—	26-12-56	600	—	—
22-4-56	5350	—	—	1-2-57	650	—	—
24-4-56	4400	—	—	4-3-57	2200	—	—
25-4-56	7900	—	—	13-4-57	3800	—	—
26-4-56	9900	—	—	14-5-57	3300	—	—
28-4-56	7200	—	—	8-6-57	1800	—	—
18-5-56	2800	—	—	26-6-57	2800	—	—
23-5-56	2400	—	—	4-7-57	700	—	—
13-6-56	2700	—	—	25-8-57	1300	7	—
14-6-56	2100	—	—	28-9-57	2000	—	—
19-6-56	2000	—	—	6-10-57	2300	—	—
21-6-56	1600	—	—	4-11-57	400	—	—
22-6-56	550	—	—	10-11-57	2500	30	124
25-6-56	4900	—	—	14-11-57	850	—	20
26-6-56	3500	—	—	28-11-57	1800	22·5	220
30-6-56	2800	—	—	4-12-57	1300	—	—
8-8-56	1600	—	—	18-12-57	1100	—	—
15-8-56	1700	—	—	2-11-58	—	17	—
19-8-56	1200	—	—	4-12-58	680	5·1	—
21-8-56	5500	—	—	14-12-58	730	3·2	—
25-8-56	2990	—	—	24-12-58	3700	—	—
28-8-56	11000	—	—	13-1-59	550	4·7	—
12-9-56	1600	—	—	14-1-59	870	4·2	—
15-9-56	2400	—	—	15-1-59	810	17	—
16-9-56	1160	—	—	31-1-59	1480	17·4	—
29-9-56	1840	—	—	6-4-59	4100	16·8	—
13-10-56	2300	—	—	19-4-59	3640	19	—
15-10-56	600	—	—	5-7-59	750	4·4	—
17-10-56	1400	—	—	13-7-59	1570	5·7	—
19-10-56	3200	—	—	12-8-59	3880	9·5	—
25-10-56	4700	—	—	26-8-59	1190	3·5	—
26-10-56	1000	—	—	31-8-59	4080	10·4	—
31-10-56	1300	—	—	24-9-59	875	6·4	—
1-11-56	900	—	—	3-10-59	1410	3·7	—

TABLE 3 — COSMIC RAY PRODUCED ISOTOPE CONCENTRATION IN RAINS AT BOMBAY: 1956-59

Date of rainfall	Atoms/ml. rain water			Date of rainfall	Atoms/ml. rain water		
	Be^7	P^{32}	S^{35}		Be^7	P^{32}	S^{35}
24-5-56	9300	—	—	6-8-57	3500	32	—
27-5-56	9250	—	—	7-8-57	2900	—	—
12-6-56	5500	—	—	11-8-57	5200	32	—
14-6-56	8000	—	—	16-8-57	5650	19	—
16-6-56	8150	—	—	18-8-57	2550	18	—
17-6-56	7900	—	—	20-8-57	3200	24	—
24-6-56	4500	—	—	22-8-57	3300	26	—
26-6-56	4100	—	—	10-11-57	2350	13	—
30-6-56	1400	—	—	11-11-57	1800	19	120
12-7-56	4400	—	—	20-6-58	940	11	230
26-7-56	6500	—	—	21-6-58	5300	65	1150
13-8-56	4100	—	—	22-6-58	4900	67	980
14-8-56	2100	—	—	26-6-58	5300	35	540
18-8-56	2500	—	—	1-7-58	2400	18	160
25-8-56	6900	—	—	2-7-58	4500	25	450
30-8-56	6600	—	—	5-7-58	4000	33	440
1-9-56	1500	—	—	7-7-58	3650	62	1700
3-9-56	7200	—	—	9-7-58	2200	13	1650
12-9-56	6350	—	—	11-7-58	1100	20	620
23-9-56	4250	—	—	12-7-58	3150	27	1360
24-9-56	1550	—	—	12-7-58	4150	43	1650
26-9-56	2250	—	—	20-7-58	6400	50	3200
27-9-56	4400	—	—	29-7-58	10000	42	3500
30-9-56	3300	—	—	3-8-58	8350	73	3450
1-10-56	1200	—	—	5-8-58	4670	46	2300
3-10-56	1650	—	—	18-8-58	3050	48	1500
6-10-56	800	—	—	19-8-58	5350	100	1850
8-10-56	4750	—	—	11-9-58	3150	55	1840
9-10-56	1800	—	—	4-6-59	2530	13·7	—
25-5-57	130	—	—	5-6-59	4370	29·0	—
22-6-57	1750	—	—	22-6-59	2640	7·5	2080
23-6-57	2000	—	—	23-6-59	1380	10·4	—
28-6-57	3900	—	—	29-6-59	1600	10·6	—
28-6-57	1400	—	—	29-6-59	1960	13·0	—
30-6-57	2600	—	—	2-7-59	1800	11·7	—
5-7-57	1700	—	—	10-7-59	3580	12·3	—
5-7-57	6200	—	—	13-7-59	2840	12·0	565
5-7-57	3300	—	—	20-7-59	1420	11·2	140
6-7-57	2500	—	—	22-7-59	5450	24·0	530
13-7-57	5900	—	—	31-7-59	2760	13·6	90
20-7-57	9100	44	690	20-8-59	9410	9·5	—
22-7-57	5700	26	690	22-8-59	3020	12·1	430
26-7-57	3350	36	—	31-8-59	810	4·4	120
5-8-57	2650	—	—				

Continued

TABLE 3 — COSMIC RAY PRODUCED ISOTOPE CONCENTRATION IN RAINS AT BOMBAY : 1956-59 — *Contd*

Date of rainfall	Atoms/ml. rain water			Date of rainfall	Atoms/ml. rain water		
	Be^7	P^{32}	S^{35}		Be^7	P^{32}	S^{35}
2-9-59	1670	8·6	—	29-9-59	2810	17·7	—
7-9-59	1930	5·7	75	1-10-59	1650	8·7	320
12-9-59	2000	10·0	53	2-10-59	1980	8·0	168
14-9-59	5010	13·3	—	4-10-59	3120	2·7	228
26-9-59	—	12·4	—	11-10-59	3220	12·8	192
28-9-59	—	21·7	—	13-10-59	4150	13·6	—

TABLE 4 — COSMIC RAY PRODUCED ISOTOPE CONCENTRATIONS IN RAIN WATER AT SHILLONG, MUSSOORIE, DELHI, PATHANKOT AND SRINAGAR : 1957-58

Date of rainfall	Atoms/ml. rain water			Date of rainfall	Atoms/ml. rain water		
	Be^7	P^{32}	S^{35}		Be^7	P^{32}	S^{35}
	SHILLONG				DELHI		
4-6-57	3000	—	—	20-11-57	7100	54	260
7-6-57	3800	—	—	11-12-57	2300	—	160
23-6-57	1200	—	—	28-1-58	1450	—	—
4-7-57	700	—	—				
11-7-57	430	—	—				
2-8-57	530	—	—				
4-8-57	150	—	—				
29-8-57	720	3·7	—				
5-9-57	780	3·5	—				
7-9-57	270	3·0	—		PATHANKOT		
26-9-57	350	—	—				
26-9-57	260	—	—	20-11-57	9500	105	—
5-10-57	165	—	—	7-12-57	7400	—	590
6-10-57	50	—	—	11-12-57	3400	39	170
11-10-57	1100	—	—				
12-10-57	2800	—	—				
	MUSSOORIE						
1-6-57	3900	—	—				
10-7-57	2600	—	—		SRINAGAR		
11-8-57	2300	12	—				
31-8-57	1500	10	—	20-11-57	3600	45	245
13-9-57	600	6	—	24-11-57	1160	—	—
12-10-57	6400	—	—	2-12-57	5500	—	420
20-11-57	5000	18	275	5-12-57	5700	43	—
12-12-57	2800	—	350	11-12-57	6300	50	—

The ' air ' data have only become possible recently due to the development of suitable air-sampling techniques in U.S.A. Both aircrafts and balloons have been used for high altitude sampling. The measurements refer to latitudes 40°S–70°N and altitudes 10,000–70,000 ft[4,15,16].

The results of the measurements in air (above the troposphere and in the troposphere) chiefly based on the data of Rama and Honda[4] who have studied the absolute concentrations of the three isotopes Be^7, P^{33} and P^{32} are summarized below.

In air well above the tropopause:

(i) The absolute concentrations of the isotopes P^{33} and P^{32} are in equilibrium with the production rates, while those of Be^7 are up to 30–50 per cent lower.

(ii) The ratio of the disintegration rates of P^{33} and P^{32} lie between 0·9 and 1·1. The corresponding expected secular equilibrium value for a static atmosphere is *c.* 1·0.

(iii) The ratio of the disintegration rates of Be^7 and P^{32} lie between 55 and 75. The corresponding expected secular equilibrium value for a static atmosphere is *c.* 100.

(iv) There is a tendency for an increase in the Be^7/P^{32} ratio with height above tropopause.

In the tropospheric air:

(v) The absolute concentrations of isotopes are much less, being markedly lower for the longer lived isotope Be^7, than the corresponding equilibrium value.

(vi) The isotope concentrations are fairly uniform throughout the troposphere.

(vii) The ratio of the disintegration rates of P^{33} and P^{32} lie between 0·5 and 0·9.

(viii) The ratio of the disintegration rates of Be^7 and P^{32} lie between 17 and 54.

The measurements are not yet extensive enough to discuss the data as a function of latitude and altitude in the stratosphere. They, however, clearly show certain definite characteristics of the stratospheric and tropospheric circulation. Observations (i) to (iv) show that large-scale transports, organized or turbulent, between two regions of significantly different production rates, occur on time scales much longer than weeks[4]. Stratospheric-tropospheric mixing effects are observable up to a few thousand feet above the tropopause. The stratospheric Be^7 data[4,15,16] show that the departures from the expected secular equilibrium values for a static atmosphere are less than 50 per cent. This is indicative of the fact that the transport

velocities can be studied using this isotope. The extension of such measurements to the relatively longer lived isotopes, S^{35} and Na^{22} is desirable.

The tropospheric data clearly show the importance of the processes of turbulence and scavengings by wet precipitations. Isotope ratios compare well with those in rain water; this indicates that rain removes these isotopes effectively.

Isotope concentrations in rain water measured during 1956–59 show that the fall-out of Be^7 and P^{32} are not dependent on latitude. The absolute fall-out rates are consistent with the picture that their fall-out occurs mainly due to their production in the troposphere; the time involved in the exchange of material across the tropopause is so large that most of their activity undergoes radioactive decay in the stratosphere.

The ratio of the disintegration rates of the isotopes Be^7 and P^{32} in individual rains ranges from 16 to 65 in most of the samples. This is similar to the results of Rama and Honda[4] for the tropospheric air. The distribution in the ratios suggests that no substantial intrusions of stratospheric air occur in the troposphere[11] and that the mean removal time of isotopes from the troposphere is 40 days[6]. The absolute fall-out rates of isotopes are also consistent with this removal period.

The experimental results discussed above clearly demonstrate the potentialities of isotope studies in air and wet precipitations. A study of the nature of the large-scale atmospheric circulation in greater details is necessary.

References

1. Arnold, J. R., Honda, M. & Lal, D., *J. geophys. Res.*, **66** (1961), 3519.
2. Arnold, J. R., *Annu. Rev. nucl. Sci.*, **11** (1961), 349.
3. Lal, D. & Peters, B., *Progress of Cosmic Ray Physics and Elementary Particle Physics*, Vol. 6 (North Holland Publishing Co., Amsterdam), 1962, 1.
4. Rama & Honda, M., *J. geophys. Res.*, **66** (1961), 3533.
5. Rama & Honda, M., *J. geophys. Res.*, **66** (1961), 3227.
6. Lal, D., Arnold, J. R. & Honda, M., *Phys. Rev.*, **118** (1960), 1626.
7. Lal, D., Malhotra, P. K. & Peters, B., *J. atmos. terr. Phys.*, **12** (1958), 306.
8. Peters, B., *Cosmic ray produced isotopes as stratospheric tracers*, Proceedings of Helsinki Conference, 1960.
9. Rama Thor & Zutshi, P. K., *Tellus*, **10** (1958), 99.
10. Goel, P. S., Narsappaya, N., Prabhakara, C., Rama Thor & Zutshi, P. K., *Tellus*, **11** (1959), 91.
11. Peters, B., *J. atoms. terr. Phys.*, **13** (1959), 351.
12. Nilsson, R., Olsson, I., Berggren, A. & Sieghalm, K., *Ark. Geophys.*, **3** (1959), 111.
13. Lal, D., Rama & Zutshi, P. K., *J. geophys. Res.*, **65** (1960), 669.
14. Rama, *J. geophys. Res.*, **65** (1960), 3773.
15. List, R. J. & Telegdas, K., *The pattern of global atmospheric radioactivity*, Preprint, May 1960.
16. Hasp, *High altitude sampling programme*, Defence Atomic Support Agency, Washington, Rep. No. 539 B, 1961.

Observations of Fall-out in India during the Period of Cessation of Nuclear Tests. K. G. Vohra & V. S. Bhatnagar, Atomic Energy Establishment, Trombay, Bombay [*Nature, Lond.*, **189** (1911), 286–88].

Recent measurements of fall-out in different parts of the world have provided evidence of shorter residence time of fission products in the stratosphere than had been estimated earlier.

Estimations of the atmospheric residence time, based on the measurement of fall-out in India, have been made for the high-yield tests carried out in the polar regions during October 1958 by measuring (i) ground-level airborne activity and (ii) the change with time of Zr^{95}/Cs^{137} activity in samples of rain water from Bombay and Srinagar during December 1958–September 1959. Both the estimations give a value of 60 days for the residence time in the atmosphere of fission products debris.

The obvious consequence of short residence time in the atmosphere is an increase in the external γ-radiation dose for several months after high-yield tests. The radiation dose from γ-emitting isotopes ($Zr^{95}+Nb^{95}$), ($Ce^{144}+Pr^{144}$), Ru^{106} and Cs^{137} after the October 1958 tests has also been estimated from observed levels of activity. (*Abstract*)

AUTHOR INDEX